Univerzita Karlova

Přírodovědecká fakulta

Katedra fyziologie

Vliv variací v genech *GRIN* na biogenezi a funkční vlastnosti NMDA receptoru

Disertační práce

Mgr. Viktor Kuchtiak

Praha 2024

Školitel: RNDr. Aleš Balík, Ph.D.

Charles University

Faculty of Science

Department of Physiology

The effect of variations in *GRIN* genes on the biogenesis and functional properties of the NMDA receptor

Doctoral thesis

Mgr. Viktor Kuchtiak

Prague 2024

Supervisor: RNDr. Aleš Balík, Ph.D.

Prohlášení

Prohlašuji, že jsem doktorskou disertační práci vypracoval samostatně a uvedl veškeré použité informační zdroje. Tato práce ani její podstatná část nebyla předložena k získání jiného či stejného akademického titulu.

Declaration

I declare that I have written my dissertation independently and have cited all sources of information used. Neither this thesis nor any substantial part of it was submitted for another or the same academic degree.

Prague, 12. 1. 2024 Mgr. Viktor Kuchtiak

Acknowledgement

I would like to express my sincere gratitude to my supervisor, RNDr. Ales Balík Ph.D., for his guidance throughout my studies, for engaging in scientific discussions, for teaching me various skills, and for giving me the opportunity to participate in various scientific experiences. Without him, I really would not have started or finished my Ph.D. studies.

I would like to thank my colleague, MSc. Eni Tomović, with whom I had the opportunity to discuss most of the experiments as well as the joys and sorrows of everyday life. I would also like to thank Prof. MUDr. Ladislav Vyklický, DrSc., and the entire Department of Cellular Neurophysiology for their help, advice, and pleasant working environment, of which everyone is a part.

Many thanks to my friends and family for supporting me throughout my studies and for always bringing laughter and joy. A special thanks goes to my parents, Beatrix and Milan, who have always stood by me, tried to help me whenever they could, and whom I cannot thank enough for their endless support towards me. Finally, I would like to thank my fiancée, Emily, whose kindness, understanding, wisdom, and love have sustained me throughout my studies. She has stood by me through the difficult and joyful moments of my life, and without her, I could hardly have written this thesis.

Scientific acknowledgement

Here, I would like to acknowledge all scientific contributions to this doctoral thesis. I would like to thank the following people and institutions:

National Institute of Mental Health, Klecany, and MUDr. Filip Španiel, Ph.D., prof. MUDr. Jiří Horáček, Ph.D., FCMA, and Mgr. David Greguš for providing genomic DNA from schizophrenia patients and control subjects, and for estimating the BrainAGE index,

Genomics Core Facility, EMBL, Heidelberg, and RNDr. Vladimír Beneš, CSc. for performing Illumina next-generation sequencing,

RNDr. Kateřina Hirschfeldová, Ph.D., for her help with sequencing data analysis,

the laboratory of Sharon Swanger, Ph.D., for performing immunoprecipitation and Western blot analysis,

MSc. Eni Tomović, MSc. Bohdan Kysilov Ph.D., and Mgr. Miloslav Kořínek, Ph.D., for performing electrophysiological experiments,

Imaging Methods Core Facility in BIOCEV and Mgr. David Liebl, and Ph.D., RNDr. Lenka Koptašiková, for their assistance and help with electron microscopy experiments,

and Ing. Jiří Černý, Ph.D., for molecular modelling.

Abstrakt

Exprese a aktivita ionotropních glutamátových receptorů řídí přenos signálu na excitačních synapsích v centrálním nervovém systému. Hlavní skupinou jsou pro vápník propustné NMDA receptory, jež jsou důležité pro různé formy synaptické plasticity, klíčového mechanismu v procesu učení a tvorby paměti. NMDA receptory jsou heterotetramerní komplexy a jsou zastoupeny třemi typy podjednotek: GluN1, GluN2A-D a GluN3A-B. Každá podjednotka se skládá ze čtyř domén, přičemž intracelulární C-terminální doména tvoří až polovinu celé podjednotky NMDA receptoru (GluN2A/2B). Řada důkazů ukazuje na to, že hypofunkce NMDA receptorů hraje důležitou roli v patogenezi neuropsychiatrických poruch, včetně schizofrenie. Schizofrenie se vyznačuje vysokou mírou dědičnosti, avšak její genetické pozadí není zatím dostatečně dobře probádáno. Předchozí studie identifikovaly v lidském genomu několik jednotlivých lokusů, které přispívají k náchylnosti k onemocnění, včetně *GRIN* genů kódujících NMDA receptory.

Pomocí sekvenování jsem v kohortě pacientů postižených schizofrenií a kontrolních subjektů identifikovali a anotovali genetické varianty ve všech genech *GRIN*. Předložená disertační práce je zaměřena na funkční analýzu genetických variací v oblastech kódujících promotory a intracelulární domény receptorů. Genetické variace v promotorových oblastech jsou považovány za potenciální zdroj vzniku patofyziologie, díky jejich možným dopadům na expresi jednotlivých genů. C-koncová doména NMDA receptoru je pak klíčová pro transport receptoru, jeho internalizaci, recyklaci nebo degradaci a funguje jako centrum proteinových interakcí. Missense a nebo nonsense varianty v rámci její kódující sekvence proto mohou mít funkční následky.

Výsledky naší analýzy genetických variant v promotorových oblastech *GRIN* genů prokázaly, že několik variant a promotorových haplotypů je asociováno se schizofrenií, a že zároveň tyto varianty mohou měnit expresní aktivitu promotorů. Výsledky analýzy missense variant nalezených v rámci C-koncové domény podjednotky GluN2A ukazují, že varianty mohou způsobovat poruchy v přenosu receptorů, synaptickém ukotvení, proteinových interakcích nebo funkci kanálů. Zjistili jsme také, že několik s onemocněním asociovaných nonsense variant a variant posunu čtecího rámce v intracelulární doméně podjednotek GluN2A a GluN2B mění jejich povrchovou expresi nebo synaptickou lokalizaci, a také jsme ukázali význam proximální oblasti této domény pro funkci receptorového kanálu. Celkově tak naše výsledky ukazují význam obou oblastí pro expresi a lokalizaci NMDA receptoru, poskytují pohled na potenciální patofyziologické mechanismy, které mohou přispívat k variantnímu fenotypu, a podporují hypotézu hypofunkce NMDA receptorů pro vznik a vývoj schizofrenie.

Klíčová slova: NMDA receptor, schizofrenie, genetické variace, funkční analýza

Abstract

The expression and activity of ionotropic glutamate receptors control signal transduction at the excitatory synapses in the central nervous system. The major class are the calcium-permeable NMDA receptors that are fundamental for the various forms of synaptic plasticity, a key mechanism in the process of learning and memory formation. NMDA receptors are heterotetrameric and are represented by three types of subunits: GluN1, GluN2A-D, and GluN3A-B. Each subunit consists of four domains, with the intracellular C-terminal domain accounting for up to half of the entire NMDA receptor subunit (GluN2A/2B). A body of evidence indicates that the hypofunction of the NMDA receptor plays an important role in the pathogenesis of several neuropsychiatric disorders, including schizophrenia. Schizophrenia is characterised by a high degree of heritability, but its genetic background is not yet fully understood. Previous studies have identified in the human genome several individual loci that contribute to disease susceptibility, including the *GRIN* genes encoding NMDA receptors.

Using a sequencing approach, we identified and annotated genetic variations across all *GRIN* genes in a cohort of schizophrenia patients and control subjects. The submitted doctoral thesis focuses on the functional analysis of the genetic variation in the regions that encode the promoters and the intracellular domains of the receptor. Genetic variations in promoter regions are considered a potential source for the emergence of pathophysiology due to their possible effects on the extent of gene expression. The C-terminal domain of the NMDA receptor is crucial for receptor trafficking, internalisation, recycling, or degradation, and it acts as a hub for protein interactions. Therefore, missense and nonsesnse variants within its coding sequence may have functional consequences.

The results of our analysis of genetic variants within the *GRIN* promoter regions showed that several variants and promoter haplotypes are associated with schizophrenia, and these variants can also alter the expression activity of the entire promoter. Results from the analysis of missense variants within the C-terminal domain of the GluN2A subunit demonstrate that variants can cause impairments in receptor trafficking, synaptic anchoring, protein interactions, or channel function. We also found that several disease-associated nonsense and frame-shit variants in the intracellular domain of the GluN2A and GluN2B subunits alter their surface expression or synaptic localisation, and we showed the importance of the proximal region of the domain for receptor ion channel function. Taken together, our results demonstrate the importance of both regions for expression and localisation of the NMDA receptor, provide a view on the potential pathophysiological mechanisms that may contribute to the variant phenotype, and support the hypothesis of NMDA receptor hypofunction for the emergence and development of schizophrenia.

Key words: NMDA receptor, schizophrenia, genetic variations, functional analysis

Table of contents

List of abbreviations:

3' UTR	3' untranslated region
5' UTR	5' untranslated region
7-CKA	7-chlorokynurenic acid
ABD	Agonist binding domain
aCGH	Array comparative genomic hybridization
AML1	Acute myeloid leukemia 1 protein
AMPA	α-amino-3-hydroxy-5-methyl-4-isoxazolepropionic acid
AMPAR	AMPA receptor
ANOVA	Analysis of variance
APV / AP-5	5-phosphonovaleric acid
ARC	Activity-regulated cytoskeleton-associated protein
Arf	ADP-rybosilation factors
ATD	Amino-terminal domain
BDNF	Brain-derived neurotrophic factor
Brag	Brefeldin A-resistant Arf guanine nucleotide exchange factor
BRG1	Brahma-related gene 1
CADD	Combined annotation dependent depletion
Calcineurin	Ca2+/calmodulin-dependent protein phosphatase
CaM	Calmodulin
CaMK	Ca2+/calmodulin-dependent protein kinase
CASK	Calcium/calmodulin-dependent serine protein kinase
CBP	CREB binding protein
Cdk5	Cyclin-dependent kinase 5
CERST	Calcium Responsive Transactivator
CINAP	CASK-interacting nucleosome assembly protein
CIPP	Channel-interacting PDZ protein
CK2	Cdk casein kinase 2
CNS	Central nervous system
CNV	Copy-number variant
COUP-TF	Chicken ovalbumin upstream promoter transcription factor

CRE	cAMP response element
CREB	cAMP response element-binding protein
CSF	Cerebrospinal fluid
CtBP1	C-terminal binding protein 1
CTD	C-terminal domain
DAPK1	Death-associated protein kinase 1
DEP	Immunodepleted lysate
DMEM	Dulbecco's Modified Eagle's medium
EC_{50}	Half maximal effective concentration
ECS	Extracellular solution
eGFP	Enhanced green fluorescent protein
EGR1	Early growth response protein 1
ELP	Embryonic long terminal repeat-binding protein
EPD	Eukaryotic promoter database
EPSCs	Excitatory postsynaptic currents
eQTL	expression Quantitative trait loci
ER	Endoplasmic reticulum
ERK	Extracellular signal-regulated kinase
FES	First-episode schizophrenia
Flot1	Flotillin-1
FTZ-F1	Murine fushi tarazu factor 1
GABA	Gamma-aminobutyric acid
GAD1	Glutamate decarboxylase 1
GERP	Genomic evolutionary rate profiling
GFP	Green fluorescent protein
GIPC	GAIP Interacting Protein C-terminus
GluN2A-NMDARs	GluN2A-containing NMDARs
GluN2B-NMDARs	GluN2B-containing NMDARs
GM	Gray matter
GWAS	Genome-wide association study
HDAC1	Histone deacetylase complex 1

HIC2	Hypermethylated in cancer 2 protein
HIF-1α	Hypoxia-inducible factor-1α
ICS	Intracelullar solution
iGluR	Ionotropic glutamate receptor
IKKα	IκB kinase α
InDels	Insertion deletion variants
Inr	Initiator element
IP	Immunoprecipitate
KIF17	Kinesin-like protein 17
KLF9	Krueppel-like factor 9
LTD	Long-term depression
LTP	Long-term potentiation
MAF	Minor allele frequency
MAGI2	Membrane-associated guanylate kinase inverted 2
MAGUK	Membrane-associated guanylate kinases
MAZ	Myc-associated zinc finger protein
MAZ	Myc-associated zinc finger protein
MEF2C	Myocyte enhancer factor 2C
mEPSCs	Miniature excitatory postsynaptic currents
MIB2	Mind Bomb-2
MK-801	(5S,10R)-(+)-5-Methyl-10,11-dihydro-5H-dibenzo[a,d]cyclohepten-5,10-imine hydrogen maleate
MLPA	Multiplex ligation-dependent probe amplification
NFE	non-Finnish European
NF-I/CTF	Nuclear factor I / CCAAT box-binding transcription factor
NF-κB	Nuclear factor kappa-light-chain-enhancer of activated B cells
NGF	Nerve growth factor
NGS	Next-generation sequencing
NMDA	*N*-methyl-D-aspartate
NMDAR	NMDA receptor
NRF-1	Nuclear Respiratory Factor 1

OPD	o-Phenylenediamine dihydrochloride
PCP	Phencyclidine
PCR	Polymerase chain reaction
PI3K	Phosphatidylinositol 3-kinase
PKA	Protein kinase A
PKC	Protein kinase C
PNASS	Positive and Negative Symptom Scale
PP1	Protein phosphatase 1
PSD	Postsynaptic density
RACK1	Receptor for activated C kinase-1
RasGRF1	Ras-guanine-nucleotide-releasing factor
RE1/NRSE	RE1-like element / neuron-restrictive silencer element
REST/NRSF	RE1-Silencing Transcription factor / Neuron-restrictive silencer factor
RFN10	Ring finger protein 10
Rph3A	Rabphilin-3A
SEM	Standard error of the mean
SF-1	Steroidogenic factor 1
SGK1	Serum glucocorticoid kinase 1
SCH	Schizophrenia
T1W	T1-weighted
Tbr-1	T-box brain 1 transcription factor
TF	Transcription factor
TGN	Trans-Golgi network
TK	Thymidine kinase
TMD	Transmembrane domain
TrkB	Tropomyosin receptor kinase B
TSS	Transcription start site
WES	Whole exome sequencing
WM	White matter
WT	Wild-type
ZNF135	Zinc Finger Protein 135

1 Introduction

The function of excitatory synapses relies on the expression and activity of ionotropic glutamate receptors (iGluRs), including calcium-permeable NMDA receptors (NMDARs). These receptors play a critical role in neurotransmission and are involved in the mechanisms of synaptic plasticity, learning, and the formation of neural networks during development. Their dysfunction, leading to pathophysiological conditions, is often associated with neuropsychiatric disorders, including schizophrenia (SCH).

The prominent theory on the pathophysiological mechanism of SCH is the glutamatergic hypothesis, which is based on SCH animal models, pharmacology, or next-generation sequencing (NGS) data in case-control studies. Together, these studies also suggested impaired function of NMDARs and variants within their *GRIN* genes as risk factors for SCH.

In this doctoral thesis, we further investigate the relationship between NMDAR dysfunction and SCH. We performed NGS of all seven *GRIN* genes, in sixty-three first-episode schizophrenia (FES) patients and thirty-two control subjects. Using the obtained NGS dataset, we annotated both common and rare variants identified in both groups. Special attention was given to genetic variations within the less-explored promoter region of the *GRIN* genes, which could affect receptor expression, and to the C-terminal domain (CTD) of NMDARs, a region often associated with genetic variability in SCH.

The doctoral thesis aims to provide new information on how identified genetic variants within the promoter region of *GRIN* genes can influence gene expression. Additionally, the objective is to describe how disease-associated variants in the CTD affect protein function and identify the functional determinants of this domain. Finally, we believe that our studies will bring new insights into the relationship between the receptor and disease.

2 Literature review

2.1. NMDA receptors

NMDA receptors (NMDARs) are ligand-gated ion channels belonging to the family of ionotropic glutamate receptors. They are named after their specific agonist, *N*-methyl-D-aspartate (NMDA) and are predominantly found postsynaptically in 60 – 70 % of all synapses in the central nervous system (CNS) (Nadler, 2012; Vyklicky et al., 2014).

NMDARs consist of three subunits: GluN1, GluN2, and GluN3. The GluN1 subunit is encoded by one gene (*GRIN1*), which can generate eight variants due to alternative splicing. The GluN2 subunit is encoded by four genes (*GRIN2A, GRIN2B, GRIN2C,* and *GRIN2D*) that give rise to the four isoforms GluN2A, GluN2B, GluN2C, and GluN2D. The GluN3 subunit is encoded by two genes (*GRIN3A, and GRIN3B*), resulting in the GluN3A and GluN3B isoforms. A functional NMDA receptor comprises two obligatory GluN1 subunits and two subunits of different combinations of GluN2A–D and/or GluN3A–B. Receptor assembly takes place in the endoplasmic reticulum (ER) under tight quality control mechanisms (Traynelis et al., 2010; Hansen et al., 2021).

Each NMDAR subunit consists of four domains: an extracellular amino-terminal (ATD) and agonist binding domain (ABD), a transmembrane domain (TMD), and an intracellular C-terminal domain (CTD). ATD contains binding sites for allosteric modulators, bivalent cations, or extracellular proteins. The ABD is composed of two sections of amino acid chains, S1 and S2, which form the binding pocket for agonists. The extracellular domains are also *N*-glycosylated. The TMD consists of three transmembrane helices (M1, M3, and M4) and one transmembrane loop (M2) that forms the ion-selective pore of the receptor channel. The intracellular CTD contains almost no known structural motifs and belongs to a class of intrinsically disordered regions (Fig. 1). However, within the domain, there are short segments, often motifs of protein interactions, with a theoretically predictable arrangement (Traynelis et al., 2010; Hansen et al., 2021; Warnet et al., 2021).

During biogenesis, NMDAR assembles as a dimer of two dimers. The initial formation of dimers is mediated by the ATD of subunits. The subsequent formation of the tetramer is enabled by interactions between the ATD and ABD of the given dimers. After assembly and ER quality control, most receptors traffic through the somatic Glogli apparatus to be sorted into endosomes that are exocytosed to the surface membrane (Traynelis et al., 2010; Hansen et al., 2021).

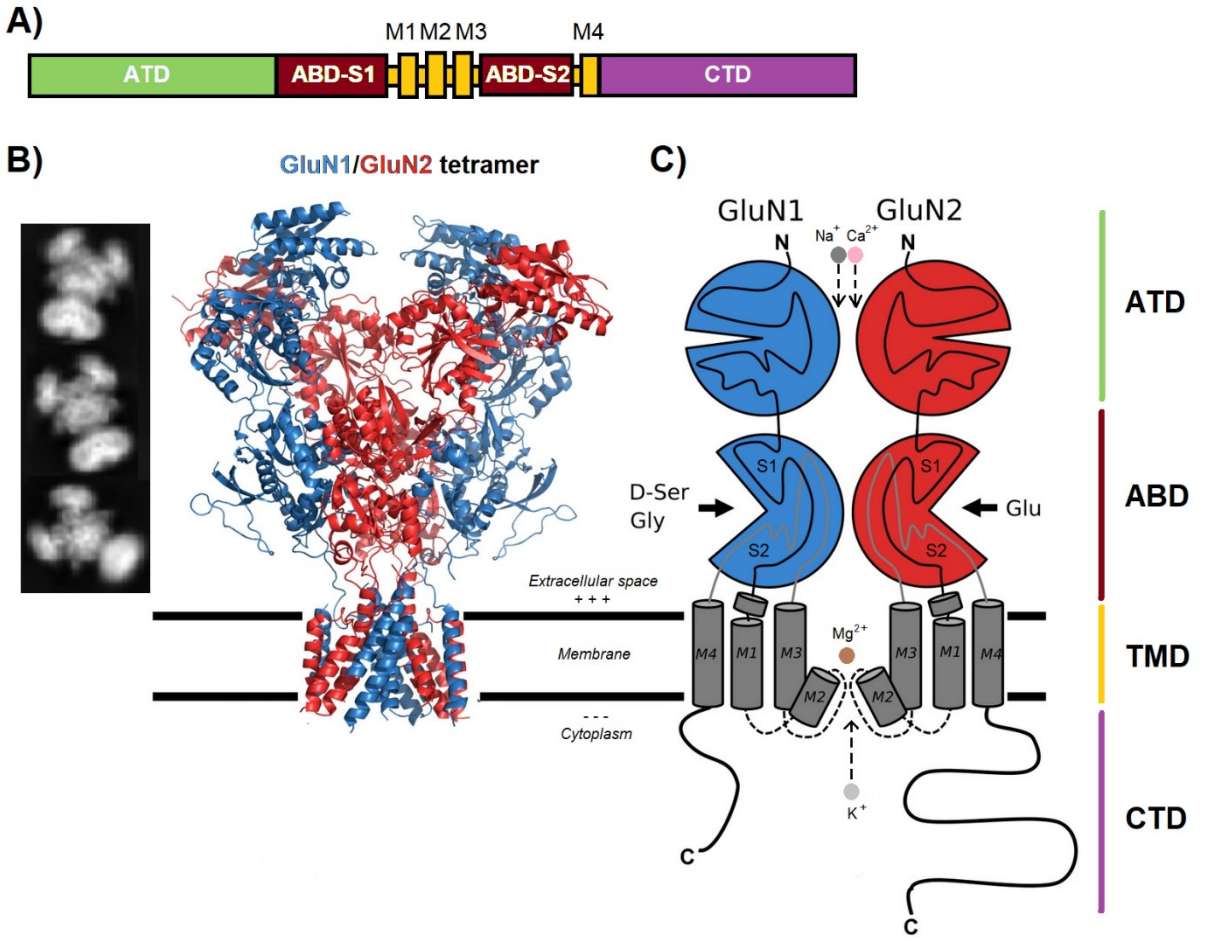

Fig. 1: **Structure and domain organization of the NMDAR**. **A)** A linear representation of a GluN subunit polypeptide chain. **B)** The GluN1/GluN2 NMDA receptor tetramer cryo-EM images and crystal structure (side view), the CTD is not present in the crystal structure and therefore not shown. **C)** The GluN1 and GluN2 subunit topologies with agonists and ions representations. Taken and modified from Chou et al., 2020, and Warnet et al., 2021.

The receptor is activated by the simultaneous binding of two co-agonists, glutamate to GluN2 subunits and glycine or D-serine to GluN3 and obligatory GluN1 subunits. Depolarization of the postsynaptic membrane is also necessary in the receptor containing GluN2 subunits because the ion channel pore of this receptor assembly is blocked by Mg^{2+} ions. After depolarization, mediated mainly by α-amino-3-hydroxy-5-methyl-4-isoxazolepropionic acid (AMPA) types of iGluRs, Mg^{2+} ions dissociate from the ion channel pore. After the activation of the NMDARs, K^+, Na^+, and Ca^{2+} ions are enabled to pass through the channel pore. The high permeability of receptors for Ca^{2+} ions occurs only in receptors consisting of GluN2 subunits, especially GluN2A and B (fig. 1C)) (Blanke & VanDongen, 2009; Paoletti, 2011; Hansen et al., 2021).

In addition to basal synaptic transmission, Ca^{2+} permeable NMDARs are involved in a variety of cellular mechanisms. Ca^{2+} ions act as a second messenger to activate several intracellular signaling pathways, leading to a number of cellular responses. NMDARs are therefore involved in the mechanisms of synaptic plasticity, long-term potentiation (LTP), and long-term

depression (LTD). They are fundamental to the mechanism of excitotoxicity, and their dysfunction leads to the development of many neurological (neurodevelopmental and neuropsychiatric) diseases (Lüscher & Malenka, 2012; Q. Zhou & Sheng, 2013; Lai et al., 2014).

NMDARs are abundantly expressed in the brain, although each subunit shows a different spatiotemporal pattern of expression. Among all NMDAR subunits, the GluN1 subunits have naturally the highest expression within all brain anatomical structures. The highest expression is found in the striatum, with an 87.5 % expression ratio of all NMDAR subunits. On the other hand, the lowest expression of the GluN1 subunit is described in the cerebral cortex, with a 67 % expression ratio of all NMDAR subunits, where also other subunits, such as GluN2A and GluN2B, are highly expressed. The GluN2A subunit was discovered to be highly expressed, primarily in the hippocampus but also in the striatum, midbrain, cerebellum, and cerebral cortex, with relatively lower expression in the hypothalamus and olfactory bulb. The GluN2B subunit has higher expression in the cerebral cortex, striatum, hippocampus, and olfactory bulb, while lower expression was described for the cerebellum or hypothalamus. The highest expression of the GluN2C subunit is found in the cerebellum, and oppositely, the lowest is found in the midbrain, and hypothalamus. Conversely, the highest expression of the GluN2D subunit is in the hypothalamus and midbrain with low expression in the cerebellum or cerebral cortex. The GluN3A subunit is highly expressed in the hypothalamus and midbrain, and it is weakly expressed in the hippocampus. Finally, the highest levels of GluN3B subunits are present in the hippocampus, cerebellar cortex, or corpus callosum, while low expression is described for the cerebral cortex or midbrain (Akazawa et al., 1994; Goebel & Poosch, 1999; Andersson et al., 2001).

The expression of NMDARs subunits is also subjected to the development of the CNS when GluN2B and GluN2D subunits are highly expressed during the prenatal period, while expression of GluN2A and GluN2C is noticeable around delivery. Further, expression of GluN2B and GluN2C subunits is highly decreased during the postnatal period, while expression of GluN2A and GluN2D rises until adulthood. These observations point to the important developmental switch for GluN2A and GluN2B subunits (Monyer et al., 1994). Similar developmental switches can be observed for the GluN3A and GluN3B subunits. While GluN3A subunit expression rises until eight postnatal days and subsequently declines until adulthood, expression of the GluN3B subunit increases during development until adulthood (Wong et al., 2002; Fukaya et al., 2005).

2.1.1. Regulation of transcription: Promoters and 5’ untranslated regions of *GRIN* genes

NMDAR protein expression is highly regulated at the gene level. As with other genes, the promoter and 5’ untranslated (5' UTR) regions are critical for gene expression, allowing the binding of polymerase and a wide range of transcription factors (TFs).

2.1.1.1. GRIN1

Fig. 2: **Schematic diagram of the promoter and 5’ UTR region of the *GRIN1 gene***. The promoter is shown as a thin line; the 5’ UTR exon sequence is represented by an open bar; a blackened bar designates the protein coding domains; TSSs and ATG are marked by arrows; regulatory elements and binding sites for transcription factors are labelled by name (above), coordinates (bellow, minus numbers indicate the upstream position relative to the start codon ATG), and letters inside indicate species origin (R = rat, H = human, C = conserved for rat, human, and mouse)

In the rat *GRIN1* promoter, two transcription start sites (TSSs) were identified at -276[1] bp and -238 bp relative to the ATG start codon[2]. The minimal promoter region essential for *GRIN1* gene expression, although with relatively low activity, was defined within the -356 bp region. Expanding the sequence to -3000 bp resulted in approximately a twofold increase in *GRIN1* expression. The 5’ UTR of the *GRIN1* gene (exon1) contains binding sites for transcription factors AP2 (-119 bp to -111 bp), SP1 and SP4 (-77 bp to -72 bp; homologous motif for mouse, rat, and human genes) and a RE1-like element / neuron-restrictive silencer element (RE1/NRSE) (-150 bp to -134 bp). RE1/NRSE silencers control expression in a neuronal-specific manner. The silencer element binds RE1-Silencing Transcription factor / Neuron-restrictive silencer factor (REST/NRSF) to block the expression of the *GRIN1* gene in non-neuronal cells. On the other hand, REST/NRSF is downregulated in neuronal cells, allowing high expression of the *GRIN1* gene. Although the absence of REST/NRSF is necessary, it is not fully sufficient for *GRIN1* expression in neuronal cells (Bai & Kusiak, 1993, 1995; Bai et al., 1998; Okamoto et al., 1999; Bai et al., 2003).

GC-box is located in proximity to TSSs in the upstream promoter region. GC-box controls gene expression during neuronal differentiation, and it is recognised by SP1, 3, and 4 as well as

[1] *The minus indicates the upstream and plus downstream positions from the dedicated coordinate*
[2] *The coordinates of regulatory elements for the promoter and 5’ UTR of the GRIN1 gene are relative to the start codon ATG*

by myc-associated zinc finger protein (MAZ) transcription factors, which enhance promoter activity (Bai & Kusiak, 1993; A. Liu et al., 2001; Okamoto et al., 2002). Within the human *GRIN1* promoter, two other putative binding sites for SP1 were identified (-387 bp to -381 bp and -1193 bp to -1187 bp) (Zimmer et al., 1995). Furthermore, a conserved SP binding site was described in rat, mouse, and human *GRIN1* promoters (-480 bp to -473 bp), which serves to bind SP4 factor and subsequently upregulate transcription of the gene in an activity-dependent manner (Priya et al., 2013).

More upstream in the rat *GRIN1* promoter region, there are two CAAT-boxes, putative binding sites for Nuclear factor I / CCAAT box-binding transcription factor (NF-I/CTF) (-897 bp to -891 bp and -2047 bp to -2042 bp) (Bai & Kusiak, 1993). Within the human *GRIN1* promoter is located also nonpalindromic T-box element (-1020 bp to -1014 bp), recognised by the T-box brain 1 transcription factor (Tbr-1), which further binds calcium/calmodulin-dependent serine protein kinase (CASK). Binding of the Tbr-1/CASK complex to the T-box element results likely in upregulation of the *GRIN1* gene (T.-F. Wang et al., 2004).

Additionally, in the rat *GRIN1* promoter, there are two localised AP2 binding sites (-1415 bp to -1407 bp and -1529 bp to -1522 bp) and one distal AP1 binding site (-2877 bp to -2872 bp). In the distal promoter region is localised cAMP response element (CRE) (-1829 bp to -1823 bp). Cre elements bind to cAMP response element-binding protein (CREB), a transcription factor that is highly expressed in glutamatergic and dopaminergic neurons and regulates the expression of many neuron-specific genes. The majority of promoters are characterised by the presence of conserved consensus sequences, such as the TATA or CAAT box, for assembly of the transcription machinery and initiation of transcription. However, there was not found any TATA or CAAT box in proximity to TSSs (Bai & Kusiak, 1993), although one putative TATA box is located from 623 bp to 630 bp upstream from the start codon within the human *GRIN1* promoter (Zimmer et al., 1995).

The activity of the *GRIN1* promoter is enhanced by nerve growth factor (NGF) by 3–4 fold. Responsive elements for NGF reside in the proximal region around the GC-box. Proposed signalling pathways for NGF upregulation of the *GRIN1* promoter include Ras/extracellular signal-regulated kinase (ERK) and phosphatidylinositol 3-kinase (PI3K) with its downstream target serum glucocorticoid kinase 1 (SGK1; in an NF-κB-independent manner), and also suggest SP1 transcription factor as a substrate for NGF-activated ERK (Bai & Kusiak, 1997; A. Liu et al., 2001; Tai et al., 2009). SP1 additionally interacts with myocyte enhancer factor 2C (MEF2C), which binds a sequence between -805 bp and -796 bp (identified for the rat *GRIN1* promoter) and enhances the activity of the *GRIN1* promoter. However, while SP1 is critical for the regulation of promoter activity by NGF, MEF2C acts more as an enhancer

(Krainc et al., 1998). The distal area of the promoter (-3295 bp to -3285 bp) also contains a putative Nuclear factor kappa-light-chain-enhancer of activated B cells (NF-κB) binding site that preferentially binds SP transcription factors 1, 3, and 4. While binding of SP1 to the site upregulates *GRIN1* gene expression in differentiated neurons, binding of the SP3 factor upregulates its expression in undifferentiated cells (A. Liu et al., 2004).

GRIN1 expression is also regulated by the binding of hypoxia-inducible factor-1α (HIF-1α) to its element (-749 bp to -482 bp, rat *GRIN1* promoter), and it is positively regulated by neuronal activity through the transcription factor Nuclear Respiratory Factor 1 (NRF-1) via an atypical NRF-1 binding site containing a GCA core located in proximity to TSS (-366 bp to -331 bp, conserved motif for rat, human, and mouse) (Yeh et al., 2008; Dhar & Wong-Riley, 2009).

Within the human *GRIN1* 5' UTR and promoter region, other putative transcription factor binding sites have also been described. Specifically, REST (-227 bp to -200 bp), early growth response protein 1 (EGR1) (-390 bp to -376 bp and -1422 bp to -1409 bp), CREB1 (-685 bp to -673 bp), Hypermethylated in cancer 2 protein (HIC2) (-650 bp to -642), Myc-associated zinc finger protein (MAZ) (-1305 bp to -1295 bp), Krueppel-like factor 9 (KLF9) (-1610 bp to -1595), Zinc finger protein 135 (ZNF135) (-1756 bp to -1742 bp), and REB1 (-2107 bp to -2087). Additionally, it was shown that regions between -337 bp to -159 bp and -704 to -556 bp in the human *GRIN1* gene are responsible for inhibition of transcription. On the other hand, the region from -556 to -337 bp is involved in the upregulation of gene expression. It's also suggested that the region between -1703 bp and -1539 bp upregulates, while the region between -1843 bp to -1703 bp downregulates gene expression (Y. Liu et al., 2022).

2.1.1.2. GRIN2A

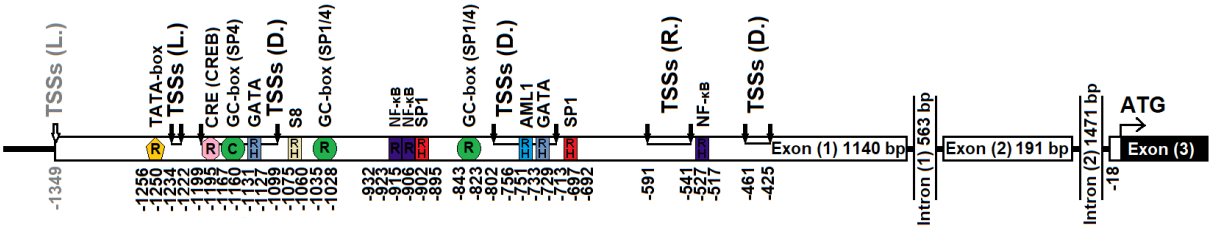

Fig. 3: **Schematic diagram of the promoter and the 5' UTR region of the *GRIN2A* gene**. The promoter is shown as a thin line; the 5' UTR exons sequence is represented by an open bar; a blackened bar designates the protein coding domains; two parallel vertical lines indicate introns; clusters of TSSs and ATG are marked by arrows; letters next to the TSSs indicate their origin (D. = Desai et al., 2002; R. = Richter et al., 2002; L. = A. Liu et al., 2003); regulatory elements and binding sites for transcription factors are labelled by name (above), coordinates (bellow, minus numbers indicate the upstream position relative to the start codon ATG (introns are not counted)), and letters inside indicate species origin (R = rat, H = human, C = conserved for rat, human, and mouse).

5' UTR of the *GRIN2A* rat gene includes an -18 bp upstream sequence from the ATG start codon (exon 3) interrupted by 1471 bp long intron 2. Upstream from intron 2 is located the 191

bp long second part of 5' UTR (exon 2), which is also interrupted by another 563 bp long intron 1. Upstream from intron 1 is an 1140 bp long sequence of untranslated Exon 1, with multiple clusters of TSSs. The exact positions of TSSs differ among studies, but all of them are located in exon 1 (Desai et al., 2002; Richter et al., 2002; A. Liu et al., 2003).

Analysis of the *GRIN2A* mouse promoter identified the sequence between -486 bp and -447 bp from ATG (introns are not counted)[3] sufficient to maintain neuronal preference for gene expression. Meanwhile, the sequence upstream of -1079 bp was critical for increasing *GRIN2A* expression in neurons, and the region between -1253 and -1180 bp was necessary for upregulation of the *GRIN2A* gene in mature neurons. This region contains a putative CRE binding site (-1195 bp), a potentially important site that allows neuronal upregulation of *GRIN2A* gene expression. Rather than silencing in non-neuronal cells, the selectivity for *GRIN2A* expression in neurons is driven by transcriptional activation. (Desai et al., 2002).

The core of the rat promoter is composed of exon 1, and it is positively regulated by SP transcription factors, whose overexpression results in increased activity of the *GRIN2A* promoter. However, the sequence upstream of exon 1 is required for complete activity of the promoter. Within the promoter core (and exon 1), three GC boxes were identified (-843 bp to -823 bp, -1039 bp to -1028 bp, and -1167 bp to -1160 bp) that bind the transcription factors SP1 and 4. The most distal GC-box serves specifically for the binding of SP4 factor, whose binding results in upregulation of gene transcription in an activity-dependent manner (Richter et al., 2002; A. Liu et al., 2003; Priya et al., 2013).

No typical TATA box (except for an atypical one at -1256 bp to -1250 bp) or CAAT box was localised within the rat or human *GRIN2A* promoter. However, several putative transcription factor binding sites were identified. Specifically, S8 (-1075 bp to -1060 bp), SP1 (-697 bp to -692 bp, -902 bp to -895 bp), GATA (-733 bp to -729 bp, -1131 bp to -1127 bp), Acute myeloid leukemia 1 protein (AML1) (-756 bp to -751 bp), and NF-κB (-527 bp to -517 bp). Two other identified NF-κB binding sites in the *GRIN2A* promoter (-915 bp to -906 bp, and -932 bp to -923 bp) are involved in the up-regulation of the *GRIN2A* gene by NF-κB. One possible pathway of action leads through the SGK1 activation of IκB kinase α (IKKα), which in turn activates NF-κB (Richter et al., 2002; A. Liu et al., 2003; Tai et al., 2009).

Comparison of the rat and human 5' UTR sequences revealed high homology (>84.5%) (Richter et al., 2002).

[3] *The coordinates of regulatory elements for the promoter and 5' UTR of the GRIN2A gene are relative to the start codon ATG (introns are not counted).*

2.1.1.3. *GRIN2B*

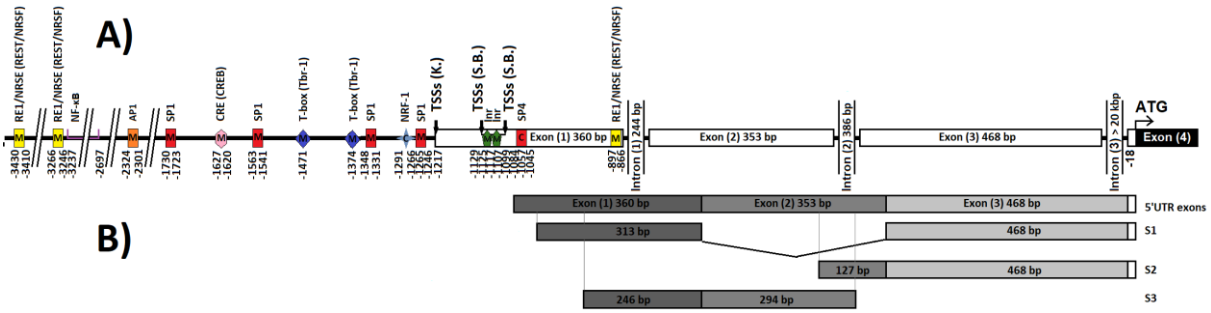

Fig. 4: **Schematic diagram of the promoter and the 5' UTR region of the *GRIN2B* gene**. **A**) The promoter is shown as a thin line; the 5' UTR exons sequence is represented by an open bar; a blackened bar designates the protein coding domains; two parallel vertical lines indicate introns; clusters of TSSs and ATG are marked by arrows; letters next to the TSSs indicate their origin (K. = Klein et al., 1998; S.B. = Sasner & Buonanno, 1996); regulatory elements and binding sites for transcription factors are labelled by name (above), coordinates (bellow, minus numbers indicate the upstream position relative to the start codon ATG (introns are not counted)), and letters inside indicate species origin (M = mouse, C = conserved for rat, human, and mouse). **B**) Schematic view of the alternatively spliced untranslated exons of the *GRIN2B* gene.

The 5' UTR of the *GRIN2B* mouse gene has three different compositions given by alternative splicing of untranslated exons. The start codon of the *GRIN2B* gene is located at exon 4 (18 bp downstream of the 5' end). Upstream from the start codon is the more than 20 kbp sequence of intron 3. Further upstream are located exon 3 (468 bp), intron 2 (386 bp), exon 2 (353 bp), intron 1 (244 bp), and exon 1 (360 bp). The most abundant splice variant retains 313 bp 3' – end part of exon 1, excluding exon 2 and retaining other exons (Fig. 4B S1). Minor splice variants compromise either 127 bp 3' – end part of exon 2 together with exon 3 (Fig. 4B S2) or 246 bp of 3' – end part of exon 1 together with 294 bp of 5' – end part of exon 2 (Fig 4B S3). The 5' UTR sequence of the mouse *GRIN2B* gene displays strong homology to the 5' UTR sequence of the rat and human *GRIN2B* gene (Klein et al., 1998).

The promoter of the *GRIN2B* mouse gene includes a major cluster of multiple TSSs located (within 45 bp) at the untranslated exon 1, which are responsible for most of the generated transcripts (Sasner & Buonanno, 1996). However, Klein et al., (1998) suggest the major TSS is located 88 bp upstream of the 5' – end major TSS found by Sasner and Buonanno (1996). In addition, TSSs were also identified in the untranslated exon 3 (in the splice variant lacking exon 2), and a cluster of TSSs was also located upstream of exon 1, although both sites are only responsible for the generation of less than 5% of all transcripts. No consensus TATA or CAAT boxes were located upstream of the major TSSs, but two initiator (Inr) elements were located downstream of the TSSs (-1125 bp to -1117 bp and -1107 bp to -1099 bp)[4].

[4] The *coordinates of regulatory elements for the promoter and 5' UTR of the GRIN2B gene are relative to the start codon ATG (introns are not counted)*

No evidence was found for the use of different TSSs during development or in specific brain structures. A region of 805 bp (-1679 bp to -838 bp) appears to be crucial for selective transcription of the *GRIN2B* gene in brain tissue. Interestingly, when the sequence of 805 bp was extended to include sequences of the 1st and 2nd introns and the 2nd and 3rd exons, promoter activity dramatically dropped, suggesting the presence of a suppressor element within this sequence. The sequences encompassing the 1st and 2nd introns and the 2nd and 3rd exons may therefore be important in regulating the developmental profile and developmental switch of the GluN2B subunit (Sasner & Buonanno, 1996).

Analysis of the 1st untranslated exon reveals a putative element RE1/NRSE, at the 3' – end part of the exon, which is intended to bind the transcriptional suppressor REST/NRSF (-879 bp to -866 bp), but the site does not appear to be functional or to confer neural-selective expression (Sasner & Buonanno, 1996). However, five other putative RE1/NRSE motifs were localised between -3958 bp and -2624 bp. Among them, two RE1/NRSE motifs at positions from -3266 bp to -3246 bp and -3430 bp to -3410 bp display functional importance. Mutations in both elements increased promoter activity, and overexpression of NRSF together with luciferase reporter promoter constructs showed decreased promoter activity. (Qiang et al., 2005).

Upstream from the 1st untranslated exon of the *GRIN2B* gene, four binding sites for the transcription factor SP1 (-1246 bp to -1265 bp, -1348 bp to -1331 bp, -1563 bp to -1541 bp, -1730 bp to -1723 bp) and a binding site for the CREB (-1627 bp to -1620 bp) were also found, which may link the gene regulation to Ca^{2+} signalling pathways (Klein et al., 1998). Later, it was observed that mutations in the CREB binding site of the *GRIN2B* promoter significantly reduced the transcription of the gene (Rani et al., 2005).

It was also shown that Calcium Responsive Transactivator (CERST), brahma-related gene 1 (BRG1, binds SP1), CREB binding protein (CBP), and histone deacetylase complex 1 (HDAC1) form a complex that binds to the *GRIN2B* promoter. *GRIN2B* promoter activity is then upregulated in a neuronal activity-dependent and NMDAR-dependent manner by CREST. This was supported by the observation of the lack of neuronal activity-dependent upregulation of GluN2B expression in CREST-null neurons. Neuronal stimulation results in increased CBP recruitment and decreased HDAC1 recruitment. The proposed mechanism suggested a neuronal activity-dependent switch of complex from *GRIN2B* repressor to activator, where CREST plays a crucial role by linking SP1/BRG1 and CREB/CBP (Qiu & Ghosh, 2008).

Two T-box elements within the mouse *GRIN2B* gene are located at positions -1471 bp and -1374 bp relative to TSS (conserved T-boxes for the rat and human *GRIN2B* genes). The elements are recognised by transcription factor Tbr-1, which forms a complex with CASK and

CASK-interacting nucleosome assembly protein (CINAP). The Tbr-1/CASK/CINAP protein complex upregulates the promoter activity of the *GRIN2B* gene. Mutation of the CASK protein results in decreased *GRIN2B* promoter activity by disrupting the protein complex, whereas overexpression of Tbr-1 or CASK results in increased *GRIN2B* promoter activity. In contrast, knock-down of Tbr-1 or CINAP decreased promoter activity of the *GRIN2B* gene. Additionally, NMDA stimulation of neurons reduces CINAP protein levels via the proteasomal degradation pathway and results in decreased promoter activity of the *GRIN2B* gene and a decreased protein level of the GluN2B subunit. The results thus reveal an interesting synaptic regulatory pathway of the GluN2B subunit via the Tbr-1/CASK/CINAP protein complex (T.-F. Wang et al., 2004; G.-S. Wang et al., 2004; Huang & Hsueh, 2009).

Within the promoter of the *GRIN2B* gene was also located a functional AP1 binding site (-2324 to -2301 bp), whose mutation results in significantly reduced promoter activity, suggesting that AP1, through binding to the promoter, upregulates the *GRIN2B* gene (Qiang & Ticku, 2005). Similarly to the *GRIN1* gene*,* the *GRIN2B* gene is also positively regulated in a neuronal activity-dependent manner by NRF-1, which binds an atypical NRF-1 binding site containing a GCA core located in proximity to TSS (-1291 bp to -1266 bp, conserved for rat, human, and mouse) (Dhar & Wong-Riley, 2009). Promoter activity of the *GRIN2B* gene is also increased by NF-κB, which is activated by SGK1 through the IKKα. The NF-κB binding site(s) is located between -3237 bp and -2697 bp (Tai et al., 2009). Additionally, the *GRIN2B* gene is also upregulated by transcription factor SP4 via a homologous SP binding motif, present in mouse, rat, and human genes at -1057 bp to -1045 bp (Priya et al., 2013).

2.1.1.4. GRIN2C

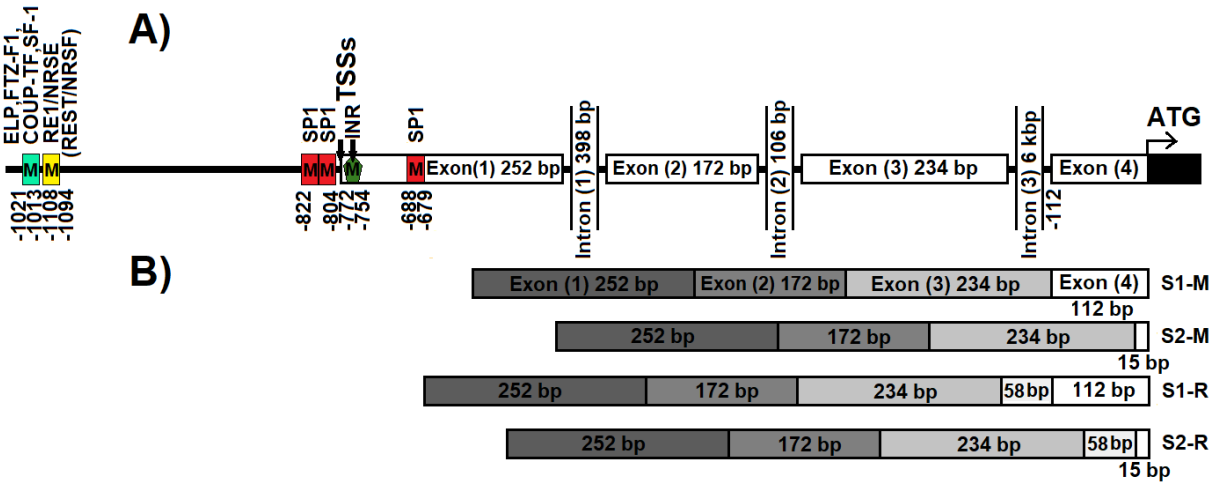

Fig. 5: **Schematic diagram of the proximal promoter and the 5' UTR region of the *GRIN2C* gene**. **A**) The promoter is shown as a thin line; the 5' UTR exons sequence is represented by an open bar; a blackened bar designates the protein coding domains; two parallel vertical lines indicate introns; TSSs and ATG are marked by arrows; regulatory elements and binding sites for transcription factors are labelled by name (above), coordinates (bellow, minus numbers indicate the upstream position relative to the start codon ATG (introns are not counted)) and letters inside indicate species origin (M = mouse). **B**) Schematic view of the alternatively spliced, untranslated exons of the *GRIN2C* gene.

The start codon of the *GRIN2C* rat gene is located within exon 4. The 5' UTR of the *GRIN2C* gene is composed of 112 bp of exon 4, followed upstream by intron 3 (approximately 6 kbp), exon 3 (234 bp), intron 2 (106 bp), exon 2 (172 bp), intron 1 (398 bp), and 252 bp of exon 1. Two TSSs were identified within the untranslated exon 1 at the -772 bp and -754 bp positions, with the TSS at the -754 bp position appearing to be of major importance. The 5' UTR of rat and mouse *GRINC2* genes is homologous. The composition of 5' UTR then depends on the alternative splicing, which differs between species. In mice, two splice variants of 5' UTR differ by 97 bp of the exon 4 (Fig. 5B S1-M, S2-M). In the rat, additional two splice variants were found due to the presence of an extra 58 bp long exon located between exons 3 and 4 (Fig. 5B S1-R, S2-R) (Suchanek et al., 1995; Nagasawa et al., 1996).

Within the promoter of the *GRIN2C* gene, an Inr element was identified at the position of a putative minor TSS in exon 1. Deletion of exon 1 results in increased promoter activity of the *GRIN2C* gene, indicating the presence of a transcriptional silencer within exon 1. The upstream sequence of major TSS lacks the CAAT box or TATA box. In the promoter sequence, several putative binding sites for TFs were located: RE1/NRSE (-1108 bp to -1094 bp), embryonic long terminal repeat-binding protein (ELP) (-1021 bp to -1013 bp), and two (or possibly one combined) SP1 binding site(s) (-813 bp to -804 bp and -822 bp to -817). Functional analysis of the mentioned SP1 binding sites confirmed SP1 binding but showed minimal regulatory impact on transcriptional regulation of the *GRIN2C* gene. The ELP binding

motif then overlaps with binding motifs for transcription factors such as murine fushi tarazu factor 1 (FTZ-F1), chicken ovalbumin upstream promoter transcription factor (COUP-TF) and steroidogenic factor 1 (SF-1). Functional analysis then suggested SF-1 as a positive modulator for transcription of the *GRIN2C* gene (Suchanek et al., 1995; Nagasawa et al., 1996; Pieri et al., 1999).

Within exon 1, there was located also a putative binding site for transcription factor EGR1 (-692 bp to -684 bp) and two other overlapping putative binding sites for SP1 (-688 bp to -683 bp and -684 bp to -679 bp). An additional putative binding site for SP1 was also located in the middle of intron 1 (Nagasawa et al., 1996).

Within the granular cells, the GluN2C subunit is upregulated by Brain-derived neurotrophic factor (BDNF) via the Tropomyosin receptor kinase B (TrkB) - ERK 1/2 cascade. However, strong depolarization results in Ca^{2+} entry through voltage-sensitive Ca^{2+} channels, leading to an increase in intracellular Ca^{2+} activated Ca^{2+}/calmodulin-dependent protein phosphatase (Calcineurin), which in turn blocks GluN2C upregulation. Interestingly, depolarization also results in upregulation of BDNF via Ca2+/calmodulin-dependent protein kinase (CaMK), suggesting a convergent mechanism of the BDNF and Ca^{2+} signaling cascades for regulation of the GluN2C subunit (Suzuki et al., 2005).

Additionally, expression of GluN2C subunits is increased by transcription factor neuregulin-β via synaptic activity of NMDARs (Ozaki et al., 1997).

2.1.1.1.5 GRIN2D, GRIN3A, GRIN3B

According to my knowledge, neither the characterisation of 5’ UTRs and/or promoters of the genes nor their transcriptional regulation have been described to the current date.

2.1.2. Intracellular domain of GluN2A/2B subunit

The CTD of NMDAR is the domain with the lowest homology between receptor subunits. While the GluN1 subunit has only 50 amino acids long CTD, the CTD of GluN2B possesses 660 amino acids. The CTD of GluN2A and GluN2B subunits is even their largest domain (Fig. 6). The CTD of the GluN2A subunit is additionally subject to alternative splicing, based on which two isoforms arise. The short isoform is primate-specific, where 186 amino acids are excised from the full GluN2A CTD and replaced by a new 23 amino acids. The CTD of NMDAR binds to several scaffold, adaptor, cytoskeletal, and other proteins and plays an important role in intracellular signalling. During the evolution, the CTD of GluN2 subunits several times increased in length and evolved to be a flexible hub, organising postsynaptic signaling. This evolution may contribute to species differences in behaviour, particularly in cognitive function (Ryan et al., 2008, 2013; Warming et al., 2019).

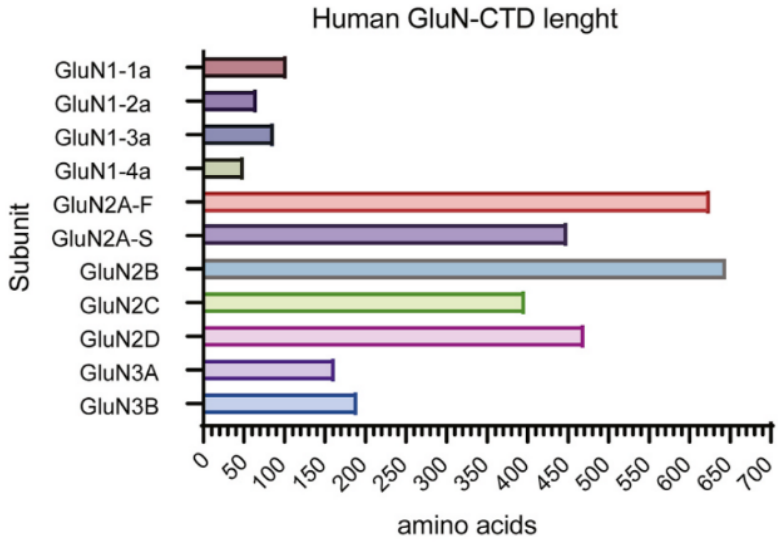

Fig. 6: **The histogram of NMDAR subunit CTD length**. Each bar demonstrates NMDAR subunit CTD length expressed as the number of amino acids. GluN1 subunits have four different variants based on alternative splicing of their CTD. GluN2A-F stands for the full CTD domain of the subunit, and GluN2A-S refers to the short primate-specific isoform of the subunit CTD. Taken and modified from Ishchenko et al., 2021.

The heterotetrameric NMDAR complex is formed in the ER from two obligatory GluN1 subunits and two various GluN2 or GluN3 subunits. GluN2 subunits contain an ER retention motif in the TMD (M3), which is masked after receptor assembly for the subsequent receptor exit from the ER. Formation of the complex is a CTD-independent process, and only fully assembled and properly folded complexes reach the cell surface. However, within the CTD of GluN2A and GluN2B subunits was found the ER releasing motif (hGluN2A $HLFY_{839-842}$, hGluN2B $HLFY_{840-843}$), located directly after the TMD (M4), that is necessary for the assembled complex to exit from the ER. The first three amino acids of the motif are crucial for surface expression of functional NMDA receptors, and at the same time they enable the receptors to overcome ER retention motifs found within the CTD of GluN1 subunits (Hawkins et al., 2004; W. Yang et al., 2007; Horak et al., 2008). Additionally, an ER retention motif was recently discovered within the CTD of the GluN2A subunit ($KKK_{879-881}$) (Q.-Q. Li et al., 2022b).

At the intermediate compartment (between ER and Golgi) and Trans-Golgi network (TGN), the multiprotein complex NMDAR-Membrane-associated guanylate kinases (MAGUK)-exocyst is formed (via binding of MAGUK member SAP102 to member of the exocyst complex Sec8). The complex is responsible for receptor trafficking, and disruption of the interactions within the complex disturbs correct NMDAR surface delivery (Sans et al., 2003; Standley et al., 2012). The complex also includes protein mPins, which function in the formation of the NMDAR – MAGUK complex and enhance the trafficking of MAGUKs (e.g. PSD-95 or SAP102) and NMDARs to synapses (Sans et al., 2005). For the transport of multiprotein complexes to the dendritic spines, kinesin motor proteins are required. In the case of GluN2B subunit-containing vesicles, transport is controlled by the Kinesin-like protein 17 (KIF17), and downregulation of KIF17 significantly impairs GluN2B surface expression and its synaptic localisation. KIF17 interacts with the auxiliary protein mLin10, a member of a tripartite protein complex that includes the proteins mLin-2 (CASK, member of the MAGUK family) and mLin-7, which bind the GluN2B subunit. CaMKII-dependent phosphorylation of KIF17 disrupts interaction with mLin10, thereby releasing NDMARs from its microtubule-based transport (Guillaud et al., 2003, 2008; Setou et al., 2000). NMDAR trafficking to the synapse may also be mediated by other kinesin motor proteins, like KIF5b, KIF3b, or KIF1A, which interact further with MAGUK proteins (Wu et al., 2016; R. Lin et al., 2019; Alsabban et al., 2020). Additionally, NMDARs can be delivered to the synapse via a non-conventional pathway, including a specialized ER sub-compartment and dendritic Golgi outposts (bypassing the somatic Golgi). This pathway also requires KIF17 and postsynaptic adaptor proteins from the MAGUK family, mLin2, and SAP97 (Jeyifous et al., 2009).

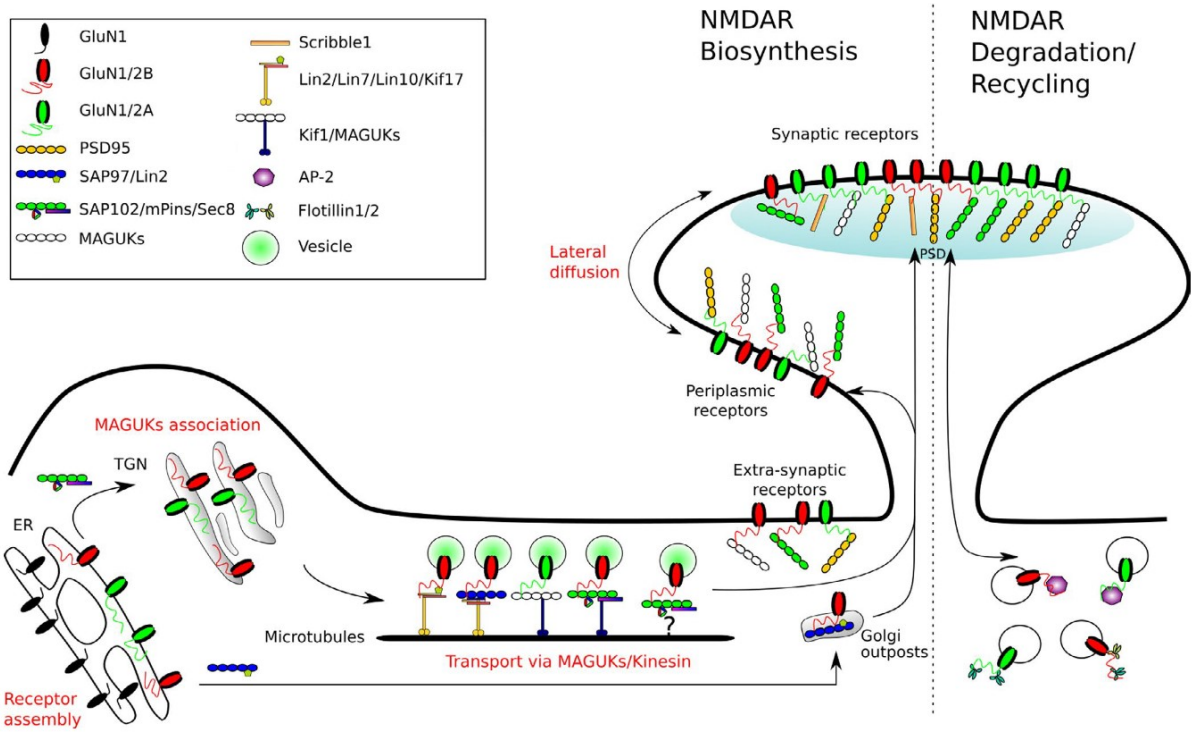

Fig. 7: **Schematic representation of NMDAR trafficking**. NMDARs can leave the endoplasmic reticulum (ER) when GluN1 and GluN2/3 subunits have assembled. Once the NMDAR is associated with MAGUKs, it is further carried to the trans-Golgi network (TGN), from where it is then delivered to the synapse via microtubules and kinesin interactions. Additionally, NMDAR can travel directly to the postsynaptic density through its interaction with SAP97/Lin2, resulting in its transport to Golgi outposts close to the synapse. By interacting with scaffolding proteins, particularly PSD-95, the CTD of GluN1 and GluN2/3 subunits anchors in the postsynaptic density. The receptor's lateral mobility enables it to move out of the postsynaptic density and into the pool of extrasynaptic receptors. Endocytosis can reduce surface expression via clathrin-dependent pathways and via interactions with AP-2 and flotillin. Taken and modified from Warnet et al., 2021.

The GluN2A and GluN2B subunits contain a membrane-proximal endocytic motif within the CTD (hGluN2A $YWKL_{842-845}$, hGluN2B $YWQF_{843-846}$) that mediates endocytosis and targets internalised receptors along a degradative pathway to late endosomes. Furthermore, a distal endocytic motif, discovered in the CTD of GluN2B subunits (hGluN2B $YEKL_{1474-1477}$), preferentially promotes recycling of internalised NMDARs through the early and recycling endosome. On the other hand, an analogous motif in the GluN2A subunit does not mediate endocytosis, but a dileucine motif ($LL_{1319–1320}$) was discovered to regulate receptor internalisation. The endocytic pathway of GluN2A CTD-mediated internalisation preferentially leads through the early to late endosome. In general, internalisation is mostly mediated by AP-2 binding to endocytic motifs, followed by clathrin-mediated endocytosis. In addition, the endocytic motifs of both subunits can be bound to other adaptor complexes, such as AP-1, AP-3, and AP-4. GluN2B subunits have a higher rate of internalisation than GluN2A subunits and have a clear preference for the recycling pathway. The rate of internalisation is also affected by the binding of MAGUKs within the CTD of GluN2A and B subunits, which causes inhibition of endocytosis and therefore an increase in surface expression (Roche et al., 2001; Lavezzari et al., 2003, 2004; Scott et al., 2004). Additionally, the lipid raft-associated protein flotillin-1 (Flot1) interacts with CTDs of both subunits, and promoting clathrin-independent internalisation of NMDARs, an additive mechanism to AP-2 clathrin-mediated endocytosis (Glebov et al., 2006; Swanwick et al., 2009).

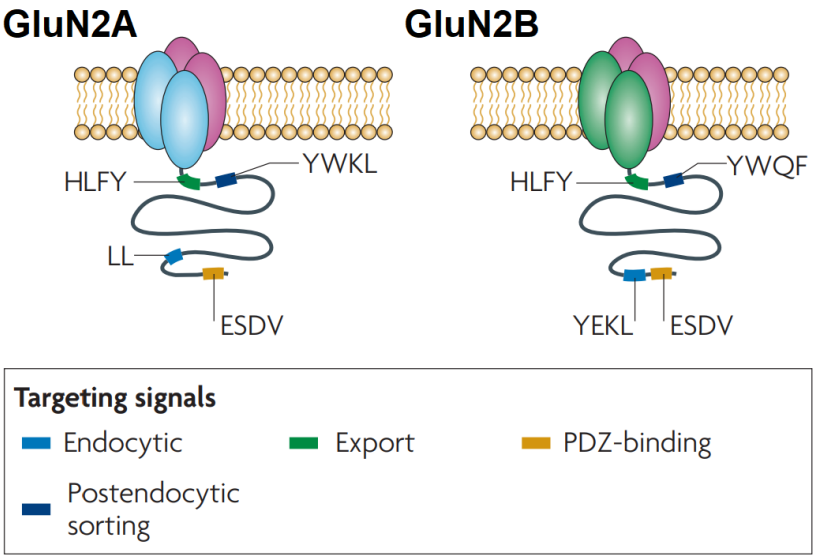

Fig. 8: **NMDAR subunit targeting signals**. An ER export signal (HLFY) found in the GluN2A/2B subunits facilitates receptor transport to the cell surface. NMDARs are directed to late endosomes for degradation by membrane-proximal signals in the CTD of the GluN2A (YWKL) and GluN2B (YWQF) subunits. Clathrin-dependent endocytosis is initiated by internalisation signals in GluN2A (LL) and GluN2B (YEKL) subunits that bind the clathrin adaptor protein AP-2. The interaction of NMDARs with scaffolding proteins (MAGUK family) is mediated by the PDZ recognition motif (ESDV) in GluN2A/2B CTD, which facilitates receptor trafficking to the cell surface.Taken and modified from Lau & Zukin, 2007.

While mice expressing the GluN2B subunit with truncated CTD (859*) die perinatally, mice expressing the truncated GluN2A subunit (863*) are viable, but they exhibit impaired synaptic plasticity. In both subunits, truncation of CTD does not interfere with the formation of functional receptor channels. The mRNA expression level of GluN2A and B subunits with truncated CTD in gene-targeted mice appeared to not differ from wild-type (WT) mice. However, mice expressing truncated GluN2B subunits show a decreased protein expression level, which was not observed in the altered GluN2A subunit (Sprengel et al., 1998). Nevertheless, the decrease in protein expression was not shown in another study with mice expressing the GluN2B subunit with truncated CTD (998*), perhaps because of the different position of truncation (Mori et al., 1998). Mice expressing a truncated CTD of GluN2A or B subunits then exhibited disturbed clustering and synaptic localisation of NMDARs. Neurons expressing truncated GluN2A subunits exhibited strongly reduced synaptic enrichment and NMDAR-mediated excitatory postsynaptic currents (EPSCs). Slower rise and decay times of NMDAR EPSCs, together with the delayed onset of the NMDA component, also indicate that receptors appeared to localise more distantly from the synapse (Steigerwald et al., 2000; Rossi et al., 2002; Köhr et al., 2003). Similarly, in mice with truncated CTD of the GluN2B subunit, neurons showed a smaller number and size of NMDAR clusters, which were less co-localised with synaptic markers, and their NMDAR-mediated EPSPs were reduced (Mohrmann et al., 2002; Mori et al., 1998). This

all strongly suggests that the CTD of GluN2A and B subunits is crucial for the precise synaptic localisation of NMDARs.

The CTD of GluN2A and B subunits also affect the channel properties of NMDARs, when mice expressing the receptor with truncated CTD has significantly decreased the channel open probability of NDMARs (Mohrmann et al., 2002; Rossi et al., 2002). Maki et al. proposed that channel kinetic is altered due to both, longer openings and desensitized intervals (Maki et al., 2012). While Punnakkal et al. suggest the faster decay time as the main contributor to the altered channel open probability (Punnakkal et al., 2012). The first 100 amino acids of the CTD, together with changes in posttranslational modifications, are then critical for these changes. Furthermore, swapping of CTDs between GluN2A and B subunits does not alter channel properties, indicating that the electrophysical properties of NMDARs are independent of the subtype-specific CTD (Maki et al., 2012; Punnakkal et al., 2012). Truncation of GluN2A CTD also had another effect on ion channel properties when truncated receptors had increased glycine potentiation (Puddifoot et al., 2009). In addition, it was shown that CTD of GluN2A subunits can affect the desensitization of receptor ion channels via calcineurin-mediated dephosphorylation of serins 900 and 929, which increases desensitization and, in turn, reduces channel open probability and thus reduces synaptic NMDAR currents. In contrast, protein protein kinase A (PKA)-mediated phosphorylation of these residues has the opposite effect (Krupp et al., 2002; Townsend et al., 2004; Maki et al., 2013). PKA phosphorylation of serine 1166 in the CTD of GluN2B subunits potentiates NMDAR signaling through increased activation and resensitization rates of the receptor (Aman et al., 2014; Murphy et al., 2014). The serines in CTD of GluN2A (S1291, S1312) and GluN2B (S1303 and S1323) can be additionally phosphorylated by protein kinase C (PKC), which leads to potentiation of the receptor (Liao et al., 2001; Jones & Leonard, 2005). Serine 1303 in the GluN2B subunit is phosphorylated as well by death-associated protein kinase 1 (DAPK1), which binds directly to CTD between 1292–1304 residues, and its phosphorylation causes an increase in channel conductance (Tu et al., 2010). GluN2A-mediated currents are also potentiated by phosphorylation at tyrosines 1105, 1267, 1325, and 1387 (Zheng et al., 1998; Taniguchi et al., 2009).

Interestingly, truncation of the CTD of GluN2 subunits significantly influences the activity of positive or negative allosteric modulators and their effects on ion-channel properties. The allosteric modulators are thus likely sensitive to intracellular ion levels, posttranslational modifications, or protein-protein interactions within CTD. For example, the neurosteriod pregnenolone sulphate (PS), a positive allosteric modulator for GluN2A/2B subunits, has subununit-specific effects after CTD deletion. Deletion of CTD in GluN2A leads to a changing

effect of PS on negative allosteric modulation, while in the case of GluN2B, there is only a reduction in PS positive allosteric modulator activity (Sapkota et al., 2019).

Regarding the behavioural effects, deletion of CTD in GluN2A and B subunits affects learning, emotion, motivation, and motor function. In addition, swapping CTD between subunits points to behaviour dependent on the CTD of a specific subunit. Differential functions of CTD are perhaps provided by distinct protein interaction patterns between subunits, where particularly interesting are the MAGUK proteins, which create subunit-specific protein complexes (Ryan et al., 2013). Additionally, mice with GluN2A subunits containing CTD from GluN2B subunits have enhanced NMDA-mediated toxicity, suggesting a stronger role of GluN2B CTD in cell death signaling (Martel et al., 2012).

Since the developmental switch occurs, the adult brain expresses more of the GluN2A subunit, which has a stronger contribution to LTP. Mice expressing GluN2A subunits with deleted CTD had deficient LTP signaling, because LTP was exclusively dependent on the presence of GluN2B subunits in synapses. This points to an important role for CTD in molecular mechanisms of learning and memory by regulating signaling pathways (Sprengel et al., 1998b; Rossi et al., 2002; Köhr et al., 2003).

The protein interactions within CTD are then crucial for synaptic localisation in terms of trafficking to synapses as well as for stabilization of receptors at synapses. Protein interactions specific to each subunit also affect the mobility of the receptor, which can be seen on less mobile receptors containing the GluN2A subunit compared to receptors with the GluN2B subunit. Recombinant GluN2A and GluN2B subunits with mutated or truncated evolutionary conserved PDZ binding motif ESDV (last four amino acids within CTD), which is the binding place for MAGUKs proteins, showed reduced delivery of recombinant receptors to synapses and impaired anchoring of cell-surface clusters at postsynaptic targets (Barria & Malinow, 2002; Prybylowski et al., 2005; Groc et al., 2006; Standley et al., 2012). MAGUK family proteins, including PSD-93, PSD-95, SAP97, or SAP102, have a differential affinity for GluN2 subunits and distinctive effects on receptor surface expression. Overexpression of PSD-93 and PSD-95, but not SAP97 and SAP102, enhanced surface expression of GluN2A and GluN2B containing NMDARs (Sans et al., 2000; Al-Hallaq et al., 2007; Cousins et al., 2008). PSD-95 and SAP102 have, except for the ESDV binding motif for their PDZ domain, other binding domains. PSD-95 binds to the CTD of the GluN2A subunit via an Src homology 3 domain (SH3)-binding motif PSDPYK (1382–1389) that associates with the SH3 domain of PSD-95. The CTD of the GluN2B subunit is bound to PSD-95 additionally by the sequence DLTDIYKE (1149–1157) and to SAP102 by the DD binding motif (1393–1394) (Cousins et al., 2009; Cousins & Stephenson, 2012; Chen et al., 2012).

In addition, the GluN2A subunit and PSD-95 interact with the dendritic spine-enriched protein Rabphilin-3A (Rph3A) to create a ternary complex that regulates NMDAR stabilization at postsynaptic membranes. Particularly, Rph3A is involved in the blocking of endocytosis and supports GluN2A synaptic retention at the synaptic membrane. Silencing Rph3A or perturbing its interaction with GluN2A subunits leads to a decrease in synaptic localisation, stability, and responses, together with suppressing the synaptic and extrasynaptic surface clustering of GluN2A-NMDARs (Stanic et al., 2015; L. Yang et al., 2023). On the other hand, C-terminal binding protein 1 (CtBP1), which also interacts with the CTD of the GluN2A subunit, decreases receptor surface expression (Cousins & Stephenson, 2019). Another scaffold protein interacting with GluN2A and, to a lesser extent, with GluN2B is IQGAP1. IQGAP1 coupling NMDARs with ERK1 and ERK2 signaling pathway. Mice lacking the IQGAP1 gene exhibited reduced surface expression of GluN2A, disturbed LTP, and impaired ERK signaling accompanied by a reduction in spine density in brain regions involved in learning, emotion, and motivation (Gao et al., 2011). On the other hand, the GluN2B subunit is coupled with ERK signaling pathways predominantly via the interaction of its CTD with Ca^{2+}/calmodulin-dependent Ras-guanine-nucleotide-releasing factor (RasGRF1) (Krapivinsky et al., 2003). Furthermore, the CTD of the GluN2A subunit also binds Ring finger protein 10 (RFN10), which acts as a synaptonuclear messenger. Activation of GluN2A-containing NMDARs (GluN2A-NMDARs) and induction of LTP result in translocation of calcium-activated RFN10 to the nucleus. LTP maintenance is then prevented by RNF10 silencing. (Dinamarca et al., 2016).

FRMPD2 is a scaffold protein that interacts with GluN2A subunit with higher affinity than with the GluN2B subunit PDZ binding motif. FRMPD2 is necessary for receptor stabilization at a synapse, and its disruption leads to a decreased level of synaptic NMDARs (Lu et al., 2018, 2019). Scaffold protein Scribble1, required for synaptogenesis and synaptic plasticity, binds to the PDZ binding motif as well and controls the number of NMDARs at the synapse. Scribble1 promotes recycling of internalised NMDARs containing the GluN2A and GluN2B subunits via interaction with AP-2 in a use-dependent manner (Piguel et al., 2014). On the GluN2A PDZ binding motif is bound the GAIP Interacting Protein C-terminus (GIPC), which associates with surface as well as internalised NMDA receptors. It is suggested that GIPC may be preferentially associated with the extrasynaptic pool of NMDARs and may play a role in their organization and trafficking (Yi et al., 2007). Other proteins that bind to the PDZ binding motifs of the CTD of both subunits and serve as scaffold proteins include membrane-associated guanylate kinase inverted 2 (MAGI2) or channel-interacting PDZ protein (CIPP). (Hirao et al., 1998; Kurschner et al., 1998).

Calcium-binding messenger protein calmodulin (CaM) interacts with GluN2A CTD between amino acids 875–1029 as a calcium-dependent binding partner through interaction with tryptophan 1014 (Bajaj et al., 2014). CaMKII is highly involved in synaptic plasticity and interacts with the CTD of both GluN2A and GluN2B subunits of NMDARs. CaMKII binds two regions in the GluN2B CTD and phosphorylates the GluN2B subunit at serine 1303 and thereby increases desensitization of the receptor. Region around serine 1303 binds except CAMKII also DAPK1, which mediates neuronal death through an extrasynaptic pool of GluN2B subunits. (Omkumar et al., 1996; Bayer et al., 2001; Sessoms-Sikes et al., 2005; Buonarati et al., 2020). In the case of GluN2A subunits, it was reported that binding of CaMKII to its CTD leads to disruption of the GluN2A/PSD-95 interaction (Strack & Colbran, 1998; Gardoni, Schrama, et al., 2001; Gardoni, Bellone, et al., 2001). Cyclin-dependent kinase 5 (Cdk5) and PI3K are two other kinases involved in synaptic transmission and plasticity that interact directly with the CTD of both GluN2 subunits (Hisatsune et al., 1999; B.-S. Li et al., 2001; F. J. S. Lee et al., 2002; J. Wang et al., 2003).

Furthermore, CTD of GluN2A and GluN2B subunits interacts with cytoskeleton-associated proteins, including Activity-regulated cytoskeleton-associated protein (ARC), myosin chains, spectrin, α-actinin, or neurofilament-light, to remodel the cytoskeleton. These interactions are often dynamically regulated by phosphorylation of CTD or by calcium signalling (Wyszynski et al., 1997; Wechsler & Teichberg, 1998; Rong et al., 2001; Ratnam & Teichberg, 2005; Amparan et al., 2005; Bajaj et al., 2009).

The CTD of GluN2A and GluN2B subunits also binds Brefeldin A-resistant Arf guanine nucleotide exchange factors 1 and 2 (Brag1/2), which mediates the exchange of GDP to GTP at ADP-rybosilation factors (Arf) and takes part in the development of mature glutamatergic synapses (Sakagami et al., 2008; Elagabani et al., 2016). Another scaffold protein, receptor for activated C kinase-1 (RACK1), interacts directly with the CTD of the GluN2B subunit and simultaneously with Fyn kinase and inhibits phosphorylation of GluN2B CTD by Fyn kinases, resulting in decreased NMDA receptor-mediated currents (Yaka et al., 2002). The CTD of the GluN2B subunit also exhibits binding to Spinophilin, which in turn decreases protein phosphatase 1 (PP1) binding to GluN2B and enhances its phosphorylation (Salek et al., 2019). Moreover, 14-3-3 proteins have an important role in the synaptic localisation of GluN2A and GluN2B containing NMDARs by promoting their surface delivery through direct interaction with CTDs or interaction with other proteins that bind to their CTDs (G. S. Lee et al., 2021).

Furthermore, the GluN2A subunit CTD binds directly to the dopamine receptor D1R (activation of D1R reduces the surface expression of GluN2A-NMDAR), the human tyrosine phosphatase PTPN4 (anti-apoptic effect), and the E3 ubiquitin ligase Nedd4 (possibly results

in ubiquitination and internalisation of GluN2A-NMDAR), while the CTD of the GluN2B subunit binds dopamine receptor D2R (activation of D2R disrupts the binding between GluN2B and CaMKII), the GTPase-activating protein p250GAP (binds RhoA and takes part in NMDAR activity-dependent actin reorganization in dendritic spines), and the E3 ubiquitin ligase Mind Bomb-2 (MIB2) (results in GluN2B-NMDAR down-regulation) (Nakazawa et al., 2003, 2008; Jurd et al., 2008; Babault et al., 2011; Gautam et al., 2013; Fan et al., 2014).

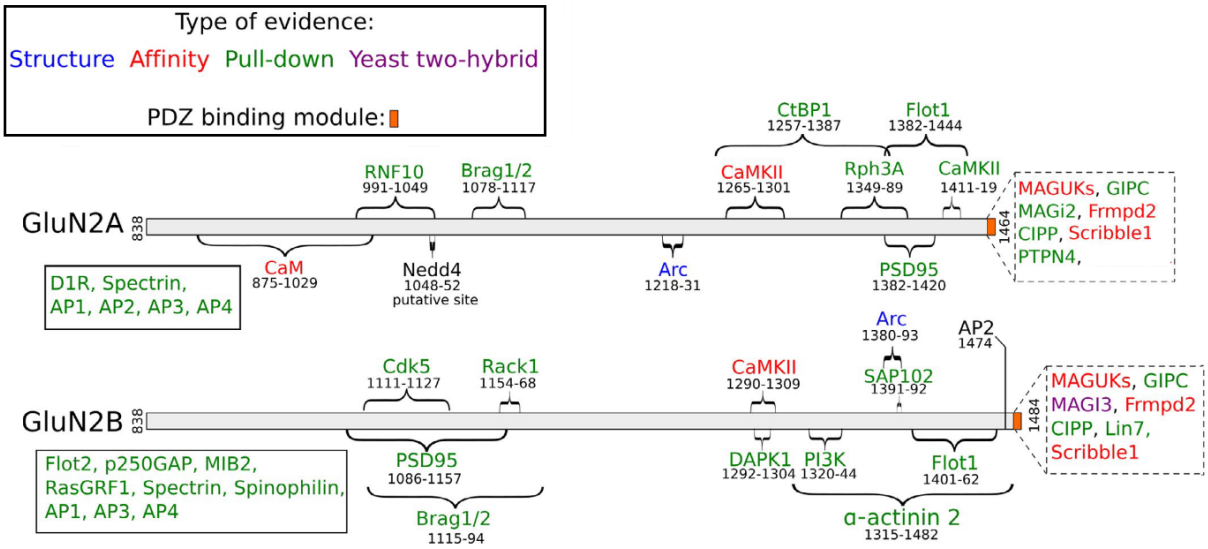

Fig. 9: **Protein interactions of the GluN2A and GluN2B subunits CTD.** Only direct physical interactions are included. The real binding region could be smaller than depicted. The interactors shown in boxes have not been assigned to CTD sub-sections. The interactors are color-coded to show the type of data used to characterise the interaction. "Structure" refers to the complexes found in the PDB. "Affinity" involves biophysical research where the strength of the binding is measured. "Pull-down" refers to the combination of all co-purification experiments, including immunoprecipitation. If more than one method has been used to describe an interaction, the method closest to the left is used. Taken and modified from Warnet et al., 2021

In general, numerous posttranslational modifications of CTD affect the functional consequences of NMDAR activity. An use-dependent dephosphorylation of NMDARs leads to a reduced number of synaptic NMDARs, which is achieved by increased endocytosis of the receptors mediated by AP-2 and dynamin, where tyrosine 842 within the CTD of the GluN2A subunit is part of a consensus binding motif for the AP-2. Dephosphorylation of tyrosine 842 within the CTD of GluN2A subunits reduces NMDA peak currents by increasing internalisation. The first 37 amino acids localised directly after M4 are required for the reduction of current. Tyrosine 842 within GluN2A and tyrosine 837 within GluN1 possibly create a ring of intracellular tyrosines that stabilizes GluN1/2A responses. Specifically, for GluN2B subunits, tyrosine 1474, part of the distal endocytic motif YEKL, is phosphorylated by Fyn and Src kinases. This phosphorylation inhibits the binding of AP-2, thereby decreasing internalisation and promoting surface expression of NMDA receptors. The phosphorylation by Fyn kinase

depends on the phosphorylation status of GluN2B at tyrosine 1070, which is required for binding of Fyn kinase to CTD, and later leads to enhanced phosphorylation of GluN2B at tyrosine 1474. Meanwhile, Src kinase phosphorylation is regulated by Cdk5, which, when inhibited, leads to increased Src binding to PSD-95 and Src kinase phosphorylation of tyrosine 1474 (Vissel et al., 2001; Cheung & Gurd, 2001; Prybylowski et al., 2005; S. Zhang et al., 2008; W. Lu et al., 2015). Moreover, Cdk casein kinase 2 (CK2) phosphorylates serine 1482 in the GluN2B subunit, part of the PDZ-binding motif ESDV, which in turn leads to inhibition of binding PSD-95 and SAP102 to the CTD of the GluN2B subunit. Phosphorylation of serine 1482 then increases endocytosis via a coordinated dephosphorylation of tyrosine 1474 in the YEKL endocytic motif. Activity-dependent phosphorylation by CK2 is regulated via CaMKII, which may induce a conformational change of CTD, leading to exposure of the PDZ-binding motif for CK2 phosphorylation. Although GluN2A subunits are not phosphorylated by CK2, activity-dependent phosphorylation of GluN2B drives its internalisation from synapses, resulting in a compensatory increase of GluN2A subunits at synapses. CK2 expression rises during development and thus may contribute to the developmental switch between GluN2A and GluN2B subunits (Chung et al., 2004; Sanz-Clemente et al., 2010). Targeting of NMDARs to the synapse membrane is also controlled via PKC phosphorylation of CTD (GluN2A – S929 / GluN2B – S1415) and subsequent physical interaction with voltage calcium channel α2δ-1 (M.-H. Zhou et al., 2021).

In addition, GluN2A and GluN2B subunits have two distinct clusters of palmitoylation sites in their CTD. Palmitoylation in the first cluster leads to an increase in phosphorylation of tyrosine in the membrane-proximal endocytic motif (GluN2A - Y842, GluN2B - Y843), which subsequently stabilizes the surface expression and synaptic localisation of NMDARs. In contrast, palmitoylation within the second cluster causes NMDAR retention in the Golgi apparatus; thus, decreasing receptor surface expression. However, mutation of the second cluster, which disables its palmitoylation, does not increase the synaptic pool of NMDARs. Palmitoylation also promotes the anchoring of the CTD to the plasma membrane and facilitates channel opening. Interestingly, palmitoylation of GluN2 CTD is activity-dependent, where neuronal activity leads to a decreased level of palmitoylation. The mechanism of depalmitoylation is induced by increased calcium concentrations during neuronal activity. Activity-dependent depalmitoylation is accompanied by a reduction in the probability of channel opening and an increased rate of internalisation; thus acting in turn as a fast negative feedback loop for increased neuronal activity (Hayashi et al., 2009; Mattison et al., 2012; Hubalkova et al., 2021).

Massive parallel sequencing of individual human genomes brought a large amount of data and revealed variants in genes encoding subunits of NMDA receptors, including CTD. Several

genetic variants have also been identified in the GluN2A and GluN2B subunits of the NMDA receptor. These variants have been found in patients diagnosed with epilepsy, mental retardation, SCH, or autism spectrum disorder. To date, very few genetic variants in the CTD region have been functionally characterised, even though many of them are nonsense variants that lead to the truncation of this domain (Firth et al., 2009; Endele et al., 2010; Tarabeux et al., 2011; Rauch et al., 2012; Lesca et al., 2013; Lemke et al., 2013; O'Roak et al., 2014; Lal et al., 2015; Retterer et al., 2016; Platzer et al., 2017; Stessman et al., 2017; von Stülpnagel et al., 2017). Functional analysis of disease-associated missense variants in the CTD of the GluN2B subunit revealed impaired binding to MAGUKs proteins (S1415L, L1424F, S1452F), a decrease in the number of dendritic spines (S1415L), deficiencies in surface expression (S1415L), and decreased trafficking and targeting of the receptor to the synapse (S1415L) (S. Liu et al., 2017). Another variant within the CTD of the GluN2B subunit (K1091T) is associated with epilepsy and intellectual disability. This variant created a Casein kinase 2 phosphorylation site and displayed a deficiency in its interaction with PSD-95, accompanied by reduced surface expression, dendritic spine number, excitatory synaptic transmission, and glutamate affinity (X. Wang et al., 2023). Similarly, a missense variant within the CTD of the GluN2A subunit associated with patients with epilepsy (S1459G) displayed deficits in binding to MAGUKs protein member PSD-95 and protein SNX27, resulting in reduced spine density, trafficking deficits, and decreased excitatory synaptic transmission (Mota Vieira et al., 2020). Another variant located within the CTD of the GluN2A subunit (K879R) resides in a recently identified ER retention motif ($KKK_{879\text{-}881}$), which results in enhanced receptor surface expression and GluN2A-NMDAR EPSCs. A knock-in mouse model of the variant then additionally exhibited defects in synaptic transmission and impaired learning and memory, possibly due to impaired mechanisms of LTP and LTD (Q.-Q. Li et al., 2022a). The most recent publication functionally analysing a variant located in the CTD of the GluN2A subunit evaluated the frame-shift variant (P1199Rfs*32) identified in epilepsy patients. Although the variant did not impair receptor trafficking to the postsynaptic membrane, its extrasynaptic expression was increased, and neurons expressing the variant exhibited fewer synapses and decreased spine density. The hypothesized mechanism involved the loss of all PDZ interactions except for the recycling protein Scribble1, which facilitates the recycling of variant NMDAR (Vieira et al., 2023).

2.2. Schizophrenia

SCH is a complex neuropsychiatric disorder with heterogeneous behavioural and cognitive symptoms affecting up to 1% of the world population. Affected people usually require drug treatment, and their life expectancy is reduced by 10 – 20 years compared to the general population. SCH significantly affects their daily lives, including their ability to sustain

employment or maintain social relationships, showing strong socio-economic impacts of SCH (Kahn et al., 2015; Owen et al., 2016).

The SCH symptoms can be divided into “positive”, “negative”, and cognitive. Positive symptoms include an inability to behave and act in accordance with reality and can be referred as psychosis. Psychosis is manifested by hallucinations, delusions, emotional disfunctions, or disorganized behaviour and speech. Negative symptoms are manifested by apathy, lethargy, affective flattening, anhedonia, or withdrawal from social events or settings. Cognitive symptoms then include a wide spectrum of cognitive dysfunctions like deficits in attention, working memory, and executive function. SCH is typically diagnosed in late adolescence, when the first psychotic symptoms manifest. However, the onset of the disease already starts in early adolescence as a prodromal phase, when a decline in cognitive and interpersonal abilities first appears. Risk factors for the development of SCH include at first heredity (approximately 80%), further prenatal and perinatal complications, paternal age, sex (SCH is more frequent in men), urban environment, migration status, drug abuse, or social adversity (physical abuse, sexual abuse, maltreatment, bullying) (Kahn et al., 2015; Owen et al., 2016).

SCH is thought to be caused by a complex interaction of genetic and environmental risk factors that influence early brain development. MRI scans of schizophrenic brains revealed a reduction in total grey and white matter as well as whole-brain volume, together with increased relative brain age compared to healthy controls. Additionally, it was observed that there was altered activation in cortical and subcortical structures in patients with SCH, corresponding to abnormal information processing reported in patients. These observations are currently understood as alternations in the connectivity of neuronal circuits (Kahn et al., 2015; Schnack et al., 2016; Birnbaum & Weinberger, 2017; Hajek et al., 2019).

From a molecular perspective, pathophysiological mechanisms refer mostly to the altered synaptic architecture and neuronal transmission resulting in abnormal brain information processing. Before the current increase in evidence of genetic links to SCH, three neurotransmitters, dopamine, glutamate, and gamma-aminobutyric acid (GABA), were implicated as pathogenetic factors by post-mortem brain studies. The evidence of impaired GABAergic functions was most consistent. Observations suggested primarily downregulated expression of the GABA synthetic enzyme glutamate decarboxylase 1 (GAD1), resulting in reduced GABA neuronal activity. However, the implication of decreased GABA neuronal activity for SCH pathophysiology are unclear and possibly reflect secondary adaptation to reduced synaptic transmission and impaired excitatory glutamate neuronal activity (Kahn et al., 2015; Berdenis van Berlekom et al., 2020).

Among the most discussed pathophysiological mechanisms of SCH belong historically to the dopamine and glutamatergic hypotheses. The dopamine hypothesis could explain mainly positive symptoms, the glutamatergic hypothesis might account for negative and cognitive symptoms. Nevertheless, dopaminergic and glutamatergic transmissions can influence each other, therefore, mutual regulation of both transmissions may play an important role in the development of SCH (Uno & Coyle, 2019; McCutcheon et al., 2020; Kruse & Bustillo, 2022).

The dopamine hypothesis is originally based on the discovery of the first antipsychotic drug chlorpromazine, later shown as an antagonist of dopamine receptor D2. Over the years, several pharmacology treatments affecting the dopaminergic system were applied to treat psychosis. An antipsychotic effect was proven for reserpine, which causes depletion of dopamine in synaptic vesicles via inhibiting the vesicular monoamine transporter, or alpha-methyl-para-tyrosine, which inhibits tyrosine hydroxylase, the essential enzyme for dopamine synthesis. In parallel, it was shown that amphetamine, which inhibits the dopamine transporter, increased dopamine concentration within the synaptic cleft, which has a psychotic effect similar to the acute phase of paranoid SCH. These observations led to the hypothesis that SCH pathophysiology is connected to excessive stimulation of dopaminergic transmission. However, treatment with antipsychotic drugs did not have an effect on the negative or cognitive symptoms of SCH, and the dopamine hypothesis is limited in its explanation of those symptoms. Moreover, the main features of SCH are linked with cortical pathology, which correlates with negative and cognitive symptoms but not with psychosis in SCH patients (Uno & Coyle, 2019; McCutcheon et al., 2020).

The glutamate hypothesis has its origin in the development and usage of dissociative anaesthetics ketamine and phencyclidine (PCP), which induce SCH-like symptoms, including all three categories of symptoms defining SCH. Later, it was discovered that ketamine and PCP are noncompetitive antagonists of the NMDARs, suggesting the theory that SCH results from the hypofunction of the NMDAR. Interestingly, the autoimmune disorder anti-NMDAR encephalitis produces antibodies against the extracellular domain of NMDARs, resulting in the downregulation of NMDARs by their internalisation. This disorder manifests similar symptoms as SCH, further supporting the hypothesis of NMDAR hypofunction. Unlike dopamine neurons, which are limited to defined anatomical pathways, glutamate signaling occurs throughout the whole brain, consequently, dysfunction of this system has the potential to account for a broad range of impairments associated with SCH. The glutamate theory is then also supported by genetic animal models that exhibit SCH-like symptoms and pathology. For instance, a mouse knock-out (KO) model of the enzyme serine racemase, which produces the one co-agonist of NMDAR D-serine, demonstrates a phenotype that closely resembles many features of SCH, such as enlarged lateral ventricles, cortical atrophy, decreased dendritic

length, decreased spine density, or downregulation of cortical GABAergic interneurons (Balu & Coyle, 2015; Uno & Coyle, 2019; Kruse & Bustillo, 2022).

In the last two decades, with the development of NGS, the study of the genetic nature of SCH has made great progress, as various areas of the genome or specific genes that are altered in SCH patients have been defined. In line with observations, genetic variants with a range of population frequencies, together with rare or *de-novo* variants, can significantly contribute to the risk of SCH. These genetic variants are especially frequent in the genes encoding for a number of synaptic proteins like dopamine or glutamate receptors, voltage-dependent calcium channels, postsynaptic scaffold proteins, or major histocompatibility complexes. However, it is not possible to identify a causal change that would be the only cause of the onset and development of the disease, suggesting a polygenetic character of the SCH, where multiple risk genes of modest effect interact with environmental risk factors to cause the phenotype. Nevertheless, it is important to identify specific genetic changes that alter the functions of specific proteins or mechanisms, such as excitatory transmission. By analysing these changes, it will be possible to determine a target, which can then be corrected with pharmacological or other (molecular genetic) treatment; thus reversing or modifying the manifestations of the disease in individual patients (Walsh et al., 2008; Purcell et al., 2014; Owen et al., 2016; Sekar et al., 2016; Kruse & Bustillo, 2022).

2.2.1. Genetic risk for schizophrenia

SCH is a highly hereditary disorder where the identification of specific risk genes is essential for understanding disease pathophysiology. Three general approaches have predominantly been used to identify specific genetic risk factors in SCH. The first two, Genome-wide association study (GWAS) and Whole exome sequencing (WES) are based on NGS, identifying common and rare variants, typically single nucleotide variants, within all genomes or exomes, respectively. Depending on the position, identified variants have the potential to be considerable SCH risk factors. The third approach uses multiplex ligation-dependent probe amplification (MLPA), array comparative genomic hybridization (aCGH), or specific software tools for NGS data processing to identify copy-number variants (CNVs) with various potential impacts on SCH (Moreno-Cabrera et al., 2020; Kruse & Bustillo, 2022).

Recently, the largest GWAS on 76 755 SCH cases and 243 649 control subjects reported the association of common variants at 287 distinct genomic loci and identified 120 genes (106 protein-coding) with SCH-associated variants. Genes with the associated variants are expressed predominantly in excitatory and inhibitory neurons. Within those genes, 16 of them contained non-synonymous or untranslated region variation. Additionally, there were also described rare disruptive coding variants for the glutamate receptor subunit *GRIN2A* and

transcription factor SP4, which were also convergent for common and rare variants associated with SCH (Trubetskoy et al., 2022).

The largest WES on 24,248 SCH patients and 97,322 controls revealed 10 genes with rare coding variants significantly associated with SCH. These genes are expressed in the central nervous system, and they participate in several mechanisms, including the formation, structure, and function of the synapse. The study also confirmed *GRIN2A* gene variations to be significantly disease-associated. Besides, genes selected from SCH common variant analyses were also enriched by rare variants, implying that common and rare genetic risk factors converge on the same underlying pathogenic biological processes (Singh et al., 2022).

In the study on 662 SCH proband-parent trios and 2623 controls, it was found that rare *de novo* CNVs are significantly more prevalent in the group of patients. Among the studied genes, the *GRIN* genes were the most enriched by *de novo* and rare CNVs, which was confirmed further by the analysis of 7907 SCH patients and 10 585 control subjects (Kirov et al., 2012). These findings were also supported by the largest CNVs study on 21,094 SCH patients and 20,227 controls, where eight genes with deletions were also reported that raised the risk of SCH, including genes for synaptic cell adhesion and scaffolding proteins or the NMDAR *GRIN1* gene (Marshall et al., 2017).

In general, reported variants associated with SCH were represented mainly in proteins involved in glutamatergic neurotransmission, especially in postsynaptic proteins like ARC or NMDARs complexes. The finding thus confirms an important role for NMDAR in the pathogenesis of SCH. Additionally, it is important to note that the majority of these genetic variants were found in non-coding regions of the genome and have unknown effects. However, it was also shown that a number of SCH-associated non-coding variants are located within regulatory elements of genes like promoter and enhancer regions, suggesting a functional relationship between non-coding variants and 3D genomic architecture (Fromer et al., 2014; Roussos et al., 2014; Javierre et al., 2016; Marshall et al., 2017; Singh et al., 2022; Trubetskoy et al., 2022).

2.3. Schizophrenia-associated genetic variations in *GRIN* genes

The SCH-associated genetic variations were identified across all *GRIN* genes.

Within the promoter and 5' UTR region of *GRIN* genes, disease-associated variants were described for the *GRIIN1*, *GRIN2A*, and *GRIN2B* genes, but not for the *GRIN2C*, *GRIN2D*, *GRIN3A*, and *GRIN3B* genes. The lack of SCH-associated variations for these genes may be due to a lack of research when the most attention was paid to the genes *GRIN1*, *GRIN2A*, and *GRIN2B*, which encode the majority of NMDARs in the hippocampus and cortex, and

at the same time, these genes encode the NMDAR subunits, which play a fundamental role in the mechanisms of synaptic plasticity. On the other hand, SCH-associated variants within the protein-coding region were identified in all *GRIN* genes. A number of studies also reported SCH-associated intronic variants and synonymous variants in the protein-coding region (Nishiguchi et al., 2000; Sakurai et al., 2000; Rice et al., 2001; Paus et al., 2004; Makino et al., 2005; Y.-C. Shen et al., 2009; Tarabeux et al., 2011; Williams et al., 2012; Y. Yang et al., 2015; Poltavskaya et al., 2021). The intronic and synonymous protein-coding variants can contribute to the pathophysiology of SCH by affecting the affinity of potential transcriptional regulators within these regions or by affecting the splicing of introns/exons. 3' UTR variants could potentially also affect transcription or translational regulation, but only a few studies have characterised this region of the *GRIN* genes with regard to SCH (Y. Zhang et al., 2015). Based on the aforementioned, this chapter will not include disease-associated common and rare variants within introns and the 3' UTR of the genes, as well as synonymous variants in the protein-coding region of the *GRIN* genes, whose functional consequences are rather minor and also difficult to analyse.

2.3.1. Promoter and 5’ UTR region of *GRIN* genes

2.3.1.1. GRIN1

A study involving 100 chronic SCH patients discovered 28 unique variants in the *GRIN1* gene. Among those variants, eight were part of the promoter and 5’ UTR region, two of them were common variants (C-1743T[5] (rs7032504), G-855C (rs11146020)), and six of them were rare variants (C-1744T, C-1537G, G-1140A (rs144123109), A-1106G (rs147317792), T-721G (rs949092578), and A-567G (rs1000173957)). However, comparison of variants in a case-control study is missing (Rice et al., 2001).

In the case-control study of 139 schizophrenic patients and 145 controls of the Italian population, the G-855C (rs11146020) variant was found in the *GRIN1* promoter, which was significantly associated with an increasing risk of SCH (Begni et al., 2003). The finding was then also supported by a study of 200 SCH patients and 200 controls from the Iranian population and by another study of 354 SCH patients and 323 controls from the German population (Galehdari, 2009, s. 100; Georgi et al., 2007). The hypothesized mechanism suggests a change in the consensus binding sequence for transcription factor NF-κB. Alterations in this binding site are caused by changes in the G-rich sequence, where the G allele is involved in G-quadruplex formation, while the C allele in this sequence leads

[5] The number indicates the relative distance from the start codon of the *GRIN1* gene

to single strand configuration. This change resulted in reduced gene expression and NMDAR activity (Chaudhary et al., 2017).

However, the association of the G-855C variant with SCH was not confirmed in studies of the Chinese Han (Taiwan) population (102 schizophrenics and 94 controls) or the Canadian population (86 nuclear families and 91 case-control pairs) (Hung et al., 2002; Martucci et al., 2003). Another study of the 707 SCH patients, 689 control subjects, and 353 family trios from the Chinese Han population then confirmed that the G-855C variant was significantly associated with SCH, but their finding suggested that the G allele was in contrast associated with SCH (Zhao et al., 2006). This results were later confirmed by another study of the Chinese Han population (Y. Liu et al., 2019). On the other hand, a study of 253 SCH patients and 140 healthy controls from the Chinese population found no association of the *GRIN1* promoter variant G-855C with the disease, although they suggested that the combination of variant G-855C together with variants in the *GRIN2B* gene (T4197C and T5988C) may be significant risk factors for the etiology of SCH (Qin et al., 2005).

The case-control study of 196 Japanese patients and 216 controls of the *GRIN1* 5' UTR (+51 bp to -941 bp relative to the start codon) identified 17 variants without disease association. Of the 17 variants, four of them were rare variants detected only in the group of patients, namely C-489T, G-388A, G-381A, and G-373A. The rare variants may therefore confer a possible risk for SCH (Tani et al., 2002).

The most recent study of 309 SCH patients and 316 healthy controls from the Chinese Han population identified seven variants, including T-2019C (rs112421622), insT-1962/1961 (rs138961287), G-1945T (rs117783907), G-1934A (rs181682830), C-1742T (rs7032504), G-1140A (rs144123109), and G-855C (rs11146020). The genotype frequencies of three variants were significantly different between cases and controls. Specifically, insT-1962/1961 with a preference for delTdelT in cases, and G-1945T and G-855C with a preference for GG in cases. Additionally, the G-1945T variant also showed a significantly different allele frequency, with a preference for the G allele in patients. The study also described two major haplotypes (after excluding four variants with very low frequencies) and found a significant difference in the haplotype frequency distribution, where the haplotype delT:G:G:C:GG (insT-1962/1961:G-1945T:G-1934A:C-1742T:G-1140A:G-855C) was more frequent in SCH patients. The reported haplotypes were further analysed by luciferase reporter assay, but no difference in promoter activity was observed (Y. Liu et al., 2019).

2.3.1.2. GRIN2A

A case-control study of 672 schizophrenics and 686 controls of the Japan population reveals significantly longer microsatellite $(GT)_n$ repeats in the *GRIN2A* promoter for SCH patients (rs3219790). Longer $(GT)_n$ repeat was leading to decreased transcription of the gene and severity of symptoms in chronic patients correlated with repeat size (Itokawa, Yamada, Iwayama-Shigeno, et al., 2003; Itokawa, Yamada, Yoshitsugu, et al., 2003; Iwayama-Shigeno et al., 2005). The results were also supported by a similar study on 122 Chinese sib-pair families and on the study of 420 schizophrenic patients and 410 healthy patients of the Chinese population (Tang et al., 2006). Additionally, comparisons in the serum level of NMDAR coagonist D-serine between patients and controls with the same length of $(GT)_n$ repeat showed a lower concentration of D-serine in the group of patients (R. Liu et al., 2015). Interestingly, longer $(GT)_n$ repeats correlated as well with the smaller volume of the hippocampus and amygdala, providing evidence of the role of the NMDA receptor in human brain development (Inoue et al., 2010). These findings are in line with the general finding of smaller brain volume in SCH, which indicates that the $(GT)_n$ repeat in the *GRIN2A* promoter may play an important role in the disease; thus, supporting the hypothesis of the hypofunction of glutamatergic neurotransmission for etiology of SCH.

2.3.1.3. GRIN2B

The study on 100 SCH patients and 100 healthy controls of the Japanese population identified, in the promoter region of the *GRIN2B* gene, T-200G (relative to TSS, rs1019385) variant as significantly associated with SCH. The frequency of the G allele was significantly higher in the schizophrenic patients compared to healthy controls. It was also shown that the reported variant is part of the transcription factor SP1 binding site and that the presence of the G allele leads to a significant downregulation of gene expression due to deficient NGF-induced SP1 binding. This suggests that the T-200G variant may be involved in the development of SCH (Miyatake et al., 2002). The finding was also supported by the study on 180 matched SCH case-control pairs and 86 SCH nuclear family trios of the Canadian population. The study further calculated the haplotype frequencies for T-200G and two identified variants in the 3' UTR of the *GRIN2B* gene (A5806C, and T5988C) and observed that haplotype T:C:C was transmitted more frequently in the controls, while haplotype G:C:T had a significantly higher frequency in cases (T-200G:A5806C:T5988C) (Martucci et al., 2006). However, another study on an Italian cohort of 188 SCH patients and 156 healthy subjects did not confirm previous observations and found the T-200G variant to be relatively equally distributed between patients and controls (Di Maria et al., 2004).

2.2.2.4. GRIN2C, GRIN2D, GRIN3A, GRIN3B

To date, none of the identified genetic variations in the promoter region or 5' UTR have been associated with SCH.

2.2.3. Protein-coding region of *GRIN* genes

Several SCH-associated variations have been identified within the protein-coding region of *GRIN* genes. The chapter focuses on the genetic variants (missense, nonsense, frame-shift, and splice site) that change the amino acid sequence of proteins. Identified genetic variants are mainly rare or *de novo* variants observed only in SCH patients, while only a few are SCH-associated common variants. The majority of these variants are missense variants (92%). Two nonsense variants were found in the *GRIN3A* gene, four frame-shift variants were identified in the *GRIN2B* (1x), *GRIN2C* (2x), and *GRIN3B* (1x) genes, and one *splice-site* variant affecting the splicing of introns and exons was described for the *GRIN2D* gene (Tab. 1). Considering the SCH phenotype, it is understandable that the associated genetic variants are predominantly missense variants, which tend to have a smaller impact on protein function compared to nonsense or frame-shift variants, which truncate the protein and thus affect protein function in a profound manner.

Nevertheless, only a few SCH-associated genetic variants were functionally characterised. Specifically, within GluN2A subunits encoded by the *GRIN2A* gene, the V452M variant causes 3,4-fold increase in glutamate potency (X.-R. Liu et al., 2021). Within GluN2B subunits encoded by the *GRIN2B* gene, the L825V variant reduces the probability of opening the receptor ion channel by 86% (Vyklicky et al., 2018), L1424F variant significantly decreases glutamate potency, the S1452F variant significantly increases glycine potency, and the L1424F and S1452F variants exhibit impaired binding to MAGUK proteins (S. Liu et al., 2017).

Tab. 1: **Schizophrenia-associated genetic variants in protein-coding region of *GRIN* genes**

Gene	Domain	Protein change	Type	References
GRIN1	ATD	p.R306Q	missense	(Tarabeux et al., 2011)
	ATD	p.A349S	missense	(Tarabeux et al., 2011)
	ATD	p.A349T	missense	(Yu et al., 2018)
GRIN2A	ATD	p.P140A	missense	(Yu et al., 2018)
	ATD	p.A149V	missense	(Yu et al., 2018)
	ATD	p.T189N	missense	(Tarabeux et al., 2011)
	ABD	p.V452M	missense	(Tarabeux et al., 2011)
	CTD	p.V852M	missense	(Tarabeux et al., 2011)
	CTD	p.D884N	missense	(Yu et al., 2018)
	CTD	p.Q964E	missense	(Yu et al., 2018)
	CTD	p.A968T	missense	(XiangWei et al., 2018)
	CTD	p.V998M	missense	(Tarabeux et al., 2011)
	CTD	p.T1064A	missense	(Tarabeux et al., 2011)
	CTD	p.H1129R	missense	(Yu et al., 2018)
	CTD	p.R1159P	missense	(Tarabeux et al., 2011)
	CTD	p.T1229S	missense	(Tarabeux et al., 2011)
	CTD	p.I1295T	missense	(Fromer et al., 2014)
GRIN2B	ATD	p.V18I	missense	(Tarabeux et al., 2011)
	ATD	p.I50N	missense	(Tarabeux et al., 2011)
	ATD	p.V65I	missense	(Williams et al., 2012)
	ATD	p.A271V	missense	(Williams et al., 2012)
	ATD	p.L362M	missense	(Tarabeux et al., 2011)
	TMD	p.L825V	missense	(Awadalla et al., 2010)
	CTD	p.Q1014R	missense	(Tarabeux et al., 2011)
	CTD	p.G1026S	missense	(Williams et al., 2012)
	CTD	p.A1267T	missense	(Williams et al., 2012)
	CTD	p.K1292R	missense	(Grozeva et al., 2015; Takasaki et al., 2016)
	CTD	p.N1352fs*0	frame-shift	(Tarabeux et al., 2011)
	CTD	p.L1424F	missense	(Tarabeux et al., 2011)
	CTD	p.S1452F	missense	(Tarabeux et al., 2011)
GRIN2C	ATD	p.R47C	missense	(Yu et al., 2018)
	ATD	p.A166V	missense	(Tarabeux et al., 2011)
	ATD	p.P132fs*192	frame-shift	(Yu et al., 2018)
	ATD	p.T407M	missense	(Yu et al., 2018)
	ABD	p.K451N	missense	(Yu et al., 2018)
	ABD	p.R488C	missense	(Yu et al., 2018)
	TMD	p.A641T	missense	(Tarabeux et al., 2011)
	ABD	p.R679C	missense	(Tarabeux et al., 2011)
	CTD	p.S911I	missense	(Tarabeux et al., 2011)
	CTD	p.S995L	missense	(Tarabeux et al., 2011)
	CTD	p.S989P	missense	(Tarabeux et al., 2011)
	CTD	p.H1187fs*7	frame-shift	(Tarabeux et al., 2011)
	CTD	p.T1196I	missense	(Tarabeux et al., 2011)

Gene	Domain	Protein change	Type	References
GRIN2D	ATD	p.R237L	missense	(Tarabeux et al., 2011)
	ATD	p.R308C	missense	(Yu et al., 2018)
	ABD	p.L466V	missense	(Tarabeux et al., 2011)
	ABD	p.S471N	missense	(Yu et al., 2018)
	ABD	p.S471X472 (G/A)	splice-site	(Yu et al., 2018)
	ABD	p.P472T	missense	(Yu et al., 2018)
	ABD	p.M733V	missense	(Tarabeux et al., 2011)
	ABD	p.R821Q	missense	(Yu et al., 2018)
	CTD	p.R872H	missense	(Tarabeux et al., 2011)
	CTD	p.M883I	missense	(Tarabeux et al., 2011)
	CTD	p.A901I	missense	(Tarabeux et al., 2011)
	CTD	p.A922V	missense	(Tarabeux et al., 2011)
	CTD	p.A982P	missense	(Tarabeux et al., 2011)
	CTD	p.G1317S	missense	(Tarabeux et al., 2011)
GRIN3A	ATD	p.S72I	missense	(Tarabeux et al., 2011)
	ATD	p.D133N	missense	(Y.-C. Shen et al., 2009)
	ATD	p.R337W	missense	(Yu et al., 2018)
	ATD	p.V389I	missense	(Yu et al., 2018)
	ATD	p.R480G	missense	(Takata et al., 2013)
	ATD	p.G487V	missense	(Tarabeux et al., 2011)
	ATD	p.K488E	missense	(Yu et al., 2018)
	ATD	p.Y493F	missense	(Tarabeux et al., 2011)
	ABD	p.Q508*	nonsense	(Tarabeux et al., 2011)
	ABD	p.N565S	missense	(Tarabeux et al., 2011)
	CTD	p.I1028N	missense	(Tarabeux et al., 2011)
	CTD	p.R1024*	nonsense	(Y.-C. Shen et al., 2009)
	CTD	p.Q1091H	missense	(Y.-C. Shen et al., 2009)
GRIN3B	ATD	p.T181I	missense	(Yu et al., 2018)
	ATD	p.G185S	missense	(Yu et al., 2018)
	ATD	p.R194W	missense	(Tarabeux et al., 2011)
	ATD	p.R247Q	missense	(Tarabeux et al., 2011)
	ATD	p.R336C	missense	(Tarabeux et al., 2011)
	ATD	p.R340Q	missense	(Yu et al., 2018)
	ATD	p.R350H	missense	(Tarabeux et al., 2011)
	ATD	p.G358D	missense	(Yu et al., 2018)
	ATD	p.P381L	missense	(Tarabeux et al., 2011)
	ABD	p.G465fs*17	frame-shift	(Matsuno et al., 2015; HORNIG et al., 2017)
	ABD	p.E470H	missense	(Tarabeux et al., 2011)
	ABD	p.V500M	missense	(Yu et al., 2018)
	TMD	p.M570K	missense	(Yu et al., 2018)
	TMD	p.A583V	missense	(Tarabeux et al., 2011)
	TMD	p.E598C	missense	(Tarabeux et al., 2011)
	TMD	p.R608H	missense	(Tarabeux et al., 2011)
	ABD	p.E675K	missense	(Yu et al., 2018)

Gene	Domain	Protein change	Type	References
GRIN3B	ABD	p.Y773C	missense	(Yu et al., 2018)
	CTD	p.V928M	missense	(Tarabeux et al., 2011)
	CTD	p.A948V	missense	(Tarabeux et al., 2011)

*Abbreviations: fs, frameshift; *, termination codon*

Our review of NMDAR genetic variants location and representation in the protein-coding region of *GRIN* genes points to the conclusion that the less affected gene is *GRIN1*, which encodes the GluN1 subunit of NMDAR (only 3,4% of all variants). Genes *GRIN2A, GRIN2B, GRIN2C, GRIN2D*, and *GRIN3A* contain a similar number of genetic variants (14 to 15% of all variants are present for each gene). On the other hand, an excess of genetic variants is observed for the *GRIN3B* gene (22,5% of all variants) (Fig. 10 A) and C)). The GluN1 is obligatory subunit in NMDAR, therefore, genetic variants within the *GRIN1* gene are under higher selection pressure compared to other subunits, and the low number of SCH-associated genetic variants is not surprising. On the contrary, the GluN3B subunit encoded by the *GRIN3B* gene has relatively low expression, and its function has not been, so far, linked to the crucial physiological processes as in the case of the GluN2A or GluN2B subunits; thus, the possible selection pressure is lower.

Regarding the location of genetic variants, most of them are present in ATD (38,2% of all variants) and CTD (37,1% of all variants), followed by ABD (19,1% of all variants), and the less affected domain is TMD (6,7% of all variants) (Fig. 10 A) and B)). When considering the SCH phenotype, the observed distribution is comprehensible. ABD and TMD are vital for NMDAR ion channel function, while CTD and ATD are regulatory domains that mediate the binding of modulators or other proteins. The majority of ATD variants are present in the *GRIN3A* and *GRIN3B* genes, and the majority of CTD variants are present in the *GRIN2A* and *GRIN2B* genes, which encode the longest CTD domains among NMDAR subunits and mediate the most NMDAR protein-protein interactions.

A)

	ATD	ABD	TMD	CTD	Total	Total (%)
GRIN1	3	0	0	0	**3**	3,4
GRIN2A	3	1	0	10	**13**	14,6
GRIN2B	5	0	1	7	**13**	14,6
GRIN2C	4	3	1	5	**13**	14,6
GRIN2D	2	6	0	6	**14**	15,7
GRIN3A	8	2	0	3	**13**	14,6
GRIN3B	9	5	4	2	**20**	22,5
Total	34	17	6	33	**89**	100
Total (%)	38,2	19,1	6,7	37,1	100	

B)

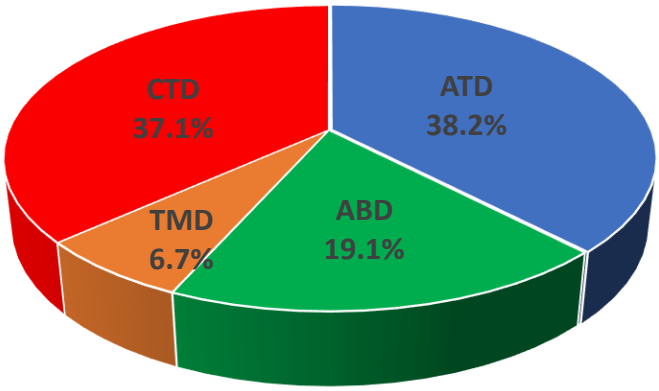

C)

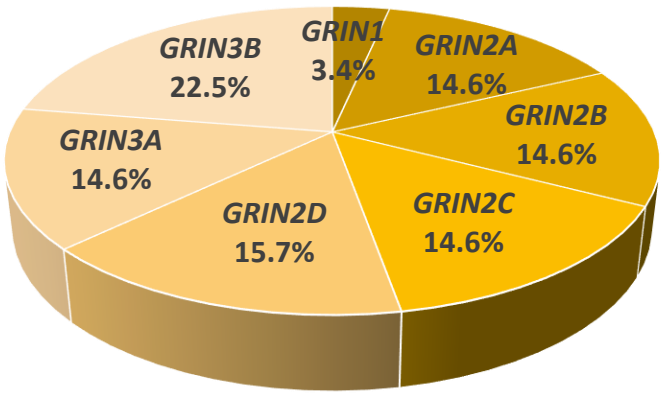

Fig. 10: **Schizophrenia-associated genetic variants differ among *GRIN* genes and NMDAR domains**. **A**) Summary of the NMDAR variant's location with *GRIN* genes representation. **B**) Percentual representation of the NMDAR variant's location. **C**) Percentual representation of SCH-associated variants for *GRIN* genes.

3 Aims of the thesis

The objective of the thesis is the functional characterisation of disease-associated genetic variants of NMDAR genes. We particularly investigated the less-studied promoter regions of these genes and the intracellular domains of the NMDAR.

The aims:

1. **Identification of common and rare variants within the NMDAR genes using our NGS dataset from SCH and control subjects.**
2. **Evaluation of the effect of genetic variants within the promoter region of NMDAR genes.**
    2.1. Annotation of promoter variants, determination of promoter genetic haplotypes, and functional characterisation of the haplotypes in the *GRIN* genes.
    2.2. Assessment of the hypothesis of NMDAR hypofunction in SCH with respect to promoters.
3. **Functional characterisation of missense variants identified within the CTD of the GluN2A NMDAR subunit.**
    3.1. Annotation of NMDAR non-synonymous coding variants from our NGS dataset
    3.2. Functional analysis of GluN2A CTD missense variants
4. **Characterisation of functional determinants of the GluN2A and GluN2B subunits' CTD.**
    4.1. Functional characterisation of GluN2A and GluN2B CTD nonsense and frame-shift variants.

4 Methods

4.1. Schizophrenia patients / Healthy controls

In this case-control study, two independent psychiatrists diagnosed sixty-three patients with FES (aged 24.6 ± 6.9 years) based on the structured MINI International Neuropsychiatric Interview (Sheehan et al., 1998a) and in accordance with the ICD-10 criteria. FES patients were diagnosed with SCH during their initial hospitalization at the Bohnice psychiatric hospital, which serves a catchment area of 1 million people living in Prague and the northern part of Central Bohemia. During the data collection period of 2014–2017, the diagnostic procedures were carried out at the National Institute of Mental Health, Klecany, CR, or the Prague Psychiatric Centre, Prague, CR. If a patient met the following requirements, they were diagnosed with FES: A) initial stay in a hospital for SCH-spectrum disorders (such as acute and transient psychotic disorders or SCH) and B) clinical interview revealed the onset of the first psychotic and/or prodromal symptoms of psychosis no earlier than 24 months prior (mean, 3.61 ± 5.05 months). Experienced psychiatrists evaluated the Positive and Negative Symptom Scale (PANSS) (Kay et al., 1987) (interclass correlation coefficient, 0.73; 95% confidence interval, 0.62-0.83). Forty-three patients were on monotherapy, four were unmedicated, and the rest were being treated with a combination of antipsychotics, with the majority of patients being treated with atypical antipsychotics (olanzapine, 29, risperidone, 15, quetiapine, 6, amisulpride, 4, clozapine, 4, aripiprazole, 7, ziprasidone, 2, zotepine, 1, haloperidol, 1). Thirty-two healthy control individuals were chosen to match age and gender with the FES subjects. In the final sample, healthy controls were slightly older and had more years of schooling compared to the FES patients (Tab. 2). The MINI was used to screen the healthy controls, and individuals were excluded if they had: A) a lifetime history of any psychiatric condition, or B) a family history of psychotic disorders up to the second degree (confirmed by diagnostic interviews and electronic medical records). Exclusion criteria for both groups included a history of seizures or serious head trauma, mental impairment, a history of substance abuse, and any MRI contraindications.

Tab. 2: **Sociodemographic and clinical information for the groups of FES and HC**

	FES (n = 63)	HC (n = 32)	*p*-Value (Two-Tailed *t*-Test)
Age, years; mean (SD)	24.62 (6.94)	27.84 (6.96)	0.0355
Female, No. (%)	24 (38.10)	17.00 (53.13)	0.16
Male, No. (%)	39 (61.90)	15.00 (46.88)	
Education, years; mean (SD)	12.72 (2.84)	16.74 (2.40)	0.00 +
Schizophrenia, No. (%)	38 (60.32)		
Other schizophrenia-spectrum disorders *, No. (%)	25.00 (39,68)		
PANSS Positive Subscale; mean (SD)	14.82 (4.91)		
PANSS Negative Subscale; mean (SD)	18.48 (6.46)		
PANSS General Psychopathology Subscale; mean (SD)	36.17 (8.87)		
PANSS total; mean (SD)	69.48 (17.35)		
Duration of untreated psychosis (months); mean (SD)	3.61 (5.05)		
Age at disease onset; mean (SD)	24.13 (6.97)		
Chlorpromazine equivalents, mg/d; mean (SD)	399.67 (192.03)		
Duration of antipsychotic treatment (months); mean (SD)	1.79 (2.96)		

*Abbreviations: PANSS, Positive and Negative Symptom Scale; FES, first-episode SCH patients; HC, healthy controls; +, Pearson's chi-squared test; *, the ICD-10 diagnosis of acute and transient psychotic disorders is congruent with the DSM-IV-defined brief psychotic disorder.*

4.2. Genomic DNA

Following the manufacturer's protocol, genomic DNA was extracted from whole blood samples using a QIAamp DNA Blood Kit. A set of target regions selected for deep sequencing were captured from ninety-five samples using a NimbleGen Custom Sequence Capture Kit. The targeted genomic regions consisted of ~15 Mb of genomic DNA sequence and were used to target all the iGluRs genes. Genomic DNA was further sheared to a mean size of 178 bp and sequenced as 75–80 bp paired-end reads using an Illumina HiSeq 2500 sequencing instrument at EMBL GeneCore. Sequence alignment to the genomic reference hg38 was performed using the bwa-mem algorithm (H. Li & Durbin, 2009). We used the Alfred command-line application (Rausch et al., 2019) to compute multi-sample quality control metrics by which the average on-target rate (± 100 bp of the target region) was calculated to be 85%. The range of duplicate readings was between 10 and 45% (mean 24%). After deduplication, nearly 90% of the targets that were successfully collected had mean coverages ≥30x for each sample. Sequencing error rates were estimated to be less than 1% across all samples based on alignments. Variant calling was performed using FreeBayes (Garrison & Marth, 2012), and the resulting vcf file was filtered for read depth and mapping quality. Subsequently, vcf files were annotated using VEP (McLaren et al., 2016). The entire alignment and variant calling method are accessible in the GitHub nRex repository (https://github.com/tobiasrausch/nRex; last accessed on December 12, 2023).

4.3. NGS data analysis

The sixteen genes that encode ionotropic glutamate receptors cover approximately 4.2 Mb and include the following regions: promoter (defined as 2000 bp upstream of the canonical transcription start site), 5'UTR, exons, introns, and 3'UTR (variable length). Genomic coordinates for these regions were determined using the GENCODE annotation (Ensembl/Havana, with consensus coding sequences chosen in accordance with CCDS), and they were saved as a BED file. Genomic variations within each gene were then retrieved and evaluated using the bcftools program from the consolidated regenotyped BCF-formatted file created by nRex. Based on the local copy of the Kaviar (Known VARiants) database and the Ensembl VEP, all the detected variants were annotated. The canonical transcripts were used as a reference point for the distribution of variations. The distribution of subjects for genetic variants was calculated for each allele. Additionally, the bedtools intersect with the wgEncode DNaseI Hypersensitivity Clusters, DNA Methylation tracks, Transcription Factor ChIP-seq data, CADD score, GERP score, and EPD, gnomAD, and ORegAnno databases records were used to annotate variations found inside promoter regions. Custom scripts were used for the data conversions and processing of the intermediate results.

4.4. Promoter cloning

Approximately 2kbp promoter of *GRIN* genes were cloned into the pGL4 Luciferase Reporter Vector (Promega). The promoter was defined as a 2000 bp upstream region from the canonical TSS (ensambl transcript). The promoters were amplified from genomic DNA samples of patients and controls by Nested polymerase chain reaction (PCR) using Q5® Hot Start High-Fidelity DNA Polymerase (NEB) according to manufacturer protocol with a 200nM primer concentration. The PCRs were additionally supplemented by betaine (200 mM) and DMSO (3%). The annealing temperature of primers was estimated using a Tm calculator (NEB, https://tmcalculator.neb.com/#!/main). The first PCR used the following outer primers:

Gene	Orientation	The sequence 5' → 3'	PCR product (bp)
GRIN1	Forward	GCTGTCTGGGCTCAGGTCTACCCCCAC	2074
	Reverse	GAGAACAGCAGGGCGAGCGTCAGCAG	
GRIN2A	Forward	TGTGCCAGACCTTGTTGACCCCTTTATTAAGGCTACTTCC	2110
	Reverse	GGAGCTGCTGAGCGAGGGAGGTAGGG	
GRIN2B	Forward	GAACCCGGTCCCAGACTGCGTCCG	2074
	Reverse	GTGGAGCATGGTCATTCCCAAAGCGTCCC	
GRIN3A	Forward	CTCAACTTTTCTAGAGTTTATTCATCTGTTTCCAGGATGGTCC	2093
	Reverse	CCGCCGCTTGCTTCCTCGGAGG	
GRIN3B	Forward	CCTGAGCTGTGCACCTAGAAATGGCCAAGATGG	2175
	Reverse	CCAGGACGCCGCACGGCTGAG	

The second PCR used the following nested primers completed with restriction sites (bold) :

Gene	Orientation	The sequence 5' → 3'	Restriction enzyme site	PCR product (bp)
GRIN1	Forward	GGTGGT**CTCGAG**GGCTCTGGCCTGCCTGAG GCGG	xhoI	1996
	Reverse	GGTGGT**AAGCTT**GGGCTCGGGCCGCGGGCC	HindIII	
GRIN2A	Forward	GGTGGT**CTCGAG**TTTTACTGCCCCCCATTTCC AGATTAG	xhoI	2000
	Reverse	GGTGGT**AAGCTT**GAGGTAACGAGGGTGGGG GGG	HindIII	
GRIN2B	Forward	GGTGGT**CTCGAG**GCTCGTAGGAAGCACAGG CTG	xhoI	2000
	Reverse	GGTGGT**AGATCT**GGGAAAAAGAGGCGGTCA GGGC	BglII	
GRIN3A	Forward	GGTGGT**GGTACC**CATACTAGGAGCTTAATAA TTGGTTGTTGAATTTAAG	KpnI	2000
	Reverse	GGTGGT**GCTAGC**TGGCCAGCAAAGGGTGGC TC	NheI	
GRIN3B	Forward	GGTGGT**GGTACC**CCTCCACGTGGCCACTTGT TCCAC	KpnI	1998
	Reverse	GGTGGT**CTCGAG**CGCAAAGTTGTCGGCGTCG CTC	xhoI	

PCR products were verified by gel electrophoresis, purified by the Monarch® PCR & DNA Cleanup Kit (NEB), and their concentration was measured using the microvolume spectrophotometer NanoDrop™ OneC (Thermo Fisher). Purified PCR products, together with an empty pGL4 backbone, were further digested with restriction enzymes (NEB). Digested products were applied to gel electrophoresis, followed by gel extraction of bands with the appropriate sizes using the Monarch® DNA Gel Extraction Kit (NEB) and measurement of the concentration by microvolume spectrophotometer. Digested PCR products were ligated overnight at 16 °C into digested backbone using T4 DNA Ligase (NEB) according to manufacturer protocol with a 3:1 ratio (insert:backbone) calculated by the Ligation Calculator (NEB, https://nebiocalculator.neb.com/#!/ligation). After ligation, the products were transformed by heat shock into XL10-Gold® Ultracompetent Cells (Agilent), followed by colony PCR and gel electrophoresis verification. Positive clones were inoculated overnight, and plasmid DNA was isolated using the E.Z.N.A.® Plasmid DNA Mini Kit (Omega Bio-Tek). Finally, pGL4 Luciferase Reporter Vectors with inserted promoters were verified by DNA sequencing (Eurofins Genomics).

The cloned promoters were further subjected to classical PCR mutagenesis or IVA (In Vivo Assembly) mutagenesis (García-Nafría et al., 2016) to generate promoters with specific haplotypes for subsequent analysis. The primers were designed manually and purchased from Eurofins Genomics. The PCR was performed using Q5® Hot Start High-Fidelity DNA

Polymerase (NEB) as described above. The PCR products were further treated by DpnI and transformed into ultracompetent XL10-Gold E. coli cells by heat shock. Positive clones were selected, and isolated DNA plasmids were verified by DNA sequencing (Eurofins Genomics).

In addition, *GRIN3B* promoter regions (485 bp) covering the $(GT)_n$ microsatellite were cloned into the pGEM®-T vector system (Promega) to visualise the size of the $(GT)_n$ repeats hidden in the NGS due to low coverage. The promoter regions were amplified from genomic DNA samples of patients and controls by PCR using Herculase II Fusion DNA Polymerase (Agilent Technologies) according to manufacturer protocol. PCR products were verified by gel electrophoresis, purified by the Monarch® PCR & DNA Cleanup Kit (NEB), and their concentration was measured using the microvolume spectrophotometer NanoDrop™ OneC (Thermo Fisher). Purified PCR products were then cloned into the pGEM®-T Vector Systems according to manufacturer protocol and transformed into ultracompetent XL10-Gold E. coli cells by heat shock. Positive clones were selected, and isolated DNA plasmids were sequenced by Sanger DNA sequencing (Eurofins Genomics).

The PCR utilized the following primers:

Gene	Orientation	The sequence 5' → 3'	PCR product (bp)
GRIN3B	Forward	CTGCCCCTAGGAACTCTTGC	485
	Reverse	CCCAGGCATTCCTCATCCTG	

4.5. Luciferase reporter assay

Human embryonic cells, HEK293T, were cultured on poly-L-lysine-coated (0.1 mg/ml, P2636, Sigma-Aldrich) 24-well culture plates supplemented with standard Dulbecco's Modified Eagle's medium (DMEM) (Sigma-Aldrich) containing 10% FCS. The cells were transfected using GenJet transfection reagent (SignaGen) according to the manufacturer protocol with 500 ng of pGL4 Luciferase Reporter Vectors containing either approximately 2 kbp of *GRIN* gene promoter cores (in triplicate for each construct) or a thymidine kinase (TK) promoter and an empty vector as a control. Transfection was performed at circa 80% confluency. 48 hours after transfection, the cells were washed on ice with PBS and incubated with 200 µl of PPBT lysis buffer (0.2% Triton X-100 in 100 mM potassium phosphate buffer, pH 7.8) for 15 minutes. Afterwards, the cells were collected into microtubes and centrifuged for 5 minutes at 11,000 g. 75 µl of cell lysate was further transferred into a 96-well microplate (Thermo Scientific™) and after adding 50 ul of Firefly luciferase buffer (20 mM Tricine, 3 mM $MgSO_4$, 0.1 mM EDTA, 33.3 mM DTT, 150 µM Coenzyme A, 500 µM ATP, 250 µM D-Luciferin, pH 7.8) by an automatic

injection system, the bioluminescence signal was immediately measured (integration time 10 sec.) using an Infinite PRO 200 multifunction modular reader (Tecan).

Conventionally, the cells are co-transfected with the pGL4 Luciferase reporter vector and the pRL Renilla Luciferase control reporter vector, and the bioluminescence signal of Luciferase/D-luciferin is typically normalised to the independent bioluminescence signal of Renilla/Coelenterazine in the dual-luciferase reporter assay. However, we observed that the expression of the pRL Renilla Luciferase control reporter vector is affecting the expression of the pGL4 Luciferase reporter vector, with higher expression of the Renilla vector leading to decreased Luciferase vector expression. Despite our attempts to use different concentrations of Renilla vector in co-transfection or to use the pRL Renilla Luciferase control reporter vector under different promoters (CMV, SV40, miniP, TK, PGK), the expression of Renilla vector affected the expression of Luciferase vector.

Therefore, we chose qPCR to quantify the concentration of the transfected pGL4 Luciferase Reporter Vector plasmid and thus normalise the bioluminescence signal of Luciferase/D-luciferin for each well. Briefly, qPCR 2x Master Mix (Top-Bio) was used according to manufacturer protocol with a 400 nM primer concentration, a 200 nM fluorescent DNA TaqMan probe concentration, and 1 ul of cell lysate (after brief vortexing) as a template. The primers were designed for the bacterial origin of replication (ori) of the plasmid; thus, maximizing the specificity of the reaction. The annealing temperature of primers was empirically estimated at 58°C. The product specificity was additionally tested by SYBR green qPCR and melting curve analysis using qPCR 2x SYBR Master Mix (Top-Bio) according to manufacturer protocol.

The qPCR used the following primers and TaqMan probe:

	Orientation	**The sequence 5' → 3'**	**Modifications**	**PCR product**
Primers	Forward	CCTAACTACGGCTACACTAGAAGAACAG	-	138 bp
	Reverse	CTTGCAAACAAAAAAACCACCGCTACC	-	
Fluorescent DNA TaqMan probe	Forward	TGCGCTCTGCTGAAGCCAGTTACC	FAM - 5' end, BHQ1 - 3' end	-

The reactions were prepared in a 96 multiwell plate (Roche), amplified by LightCycler® 480 (Roche) and analysed by LightCycler® 480 Software (Roche). The exact concentration of the transfected plasmid was determined by a dilution series of control plasmid pGL4 Luciferase Reporter Vectors containing 2 kbp of the *GRIN3A* gene promoter.

Finally, the promoter-induced bioluminescence signal was normalised to the total amount of plasmid transfected in each well. The final results were calculated as averages from normalised triplicates relative to the results of the promoter haplotype with the largest occurrence in control subjects for each gene.

4.6. Segmentation of the brain and estimation of the BrainAGE Index

The MRI data from cases and control individuals were collected using a 3T Siemens Trio MRI scanner (Siemens, Erlangen, Germany) equipped with a standard head coil. To examine the changes on gray matter volume in post hoc analyses, we utilized a structural T1-weighted (T1W) 3D-MPRAGE sequence in the MRI, with the following parameters: repetition time of 2300 ms, echo time of 4.63 ms, bandwidth of 130 Hz/pixel, field of view measuring 256 × 256 mm^2, matrix size of 256 × 256, 160–224 contiguous sagittal slices, voxel size of 1 × 1 × 1 mm^3, and a GRAPPA acceleration factor of 2.

The T1W data were segmented using SPM12 (http://www.fil.ion.ucl.ac.uk/spm/soft-ware/spm (accessed on 10 January 2024)) implemented in MATLAB 9.1 (Math Works, Natick, MA, USA). After manual reorientation, T1W images were segmented using the standard unified segmentation model within SPM12. This segmentation process generated tissue probability maps indicating the likelihood of a voxel belonging to gray matter (GM), white matter (WM), or cerebrospinal fluid (CSF).

To further refine the analysis, we applied the Diffeomorphic Anatomical Registration Through Exponentiated Lie Algebra (DARTEL) algorithm (Sheehan et al., 1998) to create a customized template for our study. This template allowed us to spatially normalise GM, WM, and CSF images for each individual within the MNI space. Subsequently, we calculated the volumes of GM, WM, and CSF using a MATLAB script called get_totals (http://www.cs.ucl.ac.uk/staff/g.ridgway/vbm/get_totals.m (accessed on 10 January 2024)). Finally, the BrainAGE index was calculated based on the volumes of GM, and the results were normalised to the reference GM volume of their chronological age.

4.7. DNA constructs

Human versions of the GluN1-1a subunit (CCDS7031.1; NM_007327), GluN2A (CCDS10539.1, NM_001134407) and GluN2B (CCDS8662.1, NM_000834) subunits in the expression vector pCI-neo were generous gifts from prof. Traynelis. PSD-95 FLAG was a gift from dr. Wei-dong Yao (Addgene plasmid #15463; RRID:Addgene_15463) and PSD-95 in the expression vector pCI-neo was a generous gift from prof. Y. Hata. Besides that, our laboratory

is in possession of the expression vectors pLEX MCS and pQBI 25 (Takara, Tokyo, Japan) containing the gene for soluble enhanced green fluorescent protein (eGFP).

For the purpose of fluorescence microscopy, the eGFP tag was introduced into the construct directly after the signal peptide in the extracellular portion of the receptor by IVA cloning. Subsequently, human versions of the GluN2A and GluN2B subunits with the eGFP tag were further cloned by classical restriction enzyme cloning into the pLEX MCS (Thermo Scientific) expression vector for lentiviral transduction. Genetic variants were introduced into all three types of constructs (pCI-neo, eGFPtag-pCI-neo, and eGFPtag-pLEX-MCS) by classical PCR mutagenesis or by IVA mutagenesis. For the purpose of electron microscopy, the 6xHis tag was introduced right before the N-terminus of the eGFP tag in the eGFP-hGluN2A WT and P1386L constructs.

Primers were designed manually and purchased from Eurofins Genomics. The PCR, DpnI treatment, transformation, and plasmid verification were performed as described in the chapter 4.4.. Amino acids are numbered according to the full-length protein, including the signal peptide, with the initiating methionine as number 1.

4.8. Analysis of surface expression by fluorescence microscopy

Human embryonic cells HEK293T were cultured on poly-L-lysine-coated (0.1 mg/ml, P2636, Sigma-Aldrich) coverslips (diameter: 18 mm; thickness: 0.13–0.16 mm) in 12-well culture plates supplemented with standard DMEM medium (Sigma-Aldrich) containing 10% FCS. One hour before transfection, the medium was replaced with a new one, enriched with NMDA receptor antagonists APV (50 µm; 5-phosphonovaleric acid), Mg^{2+} (20 mM), and ketamine (1 µg/ml). Constructs of the eGFP-hGluN2A or eGFP-hGluN2B subunit together with the hGluN1-1a subunit were co-transfected by GenJet transfection reagent (SignaGen) according to manufacturer protocol. Transfection was performed at circa 80% confluency. 24 hours after transfection, the cells were washed twice with PBS and then fixed with a 4% PFA / 4% sucrose PBS solution for 10 minutes. The cells were then washed three times with PBS solution and incubated for 30 minutes with blocking solution for the determination of surface antigens (PBS containing 50 mM NH_4Cl, 10% goat serum, and 2% fish gelatine). Next, the cells were incubated for 45 minutes with the primary anti-GFP antibody (1:1000; rabbit, AB3080P; Merck) in the same blocking solution. Subsequently, the cells were washed three times for 5 minutes with PBS solution and incubated for 45 minutes with Alexa Fluor 647 secondary antibody (1:1000; goat anti-rabbit, A-21244; Invitrogen) again in the same solution. The cells were then washed three times with PBS solution and incubated with permeabilization-blocking solution (PBS containing 50 mM NH_4Cl, 10% goat serum, 2% fish gelatine, 0.1% TritonX-100, and 0.1%

Tween20) for 30 minutes. This step was followed by incubation for 1 hour with the identical primary antibody, but in a permeabilization-blocking solution. The cells were washed again with PBS solution three times for 5 minutes and incubated for 1 hour with Alexa Fluor 555 secondary antibody (1: 1000; goat anti-rabbit, A-21428; Invitrogen) together with DAPI fluorescent dye (1: 2000; D1306; Invitrogen) in permeabilizing blocking solution. Finally, the cells were washed three times with PBS solution and mounted in ProLong-Glass mounting medium (Invitrogen) on a slide. The images were obtained on a Leica DMi8 S microscope equipped with a sCMOS camera (Leica DFC9000 GTC) and captured the next day as z-stack images (z-step size: 0,18 um) with a PlanAPO 63x (1.47 N.A.) oil-immersion objective (Leica) at 395 nm (DAPI), 555 nm (hGluN2 intracellular), and 647 nm (hGluN2 surface) excitation. Dead cells were excluded by staining the cell nuclei with DAPI. The images were analysed using ImageJ software as the maximum projection of the z-stacks, where their average intensity in channels 555 and 647 (subtracted by the intensity of the background) was measured. Surface expression was determined as the ratio of these intensities, i.e. surface and intracellular labelling.

4.9. Quantitative (chromogenic) assay of surface expression

In each experiment, monkey immortalized COS-7 cells were cultured in two 24-well culture plates coated with poly-L-lysine (0.1 mg/ml, P2636, Sigma-Aldrich) and supplemented with standard DMEM medium (Sigma-Aldrich) containing 10% FCS. One hour before transfection, the medium was replaced with a new one, enriched with the NMDA receptor antagonists APV (50 μm), Mg^{2+} (20 mM), and ketamine (1 μg/ml). Constructs of the eGFP-hGluN2A or eGFP-hGluN2B subunit together with the hGluN1-1a subunit were co-transfected by GenJet transfection reagent (SignaGen) in quadruplicates in both 12-well plates according to manufacturer protocol. In addition, each plate contained a quadruplicate transfected with the GluN1 subunit only. Transfection was performed at circa 80% confluency. 48 hours after transfection, the cells were washed twice with PBS and then fixed with a 4% PFA / 4% sucrose PBS solution for 15 minutes. The cells were then washed three times with a PBS solution and incubated for an hour with a blocking solution. Half of each plate (as well as the quadruplicate) was incubated with surface antigen blocking solution (PBS containing 50 mM NH_4Cl, 10% goat serum, and 2% fish gelatine) and the other half with permeabilizing blocking solution (PBS containing 50 mM NH_4Cl, 10% goat serum, and 2% fish gelatine, 0.1% TritonX-100, and 0.1% Tween20). This ensures that there is a duplicate of the given construct for surface and total determination on each culture plate. Subsequently, the cells were incubated with primary anti-GFP antibody (1: 500; rabbit; 11-476-C100; Exbio) in the appropriate blocking solution for 1 hour. The cells were then washed three times for 5 minutes with PBS solution and incubated for 1 hour with a secondary antibody conjugated to the enzyme HRP peroxidase (1:500; goat

anti-Rabbit AQ132P; Sigma-Aldrich). Next, the cells were washed three times with PBS solution and incubated in the dark for 30 minutes in 200 µl of of o-Phenylenediamine dihydrochloride (OPD) solution (SIGMAFAST OPD tablet set; P9187; Sigma-Aldrich), which is a substrate of HRP peroxidase. Afterwards, the absorbance at 492 nm for each well in both plates was immediately measured using an Infinite PRO 200 multifunction modular reader (Tecan). From the average absorbance value of each construct (given by the quadruplicate for surface and total labelling), the background (determined by the average absorbance value in wells transfected by the hGluN1-1a subunit itself) was subtracted. Subsequently, the average value of surface labelling was subtracted from the average value of total labelling; thus, obtaining the value of intracellular staining. Surface expression was determined as the ratio of surface and intracellular labelling.

4.10. Primary hippocampal neuronal cultures

Primary hippocampal neuronal cultures were prepared by dissection of mouse hippocampi on the first postnatal day in working media (PBS, 1% D-glucose, Pen/Strep (Merck)). After dissection, the hippocampi were washed one more time with working media and incubated in a Trypsin EDTA solution (0.05% Trypsin, 0.02% EDTA, and 0.1% D-glucose) at 37°C for 40 minutes. Afterwards, partially digested hippocampi were washed twice with Minimum Essential Media (MEM) with supplements (1% D-Glucose, Pen/Strep (Merck), Sodium Pyruvate (Gibco™), N-2 Supplement (Gibco™), 20 mM HEPES, and 10% Horse Serum (Gibco™)) and gently triturated in the same supplemented MEM solution. Finally, dissociated neurons were cultured (37 500 cells/cm^2) on poly-L-lysine-coated (0.1 mg/ml, P2636, Sigma-Aldrich) coverslips (diameter: 18 mm; thickness: 0.13–0.16 mm) in 12-well culture plates. The cultures were maintained in supplemented MEM solution for 0–1 DIV and in Neurobasal medium with supplements 0.5 mM L-Glutamine, B27 supplement (Gibco™), 25 µM β-Mercaptoethanol, and 10 ng/ml FGF-b (Alomone) for 1–14 DIV. At 7 DIV, half of the volume of Neurobasal media with supplements was replaced with fresh media.

4.11. Lentivirus production

Lentiviruses were produced by transfection of HEK293T cells cultured on poly-L-lysine-coated (0.1 mg/ml, P2636, Sigma-Aldrich) 10 cm culture dishes supplemented with standard DMEM medium (Sigma-Aldrich) containing 10% FCS. The cells were transfected at 80% confluency by GenJet transfection reagent (SignaGen) according to manufacturer protocol with the following constructs: pLEX-MCS (containing the eGFP-hGluN2A or eGFP-hGluN2B subunit), packaging plasmid (pac), and envelope plasmid (VSV-G) in a ratio of 3.5:2.3:1. 24 hours after transfection, media was collected for the first time, stored at 4°C, and replaced by fresh media.

72 hours after transfection, media were collected for the second time. The collected media were then filtered through a cellulose-acetate membrane filter with a 0.45µm pore size. Lentiviruses were concentrated by ultracentrifugation of media at 50 000 g for 2.5 hours, resuspended in DMEM, and finally aliquoted.

4.12. Analysis of synaptic localisation by fluorescence microscopy

On 4 DIV, lentiviruses containing the expression vector pLEX MCS with constructs of eGFP-hGluN2A or eGFP-hGluN2B subunits were administered to primary hippocampal neuronal cultures. On 14 DIV, neurons were washed twice with PBS and then fixed with a 4% PFA / 4% sucrose PBS solution for 10 minutes. The cells were then washed three times with PBS solution and then incubated for 30 minutes with blocking solution for the determination of surface antigens (PBS containing 50 mM NH_4Cl, 10% goat serum, and 2% fish gelatine). Next, the cells were incubated for 45 minutes with the primary anti-GFP antibody (1:500; rabbit, AB3080P; Merck) in the same blocking solution. Subsequently, the cells were washed three times for 5 minutes with PBS solution and incubated for 45 minutes with Alexa Fluor 647 secondary antibody (1:500; goat anti-rabbit, A-21244; Invitrogen) again in the same solution. Following surface antigen staining, cells were washed three times with PBS solution and incubated with permeabilization block solution (PBS containing 50 mM NH_4Cl, 10% goat serum, 2% fish gelatine, 0.1% TritonX-100, and 0.1% Tween20) for 30 minutes. This step was followed by incubation for 1 hour with primary anti-GFP antibody (1:500; rabbit, AB3080P; Merck) and with anti-PSD-95 antibody (1:500, mouse, K28/43; NeuroMab), in permeabilization blocking solution. Subsequently, the cells were washed three times for 5 minutes with PBS solution and incubated for 1 hour with Alexa Fluor 488 secondary antibody (1:500; goat anti-rabbit; A-11034; Invitrogen) and Alexa Fluor 555 (1: 500; goat anti-mouse; A-21422; Invitrogen) together with fluorescent dye DAPI (1:2000; D1306; Invitrogen) in permeabilization blocking solution. Finally, the cells were washed three times with PBS solution and mounted in ProLong-Glass mounting medium (Invitrogen) on a slide. The images were obtained on a Leica DMi8 S microscope equipped with a sCMOS camera (Leica DFC9000 GTC) and images were captured the next day as z-stack images (z-step size: 0,18 um) with a PlanAPO 63x (1.47 N.A.) oil-immersion objective (Leica) at 395 nm (DAPI), 488 nm (hGluN2A/2B intracellular), 555 nm (PSD-95), and 647 nm (hGluN2A/2B surface) excitation. Dead cells were excluded by staining the cell nuclei with DAPI. The images were then deconvolved by Huygens software using the Classic Maximum Likelihood Estimation algorithm and further analysed using ImageJ software. Synapses were determined by the postsynaptic marker PSD-95, a scaffold protein that binds directly to NMDA receptor subunits. An additional experiment also verified that the native fluorescence intensity of the eGFP protein is negligible compared to the intensity of Alexa Fluor 488. The fluorescence intensity in channel 488 is thus,

in this case, the signal of the intracellular hGluN2A/2B subunits. Images were analysed as follows: *i.* Surface expression was analysed using the maximum projection of the z-stacks. Average intensities in channels 488 and 647 (subtracted by the intensity of the background) in both the soma and dendritic spines of neurons were measured. Surface expression was determined as the ratio of these intensities, i.e., surface and intracellular labeling. *ii.* Mander's overlap coefficient determining the proportion of surface receptors covered by PSD-95 (indicating synaptic localisation) was calculated from the 20μm region of interest (ROI) of secondary dendrite using ImageJ plugin Coloc2 with automatic bisection thresholding. *iii.* The percentage of overlapping surface receptors with PSD-95 (indicating synaptic localisation) was calculated from the same ROI as described above. The analysis was done automatically by our macro. After creating maximum projection, adaptive thresholding (ImageJ plugin) was used to overcome the limitation of the conventional threshold method when the feature intensities are not homogeneous. After the creation of masks of surface receptors and PSD-95, the PSD-95 mask was subtracted from the surface receptor mask, and the percentage of overlapping pixels was calculated. Additionally, our macro-incorporated plugin Analyse Particles automatically calculated the number of puncta of surface receptors and PSD 95.

4.13. Co-localisation analysis by super-resolution STED microscopy

Human embryonic cells HEK293T were cultured and transfected as described in Chapter 4.7., except the cells were co-transfected with hGluN1-1a, eGFP-hGluN2A, and PSD-95 in a ratio of 2.66:1.33:1. 48 hours after transfection, cells were initially incubated on ice with the Fluotag-anti-GFP-STAR635P nanobody (1:100, N0304, NanoTag Biotechnologies) in blocking solution (2% BSA in PBS) to assess surface staining. To assess total staining of PSD-95, cells were washed three times with PBS for 5 minutes, fixed with a 2% PFA PBS solution for 15 minutes, and then permeabilized using a 0.1% TritonX-100 PBS solution for 10 minutes. The cells were further washed three times with PBS and incubated for 30 minutes in a blocking solution (2% BSA in PBS). PSD-95 was stained by incubation of cells with anti-PSD-95 antibody (1:1000, mouse, K28/43; NeuroMab) in blocking solution for 45 minutes, followed by three times washing by PBS for 5 minutes and incubation with secondary antibody STAR580P (1:100, goat anti-mouse, ST580, Abberior) for 45 minutes. The cells were finally washed three times for 5 minutes with PBS and mounted with ProLong Diamond medium (Invitrogen). The images were captured the next day on an Abberior Instruments Expert Line STED system equipped with a Nikon Eclipse Ti-E microscope body and a Nikon CFI Plan Apo Lambda 60× Oil, NA 1.40 objective. The sample was illuminated with pulsed 561 nm and 640 nm lasers and depleted by a pulsed 775 nm (Stimulated emission depletion) STED depletion laser of the 2D donut shape formed by a spatial light modulator. The fluorescence signal was

filtered and detected on single photon counting modules with time gates set to 0.75–8 ns. Images were scanned with a pixel size of 25 nm × 25 nm, 10 µs dwell time, and in-line interleaved acquisition mode using the Imspector software. The STED images were then deconvolved by Huygens software using the Classic Maximum Likelihood Estimation algorithm and further analysed using ImageJ software. The percentage of overlapping receptors with PSD-95 (indicating protein interaction) was calculated from the 5 x 5 µm membrane area attached to the coverslip. The analysis was performed automatically by our macro. After thresholding of both channels using Otsu's method, the masks of surface receptors and PSD-95 were created. Finally, the PSD-95 mask was subtracted from the surface receptor mask, and the percentage of overlapping pixels was calculated.

4.14. Immunoprecipitation-Western blot analysis

Human embryonic cells HEK293 (ATCC, CRL-1573) were cultured in 60 mm culture dishes with DMEM medium (high glucose, GlutaMAX supplement, Thermo Fisher Scientific, 10566-024) containing 10% FBS (Thermo Fisher Scientific, A31605-01) and 0.1X Penicillin-Streptomycin (100X, Thermo Fisher Scientific, 15140-122). The constructs hGluN1-1a, hGluN2A, and PSD-95 (rat, Addgene, 15463) were mixed at a ratio of 2.66:1.33:1 with FuGENE 6 transfection reagent (3 µl FuGENE 6:1 µg DNA, Promega, E2691) for 20 minutes before adding to cells at ~50-60% confluency. Prior to adding the FuGENE 6/DNA complex, the cell medium was supplemented with the NMDA receptor antagonists AP5 (200 µm; abcam, ab120271) and 7-CKA (200 µm; 7-chlorokynurenic acid, abcam, ab120255). 24 hours after transfection, cells were washed with DPBS and incubated with 500 µl of ice-cold NP-40 lysis buffer (50 mM Tris pH 7.5, 150 mM NaCl, 0.5% NP-40) supplemented with cOmplete™, Mini Protease Inhibitor Cocktail (Roche, 11836153001) for 15 minutes on ice. Lysed cells were collected in pre-chilled microtubes and centrifuged for 15 minutes at 17 000 g. at 4°C. The supernatant (cytosol and solubilized membrane proteins) was transferred to a pre-chilled tube and placed on ice. 20 µl of the extract was used to measure the protein concentration using the Pierce Rapid Gold BCA Assay kit (Thermo Scientific, A53226). Another 40 µl (input, 20 µl x 2 for hGluN2A and PSD-95 gels) of the extract was set aside for immunoblotting.

Dynabeads Protein G (Thermo Scientific, 10004D) were prepared for each immunoprecipitation by mixing 50 µl of beads and 400 µl of PBST (0.02% Tween 20) containing 3 µg mouse anti-PSD-95 antibody (Millipore-Sigma, MABN68 clone K28/43) in a microtube. The microtubes with beads and antibodies were incubated with rotation (14 rpm) for 30 minutes on a rotator at room temperature. After incubation, the microtubes were pulse-centrifuged and placed on a DynaMag-2 magnet (Thermo Scientific, 12321D). The

antibody-bound beads were washed with 500 µl PBST by removing the microtubes from the magnet, gently resuspending by pipette, placing the microtubes on the magnet, and aspirating the PBST. The microtubes were removed from the magnet before adding 200 µl of cell lysate. Immunoprecipitation was done overnight in the cold room with rotation (14 rpm). After ~17 hours, microtubes were pulse-centrifuged before being placing on the magnet. The supernatant (depleted lysate (DEP)) was collected for analysis. Immunoprecipitated samples were washed six times with 250 µl lysis buffer as described above. After resuspension in the final wash, the slurry was transferred to a new pre-chilled microtube. The microtubes were transferred to the magnet, and the supernatant was removed. The microtubes were then removed from the magnet, and immunoprecipitated samples were resuspended with 40 µl sample buffer (25 µl lysis buffer, 10 µl 4x Laemmli Sample Buffer (Bio-Rad, 1610747), 5 µl 2M DTT) for western blot analysis. Additionally, input and immunodepleted (DEP) samples for western blot analysis were prepared by mixing 20 µl of input / DEP (10% of lysate used in IP), 10 µl of 4x Laemmli Sample Buffer, 5 µl of 2M DTT, and 5 µl of lysis buffer. Finally, the samples were incubated at 95°C for 5 minutes prior to SDS-PAGE.

Input, immunodepleted, and IP fractions were separated on a TGX stain-free 4–15% gradient gel (Bio-Rad, 4568084) alongside 5 µl each of All Blue-stained and unstained Precision Plus protein standards (Bio-Rad, 1610373 and 1610363). The gel was run in 1X Tris/Glycine/SDS buffer (Bio-Rad, 1610732) at 60V for 20 minutes, followed by 250V for 40 minutes. The gel was imaged in the ChemiDoc MP (Bio-Rad Universal Hood III) using the stain-free detection protocol (Auto Exposure for intense bands, Bio-Rad Image Lab software). The gel was transferred onto a membrane (Bio-Rad Trans-Blot Turbo LF PVDF) in 1X Trans-blot Turbo 5X transfer buffer (20% ethanol, Bio-Rad, 10026938) using the high molecular weight program (1.3 or 2.5A, 25V, 10 min.) of the Trans-Blot Turbo System. The blot was imaged using the stain-free blot detection protocol (Auto Exposure for intense bands), then allowed to dry for 1 hour. The blot was rehydrated first in methanol, then water followed by TBS before blocking for 1 hour in 2% non-fat milk/TBS. Rabbit GluN2A (1/2000, Millipore-Sigma, AB1555P) antibody was diluted in 2% non-fat milk/TBS-T (0.05%) and incubated overnight (~17 hrs) in a cold room on a rocking platform. The blot was washed in TBS-T (0.05%) four times for a total of 30 minutes before adding mouse anti-rabbit HRP-conjugated light chain specific secondary antibody (1/50,000, Jackson ImmunoResearch, 211-032-171, 0.4 µg/µl) in 2% non-fat milk/TBS-T (0.05%) for 1 hour. The blot was washed again before adding SuperSignal West Pico PLUS western blot substrate (Thermo Scientific, 34580) for 5 minutes and imaged on the ChemiDoc MP (chemiluminescence, Signal Accumulation Mode). To probe for PSD-95, the blot was stripped for 30 minutes with Restore PLUS (Thermo Scientific, 46430), then equilibrated in PBS (2X, 10 min.) and TBS (2X, 5 min.) before re-blocking (1 hr in 2% milk/TBS).

Mouse PSD-95 antibody (1/40000, Millipore-Sigma, MABN68) was diluted in 2% milk/TBS-T (0.05%) and incubated overnight (~17 hrs) in a cold room on a rocking platform. The blot was washed in TBS-T (0.05%) four times for a total of 30 minutes before adding goat anti-mouse HRP-conjugated light chain-specific (1/10,000, Jackson ImmunoResearch, 115-035-174, 0.4 µg/µl) secondary antibody in 2% milk/TBS-T (0.05%) for 1 hour. Chemiluminescent substrate was added, followed by imaging.

Band analysis was done using the Lane and Bands tool of Bio-Rad Image Lab 5.2.1 software. Image exposures without any saturated pixels in the input or IP bands were selected for analysis. From GluN2A western blots, lanes were manually defined with the assistance of the Lane Finder tool at a uniform width of 7.98 mm. The Band Finder tool defined band signatures from lane profiles using local background subtraction with a disk size of 50 mm. The total intensity was determined by the area under the curve. Ratios of IP:input band intensities were calculated and then normalised relative to WT for each biological replicate of the GluN2A variants.

4.14. Electrophysiology – HEK293T cells

HEK293T cells were cultured in high glucose DMEM (SIGMA Life Science) with 10% fetal bovine serum at 37°C in 5% CO_2. 24h–48h before transfection, cells were plated on 31-mm polylysine-coated glass coverslips in 6-well plates. Equal amounts of expression vectors encoding hGluN1-1a, WT or mutated type hGluN2A/2B, and GFP in the absence or presence of PSD-95 were co-transfected by GenJet transfection reagent (SignaGen) according to manufacturer protocol. eGFP epifluorescence was then used to reveal transfected cells.

Experiments were performed 24–48h after transfection of HEK293T. Whole-cell voltage-clamp recordings of membrane currents were made with a patch clamp amplifier (AxonTm Digidata 1550A, Axon Instruments), after series resistence and capacitance compensation of 90%, at a holding potential of -60 mV. Agonist-induced whole-cell responses were low-pass filtered at 2 kHz, sampled at 5 kHz, and analysed using pClamp software version 11.2 (Molecular Devices).

Patch pipettes (3–6MΩ) were pulled from borosilicate glass using a MODEL P-1000 micropipette puller (Sutter Instrument) and filled with an intracelullar solution (ICS) containing (in mM): 120 gluconic acid delta latone, 15 CsCl, 10 BAPTA, 10 HEPES, 1 $CaCl_2.2H_20$, 3 $MgCl_2.6H20$, and 2 ATP-Mg salt (adjusted pH to 7.2 with 50% CsOH). Extracellular solution (ECS) for HEK293T recordings contained (in mM): 160 NaCl, 2.5 KCl, 10 HEPES, 10 glucose, 0.7 $CaCl_2$, and 0.2 EDTA (pH-adjusted to 7.3 with NaOH).

Recordings of HEK293T NMDAR responses were induced by 1 μM, 3 μM, or 1 mM glutamate together with 30 μM of glycine. (5S,10R)-(+)-5-Methyl-10,11-dihydro-5H-dibenzo[a,d] cyclohepten-5,10-imine hydrogen maleate (MK-801) was dissolved in MilliQ water and stored at -20°C. The compounds were added to the extracellular solution, and they were applied after reaching a steady-state response to agonists application by a fast multichannel perfusion system.

Agonist dose-response (*I*) analysis were fit to the following equation:

$$I = 1/\left(1 + (EC_{50}/[agonist])^{h}\right)$$

in which EC_{50} is the concentration of agonist that produces a half-maximal response, [agonist] is the concentration of agonist, and h is the Hill slope.

Desensitization (*D*) of the WT or mutated NMDAR was calculated as:

$$D = \left(\frac{Ip - Iss}{Ip}\right) \text{x } 100$$

, where *Ip* is the amplitude of the response to 1 mM glutamate and *Iss* is the steady state.

The degree of testing compound potentiation (E) was calculated as:

$$E = (I_S - I_A)/I_A \times 100$$

, where I_A is the amplitude of the response to the agonist and I_S is the amplitude of the response recorded in the presence of the agonist and the testing compound.

Weighted deactivation time constants for glutamate and MK-801 channel block analysis were fit using the following equation:

$$Tau_w = Tau_{slow}(A_{slow}/(A_{slow} + A_{fast})) + Tau_{fast}(A_{fast}/(A_{slow} + A_{fast}))$$

, where Tau_{slow} is the slow deactivation time constant, Tau_{fast} is the fast deactivation time constant, A_{slow} is the amplitude of the slow deactivation component, and A_{fast} is the amplitude of the fast deactivation component.

The peak channel open probability (P_o) was assessed from the kinetics of the MK-801 (2 μM) inhibition of the response to 1uM glutamate, which blocks open ion channels with a rate constant (k_b) of 25 μM^{-1} s^{-1} ,fitted to the kinetic model using Gepasi software. Since in the presence of saturated glutamate, NMDAR exists with high probability only in double ligated states with the channel in desensitized (D), closed (R), and/or open state (O), the glutamate binding steps were not considered.

$$D \underset{k_d}{\overset{k_r}{\rightleftharpoons}} R \underset{k_c}{\overset{k_o}{\rightleftharpoons}} O \underset{k_u}{\overset{k_b}{\rightleftharpoons}} B$$

Firstly, responses induced by saturated glutamate were analysed for peak and steady state responses, and the single exponential function (τ_d) determined the onset of desensitization. Desensitization was determined from previously described equation, while (k_d) and (k_r) are kinetic constants describing the onset of desensitization and resensitization respectively.

$$k_d = D/\tau_d$$
$$k_r = (1 - D)/\tau_d$$

In the last step, (k_c) was set at an arbitrary value of 200s^{-1}, the opening rate (k_o) was fixed as a free parameter, while k_d and k_r were set to values obtained from the previous step. The channel open probability (P_o) was calculated as:

$$P_o = 100 \times \ k_o/(k_o + k_c)$$

4.16. Electrophysiology – primary neuronal culture

The primary hippocampal neuronal culture and the lentiviruses were prepared as described in chapter 4.9 and 4.10. The coverslips were additionally coated with laminin (20 ug/ml, L2020, Sigma-Aldrich). In 4 DIV, lentiviruses containing the expression vector pLEX MCS with constructs of eGFP-hGluN2A WT or P1386L subunits were administered to primary neuronal cultures. Recordings were done at room temperature on 16–18 DIV, 12–14 days after viral transduction.

The patch-clamp amplifier Axopatch 700 B (Molecular Devices, Sunnyvale, CA, USA) together with the Digidata 1550B digitizer were used to record miniature excitatory postsynaptic currents (mEPSCs). Patch pipettes (4–6 MΩ resistance) were pulled from borosilicate glass (Science Products, Hofheim, Germany) and filled with ICS composed of (in mM) 125 gluconic acid, 15 CsCl, 10 Hepes, 1 $CaCl_2$, 3 $MgCl_2$, 10 BAPTA and 2 ATP-Mg^{2+} salt (pH 7.2). Slow exchange (tau ≈ 1 s) of applied extracellular solutions was carried out via a set of parallel tubes moved by a stepper motor. ECS contained (in mM) 160 NaCl, 2.5 KCl, 10 glucose, 10 HEPES, 1 $MgCl_2$, 2 $CaCl_2$, 0.01 strychnine, 0.01 bicuculine, and 0.0005 tetrodotoxin, (pH 7,3). Moreover, 0.02 glycine and 0.002 NBQX or 0.05 AP-5 were added to pharmacologically distinguish NMDAR or AMPA/kainate receptor-mediated currents, respectively. mEPSCs were analysed no earlier than 4 s after the solution exchange. The holding potential was -70 mV. Receptor responses were low-pass filtered (2 kHz eight-pole Bessel filter) and digitally sampled at 5 kHz. Patch-clamp data were recorded and analysed using pClamp 10.1 software.

The average NMDAR mEPSCs charge transfer (pA.s) was calculated in two steps.

First, the frequency of AMPA receptor mEPSCs was calculated from 10s-time course, right before switching from the AP-5 solution application to the glycine and NBQX solution application, as:

$$f = \left(\frac{n}{t}\right)$$

, where *f* is the frequency of AMPAR mEPSCs, *n* is the number of events during time course *t.*

Second, the average NMDAR mEPSCs charge transfer (*pC*) was calculated as:

$$pC = \left(\frac{lav}{f}\right)$$

, where *lav* is the average of collective NMDAR mEPSCs from a 10s interval measured 4 s after switching from AP-5 solution application to glycine and NBQX solution application, and *f* is the frequency of AMPAR mEPSCs.

4.17. Analysis of synaptic localisation by transmission electron microscopy

The primary hippocampal neuronal culture and the lentiviruses were prepared as described in chapters 4.9 and 4.10., except that neurons were cultured on 5mm coverslips (EMS, #72296-05) in glass-bottom Mattek dishes (Mattek, #P35G-1.5-14-C). Prior to seeding the cells, a finder grid (alphanumeric carbon mask) was deposited onto coverslips for later registration of ROI during fluorescence imaging. The coverslips were then coated with poly-L-lysine (0.1 mg/ml, P2636, Sigma-Aldrich) and laminin (20 ug/ml, L2020, Sigma-Aldrich). On 4 DIV, lentiviruses containing the expression vector pLEX MCS with constructs of 6xHis-eGFP-hGluN2A WT or P1386L subunits were administered to primary neuronal cultures.

Fluorescence live-cell imaging was performed at DIV14 using a spinning disk confocal microscope (Nikon CSU-W1) and ROI with distinct eGFP-positive dendrites were registered. Receptor labelling with Ni-NTA nanoprobe conjugated to the 5nm gold was performed on live cells according to the manufacturer´s protocol (Nanoprobes, #2082) as follows: Cells were first incubated with Ni-NTA nanoprobe solution diluted 1:20 in NeurobasalTM medium (Fisher Scientific, #12348017) without *β*-mercaptoethanol for 30 min, then washed thoroughly with the same medium and fixed with Karnovsky´s fixative solution (2,5% Glutaraldehyde and 2% Formaldehyde in 0.1M PHEM buffer pH 7.4) for 1h on ice. Cells were then post-fixed with 1%

osmium tetroxide and 1.5% potassium ferricyanide solution (1 hr on ice), washed, contrasted with 1% aqueous uranyl acetate, dehydrated in ethanol and acetone, flat-embedded in epoxy resin (EMS, EMBed 812 #14120), and polymerised at 60°C for 72 hrs. Glass coverslips were removed from resin blocks by immersion in liquid nitrogen. Previously registered ROIs were relocated within the residual carbon mask on the block face. Horizontal ultrathin (60 nm) sections from each ROI were cut on an ultramicrotome (Leica EM UC7) and collected onto formvar-carbon-coated copper slot grids (EMS, #EMS2010-Cu). Sections were post-contrasted with uranyl acetate and Reynold´s lead citrate. Images of synapse cross-sections were collected on a JEM2100-Plus Transmission Electron Microscope operating at 120 kV (JEOL) and equipped with a VIPS TemCam–XF416 4K CMOS camera.

The images were analysed using ImageJ software, where only synapses with well-recognised electrodense postsynaptic density (PSD), synaptic clefts, and presynaptic vesicles were analysed. The length of the synaptic region was defined as PSD length in proximity to the postsynaptic membrane. The perisynaptic region was defined as an adjacent membrane region to the synaptic region from both sides, with the same length as the PSD length for each side of the perisynaptic region.

Next, the number of labels per 100 nm of synapse was calculated, and the relative distance of the gold particle from the central axis of the PSD (where 0 is the central axis of the PSD, 1 is the border of the synaptic region, and 3 is the border of the perisynaptic regions) was measured.

The validity of labelling was verified by labelling a negative control of an untransduced sample. The number of labels per 100 nm of synapse and the average PSD length in proximity of the postsynaptic membrane were calculated from synapse averages from transduced ROIs (n = 65 (WT)) and untransduced controls (n = 12 synapses/cells).

Finally, the relative distance from the central axis of the PSD and the number of hGluN2A per 100 nm of the synapse were calculated from cell averages (n = 4). Relative label distance from the central axis of the PSD and distribution of labelling in percent were shown and calculated from all measured labellings (n = 575 (WT), 564 (P1386L)).

4.18. Molecular modelling

In silico complexes of GluN2A and PSD-95 fragments were prepared using a local copy of AlphaFold multimer version 2.2.4 running on a NVIDIA 3090 or 4090 GPU with 24GB RAM. The amino acid sequences were taken from UniProt records Q12879 for PSD-95 and P78352

for GluN2A. The resulting models were visualised and analysed using the open-source PyMOL version 2.6.

4.19. Statistical analysis

Statistical analyses and evaluations were performed using GraphPad Prism 8 (GraphPad Software, Inc., CA, USA) and STATGRAPHICS Centurion 18 (Statgraphics Technologies, Inc., VA, USA) softwares. Outliers were identified using Grubb´s test or absolute values of studentized residuals greater than 3. The normal distribution of data was analysed using the D'Agostino and Pearson tests or the Shapiro-Wilk test in cases of small sample size. If the original data did not have a symmetric distribution and constant variance, transformations were implemented to achieve symmetry and homoscedasticity (constant variance). Data were analysed either by Fisher's exact test, unpaired or paired t test ($k = 2$), or by analysis of variance (one-way ANOVA) ($k > 2$), followed by multiple comparisons using Tukey's or Dunnett's method (versus WT). $p \leq 0.05$ was considered statistically significant throughout the study. All values are presented as means ± standard error of the mean (SEM).

5 Results

5.1. Identification of common and rare variants within the NMDAR genes

Using our NGS dataset involving subjects with SCH and control subjects, we analysed in detail the genetic variants found within all seven NMDAR genes. In the canonical transcripts of all NMDAR genes analysed, there was a markedly increased number of variants (more than 17%) observed in the SCH subjects compared to the healthy controls (Tab. 3). Within both groups, 91% of the variants were single nucleotide variants, and the remaining 9% were insertion deletion variants (InDels), with the most prevalent type being a single nucleotide deletion or duplication, accounting for 61% of the InDels.

A significant proportion (97%) of the variants exclusive to the SCH group were situated within intronic sequences. However, the majority of these variants were rare, with a minor allele frequency (MAF) of ≤ 0.016 in the SCH population, and they appeared to be randomly distributed. Besides, the intronic regions contained most of the genetic variants for both groups (94%), likely due to extensive intronic sequences (Tab. 3).

The analysis further revealed the highest average variability across all examined regions in the *GRIN2B* gene, with 7.0 variants per 1000 base pairs. This was closely followed by the *GRIN2A* (5.8), *GRIN3A* (5.6), and *GRIN3B* (4.9) genes. Subsequently, *GRIN2D* (3.8) and *GRIN2C* (2.9) genes exhibited moderate variability, while gene *GRIN1* displayed the lowest variability among all regions analysed, with only 1.0 variant detected per 1000 base pairs (Tab. 3).

Variants lacking an assigned reference number were considered novel variants, comprising 2.3% of the variants identified in the SCH cohort.

Tab. 3: **Genetic variations of NMDAR genes.** The summary of genetic variants found in the promoter regions (1500 bp upstream of a TSS), 5′UTRs, exons, introns, and 3′UTRs of seven NMDAR genes. Variants per 1000 bp is a measure of the variation rate in particular regions of the gene. The canonical Ensembl transcript corresponds to the RefSeq transcript. *Note: The RefSeq transcript in the hg38 assembly database does not always need to be a canonical transcript.*

Sample	Chr	iGluR Gene	RefSeq	Ensembl Canonical	Promotor (Existing/Novel)	Per 1000 bp	5 ′UTR (Existing/Novel)	Per 1000 bp	EXONS (Existing/Novel)	Missense/Synonymous (Novel)	Frameshift Variant	Per 1000 bp	INTRONS (Existing/Novel)	Per 1000 bp	3 ′UTR (Existing/Novel)	Per 1000 bp
SCH cases	chr9	GRIN1	NM_001185090.2	ENST00000371553.3	2/0	1.3	0/0	0.0	3/0	0/3	0	1.1	(67) 67/0	2.6	0/0	0.0
Controls	chr9	GRIN1	NM_001185090.2	ENST00000371553.3	2/0	1.3	0/0	0.0	2/0	0/2	0	0.7	(60) 56/4	2.4	0/0	0.0
SCH cases	chr16	GRIN2A	NM_001134407.3	ENST00000330684.3	28/0	18.7	0/0	0.0	7/1	(1) 4/4	0	1.8	(2162) 2112/50	5.2	31/0	3.2
Controls	chr16	GRIN2A	NM_001134407.3	ENST00000330684.3	17/0	11.3	0/0	0.0	6/0	4/2	0	1.4	(1842) 1816/26	4.5	29/0	3.0
SCH cases	chr12	GRIN2B	NM_000834.4	ENST00000609686.1	4/0	2.7	2/2	19.1	12/1	0/13 (1)	0	2.9	(1779) 1730/49	4.3	134/1	6.0
Controls	chr12	GRIN2B	NM_000834.4	ENST00000609686.1	4/0	2.7	2/0	9.5	10/0	0/10	0	2.2	(1449) 1430/19	3.5	107/1	4.8
SCH cases	chr17	GRIN2C	NM_000835.5	ENST00000293190.5	1/0	0.7	1/0	6.8	6/0	3/2	1	1.6	(31) 30/1	2.3	0/0	0.0
Controls	chr17	GRIN2C	NM_000835.5	ENST00000293190.5	1/1	1.3	0/0	0.0	7/0	3/4	0	1.9	(27) 27/0	2.0	1/0	2.4
SCH cases	chr19	GRIN2D	NM_000836.2	ENST00000263269.3	5/0	3.3	1/0	11.4	3/0	0/3	0	0.8	(109) 107/2	2.4	1/0	1.0
Controls	chr19	GRIN2D	NM_000836.2	ENST00000263269.3	2/0	1.3	1/0	11.4	3/0	1/2	0	0.8	(87) 84/3	1.9	1/0	1.0
SCH cases	chr9	GRIN3A	NM_133445.2	ENST00000361820.3	6/0	4.0	6/0	10.0	18/0	8/10	0	5.4	(760) 752/8	4.7	14/1	3.9
Controls	chr9	GRIN3A	NM_133445.2	ENST00000361820.3	4/0	2.7	5/0	8.3	15/0	6/9	0	4.5	(603) 597/6	3.7	13/2	3.9
SCH cases	chr19	GRIN3B	NM_138690.3	ENST00000234389.3	13/2	10.0	0/0	0.0	25/1	16/9 (1)	1	8.3	(38) 36/2	6.3	0/0	0.0
Controls	chr19	GRIN3B	NM_138690.3	ENST00000234389.3	11/0	7.3	0/0	0.0	19/0	10/9	0	6.1	(29) 29/0	4.8	0/0	0.0

5.2. Evaluation of the effect of genetic variants within the promoter region of NMDAR genes

Further, we closely analysed the promoter regions of the NMDAR genes *GRIN1*, *GRIN2A*, *GRIN2B*, *GRIN3A*, and *GRIN3B*. Promoter and 5´ UTR regions regulate the expression of genes; thus, their impairments could alter protein expression and lead to a change in NMDAR function. Since the 5´ UTR sequences exhibited in our NGS dataset rare or no sequence variability of clinical significance, we restricted our analysis of genetic variants to extended promoter regions of five *GRIN* genes. The GluN1 subunit, which is encoded by the *GRIN1* gene, is an obligatory subunit within NMDAR and has the highest expression of any NMDAR subunit. The GluN2A and GluN2B subunits, which are encoded by the *GRIN2A* and *GRIN2B* genes, are both highly expressed subunits in the forebrain's highly complex structures, with their developmental switch present in some brain structures. Similarly, the GluN3A and GluN3B subunits encoded by the *GRIN3A* and *GRIN3B* genes undergo developmental switching within specific brain regions, and while they are expressed to a lesser extent among the more complex brain regions, they may provide fine-tuning of neuronal and synaptic development. In the current study, we did not include the GluN2C and GluN2D subunits with their *GRIN2C* and *GRIN2D* genes since they are mostly expressed in the less complex structures of the hindbrain and midbrain and are considered to potentially have a lower impact on the development of SCH. (Akazawa et al., 1994; Goebel & Poosch, 1999; Pérez-Otaño et al., 2016).

5.2.1. Annotation of promoter variants, determination of promoter genetic haplotypes, and functional characterisation of the haplotypes

For NMDAR genes of our interest, we analysed the promoter region, which was extended up to 2,000 bp upstream of the TSS. A parsimony method developed by Clark was used to reconstruct haplotypes from sequencing data for promoter regions (Clark, 1990). Each detected promoter variant was evaluated based on several criteria: CADD score[6] (Rentzsch et al., 2019), GERP score[7] (Cooper et al., 2005), position in a validated transcriptional regulatory element, CpG island or position that may alter the effects of chromatin modification,

[6] The Combined Annotation Dependent Depletion (CADD) framework combines different annotations into a single metric by comparing variants that have survived natural selection with variants that have been simulated. A CADD score equal to or greater than 10 suggests that these variants are predicted to be among the 10% most deleterious substitutions possible within the human genome.

[7] The Genomic Evolutionary Rate Profiling (GERP) method uses maximum likelihood evolutionary rate estimation to generate position-specific estimates of evolutionary constraints. In addition, GERP is able to detect "constrained elements", where several positions together produce a signal that indicates a putative functional element. This trace only shows the position-specific scores, not the element predictions.

frequency in the population and our samples, and its trace in previously published studies (Tab. 4). Based on this detailed variant annotation, the reconstructed haplotypes from each promoter region of each gene in each sample were restricted to certain selected variants (Fig. 11). Since the different sources refer to different transcripts and thus to different numbering of the position in the promoter, we converted the relevant information to the promoter position in canonical Ensembl transcripts where necessary (Tab. 4).

Tab. 4: **Genetic variations within the promoter region of NMDAR genes.** The summary of detected genetic variations within the promoter region (2 000 bp upstream of a TSS) with its CADD score, GERP, and MAF, together with its distribution and frequency for patients and the control group. Detected variants are completed by information about the CpG island and binding site of TFs, which they are overlapping with. Genetic variants used to generate the promoter's haplotypes are highlighted. The p-value was calculated using Fisher's exact test.

Gene	Chromosome	Coordinate (hg38)	rsID	Nucleotide change	CADD score	GERP	MAF (NFE)	highest MAF	TF / CpG island	SCH	CTRL	f SCH	f CTRL	p-Value
GRIN1	chr9	137137267	rs112434899	G/A	4.18	-0.89	0.03	0.20	/	3	2	0.02	0.03	
		137137283	rs111611214	C/T	6.30	-0.19	0.03	0.20	/	3	2	0.02	0.03	
		137137542	rs117783907	G/T	1.91	-0.49	0.08	0.37	/	14	7	0.11	0.11	
		137137745	**rs7032504**	**C/T**	**8.97**	**-0.86**	**0.36**	**0.46**	**EGR1**	**37**	**27**	**0.29**	**0.42**	
		137138227	rs949087114	T/C	2.57	-3.26	0.0003	< 0.01	EGR1, CTCF	1	1	0.01	0.02	
		137138632	**rs11146020**	**G/C**	**5.81**	**-1.65**	**0.10**	**0.38**	**EGR1, CTCF**	**18**	**10**	**0.14**	**0.16**	
		137139131	**rs1204967435**	**C/T**	**13.34**	**-0.08**	**1.55e^{-5}**	**< 0.01**	**CpG, TEAD4, HES7**	**1**	**1**	**0.01**	**0.02**	
GRIN2A	chr16	10182486	rs569661294	G/A	18.97	0.14	0.004	0.03	CpG	0	2	0.00	0.03	
		10182602/10182607	rs5815566	CCCCC/CCCCC	/	-1.16	2.02e^{-4}	0.11	CpG	1	0	0.01	0.00	
		10182795	rs45467098	C/T	10.21	-2.51	0.01	0.10	CpG	1	2	0.01	0.03	
		10183211	**rs181870048**	**C/T**	**15.59**	**2.13**	**0.004**	**0.01**	**CpG, PRDM14**	**1**	**0**	**0.01**	**0.00**	
		10183406	**rs117609472**	**C/T**	**7.15**	**-4.23**	**0.11**	**0.14**	**CpG, PRDM14**	**6**	**5**	**0.05**	**0.08**	
		10183621	**rs144674641**	**A/C**	**15.59**	**-4.23**	**0.04**	**0.05**	**/**	**2**	**0**	**0.02**	**0.00**	
		10183677	**rs3785185**	**G/A**	**17.17**	**-0.39**	**0.32**	**0.41**	**/**	**42**	**18**	**0.33**	**0.28**	
		10184301	rs4780874	G/T	3.71	-1.06	0.32	0.43	/	43	17	0.34	0.27	
		10184362	rs4780876	C/T	2.19	-1.20	1.62e^{-4}	0.079	/	1	0	0.01	0.00	
GRIN2B	chr12	**13980398**	**rs3764030**	**C/T**	**17.16**	**-2.54**	**0.19**	**0.46**	**/**	**37**	**13**	**0.29**	**0.20**	
		13980457	rs76826810	G/A	19.28	1.79	0.10	0.12	/	9	5	0.07	0.08	
		13980894	rs145433203	A/ACG	/	1.89	0.07	0.32	MEIS1, MAX	3	5	0.02	0.08	
		13981450	rs117225756	T/G	4.13	-2.65	0.03	0.05	/	1	1	0.01	0.02	
		13981761	rs539720686	A/G	14.56	-0.30	0.01	0.02	CpG, ZNF263	1	2	0.01	0.03	
		13981896	rs991760522	G/A	9.75	-0.65	2.945e^{-5}	< 0.01	CpG	1	0	0.01	0.00	
		13981909	**rs1019385**	**C/A**	**0.65**	**-3.56**	**0.46**	**0.49**	**CpG, CTCF**	**70**	**30**	**0.56**	**0.47**	
		13981935	rs111988772	G/T	8.10	-0.66	0.11	0.13	CpG	10	5	0.08	0.08	
		13982130	**rs3764028**	**G/T**	**10.52**	**-0.66**	**0.03**	**0.41**	**CpG, FOXP1, CTCF**	**9**	**0**	**0.07**	**0.00**	**0.030**
		13982341	**rs1024893**	**T/A**	**12.13**	**-3.86**	**0.28**	**0.30**	**FOXP1, CTCF**	**28**	**22**	**0.22**	**0.34**	
GRIN3A	chr9	101738689	rs1012396242	C/T	20.3	2.75	1.47e^{-5}	< 0.01	CpG, CTCF, TBP	1	0	0.01	0.00	
		101739285	**rs2067056**	**T/C**	**0.68**	**-5.04**	**0.50**	**0.50**	**CpG, CTCF**	**62**	**33**	**0.49**	**0.52**	
		101739320	**rs2067057**	**A/G**	**2.02**	**-7.37**	**0.50**	**0.50**	**CTCF**	**62**	**33**	**0.49**	**0.52**	
		101739539	**rs12338602**	**C/T**	**14.46**	**1.84**	**0.22**	**0.26**	**SP1**	**28**	**17**	**0.22**	**0.27**	
		101740055	**rs62577465**	**G/A**	**9.24**	**-0.38**	**0.04**	**0.23**	**/**	**5**	**1**	**0.04**	**0.02**	
		101740126	rs116863968	G/A	4.71	2.10	0.004	0.02	/	1	0	0.01	0.00	
		101740412	rs531165825	C/T	1.29	-2.90	0	0.01	/	1	0	0.01	0.00	
		101740476	rs190501091	G/T	0.09	-3.28	0.02	0.04	/	3	1	0.02	0.02	
GRIN3B	chr19	**998618**	**rs11667281**	**C/T**	**9.03**	**-1.78**	**0.50**	**0.50**	**POLR2G, CTCF**	**66**	**42**	**0.52**	**0.66**	
		998637	rs987292965	A/G	1.60	-1.89	4.651e^{-5}	< 0.01	POLR2G, CTCF	1	0	0.01	0.00	
		998687	rs11667292	C/T	2.71	-2.67	0.50	0.50	POLR2G, CTCF	66	42	0.52	0.66	
		998689	rs77920892	C/T	2.32	-2.67	0.001	0.28	POLR2G, CTCF	1	0	0.01	0.00	
		998799	**rs11669927**	**T/C**	**0.27**	**-0.54**	**0.54**	**0.49**	**POLR2G, EGR1**	**75**	**44**	**0.60**	**0.69**	
		998856	rs12609062	C/T	2.96	-2.34	0.50	0.50	POLR2G, EGR1	60	22	0.48	0.34	
		999000	rs11672296	G/C	2.82	1.08	0.50	0.50	POLR2G, EGR1	66	42	0.52	0.66	
		999078	rs912841654	C/T	6.47	0.70	1.471e^{-5}	< 0.01	POLR2G, EGR1	1	0	0.01	0.00	
		999081	rs11669794	A/G	7.64	-0.26	0.50	0.50	POLR2G, EGR1	66	42	0.52	0.66	
		999093	/	C/T	3.52	/	/	/	POLR2G, EGR1	1	0	0.01	0.00	
		999106	rs7258402	G/A	0.11	-2.52	0.50	0.50	POLR2G, EGR1	66	42	0.52	0.66	
		999122	rs1016974610	G/T	13.21	0.06	0.001	0.01	POLR2G, EGR1	1	0	0.01	0.00	
		999319	rs80031813	C/G	1.79	-2.02	7.349e^{-5}	0.15	EGR1	1	0	0.01	0.00	
		999440	rs112661396	C/T	0.83	-1.37	0.03	0.14	EGR1, CTCF	3	2	0.02	0.03	
		999455	rs28405870	T/C	2.33	-1.74	0.50	0.50	EGR1, CTCF	66	42	0.52	0.66	
		999562	/	G/A	6.61	/	/	/	EGR1, CTCF	1	0	0.01	0.00	
		999583	rs58147703	A/G	5.08	-1.62	0.50	0.50	EGR1, CTCF	66	42	0.52	0.66	
		999674	rs11670014	A/C	3.62	-0.53	0.50	0.50	EGR1, CTCF	66	42	0.52	0.66	
		999838	rs11670089	A/G	5.81	-0.67	0.50	0.50	EGR1, CTCF	66	42	0.52	0.66	
		999973	rs537234536	C/T	1.37	-0.21	0.006	0.01	CTCF	2	0	0.02	0.00	
		999976	rs192907016	C/T	1.24	-0.21	0.004	0.18	CTCF	2	0	0.02	0.00	
		1000018	rs143597747	G/T	4.44	0.27	0.001	0.28	CTCF	1	0	0.01	0.00	
		1000053	rs34418036	T/C	4.16	-0.21	0.50	0.50	CTCF	64	41	0.51	0.64	
		1000093	rs113901306	G/C	3.51	0.27	0.03	0.14	CTCF	3	2	0.02	0.03	
		1000095	**rs35873901**	**A/G**	**5.71**	**-0.45**	**0.48**	**0.50**	**CTCF**	**63**	**41**	**0.50**	**0.64**	
		1000154	rs62134211	G/A	2.63	-1.65	0.48	0.50	CTCF	63	41	0.50	0.64	
		1000167	rs35581531	C/T	4.26	0.78	0.48	0.50	CTCF	63	41	0.50	0.64	
		1000176	**rs72971670**	**G/A**	**4.52**	**0.68**	**0.18**	**0.37**	**CTCF, JDP2, NFE2, BACH1**	**18**	**5**	**0.14**	**0.08**	

Abbreviation Key: CADD, Combined Annotation Dependent Depletion; GERP, Genomic Evolutionary Rate Profiling; MAF, Minor allele frequency; NFE, Non-Finnish European; TF, transcriptional factor

5.2.1.1. GRIN1

All promoter variants refer to the translation start site (ATG) and the TSS of the canonical *GRIN1* transcript ENST00000371561.8 from Ensembl. To elucidate the effects of the variants, bioinformatic analysis was performed to identify possible functional determinants of the promoter. A recently published study (Y. Liu et al., 2022) has highlighted a single transcriptional activation site (-337 to -556 bp relative to ATG) and two repression regions (-159 to -337 bp and -556 to -704 bp relative to ATG) within the *GRIN1* proximal promoter. The TATA box-like motif recognised by the EPD (Eukaryotic Promoter Database) starts at position 296 bp upstream from the TSS, too far to act as a functional promoter element (Ponjavic et al., 2006). Instead, the region near the TSS is GC-rich (75%) and harbours two tandem proximal GC-box-like motifs 5´ GGGCGGCGGGAGGG 3´ (40 to 53 bp upstream of the TSS) within a 24 bp GC-rich region that is divided into two highly conserved blocks (93.70% for block-1 and 99.34% for block-2, phastCons100way) interrupted by a single low-conserved nucleotide.

Another highly conserved (97.75%, phastCons100way) GC-rich motif 5´ GGAGGCG 3´ is located 81 to 88 bp upstream of the TSS, and finally a third GC-rich moderately conserved sequence, 5´ ACGCAGGCGC 3´, which is joined in the middle by a single low-conserved nucleotide (73.73% for block-1 and 88.19% for block-2, phastCons100way), is located 102 to 111 bp upstream of the TSS and is characterised as the site of H3K4me1 modification. All these GC-rich elements are covered by the -337 to -556 bp long transcriptional activation region. It appears that the proximal GC boxes are sufficient to drive neuronal-specific transcription at both the basal and induced levels required for spatially and temporally specific expression (Ross et al., 2002; Ulfhammer et al., 2016). Transcription factors known to bind the GC-rich motifs in neuronal cells include Sp1, Sp3, and Sp4. In addition, the Sp4 gene has recently been validated as a SCH risk gene (X. Zhou, 2022).

Overall, we detected seven single nucleotide variants within the extended *GRIN1* promoter, but only three of them (rs1204967435, rs11146020, and rs7032504) could have a potential functional impact according to our evaluation (Tab. 4).

The rs1204967435 (hg38:chr9:g.137139131, C>T) represents a moderately conserved nucleotide with a CADD score of 13.34 that changes the core matrix of the TEAD4:HES7 transcription factor binding site to a less similar consensus sequence. The variant is rare, with a minor allele frequency in gnomADg for the non-Finnish European (NFE) population of 0.0000155.

The rs11146020 (hg38:chr9:g.137138632, G>C) is a low conserved nucleotide with a CADD score of 5.809, but it is listed in the PharmGKB and SNPedia databases as a variant associated

with response to clozapine (an antipsychotic drug used for SCH treatment) (Hwang et al., 2011) and as a variant associated with SCH (Georgi et al., 2007; Zhao et al., 2006). In addition, the variant is located within the transcription factor binding site (ORegAnno ID: OREG1518522) (Portales-Casamar et al., 2009; Lesurf et al., 2016) for the EGR1 and CTCF transcription factors (PAZAR dataset). The minor allele frequency in gnomADg for the NFE population is 0.098.

The last variant rs7032504, (hg38:chr9:g.137137745, C>T) is a low-conserved nucleotide with a CADD score of 8.967. The variant is also located within the transcription factor binding site (ORegAnno ID: OREG1518522) (Portales-Casamar et al., 2009; Lesurf et al., 2016) for the EGR1 transcription factor (PAZAR dataset). The minor allele frequency in gnomADg for the NFE population is 0.375.

With these three variants of the extended *GRIN1* promoter, five different haplotypes were recognised (Fig. 11; Tab. 5).

The most prevalent haplotype, termed GRIN1_1 (CGC), showed a 58% occurrence in the group of patients and 42% in the group of controls. Notably, this haplotype was significantly more frequent among cases compared to controls ($p = 0.046$). However, it's important to note that this particular haplotype was also fairly well represented in the control group. Two other highly represented haplotypes were GRIN1_2 (TGC), observed in 27% of patients and 41% of control subjects, and GRIN1_3 (CCC), with a frequency of 12% in patients and 14% in controls. The remaining two haplotypes, GRIN1_4 (TCC) and GRIN1_5 (CGT), did not exceed a frequency of 5% in either the SCH or control groups, and they did not exhibit a significantly higher number of occurrences in cases compared to controls. As a result, they were not further functionally analysed (Tab. 5).

Promoter haplotypes GRIN1_1, GRIN1_2, and GRIN1_3 were further cloned into the pGL4 Luciferase Reporter Vector, and their promoter activity was tested by luciferase assay. The results were normalised to the promoter haplotype GRIN1_1, which exhibits the highest prevalence in the control group (although, in this particular case, the promoter is significantly more represented by the SCH group). The results then showed significantly higher relative luciferase activity for haplotype GRIN1_2 (5.2 times higher, $p = 0.005$) and for haplotype GRIN1_3 (4.2 times higher, $p = 0.035$), suggesting low activity of promoter haplotype GRIN1_1, which was present significantly higher in the patient group compared to control subjects (Fig. 12A).

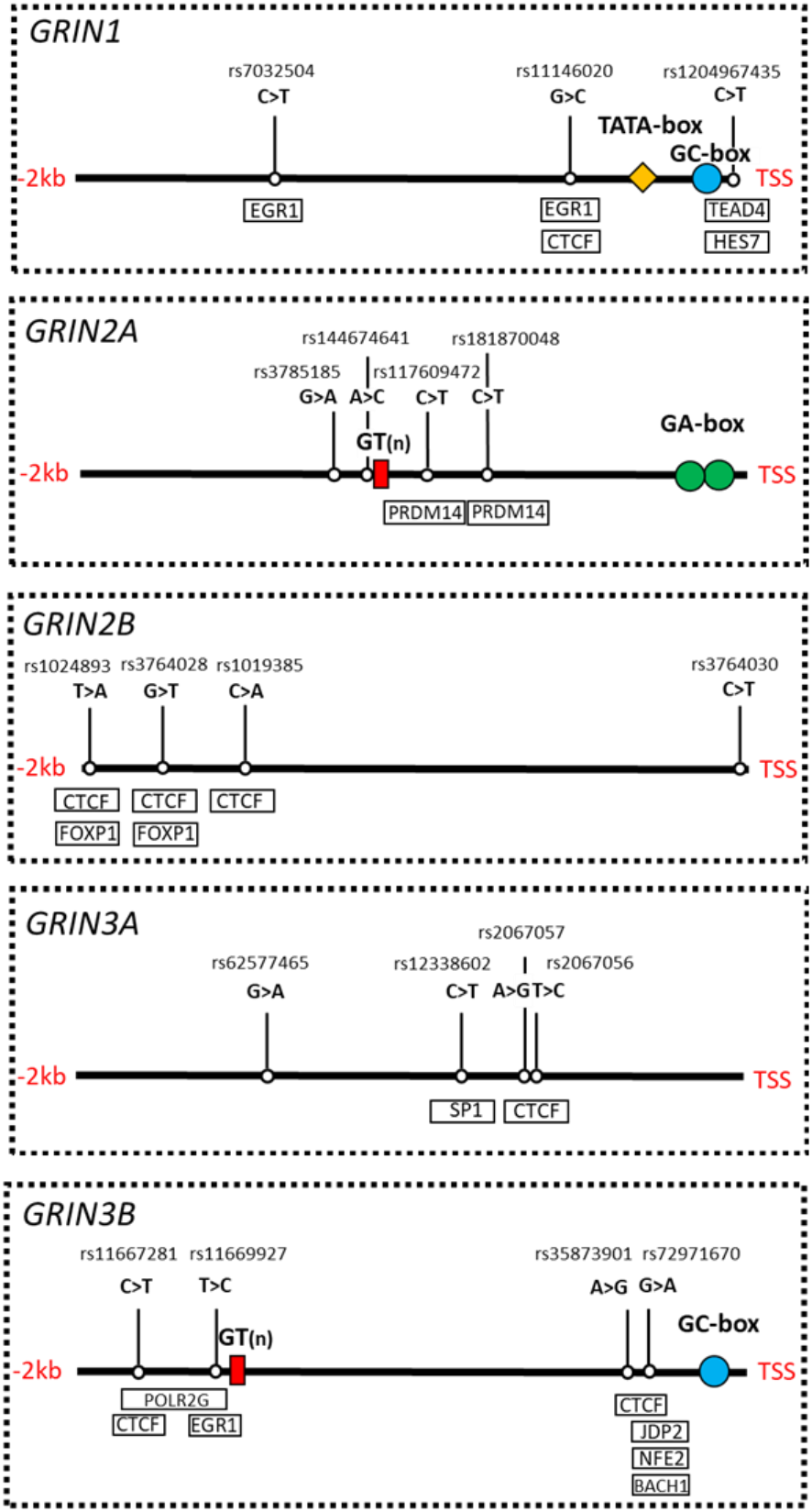

Fig. 11: **Schematic diagram of the selected NMDAR gene's promoter regions.** Promoter regions (2000 bp upstream of a TSS) are completed by genetic variations used to generate genetic haplotypes and by TF binding sites overlapping with the position of selected genetic variants. Promoter elements are given by the Eukaryotic Promoter Database (EPD).

5.2.1.2. GRIN2A

All promoter variants refer to the TSS of a canonical *GRIN2A* ENST00000330684.4 transcript from Ensembl, which corresponds to the GRIN2A2 promoter from the EPD database. Our bioinformatic analysis revealed, that TATA-less promoter is rich in GA-box motifs (5´ GGGAGG 3´). Four proximal GA-box motifs are located at positions -150 to -155, -164 to -169, -171 to -176 and -192 to -197 upstream of the TSS, but only the second motif is part of a conserved element. The region near the TSS has a GC content of 68%. Since the ETS family of transcription factors has been proposed to regulate GRIN2B transcription (Y. Jiang et al., 2017), the proximal promoter of *GRIN2A* was checked for the presence of their core binding motif (5´GGAA/T 3´) and several were found.

Eleven variants were detected in the extended promoter of both cases and controls. All variants were manually annotated, and those with predictions of possible functional effects were further analysed. The following four variants were used to reconstruct haplotypes (Tab. 4).

The first variant, rs181870048 (hg38:chr16:g.10183211 C>A = G>T in the coding strand), is a highly conserved nucleotide with a CADD score of 15.59. It resides in the region of a CpG island within an area of enhancer regulatory element (GH16J010180, GeneHancer Regulatory Elements) and a transcription factor binding site (ORegAnno ID: OREG1834849) for the PRDM14 transcription factor (PAZAR dataset). The minor allele frequency in gnomADg for the NFE population is 0.004.

The second variant, rs117609472 (hg38:chr16:g.10183406 C>T = G>A in the coding strand), is a low conserved nucleotide with a CADD score of 7.150, but still within the CpG island, a promoter enhancer region (GH16J010180, GeneHancer Regulatory Elements), and a transcription factor binding site (ORegAnno ID: OREG1834849). There is also a strong H3K27Ac modification in the surrounding region. The minor allele frequency in gnomADg for the NFE population is 0.110.

The third variant, rs144674641 (hg38:chr16:g.10183621 A>C = T>G in the coding strand), is a low-conserved nucleotide with a CADD score of 15.59. The variant is still located in the enhancer regulatory element or promoter (GH16J010180, GeneHancer Regulatory Elements) and in the region of H3K27Ac modification. The minor allele frequency in gnomADg for the NFE population is 0.042.

The last variant, rs3785185 (hg38:chr16:g.10183677 G>A = C>T in the coding strand), is a moderately conserved nucleotide with a CADD score of 17.17, again residing in the enhancer regulatory element (GH16J010180 GeneHancer Regulatory Elements) and a region of H3K27Ac and H3K4me3 modifications. The AA genotype was revealed as a risk factor for

major depressive disorder development (Yin et al., 2016). The minor allele frequency in gnomADg for the NFE population is 0.318.

Using the four variants from the *GRIN2A* promoter, five distinct haplotypes were recognised (Fig. 11; Tab. 5).

The most prevalent haplotype, GRIN2A_1 (CACC), demonstrated an equal distribution, appearing in 61% of the SCH group and 64% of the control group. Two other notably represented haplotypes were GRIN2A_2 (AACC) found in 32% of cases and 28% of control subjects, and GRIN2A_3 (GATC) with a frequency of 5% in patients and 8% in controls. In contrast, the remaining two haplotypes, GRIN2A_4 (ACCC) and GRIN2A_5 (GACT), did not exceed a frequency of 5% in either the SCH or control group, and these haplotypes were not further functionally analysed. It's important to note that none of the detected haplotypes displayed significantly higher representation for either of the groups (Tab. 5).

The promoter haplotypes GRIN2A_1, GRIN2A_2, and GRIN2A_3 were cloned into the pGL4 Luciferase Reporter Vector, and their promoter activity was measured with a luciferase assay. The data were normalised to the GRIN2A_1 promoter haplotype with the highest prevalence in the control group. The results then revealed that haplotype GRIN2A_2 (3.5 times higher, $p = 0.008$) and haplotype GRIN2A_3 (5.3 times higher, $p = 0{,}001$) had significantly higher relative luciferase activity compared to haplotype GRIN2A_1, and haplotypes GRIN2A_2 and GRIN2A_3 also exhibit a significant difference between each other as well ($p = 0.042$). Differences in relative promoter activity are difficult to interpret since each promoter haplotype has comparable patient and control subject distributions. Hence, observed differences may represent natural variability in promoter haplotypes and their activities (Fig. 12B).

Tab. 5: **Promoter's haplotypes of selected NMDAR genes.** The summary of generated haplotypes for selected NMDAR genes, together with their representation and frequency for patients and the control group. Genetic haplotypes used further in functional analysis are highlighted. The most frequent haplotypes in the control group are underlined. The p-value was calculated using Fisher's exact test.

Gene	Promoter haplotype		SCH	CTRL	f SCH	f CTRL	p-value
GRIN1	**1**	**CGC**	**73**	**27**	**0.58**	**0.42**	**0.046**
	2	**TGC**	**34**	**26**	**0.27**	**0.41**	
	3	**CCC**	**15**	**9**	**0.12**	**0.14**	
	4	TCC	3	1	0.02	0.02	
	5	CGT	1	1	0.01	0.02	
			126	64	1.00	1.00	
GRIN2A	**1**	**GACC**	**77**	**41**	**0.61**	**0.64**	
	2	**AACC**	**40**	**18**	**0.32**	**0.28**	
	3	**GATC**	**6**	**5**	**0.05**	**0.08**	
	4	ACCC	2	0	0.02	0.00	
	5	GACT	1	0	0.01	0.00	
			126	64	1.00	1.00	
GRIN2B	**1**	**TGAT**	**35**	**13**	**0.28**	**0.20**	
	2	**TGAC**	**34**	**17**	**0.27**	**0.27**	
	3	**AGCC**	**25**	**22**	**0.20**	**0.34**	**0.034**
	4	**TGCC**	**20**	**12**	**0.16**	**0.19**	
	5	**TTCC**	**9**	0	**0.07**	**0.00**	**0.030**
	6	AGCT	2	0	0.02	0.00	
	7	AGAC	1	0	0.01	0.00	
			126	64	1.00	1.00	
GRIN3A	**1**	**GCGC**	**62**	**33**	**0.49**	**0.52**	
	2	**GCAT**	**31**	**13**	**0.25**	**0.20**	
	3	**GTAT**	**28**	**17**	**0.22**	**0.27**	
	4	ACAT	5	1	0.04	0.02	
			126	64	1.00	1.00	
GRIN3B	**1**	**TCGG**	**65**	**41**	**0.52**	**0.64**	
	2	**CTAG**	**33**	**15**	**0.26**	**0.23**	
	3	**CTAA**	**18**	**5**	**0.14**	**0.08**	
	4	**CCAG**	**9**	**2**	**0.07**	**0.03**	
	5	TCAG	1	1	0.01	0.02	
			126	64	1.00	1.00	

5.2.1.3. GRIN2B

In the case of the *GRIN2B* gene, all promoter variants refer to the TSS of an original canonical Ensembl *GRIN2B* ENST00000609686.1 transcript and its corresponding promoter, the GRIN2B1 EPD promoter. The current canonical transcript version ENST00000609686.4 is extended by an additional non-coding exon and corresponds to the GRIN2B2 EPD promoter.

Our bioinformatic analysis revealed that within the *GRIN2B* promoter, there are no TATA-box or proximal GC-box motifs near the TSS in either the GRIN2B1 or GRIN2B2 promoter sequences. The nucleotides in the vicinity of the TSS (50 bp downstream and 50 bp upstream) are usually highly conserved (98–100%) in vertebrates (phastCons100way). The region near the TSS of the GRIN2B1 promoter has a GC content of 50%. GRIN2B was previously identified as a target of ETS transcription factors that bind a specific core motif of 5´GGAA/T 3´ (Sementchenko & Watson, 2000; Hollenhorst et al., 2011; Y. Jiang et al., 2017). The extended GRIN2B1 promoter was analysed and after manual annotation, the following four variants were used to reconstruct haplotypes (Tab. 4).

The rs3764030 variant (hg38:chr12:g.13980398 C>T = G>A in the coding strand) is a low-conserved nucleotide, exhibiting a CADD score of 17.16. It's located within an ENCODE Candidate Cis-Regulatory Element marked by a promoter-like signature (EH38E1594613) and shows significant H3K27Ac modification (Dunham et al., 2012). In the gnomADg database, its minor allele frequency among the NFE population is 0.191. A functional analysis suggested that this variant might be a gain-of-function variant, creating a novel ETS binding site (Y. Jiang et al., 2017). Additionally, another study associated this variant with cognitive impairment (Han et al., 2017).

The second variant, rs1019385 (hg38:chr12:g.13981909 C>A = G>T in the coding strand), is a low conserved nucleotide with a low CADD score of 0.648. It's situated within a CpG island and a CTCF binding site (ENCODE TF ChIP-seq) (Dunham et al., 2012). In the gnomADg database, its minor allele frequency among the NFE population is 0.456 (the T allele in the coding strand). The variant has records in the SNPedia and PharmGKB databases (PA166154508) and has been the subject of various studies, albeit with varying degrees of success in establishing disease associations (Kohlrausch et al., 2016; Varner et al., 2020; Vuletić et al., 2021).

The third variant, rs3764028 (hg38:chr12:g.13982130 T>G = A>C in the coding strand), is a moderately conserved nucleotide with a CADD score of 10.52, where G represents the ancestral allele. This variant resides within recognised transcription factor binding sites: ORegAnno ID: OREG1608605 (FOXP1) and OREG1372861 (CTCF) based on the PAZAR

dataset. Its record can be found in the SNPedia database. The surrounding region shows significant H3K27Ac modifications as well. In the gnomADg database, the minor allele frequency for the NFE population is 0.029 (an allele on the coding strand). Studies indicate that the ancestral C allele (on the coding strand) exhibits reduced transcriptional activity compared to the A allele (H. Jiang & Jia, 2009). Additionally, this variant has been investigated in several association studies, yielding varying degrees of success (H. Jiang & Jia, 2009; Zhong et al., 2017; Silvennoinen et al., 2020).

The last variant, rs1024893 (hg38:chr12:g.13982341 T>A = A>T in the coding strand), represents a low conserved nucleotide with a CADD score of 12.13. Similar to the previous variant, it's situated within recognised transcription factor binding sites: ORegAnno ID OREG1608605 (FOXP1) and OREG1372861 (CTCF), according to the PAZAR dataset. Moreover, it resides within an ENCODE Candidate Cis-Regulatory Element, displaying a proximal enhancer-like signature (EH38E1594618). Surrounding this variant are notable H3K27Ac and H3K4me3 modifications. Ensembl data indicates that this variant alters the fourth position of the binding matrix ENSPFM0017 (5´ATGACTCAT 3´) for transcription factors JDP2, NFE2, and BACH1. The matrix suggests that only an A (in the coding strand) is tolerated at the fourth position, and the change to T significantly diminishes the consensus binding sequence. In the gnomADg database, the minor allele frequency for the NFE population is 0.277 (T allele on the coding strand).

The above-mentioned variants were used to reconstruct seven distinct haplotypes (Fig. 11; Tab. 5).

The most prevalent haplotype within control subjects, GRIN2B_3 (AGCC), was found in 20% of the patient group and 34% of the control group. Notably, this haplotype was significantly more frequent among the control group compared to the cases ($p = 0.034$). Among SCH patients, the most prevalent promoter haplotype was GRIN2B_1, accounting for 28%, while it was represented by 20% in the control group. Two other highly represented haplotypes were GRIN2B_2 (TGAC), observed in 27% of SCH patients and 27% of control subjects, and GRIN2B_4 (TGCC), with a frequency of 16% in patients and 19% in controls. The promoter haplotype GRIN2B_5 (TTCC) was exclusively present in the patient group, accounting for 7%, resulting in significant differences between the groups ($p = 0.03$). The remaining two haplotypes, GRIN2B_6 (AGCT) and GRIN2B_7 (AGAC), were underrepresented in either the SCH or control group and were not further functionally analysed (Tab. 5).

The GRIN2B_1, GRIN2B_2, GRIN2B_3, GRIN2B_4, and GRIN2B_5 promoter haplotypes were cloned into the pGL4 Luciferase Reporter Vector. A luciferase assay was then used to measure the activity of their promoters. The data were normalised to the most prevalent

promoter haplotype, GRIN2B_3, in the control group. The results showed that haplotype GRIN2B_5, which was only found in the patients' group, had significantly higher relative luciferase activity than other haplotypes GRIN2B_1 (1.7 times higher, p = 0.043), GRIN2B_3 (1.8 times higher, p = 0.015), and GRIN2B_4 (2 times higher, p = 0.003). These differences showed an exclusive SCH promoter haplotype with low prevalence and significantly higher relative luciferase activity compared to most of the equally represented GRIN2B promoter haplotypes (Fig. 12C).

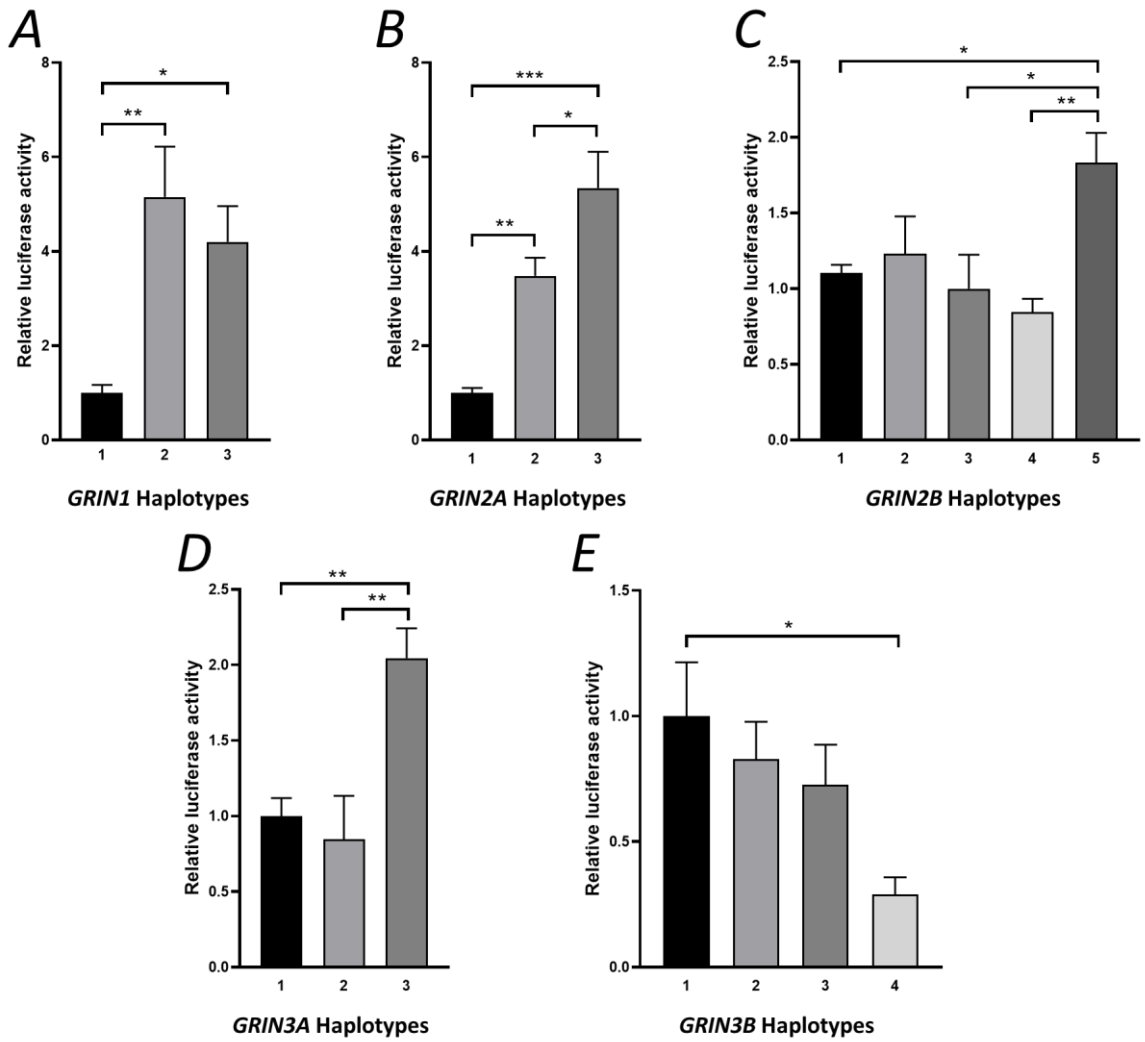

Fig. 12: **Various NMDAR gene promoter haplotypes alter its promoter activity.** Summary of relative luciferase activity for selected haplotypes of the NMDAR gene *GRIN1* (***A***), *GRIN2A* (***B***), *GRIN2B* (***C***), *GRIN3A* (***D***), and *GRIN3B* (***E***). Luciferase activity was measured in triplicate from three to four independent experiments (n = 8–12) and then normalised to the most frequent haplotype in the control group for each NMDAR gene. All summary data are presented as the mean ± SEM; *, p < 0.05, analysed by one-way ANOVA and Tukey's multiple comparison test.

5.2.1.4. GRIN3A

The promoter variants are specifically associated with the TSS of the Ensembl canonical *GRIN3A* ENST00000361820.6 transcript, which corresponds to the GRIN3A1 promoter in the EPD database. Notably, our bioinformatic analysis did not identifiy any apparent TATA-box or GC-box motifs in close proximity to this TSS. The region around the TSS maintains a GC content of 59%. Unlike previous genes studied, the 5´ UTR region of *GRIN3A* displays common variability, but none of the detected minor allele frequencies have shown significant differences between SCH cases and controls (Y.-C. Shen et al., 2009; Hirschfeldova et al., 2021).

The area adjacent to the TSS exhibits relatively low conservation. However, it contains several ENCODE Candidate Cis-Regulatory Elements, including a CpG island. Specifically, two elements bear a proximal enhancer-like signature (EH38E2713417 covering the GRIN3A_2 promoter from the EPD database and EH38E2713419), and one carries a promoter-like signature (EH38E2713418 covering the GRIN3A_1 promoter from the EPD database).

The analysis of the extended GRIN3A_1 promoter revealed four specific variants that were included in the reconstructed haplotypes (Tab.4). Overall, these detected common variants exhibit predominantly low conservation levels, characterised by low CADD scores.

The variant rs2067056 (hg38:chr9:g.101739285 T>C = A>G in the coding strand) is in complete linkage with variant rs2067057 (hg38:chr9:g.101739320 A>G = T>C in the coding strand). Both variants exhibit low conservation levels, with CADD scores of 0.675 and 2.016, respectively. They are situated within a CTCF binding region that shows moderate levels of H3K27Ac modification. In the gnomADg database, the minor allele frequency (GC haplotype on the coding strand) for the NFE population is 0.498.

The third variant, rs12338602 (hg38:chr9:g.101739539 C>T = G>A in the coding strand), is notably highly conserved, with a CADD score of 14.46. It is positioned within an ENCODE Candidate Cis-Regulatory Element distinguished by a proximal enhancer-like signature (EH38E2713419) and is suspected to harbour an SP1 transcription factor binding site. In the gnomADg database, this variant exhibits a minor allele frequency of 0.222 within the NFE population.

The final variant, rs62577465 (hg38:chr9:g101740055 G>A = C>T in the coding strand), is a moderately conserved nucleotide, possessing a CADD score of 9.235. Within the NFE population in the gnomADg database, its minor allele frequency is recorded as 0.043.

Using these variants, four distinct haplotypes were reconstructed (Fig. 11; Tab. 5).

The most prevalent GRIN3A_1 (GCGC) haplotype occurred in 49% of patients and 52% of controls. Two other notable haplotypes were GRIN3A_2 (GCAT), found in 25% of cases and 20% of controls, and GRIN3A_3 (GTAT), with a frequency of 22% in patients and 27% in controls. The remaining haplotype, GRIN3A_4 (ACAT), did not exceed a frequency of 5% in either group and wasn't further studied. None of these haplotypes showed significantly different representations between the patient and control groups (Tab. 5).

The GRIN3A_1, GRIN3A_2, and GRIN3A_3 promoter haplotypes were introduced into the pGL4 Luciferase Reporter Vector, and their promoter activities were assessed using a luciferase assay. The data were standardized against the GRIN3A_1 promoter haplotype, the most prevalent haplotype in the control group. The findings indicated that the GRIN3A_3 haplotype exhibited significantly higher relative promoter activity compared to both GRIN3A_1 (2 times higher, $p = 0.006$) and GRIN2A_3 (2.1 times higher, $p = 0.002$) promoter haplotypes. However, interpreting the observed differences in relative promoter activity is difficult due to the comparable distributions of these promoter haplotypes in both patient and control groups. Consequently, these differences may signify natural variations in promoter haplotypes and their activities (Fig. 12D).

5.2.1.5. GRIN3B

The promoter variants are specifically linked to the TSS of the Ensembl canonical *GRIN3B* ENST00000234389.3 transcript, corresponding to the GRIN3B1 promoter in the EPD database. Our bioinformatic analysis revealed that there's an absence of TATA-boxes, with only one GC-box motif situated 78 to 83 base pairs upstream from the TSS. The region surrounding the TSS exhibits a high GC content of 73% but demonstrates poor conservation (phastCons100way). However, this region encompasses several key elements: an ENCODE Candidate Cis-Regulatory Element displaying a promoter-like signature (EH38E1930683, partially covering the GRIN3B_1 promoter from the EPD database), a CpG island, and two transcription factor binding sites (ORegAnno ID: OREG1394020 and OREG1346353) for CTCF binding (PAZAR dataset). Additionally, the promoter shows enrichment in H3K4me1 and H3K4me3 modifications and is recognised as an RNA polymerase II binding site, as indicated by ChIP-seq tags data from CD4 cells (Barski et al., 2007).

The analysis of the extended *GRIN3B* promoter revealed a notable promoter haplotype known as the 15-HAP, comprising fifteen common variants. The distance between the most 5´end and 3´end detected variants within the 15-HAP spans 1,799 base pairs, encompassing the promoter signature (EH38E1930683 and GRIN3B1), along with CTCF (OREG1394020; OREG1346353; EH38E1930681) and EGR1 (OREG1495984) transcription factor binding sites.

Several variants within the 15-HAP haplotype are designated as moderately positive expression Quantitative Trait Loci (eQTL) based on GTEx Analysis V6p (https://www.gtexportal.org/home/datasets). The 15-HAP comprises the following variants: rs11667281, rs11667292, rs12609062, rs11672296, rs11669794, rs7258402, rs28405870, rs58147703, rs11670014, rs11670089, rs34418036, rs35873901, rs62134211, rs35581531, rs112743753, generating corresponding allele combinations: [CCTGAGTAAATAGCA]/[TTCCGACGCGCGATG]. The estimated minor allele frequency of the 15-HAP based on gnomADg data for the NFE population is 0.498. This region shows substantial variability, housing not only the 15-HAP haplotype but also several less common variants.

The rs11667281 (hg38:chr19:g.998618 C>T) was then selected as a tagging variant for the entirety of the 15-HAP due to its highest CADD score of 9.031. This variant is situated within the candidate CTCF binding site (EH38E1930681) and a region characterised by abundant H3K27Ac modification.

During the data analysis, two recombination events were observed. Both recombination events disrupted the 15-HAP between rs11670089 and rs34418036, which are only 215 base pairs apart. Interestingly, this disruption occurred within a region housing tandemly organized two SINE repeat elements, AluSx1 and AluSx3, suggesting that these elements could be a potential site for recombination hotspots. Based on the gathered data, the probability of recombination in this region is estimated to be around 1%.

In light of this, rs35873901 (hg38:chr19:g.1000095 A>G) was included in the reconstruction of the promoter haplotype as a second variant from the 15-HAP capable of identifying recombinants.

Selecting variants outside the scope of the 15-HAP within the extended promoter, a manual annotation process was conducted. Additional two variants were chosen from this set, and in combination with the two variants from the 15-HAP, they were employed for the reconstruction of GRIN3B promoter haplotypes (Tab. 4).

The variant rs11669927 (hg38:chr19: g.998799 T>C) is characterised as a low conserved nucleotide, displaying a CADD score of 0.268. This variant is positioned within the EGR1 (OREG1495984) transcription factor binding site. Moreover, it has been identified as a moderately positive expression Quantitative Trait Loci (eQTL) based on the GTEx Analysis V6p dataset (https://www.gtexportal.org/home/datasets). Although it is in linkage with the 15-HAP, it does not form a complete linkage (r2 is 0.752203 and D´ is 0.999994). In the gnomADg database, the minor allele frequency for the NFE population is recorded as 0.459.

The last variant, rs72971670 (hg38:chr19:g.1000176G>A), represents a moderately conserved nucleotide with a CADD score of 4.518. It is located within an element exhibiting a promoter-like signature (EH38E1930683), two suspected CTCF binding sites (OREG1394020 and OREG1346353), and a region marked with H3K4me1 modification. Additionally, according to Ensembl, this variant alters the ninth position of the binding matrix ENSPFM0017 (5´ATGACTCAT 3´) for transcription factors JDP2, NFE2, and BACH1. The substitution from G to A is suggested by the matrix to create a sequence more in line with the consensus binding sequence for these transcription factors. In the gnomADg database, the minor allele frequency for the NFE population is reported as 0.175.

Using the variants (rs11667281, rs11669927, rs35873901, and rs72971670), five distinct haplotypes were reconstructed based on their specific occurrences (Fig. 11; Tab. 5).

The most prevalent haplotype, GRIN3B_1 (TCGG), was observed in 52% of the patient group and 64% of the control group. Three others notably represented haplotypes were GRIN3B_2 (CTAG), found in 26% of patients and 23% of controls, GRIN3B_3 (CTAA), occurring in 14% of patients and 8% of control subjects, and GRIN3A_4 (CCAG), with a frequency of 9% in patients and 2% in controls. The remaining represented haplotype, GRIN3B_5 (TCAG), did not exceed a frequency of 5% in either group and was not further studied. Notably, none of these haplotypes displayed significantly different representations in specific promoter haplotypes between the patient and control groups (Tab. 5).

The GRIN3B_1, GRIN3B_2, GRIN3B_3, and GRIN3B_4 promoter haplotypes were inserted into the pGL4 Luciferase Reporter Vector to assess their promoter activity through a luciferase assay. The promoter activity was normalised to the most prevalent GRIN2A_1 promoter haplotype. The results indicated a significant decrease in relative luciferase activity for the haplotype GRIN3B_4 compared to the GRIN3B_1 haplotype (71% decrease, $p = 0.016$). The observed variations in relative promoter activity are challenging to decipher, given the similar distribution of both promoter haplotypes among patients and control subjects. However, while GRIN3B_1 showed lower representation in the patient group, GRIN3B_4 was predominantly represented by the patients (Fig. 12E).

Additionally, within the *GRIN3B* extended promoter, the $(GT)_n$ microsatellite (rs3222791) resides at position 1502 upstream of the canonical TSS. Up to the date, there is no publication describing this $(GT)_n$ repeat. However, based on the previously analysed similar $(GT)_n$ microsatellite (rs3219790) within the *GRIN2A* promoter, where longer repeats were significantly associated with SCH and increased inhibition of transcriptional activity (Itokawa, Yamada, Yoshitsugu, et al., 2003; Tang et al., 2006; R. Liu et al., 2015), we examined the *GRIN3B* $(GT)_n$ microsatellite as a potential risk factor for SCH.

Initially, we cloned various *GRIN3B* promoters (haplotype GRIN3B_1), each featuring a different number of $(GT)_n$ repeats (0, 10, 13, 16, 17, and 20). Subsequently, these *GRIN3B* promoters with varying $(GT)_n$ repeat counts were introduced into the pGL4 Luciferase reporter vector for evaluating their promoter activities via a luciferase assay. The outcomes were normalised to the promoter lacking the $(GT)_n$ repeat. The findings demonstrated a gradual reduction in relative luciferase activity with an increasing number of $(GT)_n$ repeats, exhibiting statistical significance ($p = 0.031$). Furthermore, the multiple comparison test revealed a significant difference between the promoters with 0 and 20 repeats of $(GT)_n$ (33% reduction for $(GT)_{20}$, $p = 0.043$) (Fig. 13A).

Simultaneously, we attempted to read the $(GT)_n$ repeats distributions in our dataset from NGS of patient and healthy control samples. Unfortunately, insufficient coverage of sequencing reads hindered our ability to accurately determine the number of $(GT)_n$ repeats within the studied region. Instead, we additionally cloned into the pGEM®-T vector *GRIN3B* promoter's regions covering $(GT)_n$ microsatellite from gDNA samples of 23 SCH and 22 controls and performed Sanger sequencing of the obtained clones, enabling us to visualise $(GT)_n$ repeat size. The results showed a higher occurrence of control subjects with promoters featuring a lower number of repeats, while patients were more prevalent in promoters containing longer $(GT)_n$ repeats (Fig. 13B).

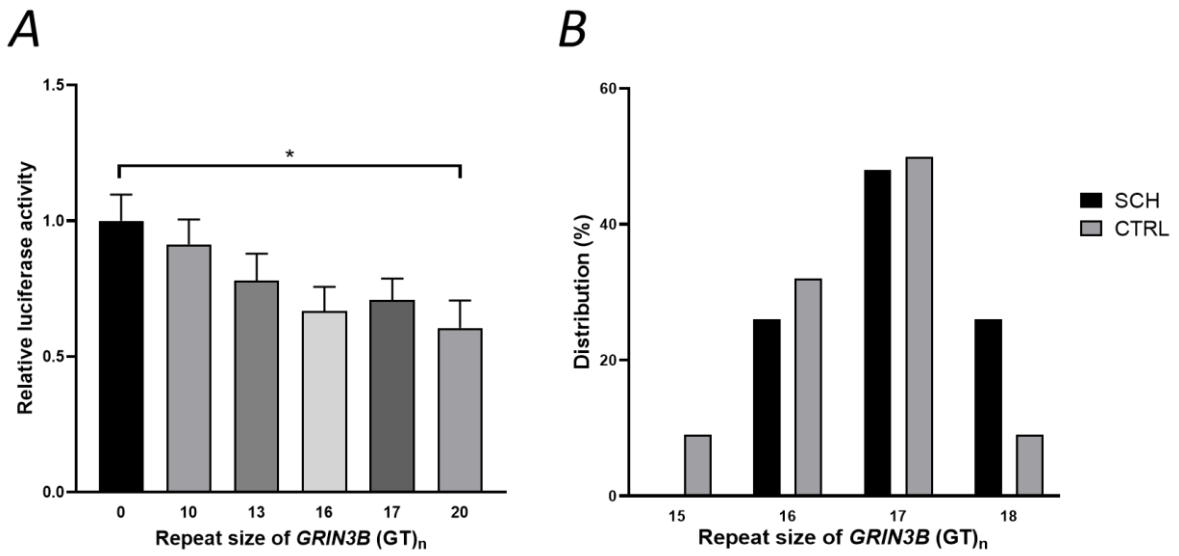

Fig. 13: **Prolonged $(GT)_n$ repeat within the promoter region of the *GRIN3B* gene leads to decreased promoter activity.** (***A***) Summary of relative luciferase activity of the *GRIN3B* gene promoter with selected $(GT)_n$ repeat size. Luciferase activity was measured in triplicate from four independent experiments (n = 12) and then normalised to the promoter without $(GT)_n$ repeat. All summary data are presented as the mean ± SEM; *, $p < 0.05$, analysed by one-way ANOVA and Tukey's multiple comparison test. (***B***) Summary of the $(GT)_n$ repeat size distribution in percentage for the SCH (n = 23) and control (CTRL) (n = 22) groups.

5.2.2. Assessment of the hypothesis of NMDAR hypofunction in schizophrenia within our research investigation of promoters

Next, we calculated the total relative activity of promoters for NMDAR genes between the patient and control groups. This provided a more accurate picture of the state of the two groups mentioned above. The promoter activity for each patient or control subject was calculated as the mean of the haplotypes of the two alleles, and the results were finally normalised to the control group (Fig. 14A). The results showed significantly decreased relative promoter activity for the patient groups in the case of the *GRIN1* promoters (20% decrease, p = 0.011, Fig. 14 A *GRIN1*) and *GRIN3B* promoters (6% decrease, p = 0.04, Fig. 14 A *GRIN3B*). The lower activity of the *GRIN1* promoter in the SCH group was mainly due to its high representation within the GRIN1_1 haplotype. In the case of the *GRIN2B* promoters, the relative promoter activity for the patient group shows a significant increase compared to the control group (7% increase, p = 0.004, Fig. 14A *GRIN2B*). The higher activity of the *GRIN2B* promoter in the SCH group was then predominantly driven by a group of patients containing the GRIN2B_5 haplotype. The remaining promoters of the *GRIN2A* and *GRIN3A* genes did not show significant differences between controls and cases (Fig. 14A, *GRIN2A*, *GRIN3*A).

Further, we linked all normalised data from the five studied NMDAR gene promoters into a single comparative analysis of relative promoter activity among the *GRIN* genes in patients and control subjects. Despite the differences in the strength of endogenous expression across NMDAR genes during development and in various brain structures, we aimed to determine if there's a general trend to decrease the expression of the NMDAR genes introducing receptor-dependent hypofunction in individuals with SCH. The results suggested a slight decrease in relative promoter activity for patients compared to the control group, bordering on significance (6% reduction, p = 0.058) (Fig. 14B).

Finally, we used data from MRI brain scans from the SCH patients and controls. MRI brain scans were further segmented, and the BrainAGE index was estimated. We utilized a multivariate pattern recognition method that measures age-related brain tissue reduction using kernel regression techniques within an extensive training database (Franke et al., 2010, 2012). The results suggested an older brain age for the group of patients compared to controls (2.3 years older, p = 0.043) (Fig. 14C). The observation of smaller GM volumes and a higher BrainAGE index was already reported by several studies (Schnack et al., 2016; Birnbaum & Weinberger, 2017; Hajek et al., 2019); however, we aimed to confirm this within our case and control subjects. Further, we corelated relative *GRIN* genes promoter activity with the BrainAGE index. The analysis indicated a positive correlation between the overall higher biological brain age and lower *GRIN* genes promoter activity in SCH patients, although the

variability in the BrainAGE index was large and differences in relative *GRIN* genes promoter activity did not reach significance (Fig. 14D).

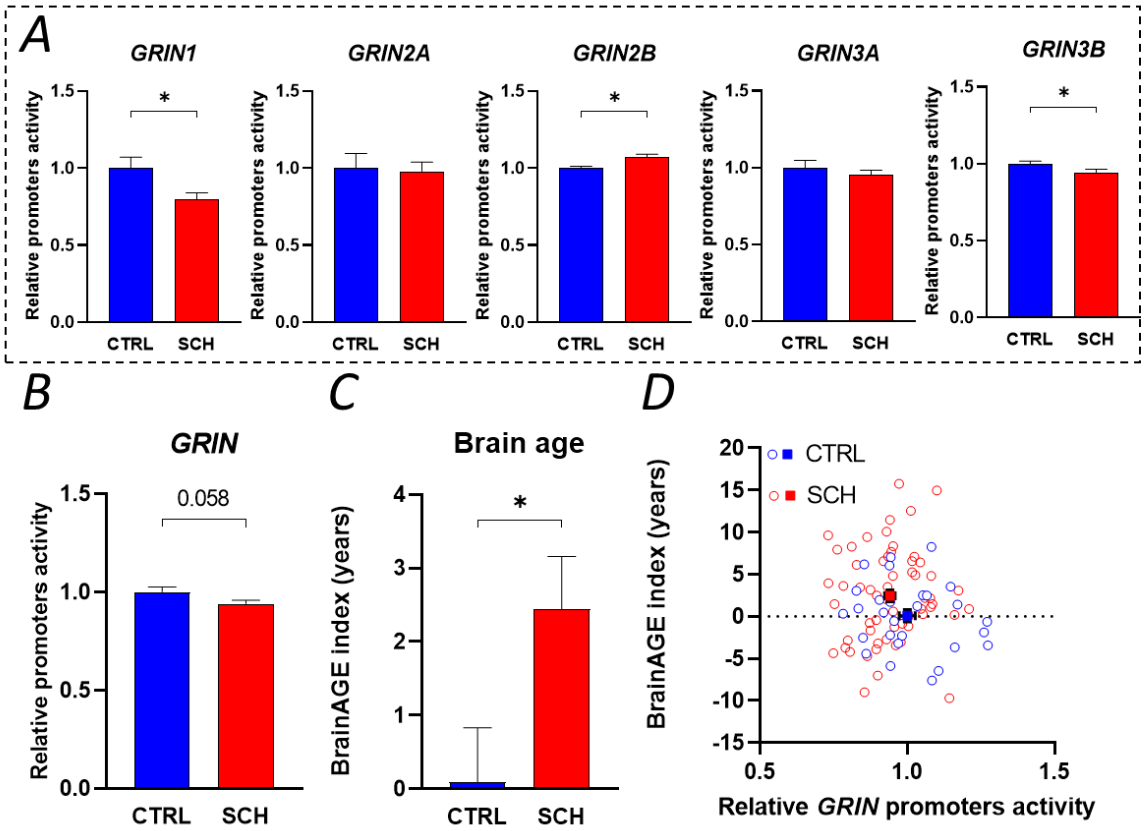

Fig. 14: **Schizophrenia leads to an increased BrainAGE index and changes in promoter activity among selected NMDAR genes, with a tendency to hypofunction.** (***A***) Summary of relative promoter luciferase activity for selected NMDAR genes for SCH (n = 63) and control groups (n = 32). Promoter activity for each patient or control subject was calculated as the mean of both alels. Relative luciferase activity was normalised to the average of the control group. (***B***) Summary of mean promoter luciferase activity for the SCH (n = 295) and control (n = 145) groups. Relative *GRIN* promoter activity was calculated as the mean of the relative promoter luciferase activity of all selected NMDAR genes. All relative luciferase activity data for each subject were normalised to the mean relative values given by the relative promoter luciferase activity of a specific gene (Fig. 14A). Only subjects with a known BrainAGE index were considered. (***C***) Summary of the BrainAGE index for the SCH (n = 59) and control (n = 29) groups. All summary data are presented as the mean ± SEM. *, $p < 0.05$, analysed by unpaired or Welch's t-test. (***D***) Correlation between Relative *GRIN* promoters' activity and BrainAge index, with the mean values marked as filled quadrates.

5.3. Functional characterisation of missense variants identified within the CTD of the GluN2A NMDAR subunit

The majority of functional analyses of genetic variants focus on missense or nonsense variants within a gene. While nonsense variants usually have serious deleterious effects on protein function, which depends on the position of the newly established stop codon, the functional consequences of missense variants leading to a single amino acid substitution are more uncertain but often have severe effects on protein properties. In the case of NMDARs, most of the missense variants studied were located within the ABD and TMD, the vital parts of the receptor, where a new variant often results in a strong change in the ion channel properties. However, as outlined in Chapter 2.2.3, most SCH-associated variants are located in the ATD and CTD of NMDAR. Although these domains have a more modulatory effect on ion channel properties, they regulate NMDAR trafficking and synaptic anchoring and are hubs for complex protein-protein interactions.

5.3.1. Annotation of NMDAR non-synonymous coding variants from our NGS dataset

From our NGS study encompassing individuals with SCH and control subjects, we annotated all variants present in coding regions within five NMDAR genes. In total, we identified sixty-two variants, predominantly rare in occurrence. Among all the variants, 44% were localised in the CTD, 27% in the ATD, 21% in the ABD, and 8% were TMD (Tab. 6).

Within the *GRIN1* gene, we identified a solitary variant situated in the TMD. This variant constitutes a deletion encompassing an entire triplet, resulting in the removal of a single amino acid while leaving the remainder of the protein unaffected. Notably, this variant was exclusively present in the patient group, leading to a significant association with the disease ($p = 0.030$) (Tab. 6).

Within the *GRIN2A* gene, we found five missense variants: one in the ATD and four in the CTD. The ATD variant was only observed in one control subject, while the CTD variants were distributed similarly between patients and controls, except for the P1386L variant, which was exclusively present in a single patient (Tab. 6).

Upon detailed annotation and revision of genetic variants, no coding variants were identified within the *GRIN2B* gene.

In the *GRIN2C* gene, we detected ten coding variants, five in the CTD, three in the ABD, and two in the ATD. Among these, eight were missense variants, one was an inframe insertion of three amino acids within the CTD, and one was a frameshift variant in the ABD, creating a premature stop codon. Notably, only one variant (rs3744215) showed a significant

association, albeit within the group of control subjects. Three variants of rare occurrence were exclusively present in individuals with SCH (Tab. 6).

In the *GRIN2D* gene, we identified six variants, one in the ATD and the remaining in the CTD. Among these, five were missense variants, and one of the variants located in the CTD was a frameshift variant that truncated the intracellular domain. The variants appeared to be evenly distributed between the two groups, although one CTD missense variant was found exclusively in the patient group (Tab. 6).

In the *GRIN3A* gene, nine coding variants were detected, four in CTD, one in ABD, and four in ATD. Eight of these variants were missense, while one, situated at the beginning of ATD, was a nonsense variant. Although the variants appeared to be distributed evenly between the two groups, the mentioned nonsense variant and two CTD missense variants were exclusively identified in patients (Tab. 6).

The last NMDAR gene, *GRIN3B*, exhibited a larger number of coding variants, totaling thirty-one variants, encompassing nine ATD, nine ABD, four TMD, and nine CTD variants. The majority were missense variants, except for two inframe amino acid deletions in CTD and two frameshift variants in ABD, resulting in a premature stop codon. Among the thirty-one variants, ten were exclusive to SCH cases. One CTD variant then showed a significant association with SCH ($p = 0.028$) (Tab. 6).

Tab. 6: **Non-synonymous genetic variations within protein-coding regions of NMDAR genes.** The summary of detected non-synonymous genetic variants within the protein coding region of the receptor subunit, together with their belonging to the receptor domain, type of variant, specific nucleotide and protein change, and distribution and frequency for patients and the control group. The p-value was calculated using Fisher's exact test.

Gene	Chromosome	Coordinate (hg38)	Domain	rsID	Nucleotide change	Protein change	Type	SCH	CTRL	f SCH	f CTRL	p-Value
GRIN1	chr9	137162431	TMD	/	c.1857_1859delGGA	p.E619del	deletion (inframe)	9	0	0.07	0.00	**0.030**
GRIN2A	chr16	9763387	CTD	rs1277391984	c.4157C>T	p.P1386L	missense	1	0	0.01	0.00	
		9764316	CTD	rs61758995	c.3228C>A	p.N1076K	missense	1	1	0.01	0.02	
		9764354	CTD	rs138809301	c.3190A>G	p.T1064A	missense	1	1	0.01	0.02	
		9764645	CTD	rs61731465	c.2899G>C	p.V967L	missense	1	1	0.01	0.02	
		9849943	ATD	rs757464009	c.1141C>T	p.H381Y	missense	0	1	0.00	0.02	
GRIN2C	chr17	74842510	CTD	rs3744215	c.3627G>T	p.R1209S	missense	21	20	0.17	0.31	0.026
		74842838	CTD	/	c.3299G>A	p.C1100Y	missense	0	2	0.00	0.03	
		74842991	CTD	/	c.3137_3138insCCCGGAGCC	p.F1046_P1047ins P-E-P	insertion (inframe)	110	60	0.87	0.94	
		74843255	CTD	/	c.2882G>A	p.G961E	missense	0	1	0.00	0.02	
		74843525	CTD	rs765016248	c.2612A>G	p.Q871R	missense	2	0	0.02	0.00	
		74844496	ABD	/	c.2360_2361delAG	p.K788fs*12	frameshift	1	0	0.01	0.00	
		74850229	ABD	rs11575879	c.1468G>A	p.V490I	missense	0	1	0.00	0.02	
		74850361	ABD	rs61754645	c.1336G>A	p.V446M	missense	2	0	0.02	0.00	
		74850716	ATD	rs375174698	c.1165C>T	p.R389C	missense	0	1	0.00	0.02	
		74854900	ATD	rs78349823	c.193C>T	p.L65F	missense	2	0	0.02	0.00	
GRIN2D	chr19	48414095	ATD	rs150870505	c.1190C>T	p.T397M	missense	0	1	0.00	0.02	
		48442997	CTD	rs1160641963	c.3071T>C	p.F1024S	missense	2	2	0.02	0.03	
		48443016	CTD	/	c.3102delC	p.A1035fs	frameshift	1	1	0.01	0.02	
		48443600	CTD	rs558749972	c.3674G>A	p.R1225H	missense	0	2	0.00	0.03	
		48443708	CTD	/	c.3782A>G	p.D1261G	missense	0	1	0.00	0.02	
		48443875	CTD	rs191119443	c.3949G>A	p.G1317S	missense	1	0	0.01	0.00	
GRIN3A	chr9	101573267	CTD	rs147490517	c.3255G>C	p.Q1085H	missense	1	0	0.01	0.00	
		101573304	CTD	rs62000403	c.3218A>T	p.N1073I	missense	6	5	0.05	0.08	
		101573337	CTD	rs71509734	c.3185A>G	p.N1062S	missense	1	0	0.01	0.00	
		101573400	CTD	rs3739722	c.3122G>A	p.R1041Q	missense	13	7	0.10	0.11	
		101623429	ABD	rs35768024	c.2502_2503delTGinsCA	p.D835N	missense	60	31	0.48	0.48	
		101670953	ATD	rs10989589	c.1459G>A	p.G487R	missense	51	31	0.40	0.48	
		101670973	ATD	rs34755188	c.1439G>A	p.R480H	missense	1	2	0.01	0.03	
		101686816	ATD	rs10989591	c.1084G>A	p.V362M	missense	40	23	0.32	0.36	
		101737814	ATD	/	c.166C>T	p.Q56*	nonsense	1	0	0.01	0.00	
GRIN3B	chr19	1000718	ATD	rs139242998	c.281C>A	p.A94E	missense	2	0	0.02	0.00	
		1000784	ATD	rs12986002	c.349C>T	p.H117Y	missense	66	41	0.52	0.64	
		1000847	ATD	rs766207454	c.410C>T	p.A137V	missense	1	1	0.01	0.02	
		1000862	ATD	rs1334049042	c.425C>T	p.P142L	missense	1	0	0.01	0.00	
		1003163	ATD	rs113181909	c.460C>T	p.P154S	missense	4	3	0.03	0.05	
		1003173	ATD	rs2240154	c.470C>T	p.T157M	missense	23	10	0.18	0.16	
		1003222	ATD	rs35592366	c.519C>A	p.D173E	missense	9	2	0.07	0.03	
		1003440	ATD	rs55646937	c.737G>A	p.R246H	missense	2	1	0.02	0.02	
		1003658	ATD	rs61744452	c.955G>A	p.A319T	missense	4	3	0.03	0.05	
		1004688	ABD	rs12978900	c.1187T>C	p.L396S	missense	6	1	0.05	0.02	
		1004711	ABD	rs4807399	c.1210C>T	p.R404W	missense	62	31	0.49	0.48	
		1004724	ABD	rs144402697	c.1223C>A	p.P408Q	missense	1	0	0.01	0.00	
		1004741	ABD	rs2240157	c.1240T>C,	p.W414R	missense	84	36	0.67	0.56	
		1004804	ABD	rs201638380	c.1303G>A	p.E435K	missense	1	0	0.01	0.00	
		1004873	ABD	rs61750461	c.1372G>A	p.A458T	missense	2	0	0.02	0.00	
		1004897	ABD	rs10666583	c.1396_1397insCGTT	p.G466fs*17	frameshift	38	20	0.30	0.31	
		1005200	TMD	rs566603277	c.1699G>A	p.G567S	missense	1	0	0.01	0.00	
		1005231	TMD	rs2240158	c.1730C>T	p.T577M	missense	50	24	0.40	0.38	
		1007839	ABD	/	c.2211delC	p.K738fs*24	frameshift	3	1	0.02	0.02	
		1007962	ABD	rs201937512	c.2305G>A	p.A769T	missense	1	0	0.01	0.00	
		1008646	TMD	rs78914045	c.2495C>A	p.A832E	missense	2	0	0.02	0.00	
		1008684	TMD	rs2285906	c.2533G>A	p.A845T	missense	26	6	0.21	0.09	0.064
		1008705	CTD	rs61744375	c.2554G>A	p.E852K	missense	1	0	0.01	0.00	
		1008880	CTD	rs2285907	c.2655G>C	p.T885T	missense	26	6	0.21	0.09	0.064
		1009184	CTD	/	c.2734_2736delCAG	p.Q912del	deletion (inframe)	18	12	0.14	0.19	
		1009229	CTD	rs755723427	c.2759G>A	p.G920D	missense	1	0	0.01	0.00	
		1009363	CTD	rs10417824	c.2896T>A	p.Y966N	missense	54	24	0.43	0.38	
		1009414	CTD	rs145392111	c.2944G>A	p.E982K	missense	4	3	0.03	0.05	
		1009480	CTD	rs10401245	c.3016C>G	p.Q1006E	missense	78	30	0.62	0.47	0.063
		1009551	CTD	/	c.3083_3109delCCCCCGCGGAGGCCCCACCACACTCTG	p.A1028-S1036del	deletion (inframe)	24	13	0.19	0.20	
		1009586	CTD	rs10401454	c.3116C>G	p.P1039R	missense	44	12	0.35	0.19	**0.028**

5.3.2. Functional analysis of GluN2A CTD missense variants

The variants in the coding regions of NMDAR genes associated with SCH were found in all *GRIN* genes. Nevertheless, the most comprehensive GWAS and WES studies of SCH patients have indicated an association of *GRIN2A* variants with the disease (Singh et al., 2022; Trubetskoy et al., 2022). Furthermore, the published studies (Chapter 2.2.3.) along with results from our NGS dataset noted the high occurrence of SCH-associated variants within the CTD of NMDARs. Therefore, we further focused on the functional analysis of four coding variants within the CTD of the *GRIN2A* gene, which encodes the GluN2A subunits of NMDAR. In the context of GluN2A subunits, the CTD, its largest domain, assumes importance for receptor regulation. We found and analysed four CTD-located variants: V967 (V967L), T1064 (T1064A), N1076 (N1076K), and P1386 (P1386L) (Fig. 15).

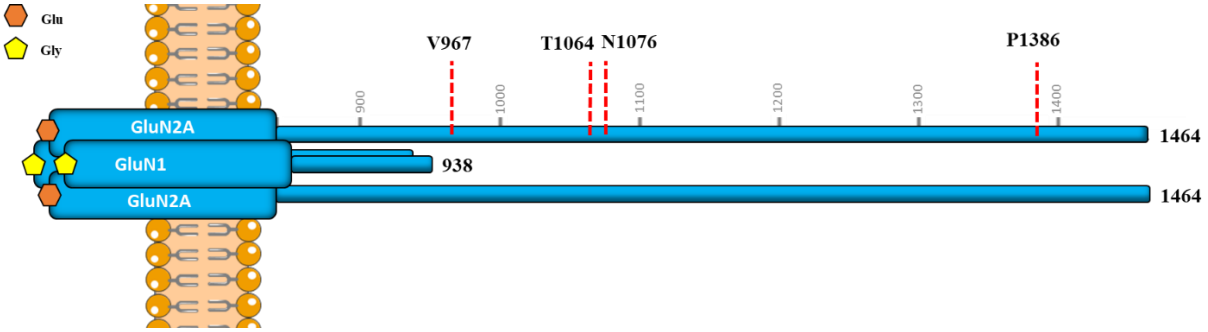

Fig. 15: **Schematic representation of the GluN1/GluN2A homodimer's CTDs with annotated sites of genetic variations.**

5.3.2.1. The effects of GluN2A CTD missense variants on surface expression in HEK293T and COS-7 cells

As multiple studies have suggested, genetic alterations within the CTD of GluN2 subunits can affect receptor trafficking and the stability of surface expression. Therefore, we used immunofluorescence microscopy and a colorimetric assay to assess the effects of the missense variants on the surface expression of NMDARs. Initially, we constructed vectors encoding eGFP-tagged hGluN2A subunits. Subsequently, these tagged subunits, whether WT or variant, were co-transfected with the hGluN1-1a subunit into HEK293T cells (for immunofluorescence microscopy) or COS-7 cells (for the colorimetric assay) to analyse the expression of NMDAR on the cell surface.

The analysis of images revealed a significant decrease in the ratio of surface-to-intracellular expression of NMDAR for all four variant receptors (hGluN1-1a/eGFP-hGluN2A-P1386L /N1076K/T1064A/V967L) compared to hGluN1-1a/eGFP-hGluN2A-WT receptors when expressed in HEK293T cells (P1386L 31% reduction, N1076K 30% reduction, T1064A 30% reduction, V967L 28% reduction compared to WT, $p = <0.002$ for all four variants) (Fig. 16 A, B). These findings were further corroborated by a quantitative colorimetric assay performed in COS-7 cells, which demonstrated a significant reduction in surface-to-intracellular NMDAR expression for all variants compared to the WT GluN2A-NMDAR (P1386L 22% reduction, N1076K 17% reduction, T1064A 25% reduction, V967L 25% reduction compared to WT, $p = <0.012$ for all four variants) (Fig. 16 C).

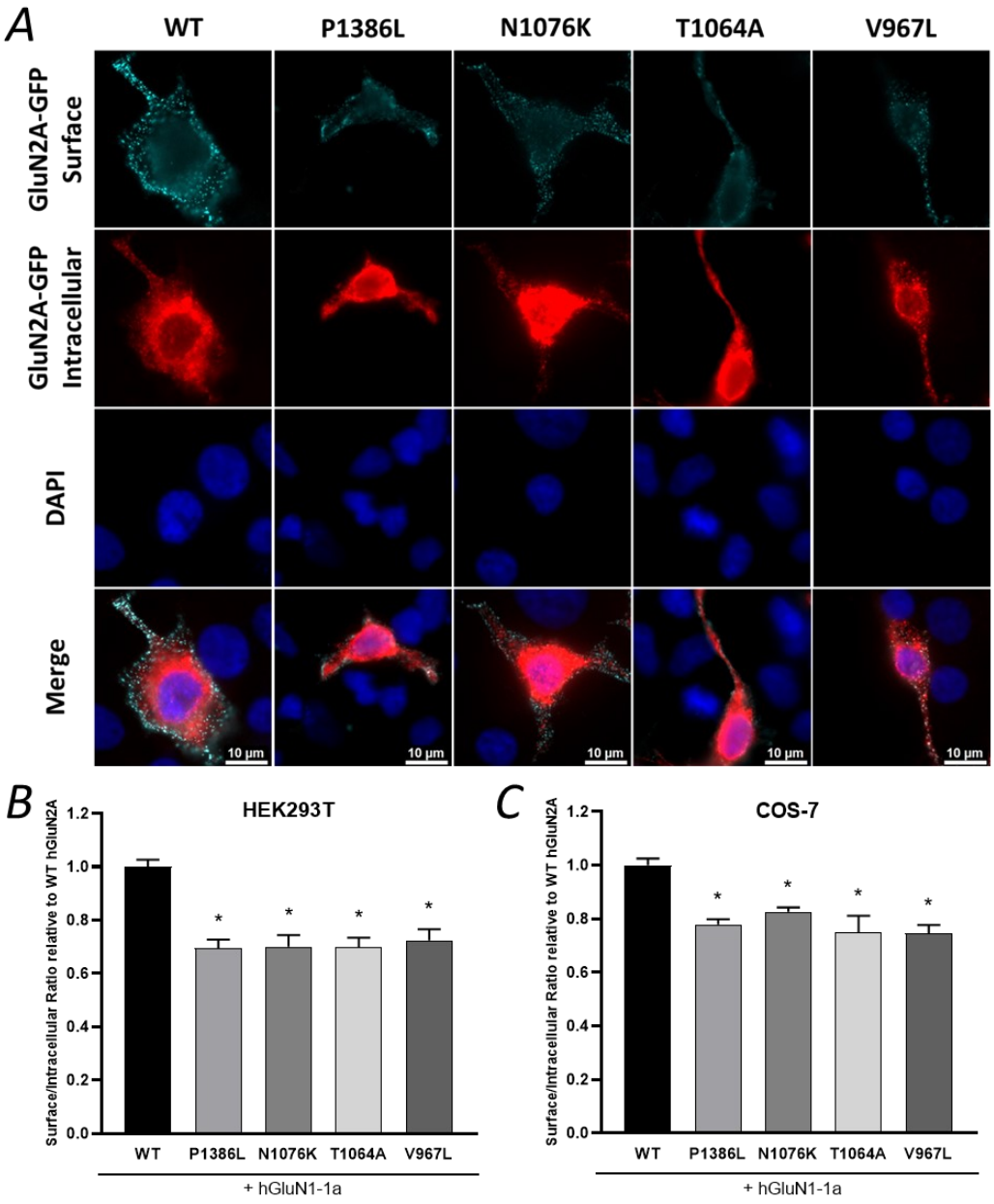

Fig. 16: **Missense variants of CTD of hGluN2A subunits decrease surface expression of NMDARs in HEK293T and COS-7 cells.** (***A***) Representative images of surface and intracellular eGFP-hGluN2A subunits measured in HEK293T cells expressing the indicated variant of CTD. Cells were co-transfected with hGluN1-1a. DAPI was used as an indicator of cell viability. (***B***) Summary of the relative surface expression (surface/intracellular ratio) of the mutated CTD of eGFP-hGluN2A subunits measured in HEK293T cells using fluorescence microscopy (n ≥ 134 cells per group from three to four independent experiments) All summary data are presented as the mean ± SEM. (***C***) Summary of the relative surface expression (surface/intracellular ratio) of the mutated CTD of eGFP-hGluN2A subunits measured in COS-7 cells using a quantitative colorimetric assay. Cells were co-transfected with hGluN1-1a. Relative surface expression was measured in quadruplicate in three to four independent experiments. All summary data are presented as the mean ± SEM. *, $p < 0.05$ versus WT, analysed by one-way ANOVA and Tukey's (*B*) or Dunnett's (*C*) multiple comparison test.

Next, we also performed patch-clamp electrophysiology experiments to assess the current density of responses evoked by glutamate (1 mM) in the presence of 30 µM glycine, which serves as indirect evidence of the number of surface-expressed NMDARs. This analysis was performed on HEK293T cells transfected with both WT and variant subunits. While all four variants exhibited a trend towards reduced current density compared to the WT receptor, only two variants, P1386L ($p = 0.039$) and N1076K ($p = 0.028$), showed a statistically significant difference in our analysis (Fig. 17A, C; summarised in Tab. 7). However, it's important to note that current densities can be affected by eventually altered ion channel properties and by transfection efficiency that can be variable between individual cells.

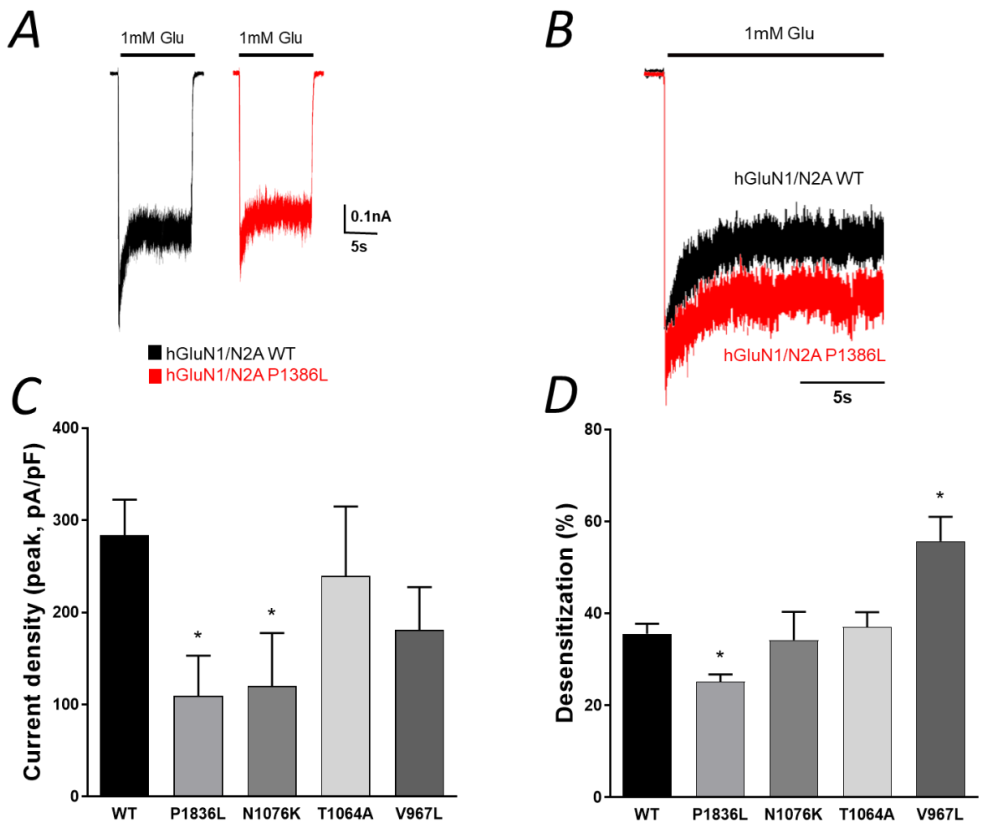

Fig. 17: **Missense variants of CTD of hGluN2A subunits alter current density and desensitization of NMDARs in HEK293T cells.** (***A***) Representative recordings of responses to 1 mM glutamate applications made in the presence of 30 µM glycine are shown for HEK293T cells expressing hGluN1-1a/hGluN2A WT or P1386L receptors. (***B***) Representative currents induced in hGluN1-1a/hGluN2A-WT or P1386L receptors by fast application of 1 mM glutamate in the continuous presence of 30 µM glycine are shown normalised with respect to the maximal response. (***C***) Summary of the mean current density evoked by 1 mM glutamate and normalised with respect to the individual HEK293T cell capacitance. (***D***) Summary of the mean desensitization in percentage calculated from the current evoked by 1 mM glutamate. All summary data are presented as the mean ± SEM. *, $p < 0.05$ versus WT, analysed by one-way ANOVA and Dunnett's multiple comparison test.

5.3.2.2. The effects of GluN2A CTD missense variants on receptor ion channel properties

Previously, the effects of variants within the CTD of NMDAR on its functional properties were reported; therefore, we performed patch-clamp electrophysiology experiments to assess the functional effects of the hGluN2A subunit variants. We co-expressed the hGluN2A-WT or variant subunits with the hGluN1-1a subunit in HEK293T cells.

Firstly, we evaluated the effects of hGluN2A variants on NMDAR desensitization, which refers to the time-dependent decline of responses in the sustained presence of an agonist. Receptors were activated at a saturating concentration of glutamate (1 mM) and in the presence of glycine (30 μM). The analysis of the responses revealed that desensitization was significantly altered in P1386L (25%, $p = 0.02$) and V967L (56%, $p = 0.002$) variants compared to WT hGluN2A-NMDAR (36%). Conversely, no significant differences were observed for the N1076K (34%) and T1064A (37%) variants (Fig. 17 B, D; summarised in Tab. 7).

Subsequently, we investigated the effects of hGluN2A variants on NMDAR deactivation kinetics. We assessed the average time constant tau for fast and slow components, along with the tau weighted for hGluN1-1a/hGluN2A WT or variant receptors. Receptors were activated by a saturating concentration of glutamate (1 mM) in the continuous presence of glycine (30 μM). While no significant changes were observed for the fast and slow components of deactivation kinetics, we noted significant decreases in tau weighted for the P1386L (96 ms, $p = 0.036$) and N1076K (90 ms, $p = 0.0267$) variants compared to the WT hGluN2A-NMDAR (237 ms). The T1064A (139 ms) and V967L (154 ms) variants also exhibited decreased tau weighted, although they did not reach statistical significance compared to the WT NMDAR (summarised in Tab. 7).

Additionally, we investigated the effects of hGluN2A variants on NMDAR response to the application of 1 μM MK-801, a use-dependent NMDAR open channel blocker, which indicates the probability of ion-channel opening. We evaluated the average rate of 1 μM MK-801 channel block of activated receptors (time constant tau) at a saturating concentration of glutamate (1 mM) in the continuous presence of glycine (30 μM). A slower response to the MK-801 application suggests a lower channel open probability, resulting in lower charge transfer over time. Our results indicated significant alterations in the time constant tau of GluN2A CTD variants compared to the WT hGluN2A-NMDAR (385 ms), only for the T1064A (1594 ms, $p = 0.007$) variant. The values of time constant tau for the P1386L (193 ms) and N1076K (223 ms) variants suggested a lower channel open probability. In contrast, the V967L (1061 ms) variant tended to exhibit a higher channel open probability (summarised in Tab. 7).

Tab. 7: **Effects of hGluN2A CTD missense variants on NMDAR functional properties.** The summary of mean current density, desensitization, deactivation kinetics, and MK-801 application kinetics indicates an open probability for hGluN1-1a/hGluN2A WT or mutated receptors. Values are the mean ± SEM with the number n in brackets. Highlighted values indicate significant differences, where * is $p < 0.05$ versus WT, analysed by one-way ANOVA and Dunnett's multiple comparison test.

hGluN2A	WT (n)	P1386L (n)	N1076K (n)	T1064A (n)	V967L (n)
Current density (peak,pA/pF)	284 ± 39 (17)	**109 ± 44* (7)**	**120 ± 58* (6)**	239 ± 76 (6)	181 ± 46 (7)
Desensitization (%)	36 ± 2 (16)	**25 ± 2* (8)**	34 ± 6 (6)	37 ± 3 (8)	**56 ± 5* (7)**
Deactivation					
τ fast (ms)	90 ± 10 (8)	73 ± 7 (6)	78 ± 10 (6)	93 ± 9 (7)	95 ± 6 (4)
τ slow (ms)	1782 ± 511 (8)	569 ± 128 (6)	564 ± 187 (6)	952 ± 360 (7)	637 ± 183 (4)
τ w (ms)	237 ± 57 (8)	**96 ± 13* (6)**	**90 ± 9* (6)**	139 ± 15 (7)	154 ± 53 (4)
MK-801 application					
τ w (ms)	385 ± 70 (11)	193 ± 16 (6)	223 ± 20 (5)	**1594 ± 561* (7)**	1061 ± 246 (8)

Finally, we analysed glutamate and glycine agonist potencies for WT and variant NMDAR, which affect the number of activated receptors. The glutamate EC_{50} (half maximal effective concentration) was significantly increased for the N1076K variant (7.6 uM, $p = 0.012$) compared to the WT hGluN2A-NMDAR (5 uM). Furthermore, the P1386L variant (6.8 uM) exhibited a tendency for increased glutamate EC_{50}, and the T1064A (3.5 uM) and V967L (3.8 uM) variants showed a tendency for decreased glutamate EC_{50} (summarised in Tab. 8).

A subsequent analysis of glycine potency reveals that the EC_{50} of variant P1386L (0.7 uM) had decreased significantly, while variant T1064A (2.1 uM) had increased significantly compared to the WT hGluN2A-NMDAR (1.3 uM). Variant N1076K (0.8 uM) demonstrated a tendency towards a decreased glycine EC_{50}, while variant V967L (1.3 uM) exhibited no changes in glycine EC_{50} (summarised in Tab. 8).

Tab. 8: **Effects of hGluN2A CTD missense variants on NMDAR agonist potency.** The summary of the mean glutamate and glycine EC_{50} for hGluN1-1a/hGluN2A WT or mutated receptors. Values are the mean ± SEM with the number n in brackets. Highlighted values indicate significant differences, where * is $p < 0.05$ versus WT, analysed by one-way ANOVA and Dunnett's multiple comparison test.

hGluN2A	GluEC50 (µM)	GlyEC50 (µM)
WT (n)	5 ± 0.5 (10)	1.3 ± 0.1 (9)
P1386L (n)	6.8 ± 0.3 (7)	**0.7 ± 0.2* (5)**
N1076K (n)	**7.6 ± 0.7* (6)**	0.8 ± 0.1 (5)
T1064A (n)	3.5 ± 0.5 (6)	**2.1 ± 0.2* (6)**
V967L (n)	3.8 ± 0.7 (7)	1.3 ± 0.1 (6)

5.3.2.3. The role of GluN2A CTD missense variants in surface expression and synaptic localisation in primary hippocampal neurons

The information obtained from surface-expression experiments on HEK293T and COS-7 cells is relevant, but there is a lack of expression of other, neuronally specific proteins to fully understand the effects of genetic variants on NMDAR function. Therefore, we performed similar experiments in the context of neuronal cells, which provides a complex environment for NMDAR function.

We used an immunofluorescence approach to investigate the surface expression of NMDARs containing WT or variant hGluN2A subunits within the soma and dendritic spines of primary hippocampal neurons. The WT or variant eGFP-tagged hGluN2A subunits were introduced into primary mouse hippocampal neurons via lentiviral particles. Within this model, the surface expression of the introduced eGFP-hGluN2A subunits relies entirely on the expression of endogenous GluN1 subunits.

Analysis of immunofluorescently stained images of cultured hippocampal neurons transduced with WT or variant eGFP-hGluN2A-NMDAR subunits revealed that surface expression in the soma of neurons was significantly reduced for variant T1064A (49% reduction, p = < 0.001) compared to the WT subunit. The remaining variants did not show significantly reduced surface expression in the soma, although the variants P1386L (10% reduction) and V967L (23% reduction) showed a tendency towards reduction (Fig. 18 A, B).

The soma of neurons is well defined morphologically and therefore easier to analyse, but the main site of action of NMDARs are excitatory synapses, localised in dendritic spines. Therefore, we focused our analysis on the dendritic spines, where synapses were labelled by staining the postsynaptic scaffold protein PSD-95. Our analysis of surface expression on dendritic spines confirmed our results obtained with HEK293T and COS-7 cells. The findings suggested a significant decrease in surface expression for all tested genetic variants of eGFP-hGluN2A-NMDAR in comparison to the WT receptors (P1386L - 27% reduction, p = <0.001; N1076K - 13% reduction, p =<0.001; T1064A - 36.% reduction, p = <0.001; V967L - 9% reduction, p = 0.047) (Fig. 18 A. C).

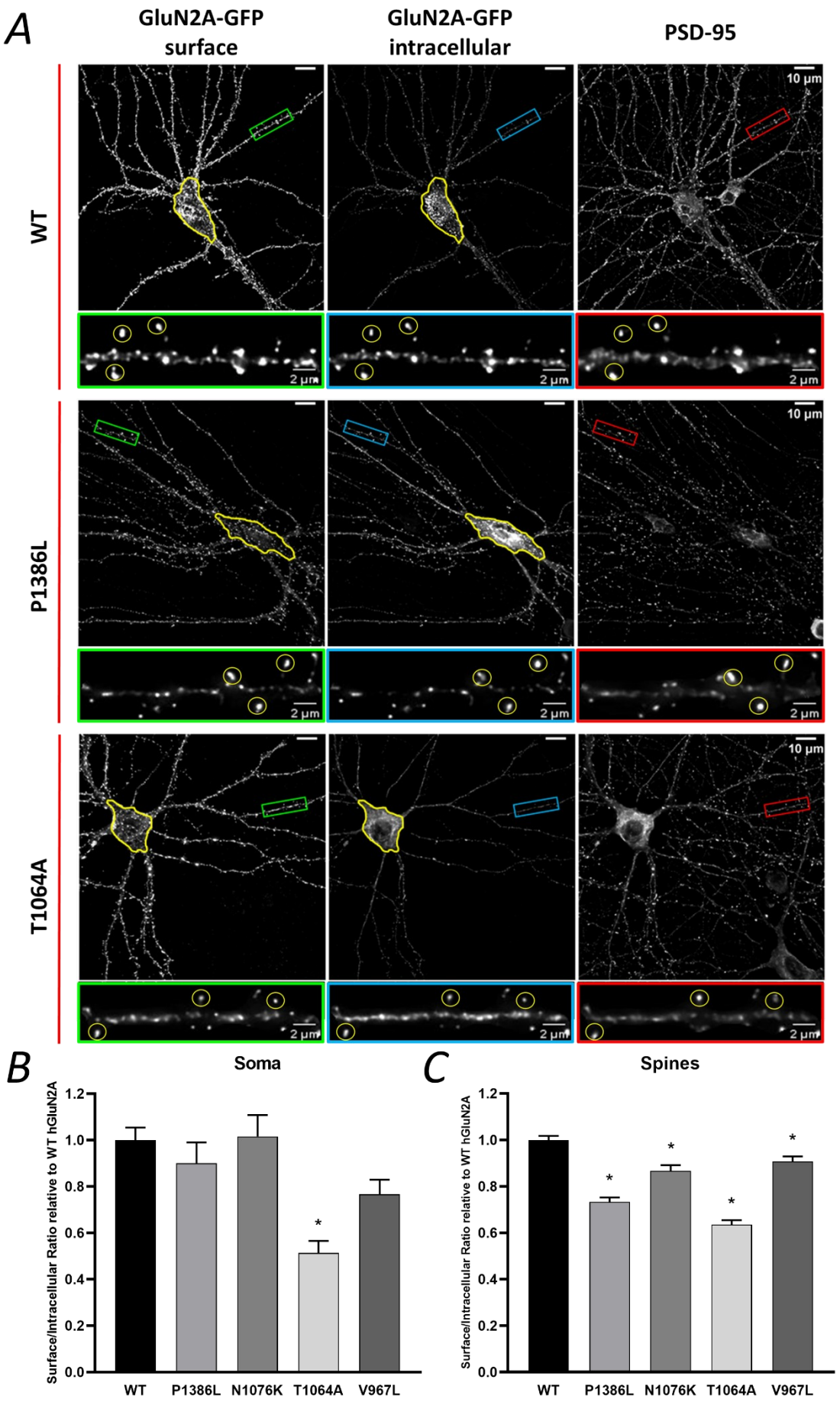
A
GluN2A-GFP surface
GluN2A-GFP intracellular
PSD-95
WT
P1386L
T1064A
10 µm
2 µm
B
Soma
Surface/Intracellular Ratio relative to WT hGluN2A
1.2
1.0
0.8
0.6
0.4
0.2
0.0
WT
P1386L
N1076K
T1064A
V967L
C
Spines
Surface/Intracellular Ratio relative to WT hGluN2A
WT
P1386L
N1076K
T1064A
V967L

Fig. 18: **Missense variants of CTD of hGluN2A subunits alter surface expression of NMDARs in hippocampal neurons.** (***A***) Representative images showing surface and intracellular immunostaining for eGFP-hGluN2A subunits and immunostaining against PSD-95. Areas marked in yellow indicate the soma of neurons used in surface expression analysis. Area marked by a bar indicating 20 ųm of secondary dendrite. Shown below are details from the marked bars, with areas marked in yellow indicating the spines of neurons used in surface expression analysis. Bars highlighted in green and red were further used for co-localisation analysis. (***B, C***) Summary of the relative surface expression (surface/intracellular ratio) of the mutated CTD of eGFP-hGluN2A subunits measured in somas (***B***) and dendritic spines (***C***) of hippocampal neurons using fluorescence microscopy (n ≥ 24 cells/somas and n ≥ 24 cells/120 spines per group from three independent experiments). All summary data are presented as the mean ± SEM. *, $p < 0.05$ versus WT, analysed by one-way ANOVA and Dunnett's multiple comparison test.

Next, we also used immunofluorescence analysis to investigate the synaptic localisation of NMDARs containing WT or variant hGluN2A subunits in primary hippocampal neurons. We stained the postsynaptic scaffold protein PSD-95 and determined the degree of co-localisation of the surface eGFP-hGluN2A and PSD-95 signals from the 20ųm ROI of secondary dendrite by applying two complementary methods of analysis: Manders' overlap coefficient to determine the proportion of surface receptors covered by PSD-95, and in addition, we wrote our own macro that calculates the percentage of overlapping pixels of surface receptors with PSD-95.

The results from our analyses suggest a trend towards reduced synaptic localisation, albeit with a minor decrease, across all variant eGFP-hGluN2A-NMDARs in comparison to the WT eGFP-hGluN2A receptor. However, the P1386L variant notably demonstrated a significant reduction in its Manders' overlap coefficient compared to the WT hGluN2A-NMDAR (11% decrease, $p = 0.008$), accompanied by a significant decrease in the percentage of overlapping pixels between surface receptors and PSD-95 compared to WT (15% decrease, $p = 0.001$). Furthermore, the N1076K variant also exhibited a significant reduction in the percentage of overlapping pixels between surface receptors and PSD-95 compared to WT (10% decrease, $p = 0.03$), although this result was not confirmed by the Manders' overlap coefficient (Fig. 19A, B, C).

Finally, we counted the total number of stained puncta of surface NMDARs and PSD-95 per distance of 20 µm of secondary dendrites to evaluate the profound effect of variant subunits on the number of synapses and receptor clusters. The results showed no significant differences between neurons expressing the WT and variant eGFP-hGluN2A subunits (data not shown).

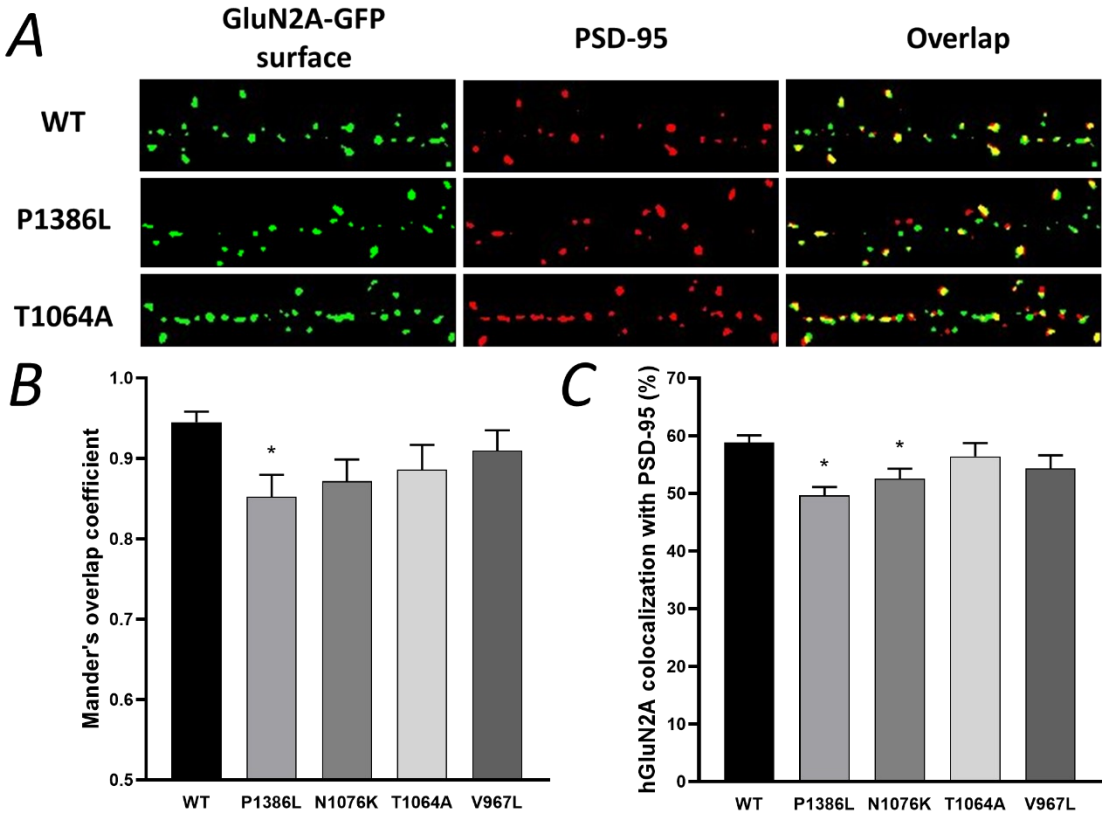

Fig. 19: **The P1386L variant of the CTD of the hGluN2A subunit decreases synaptic localisation of NMDARs in hippocampal neurons.** (***A***) Representative images showing tresholded surface receptors (green) and PSD-95 (red) with their composite image corresponding to 20 µm of secondary dendrite shown in image **Fig. 17A** used to calculate the percentage of receptors at synapses. (***B***) Summary of the co-localisation analysis between surface eGFP-hGluN2A and PSD-95 assessed by determination of Manders' overlap coefficient (n ≥ 24 cells/secondary dendrites per group from three independent experiments). (***C***) Summary of co-localisation analysis determined as percentage of overlapping pixels of surface eGFP-hGluN2A with PSD-95 (n ≥ 24 cells/secondary dendrite per group from three independent experiments). There was no significant difference between the WT and variants hGluN2A in the total number of puncta of surface receptors and PSD-95 per 20 µm of secondary dendrite (data not shown). All summary data are presented as the mean ± SEM. *, $p < 0.05$ versus WT, analysed by one-way ANOVA and Dunnett's multiple comparison test.

5.3.2.4. The effects of the GluN2A missense variant P1386L on NMDAR CTD protein interaction

In view of the impact of GluN2A-NMDAR variants on synaptic localisation, we also explored known protein interactions within or near the locations of the analysed genetic variants. Our search revealed the presence of a CaM binding site (875–1029) (Bajaj et al., 2014), which overlaps with the variant V967L. We didn't detect any protein interactors binding directly to positions of variants T1064A and N1076K. However, these variants are proximal to the binding sites of E3 ubiquitin ligase Nedd4 (1048–1052) (Gautam et al., 2013), and BRAG1/2,

(1078–1117) (Elagabani et al., 2016). For the last P1386L variant, four different protein binding sites were identified that overlapped with the position of the variant. These include CtBP1 (1257–1387) (Cousins & Stephenson, 2019), Rph3A (1349–1389) (Stanic et al., 2015), Flot1 (1382–1444) (Glebov et al., 2006), and PSD-95 (1382–1420) (Cousins et al., 2008, 2009; Cousins & Stephenson, 2012) (Fig. 20).

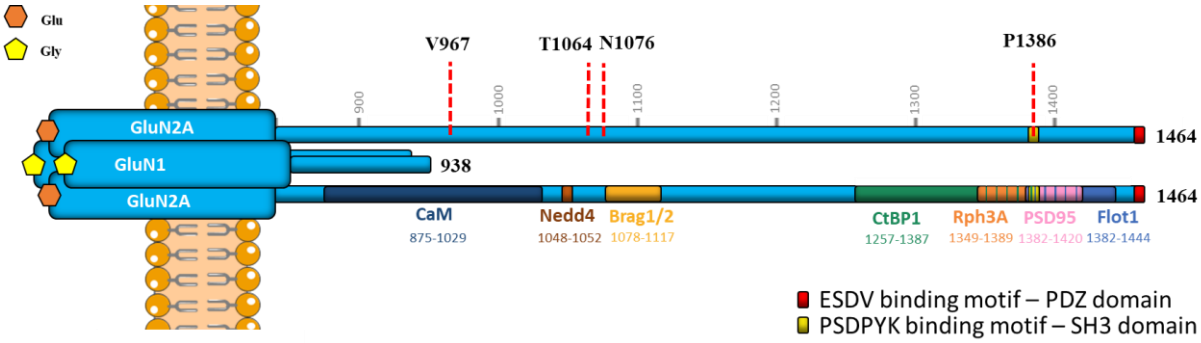

Fig. 20: **Schematic representation of the GluN1/GluN2A homodimer's CTDs with binding motifs for the PDZ and SH3 domains and protein interaction sites overlapping or in proximity to the sites of genetic variations.**

PSD-95 is one of the most abundant proteins within the postsynaptic density (PSD) and is crucial for the anchoring of NMDAR within the synapse. The primary binding motif for PSD-95 at the GluN2A subunit is the highly conserved ESDV sequence at the very end of CTD, which binds to the PDZ domain of PSD-95 (Kim & Sheng, 2004). However, Cousins et al., discovered the second binding motif, PSDPYK, known for its unconventional interaction with PSD-95 through the SH3 domain, and where variant P1386L occupies the fourth position in the motif (Cousins et al., 2008, 2009; Cousins & Stephenson, 2012) (Fig. 20).

In summary, GluN2A variant P1386L altered PSD-95 co-localisation and is placed at the core of the PSDPYK binding motif; therefore, we further analysed this interaction.

To explore the effects of the P1386L variant of hGluN2A-NMDAR on its interaction with PSD-95, we co-expressed subunits hGluN1-1a and eGFP-hGluN2A WT, or the P1386L variant, along with PSD-95 in HEK293T cells. Using immunofluorescence and super-resolution microscopy (STED), we quantified the degree of co-localisation by measuring the percentage of overlapping pixels between surface eGFP-hGluN2A and PSD-95 within a 5 x 5 µm membrane area adhering to the coverslip. The results of the analysis indicated a significant decrease in co-localisation of the P1386L variant with PSD-95 (44%, $p = < 0.001$) compared to WT receptors (58%) (Fig. 21 A, B).

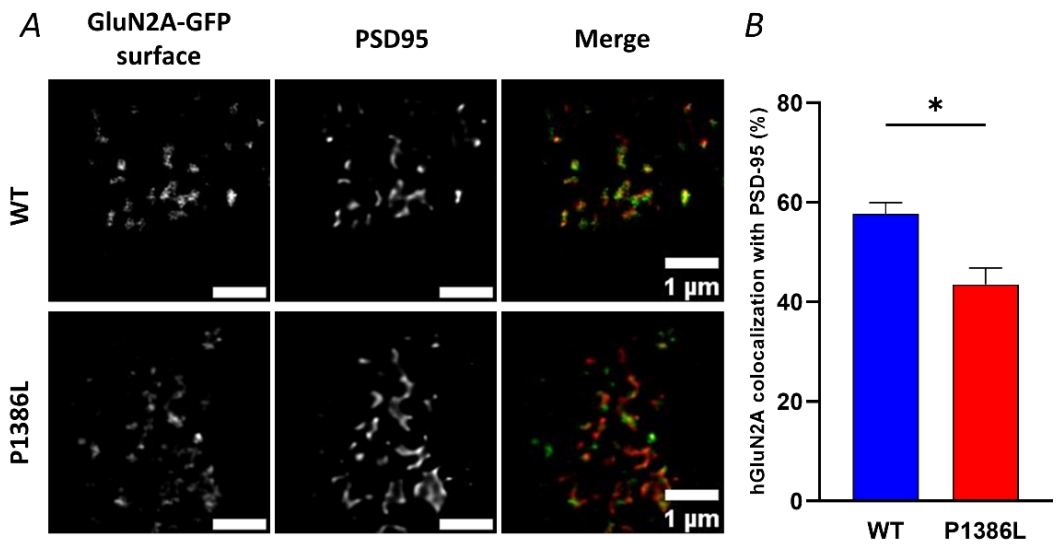

Fig. 21: **Variant P1386L in the hGluN2A subunit decreases receptor co-localisation with PSD-95.** (***A***) Representative images of HEK293T cells showing surface staining of eGFP-hGluN2A subunits and immunostaining of PSD9-95 in a 5 x 5 µm membrane area attached to the coverslip, captured by super-resolution STED microscopy (STED images are shown as deconvolved). (***B***) Summary of co-localisation analysis determined as percentage of overlapping pixels of eGFP-hGluN2A with PSD-95. (n ≥ 38 cells per group). All summary data are presented as the mean ± SEM. *, $p < 0.05$ P1386L versus WT, analysed by t test.

Previous studies have highlighted the effects of co-expressing PSD-95 on NMDAR current responses in HEK cells, specifically on the receptor's current density and its sensitivity to glutamate. The co-expression of NMDARs with PSD-95 led to a significant increase in current density compared to NMDARs expressed without PSD-95. However, this effect was significantly reduced when a stop codon was introduced before the ESDV binding motif. Furthermore, co-expression of GluN2A-NMDAR with PSD-95 enhanced the open probability of the NMDAR and its sensitivity to glutamate compared to receptors expressed alone (Rutter & Stephenson, 2000; Y. Lin et al., 2004).

We used an identical experiment to assess the effects of the P1386L variant on the functional characteristic of hGluN2A-NMDAR when co-expressed with PSD-95. We co-expressed subunits hGluN1-1a and hGluN2A WT, or the P1386L variant, and with or without PSD-95 in HEK293T cells. In addition, we also created and tested the hGluN2A construct with a truncated ESDV motif.

Initially, we evaluated the current density of responses evoked by glutamate (1 mM) in the presence of 30 µM glycine. Co-expressing hGluN2A-NMDAR WT with PSD-95 resulted in a significantly increased current density compared to hGluN2A-NMDAR WT expressed without PSD-95 (95% increase, $p = 0.002$). Conversely, the expression of PSD-95 alongside the P1386L variant or the ΔESDV construct did not exhibit a significant increase in current

density (P1386L – 38% increase, ΔESDV – 22% increase). The results suggested that the P1386L variant of hGluN2A-NMDAR altered the interaction between the CTD of the hGluN2A subunit and PSD-95 (Fig. 21A, summarised in Tab. 9).

Subsequently, we examined the influence of the hGluN2A P1386L variant and the ΔESDV construct on NMDAR glutamate sensitivity, both in the presence and absence of PSD-95. Notably, the glutamate EC_{50} of WT hGluN2A-NMDAR significantly increased when co-expressed with PSD-95 compared to WT receptors expressed alone (67% increase, $p = 0.008$). This change did not occur in the case of the P1386L variant or the ΔESDV construct of hGluN2A-NMDAR when co-expressed with PSD-95, suggesting again that the P1386L variant affects the interaction between the CTD of the hGluN2A subunit and PSD-95 (Fig. 21B, C, summarised in Tab. 9).

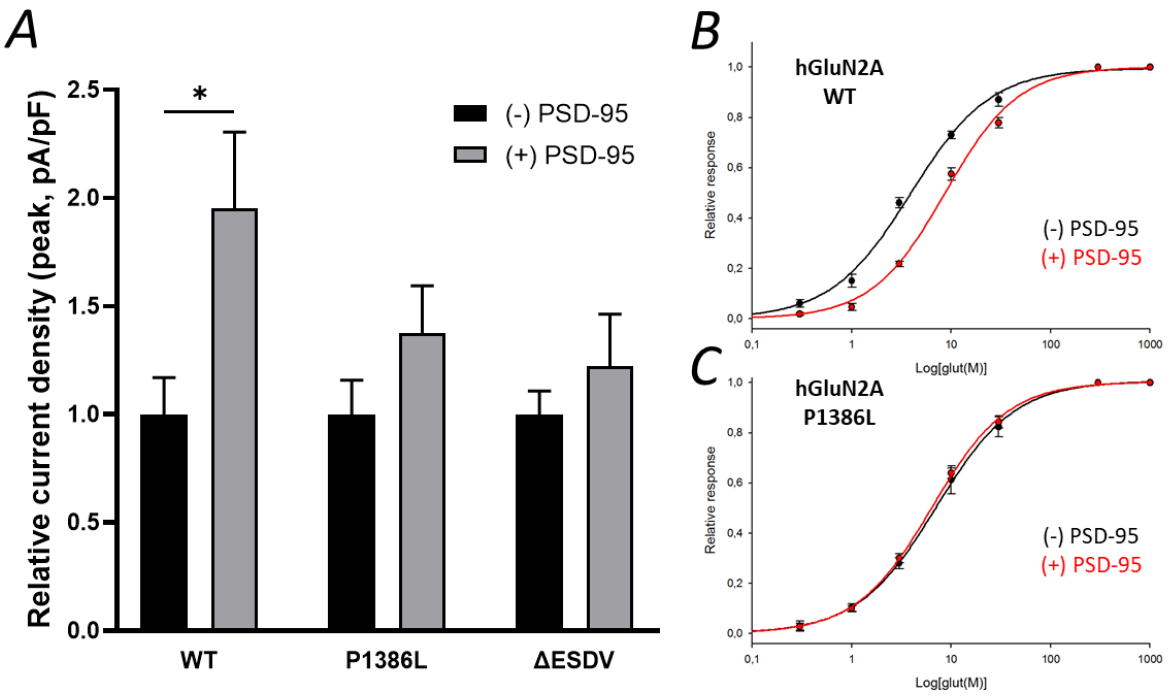

Fig. 21: **PSD-95 significantly increases glutamate EC_{50} and the current density of hGluN2A WT NMDAR, but not of the P1386L mutated receptor.** The presence of PSD-95 has a significant impact on both the glutamate EC_{50} and the current density of the hGluN1-1a/hGluN2A WT receptor. However, this effect is not observed in the case of hGluN1-1a/hGluN2A P1386L NMDAR. (***A***) The summary of the mean relative current density of hGluN1-1a/hGluN2A WT, P1386L, or ΔESDV NMDAR with or without the presence of PSD-95 normalised to the mean current density of cells not expressing PSD-95. All summary data are presented as the mean ± SEM. *, $p < 0.05$ (+) versus (-) PSD-95, analysed by one-way ANOVA and Tukey's multiple comparison test. (***B***,***C***) Relative peak dose-response relationship for glutamate activation of hGluN1-1a/hGluN2A WT (***B***) and hGluN1-1a/hGluN2A P1386L receptors (***C***).

Additionally, we assessed the desensitization and deactivation kinetics of WT or variant hGluN2A-NMDAR in the presence or absence of PSD-95. We didn't observe significant alterations in desensitization and deactivation kinetics for WT, P1386L variant, or ΔESDV hGluN2A-NMDAR in the presence of PSD-95. This is in line with the previous studies, which also didn't report any differences in these ion channel properties (summarised in Tab. 9).

Tab. 9: **Effects of PSD-95 co-transfection on NMDAR functional properties of hGluN2A WT or mutated receptors.** The summary of mean glutamate EC_{50}, current density, desensitization, and deactivation kinetics for hGluN1-1a/hGluN2A WT or mutated receptors with or without the presence of PSD-95. Values are the mean ± SEM. Highlighted values indicate significant differences between recordings with or without PSD-95, where * is $p < 0.05$ versus WT, analysed by one-way ANOVA and Tukey's multiple comparison test.

hGluN2A	WT		P1386L		ΔESDV	
PSD-95	-	+	-	+	-	+
Current density (peak,pA/pF)	**229 ± 39**	**447 ± 81***	101 ± 16	139 ± 22	192 ± 21	235 ± 46
$GluEC_{50}$ (μM)	**4,9 ± 0.6**	**8,2 ± 0.8***	7 ± 0.2	7 ± 0.8	5,6 ± 0.6	6,7 ± 0.9
Desensitization (%)	35 ± 3	29 ± 4	27 ± 3	23 ± 3	30 ± 4	26 ± 1
Deactivation						
τ fast (ms)	84 ± 21	101 ± 41	79 ± 6	85 ± 11	92 ± 18	89 ± 11
τ slow (ms)	1682 ± 321	835 ± 181	512 ± 93	505 ± 183	1982 ± 413	1282 ± 354
τ w (ms)	224 ± 36	158 ± 28	88 ± 16	80 ± 25	264 ± 24	221 ± 19
n	6	5	5	5	5	5

Although the co-localisation and electrophysiology experiments provide valuable insights into the implications of the P1386L variant, they lack direct mechanical evidence of altered interactions between these two molecules.

Therefore, to determine the effects of the P1386L variant on the interaction between the hGluN2A subunit and PSD-95, we performed co-immunoprecipitation experiments using PSD-95 antibodies to isolate protein complexes involving PSD-95, hGluN1-1a, and hGluN2A from HEK293 cells. The levels of hGluN2 P1386L detected in the immunoprecipitated (IP) fraction were found to be 85% of the hGluN2A WT levels, indicating an impairment in the interaction between PSD-95 and hGluN2A ($p = 0.009$; Fig. 22 A, B).

Furthermore, we investigated the effects of deleting the hGluN2A CTD (GluN2A-ΔCTD) to disrupt all interactions between hGluN1-1a/hGluN2A and PSD-95. Our results demonstrated that the hGluN2A protein was undetectable in the IP fraction from HEK293 cells expressing hGluN2A ΔCTD, affirming the efficacy of our co-IP method in probing PSD-95-hGluN2A interactions (Fig. 22 C).

To ultimately confirm the impact of the P1386L variant, we truncated the primary binding site for PSD-95 (hGluN2A ΔESDV) for WT and the P1386L variant receptor to discriminate between differences in the hGluN2A-PSD-95 interaction caused by the P1386L variant. The

levels of hGluN2A ΔESDV detected in the PSD-95 IP fraction were as expected low, 3.7% of hGluN2A WT levels (Fig. 22 D, E). The levels of hGluN2A P1386L ΔESDV in the IP fraction were even lower, at 2.2% of hGluN2A WT. Although hGluN2A P1386L ΔESDV levels in the IP fraction showed a considerable reduction (approximately 60%) compared to hGluN2A ΔESDV in two out of three experiments, these findings did not yield a statistically significant difference between the groups, likely due to the limited sample size (p = 0.115; Fig. 22 D, E).

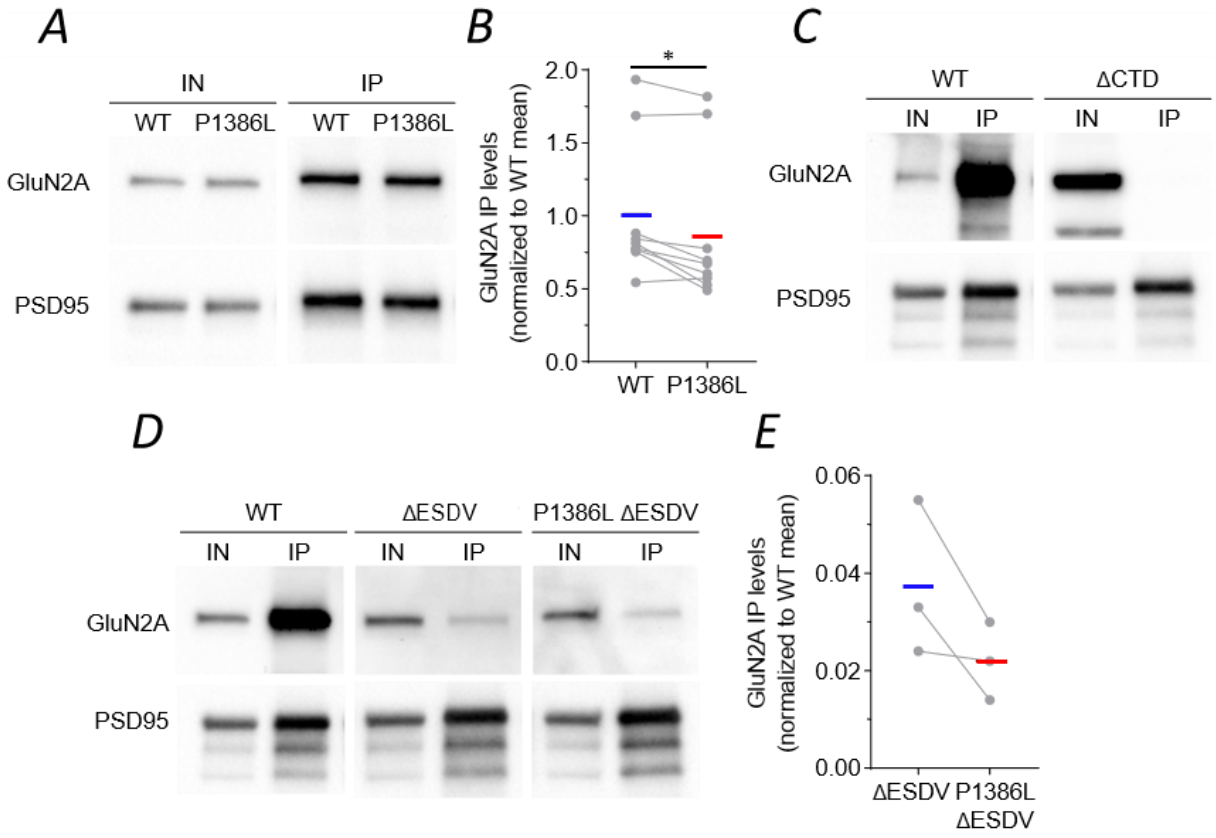

Fig. 22: **Variant P1386L in the CTD of the hGluN2A subunit reduces the interaction between PSD-95 and hGluN2A.** HEK293T cells were transfected with cDNA encoding PSD-95, hGluN1-1a, and (***A***) hGluN2A-WT or hGluN2A-P1386L (n = 9), (***C***) hGluN2A-WT or hGluN2A-ΔCTD (n = 2), (***D***) GluN2A-WT, GluN2A-ΔESDV, or GluN2A-ΔESDV-P1386L (n = 3). After 24 hr, cell lysates (input, IN) were incubated with beads conjugated to PSD-95 antibodies in order to co-immunoprecipitate (IP) PSD-95 with hGluN1-1a/hGluN2A. hGluN2A and PSD-95 levels were probed by western blotting and quantified by densitometry. The representative blots in each panel are from independent experiments. (***B, E***) The amount of hGluN2A co-immunoprecipitated with PSD-95 was normalised to the mean of the WT group and plotted as pairs within each experiment (grey symbols and lines). The blue and red lines represent the mean of each group. *, $p < 0.05$ WT versus P1386L, analysed by paired t-test.

To understand the structural consequences of the P1368L substitution, we prepared a series of *in silico* complexes of various GluN2A CTD and PSD-95 fragments using AlphaFold multimer. We modelled complexes of the GluN2A CTD fragment (containing residues 1371 to 1430 according to the Q12879 UniProt record) and PSD-95 SH3

domain (containing residues 428 to 498 according to the P78352 UniProt record). The AlphaFold miltimer modeling predicts a rich set of interacting residues between the WT GluN2A CTD fragment and the PSD-95 SH3 domain. On the other hand, the complex with the P1386L variant in the CTD fragment shows visibly much fewer contacts with the SH3 domain (Fig. 23). The model predicts that the position of the introduced leucine 1386 overlaps with the position originally occupied by the alanine 1409 in the WT. The binding of the larger hydrophobic leucine is locally stabilized; however, the binding is non-specific and competes with the interactions observed for the WT GluN2A CTD fragment.

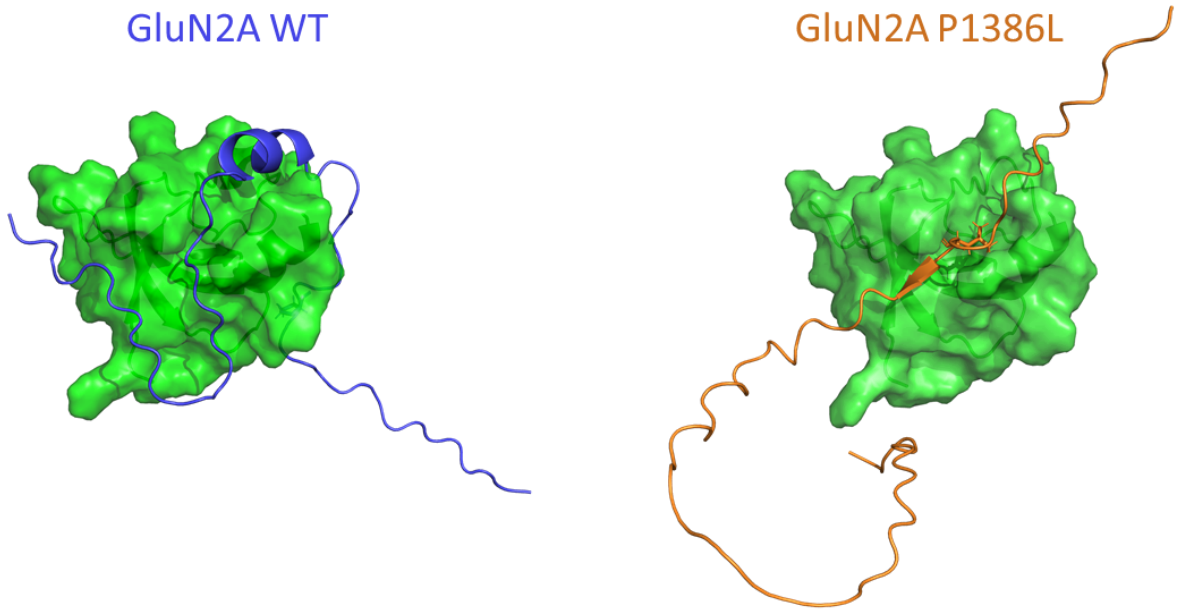

Fig. 23: **Variant P1386L in the CTD of the hGluN2A subunit reduces the amino acid interactions between the SH3 domain of PSD-95 and the CTD of the GluN2A subunit.** *In silico* complex of the SH3 domain of PSD-95 and the CTD fragment of the WT or P1386L variant with amino acids between 1371 and 1430.

5.3.2.5. The effect of the GluN2A missense variant P1386L on synaptic function

The previous findings indicating an impaired interaction between the hGluN2A P1386L variant and the presynaptic scaffold protein PSD-95 using co-localisation, electrophysiology, and co-immunoprecipitation experiments were further studied directly on the NMDAR site of action on the synapse.

To identify the precise distribution of variants within the synapse and adjacent regions, we used transmission electron microscopy (TEM) together with gold labeling in primary mouse hippocampal neurons. In our experiment, a small 6xHIS tag was introduced into lentiviral vectors for the WT or P1386L variant and, the neurons were infected. The neurons were cultured on coverslips covered by a finder grid with coordinates. and infected neurons were identified by fluorescence microscopy by the eGFP signal. Subsequently, the 6xHis-eGFP-hGluN2A-NMDAR, WT or variant, were live-labelled with a Ni-NTA nanoprobe conjugated to 5 nm gold particles, and the samples were processed for TEM. The length of-PSD in proximity to the postsynaptic membrane was used to calculate the length of the synaptic region. The perisynaptic region was defined as a membrane region adjacent to the synaptic region on both sides, with the same length as the length of PSD on each side (Fig. 24 A, B).

Since binding to the 6xHis tag by Ni-NTA nanoprobe can be less specific, we determined the average number of labels per 100 nm of synapse for neurons transduced by 6xHis-eGFP-hGluN2A WT NMDAR and for the virally untransduced negative control sample. Although we detected some unspecific labelling, transduced neurons exhibited a significantly higher average number of labels per 100 nm of synapse when compared to the negative control (2.09 vs. 0.9, $p = 0.009$); thus, enabling us to proceed with the further analysis (Fig. 24 C).

As an additional internal control, we measured the average length of the PSD for both the WT and P1386L variant 6xHis-eGFP-hGluN2A-NMDAR samples, as well as the negative control. The length of PSD remained unaltered, as we found no significant difference between the samples (WT – 283 nm, P1386L – 286 nm, NK – 248 nm) (Fig. 24 D).

Next, we measured the distance of gold particles from the central axis of the PSD to the perisynaptic edge for both the WT and P1386L variant 6xHis-eGFP-hGluN2A-NMDAR, where 0 denotes the central axis of the PSD, 1 indicates the border of the synaptic region (0 to 1 is a half of the synaptic region), and 3 represents the perisynaptic border. We then plotted all detected gold particles according to their distances and analysed their distribution across the synaptic and perisynaptic regions. The distribution displayed a clear difference between the

WT and P1386L variant receptors, which exhibited, in comparison to WT, lower labelling within the synaptic and more labelling in the perisynaptic region (Fig. 24 E, F).

To quantify this difference, we first measured the mean relative distance from the central axis of the PSD for both the WT and P1386L variant receptors. The results then show a significant increase in relative distance from the center of the synapse for P1386L 6xHis-eGFP-hGluN2A-NMDAR (1.35, $p = 0.001$) compared to the WT receptor (0.99) (Fig. 24 G).

Second, we calculated the average number of gold labels per 100 nm of the synapse and perisynapse. In the case of synapse, WT 6xHis-eGFP-hGluN2A-NMDAR (2.13) exhibited a significantly higher number of receptors compared to the P1386L variant receptor (1.4, $p = 0.005$) (Fig. 24 H). Conversely, WT 6xHis-eGFP-hGluN2A-NMDAR (1.44) exhibited a lower number of receptors in the perisynapse compared to the P1386L variant receptor (1.96), although this difference did not reach statistical significance (Fig. 24 I).

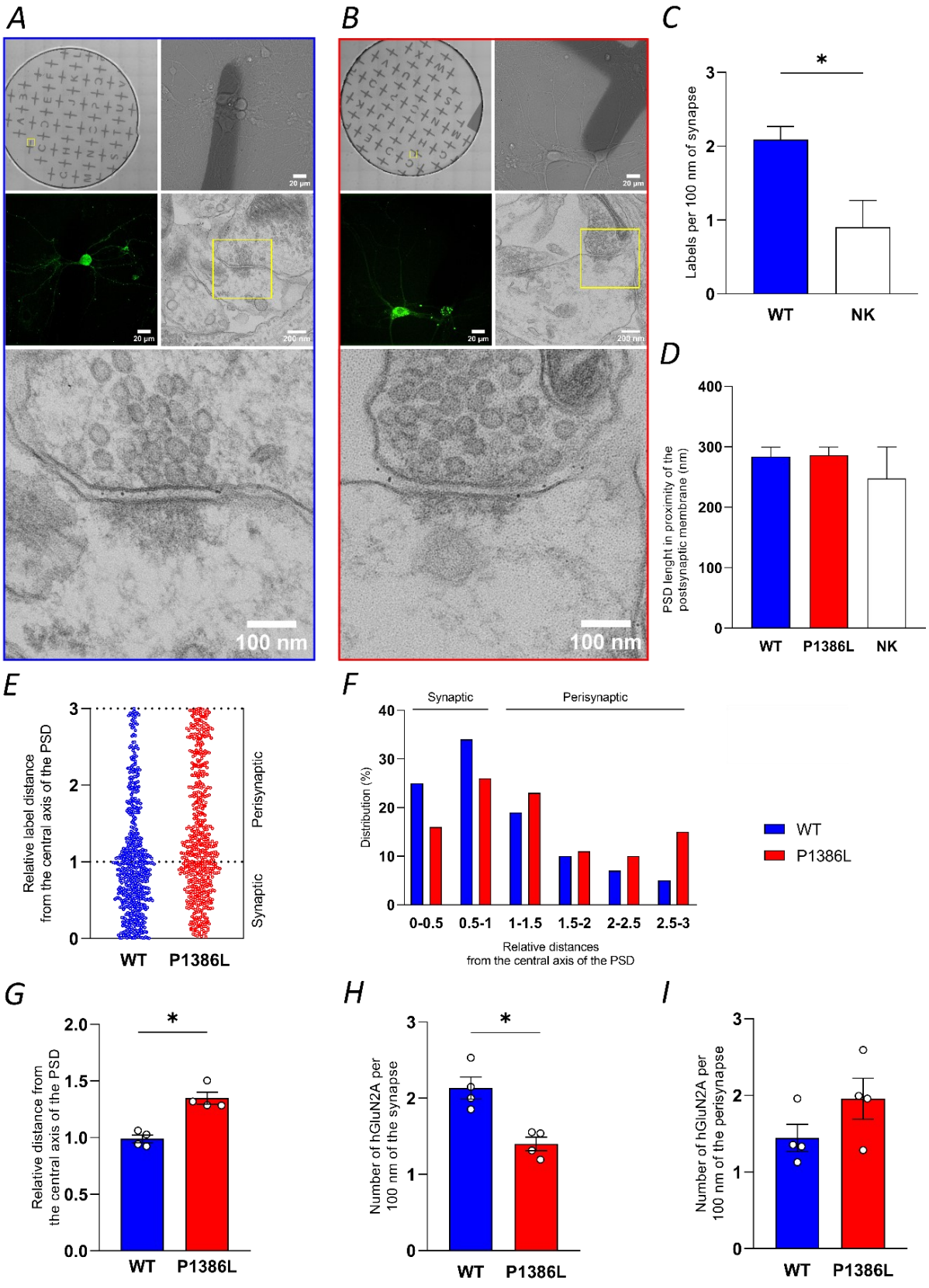
A
B
C
D
E
F
G
H
I
20 µm
200 nm
100 nm
Labels per 100 nm of synapse
WT
NK
PSD lenght in proximity of the postsynaptic membrane (nm)
P1386L
Relative label distance from the central axis of the PSD
Perisynaptic
Synaptic
Distribution (%)
Relative distances from the central axis of the PSD
0-0.5
0.5-1
1-1.5
1.5-2
2-2.5
2.5-3
Relative distance from the central axis of the PSD
Number of hGluN2A per 100 nm of the synapse
Number of hGluN2A per 100 nm of the perisynapse

Fig. 24: **The genetic variant P1386L within the CTD of the hGluN2A subunit reduces synaptic localisation of NMDARs in hippocampal neurons.** (***A***,***B***) Representative images of 6xHis-eGFP-hGluN2A WT (***A***) and P1386L (***B***) show a grid surface with coordinates (*upper left*), brightfield (*upper right*), and confocal (*middle left*) live images of neurons and TEM images of gold-stained neurons with lower (*middle right*) and higher magnification (*down*). The yellow-marked area indicates the field of view of a high-magnification TEM image. (***C***) Summary of the mean number of gold labels per 100 nm of synapse for 6xHis-eGFP-hGluN2A WT NMDARs (n = 65 synapses) and untransduced negative control samples (n = 12 synapses/cells). (***D***) Summary of the mean PSD length in proximity of the postsynaptic membrane for 6xHis-eGFP-hGluN2A WT (n = 65 synapses) and P1386L (n = 66 synapses) NMDARs and untransduced negative control samples (n = 12 synapses/cells). (***D***) Relative gold label distance from the central axis of PSD for 6xHis-eGFP-hGluN2A WT (n = 575 gold particles) and P1386L (n = 564 gold particles) NMDARs, where interval [0,1] shows synaptic and interval [1,3] perisynaptic localisation. (***F***) The distribution in percentage of gold label distances from the central axis of PSD in synaptic [0,1] and perisynaptic [1,3] regions for 6xHis-eGFP-hGluN2A WT (n = 575 gold particles) and P1386L (n = 564 gold particles) NMDARs. (***G***) Summary of the mean relative label distance from the central axis of PSD for 6xHis-eGFP-hGluN2A WT (n = 4 neurons (65 synapses)) and P1386L (n = 4 neurons (66 synapses)) NMDARs. (***H***) Summary of the mean number of hGluN2A per 100 nm of synapse for 6xHis-eGFP-hGluN2A WT (n = 4 neurons (65 synapses)) and P1386L (n = 4 neurons (66 synapses)) NMDARs. (***I***) Summary of the mean number of hGluN2A per 100 nm of perisynapse for 6xHis-eGFP-hGluN2A WT (n = 4 neurons (65 synapses)) and P1386L (n = 4 neurons (66 synapses)) NMDARs. All summary data are presented as the mean ± SEM. *, $p < 0.05$, analysed by the t test.

To functionally examine the observed difference in synaptic distribution of the WT and P1386L variant of the GluN2A subunit, we performed electrophysiology experiment on virally transduced primary hippocampal neurons. The weaker binding of the hGluN2A P1386L subunit to PSD due to impaired PSD-95 binding in synapses might be manifested in the relatively smaller NMDAR-mediated mEPSCs in cultures transduced with the hGluN2A P1386L variant subunit compared to cultures transduced with the hGluN2A WT subunit.

Therefore, we measured NMDAR mEPSCs when we applied glycine and NBQX (AMPA and kainate receptor blockers) to patched neurons. We did not record individual NMDAR mEPSCs, as is seen when AMPA/kainate mEPSCs are measured (pre-application with AP5, an NMDAR antagonist), but we observed the collective current of several overlapping NMDAR mEPSCs (Fig. 24 A). This occurrence is due to the relatively prolonged nature of NMDAR mEPSCs (> 0.3 seconds) and their frequency in our cultures, which is approximately 8 mEPSCs per second. As a result, the majority of NMDAR mEPSCs overlap with one another, avoiding the analysis of individual mEPSC.

However, from our data, we were able to estimate the average charge transfer of a single NMDAR mEPSC, a parameter we anticipated to be reduced in cultures expressing the hGluN2-P1386L subunit. The collective current's magnitude equals the average charge transfer of a single NMDAR mEPSC multiplied by the frequency of NMDAR mEPSCs. Assuming the frequency of NMDAR and AMPAR mEPSCs is the same (indicated by no expected changes in presynaptic glutamate release on a roughly 10-second timescale), the

average charge transfer of a single NMDAR mEPSC can be calculated as the collective current magnitude divided by the frequency of AMPA mEPSCs (Fig. 25 A).

In mouse neurons transduced with the hGluN2A-P1386L subunit, the estimated charge transfer of an average NMDAR mEPSC was 6.0 ± 1.1 pA.s, showing a 34% reduction compared to neurons transduced with hGluN2A-WT, which displayed an average charge transfer of 9.0 ± 1.6 pA.s (Fig. 25 B). Although this reduction aligns with our hypothesis, it did not achieve statistical significance (p = 0.15).

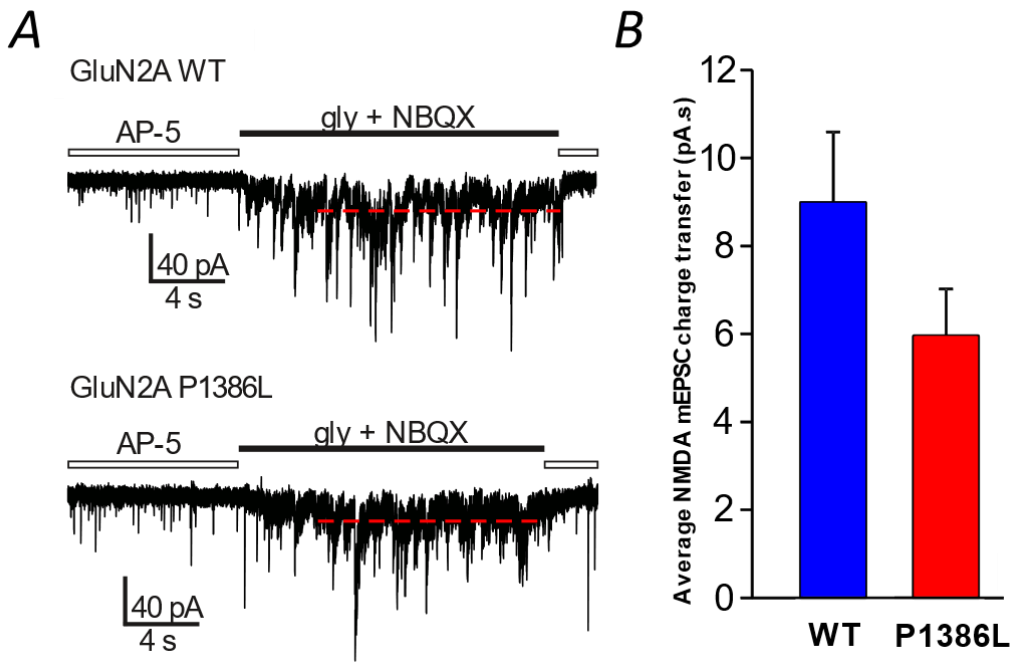

Fig. 25: **Variant P1386L in the GluN2A subunit alters NMDA mEPSC charge transfer.** (***A***). The assessment of the average charge transfer of a single NMDAR mEPSC was based on the measurement of AMPAR mEPSCs frequency fA (when AP-5 was applied), followed by the measurement of the average collective current (IC, dashed lines) of overlapping NMDAR mEPSCs (when glycine and NBQX were applied). (***B***) The average charge transfer of a single NMDAR mEPSCs is equal to IC/fA. The bar graph compares the average charge transfer of a single NMDAR mEPSCs in neurons transduced by the hGluN2A WT or P1386L subunit (n = 6 for each column, t-test p = 0.15).

All results describing the effects of the P1386L variant indicated functional and structural impairment of the PSDPYK binding motif, resulting in lower synaptic anchoring of the variant receptor, which might critically affect whole synaptic function. If the PSDPYK motif provides such an important feature for neurotransmission, we were curious how much the motif is evolutionary conserved in less complex vertebrates.

The PSDPYK motif is highly conserved throughout the species, but it is completely preserved only within mammals. However, it's intriguing that less complex vertebrates have leucine or isoleucine in the fourth position, similarly to the disease-associated variant P1386L. For

instance, birds possess amino acid substitutions in positions two and four, resulting in the motif PADLYK. Reptiles like crocodiles and rhynchocephalias exhibit the same exact motif as our variant, PSDLYK. Turtles, similar to birds, carry the PADLYK motif, while varans have an additional substitution in position three, leading to the sequence PAGLYK. Less complex species, such as amphibians and fish, show a substitution in the first position and proline substitutes for isoleucine in the fourth position, resulting in the SSDIYK motif. Chondrichthyes, like sharks, have, in addition, an insertion between positions two and three, yielding the motif SSTDIYK. Overall, only the last two amino acids of the motif are preserved through the vertebrates, while the consensus SH3 binding motif PxxP is more variable (Tab. 10).

Tab. 10: **Alternations of PSDPYK binding motif within different species.** The underline P (proline) indicates the position of the P1386L variant. Red letters indicate amino acid changes compared to the mammalian binding motif. Less complex animal species contain L (leucine) or I (isoleucine) at the fourth position of the binding motif. *Note: NMDARs in invertebrates do not contain CTD.*

Species	Class	Order	Binding motif	UniProt code
Homo sapiens	*Mammalia*	*Primates*	**PSDPYK**	UPI000000D7AB
Mus musculus	*Mammalia*	*Rodentia*	**PSDPYK**	UPI00001EA349
Gallus gallus	*Aves*	*Galliformes*	**PADLYK**	UPI0020B00B08
Crocodylus porosus	*Reptilia*	*Crocodilia*	**PSDLYK**	UPI00093B3BDE
Chelonia mydas	*Reptilia*	*Testudines*	**PADLYK**	UPI0018A1E5CF
Varanus komodoensis	*Reptilia*	*Squamata*	**PAGLYK**	UPI00133D4A2B
Sphenodon punctatus	*Reptilia*	*Sphenodontida*	**PSDLYK**	UPI000FC7DE58
Xenopus laevis	*Amphibia*	*Anura*	**SSDIYK**	UPI0001615E62
Danio rerio	*Actinopterygii*	*Cypriniformes*	**SSDIYK**	UPI0001E9186E
Callorhinchus milii	*Chondrichthyes*	*Chimaeriformes*	**SSTDIYK**	UPI0011495B26

5.4. Characterisation of functional determinants of the GluN2A and GluN2B subunits' CTD

In light of the strong effects of missense variants within the CTD of the GluN2A subunit on NMDAR function, we also, in detail, analysed the functional determinants within the CTD of the GluN2A and GluN2B NMDAR subunits. Together with the GluN1 subunits, they are both the most highly expressed subunits. The CTD is then their largest domain, but with a less understood function.

5.4.1. Functional characterisation of GluN2A/2B CTD nonsense and frameshift variants

To study the functional significance of the CTD of GluN2A and B subunits, we generated truncated hGluN2A/2B subunits with CTDs of different lengths. Truncated CTD corresponded to nonsense and frame-shift variants associated with various neurodevelopmental disorders, resulting in a premature stop codon and a truncated protein. We performed a screening of available databases (https://ncbi.nlm.nih.gov/clinvar/; http://functionalvariants.emory.edu/database/index.html) and identified ten *de-novo* nonsense and frame-shift variants, which we used for a comprehensive investigation of the consequences of subunit truncation on receptor surface expression, synaptic localisation, and ion channel properties. Additionally, we prepared and included the artificial hGluN2A R846X variant, allowing the analysis of receptors with the complete deletion of the hGluN2A CTD, similar to the disease-associated hGluN2B R847X variant (Tab. 11).

Tab. 11: **Selected *de-novo nonsense* and frame-shift variants identified in the CTDs of hGluN2A and hGluN2B subunits and characterisation of their phenotype.**

Subunit	Variant	Type	Phenotype	References
hGluN2A	S913X	nonsense	EPI, ID	(von Stülpnagel et al., 2017)
	Y943X	nonsense	EPI, ID	(Lemke et al., 2013)
	Q950X	nonsense	ANS	(Retterer et al., 2016)
	Y1387X	nonsense	EPI, ID, ASD	(Lesca et al., 2013)
hGluN2B	R847X	nonsense	ASD, ID, DD	(Firth et al., 2009; Platzer et al., 2017)
	I864SfsX20	frame-shift	ANS, DD, ID	(Retterer et al., 2016)
	Y1004X	nonsense	ASD, ID	(Platzer et al., 2017)
	R1099AfsX51	frame-shift	ASD, ID	(Rauch et al., 2012)
	Y1155X	nonsense	ASD, ID	(O'Roak et al., 2014; Stessman et al., 2017)
	S1415X	nonsense	ASD	(DB)

Abbreviation Key: ANS, abnormality of the nervous system; ASD, autism spectrum disorder, or features thereof; DD, developmental delay; EPI, epilepsy, focal or generalized seizures; ID, intellectual disability (including non-verbal); X, stop codon; fs, frame-shift; DB, Functional Variants CFERV Database (http://functionalvariants.emory.edu/database/index.html).

5.4.1.1. The effects of the GluN2A CTD nonsense and frameshift variants on surface expression in HEK293T and COS-7 cells

Identically to our investigation of GluN2A missense variants, we first examined the surface expression, because the compromised CTD can affect receptor trafficking and the stability of its surface expression. As previously, we used immunofluorescence microscopy and a colorimetric assay to analyse the surface expression of NMDAR subunits. We generated eGFP-hGluN2A/2B subunits containing different CTD variants and co-transfected these constructs along with the hGluN1-1a subunit into both HEK293T cells (for immunofluorescence microscopy) and COS-7 cells (for the colorimetric assay) to evaluate NMDAR expression on the cell surface.

Analysis of images revealed significant alterations in the surface-to-intracellular ratio of the majority of NMDAR variants. In HEK293T cells, the hGluN1-1a/eGFP-hGluN2A Y1387X variant receptor only exhibited a significantly increased surface expression, while the hGluN1-1a/eGFP-hGluN2A R846X, S913X, Y943X, and Q950X receptors displayed a significantly reduced surface expression compared to the hGluN1-1a/eGFP-hGluN2A WT receptors (Y1387X – 16% increase, $p = 0.003$; R846X – 72% decrease, $p = < 0{,}001$; S913X – 61% decrease, $p = < 0{,}001$, Y943X – 75% decrease, $p = < 0{,}001$; Q950X – 56% decrease,

p = < 0,001) (Fig. 26 A, C). Parallelly, these findings were further confirmed by a colorimetric assay in COS-7 cells, showing a similar increase in surface expression for the hGluN1-1a/eGFP-hGluN2A Y1387X receptor and a decrease for the rest of the truncated eGFP-hGluN2A subunit-containing NMDARs (Y1387X – 21% increase, p = 0.037; R846X – 85% decrease, p = < 0,001; S913X – 88% decrease, p = < 0,001; Y943X – 84% decrease, p = < 0,001; Q950X – 71% decrease, p = < 0,001) (Fig. 26 D).

Similarly, for hGluN2B subunit, in both HEK293T and COS-7 cells, the surface expression of all hGluN1-1a/eGFP-hGluN2B R847X, I864SfsX20, Y1004X, R1099AfsX51, Y1155X, and S1415X receptor variants was significantly reduced when compared to hGluN1-1a/eGFP-hGluN2B WT receptors (HEK293T: R847X – 41% decrease, p = < 0,001; I864SfsX20 – 27% decrease, p = < 0,001; Y1004X – 30% decrease, p = < 0,001; R1099AfsX51 – 33% decrease, p = < 0,001; Y1155X – 29% decrease, p = < 0,001; S1415X – 46% decrease, p = < 0,001 / COS-7: R847X – 51% decrease, p = < 0,001; I864SfsX20 – 53% decrease, p = < 0,001; Y1004X – 44% decrease, p = < 0,001; R1099AfsX51 – 44% decrease, p = < 0,001; Y1155X – 31% decrease, p = < 0,014; S1415X – 40% decrease, p = < 0,001) (Fig. 26 B, E, F).

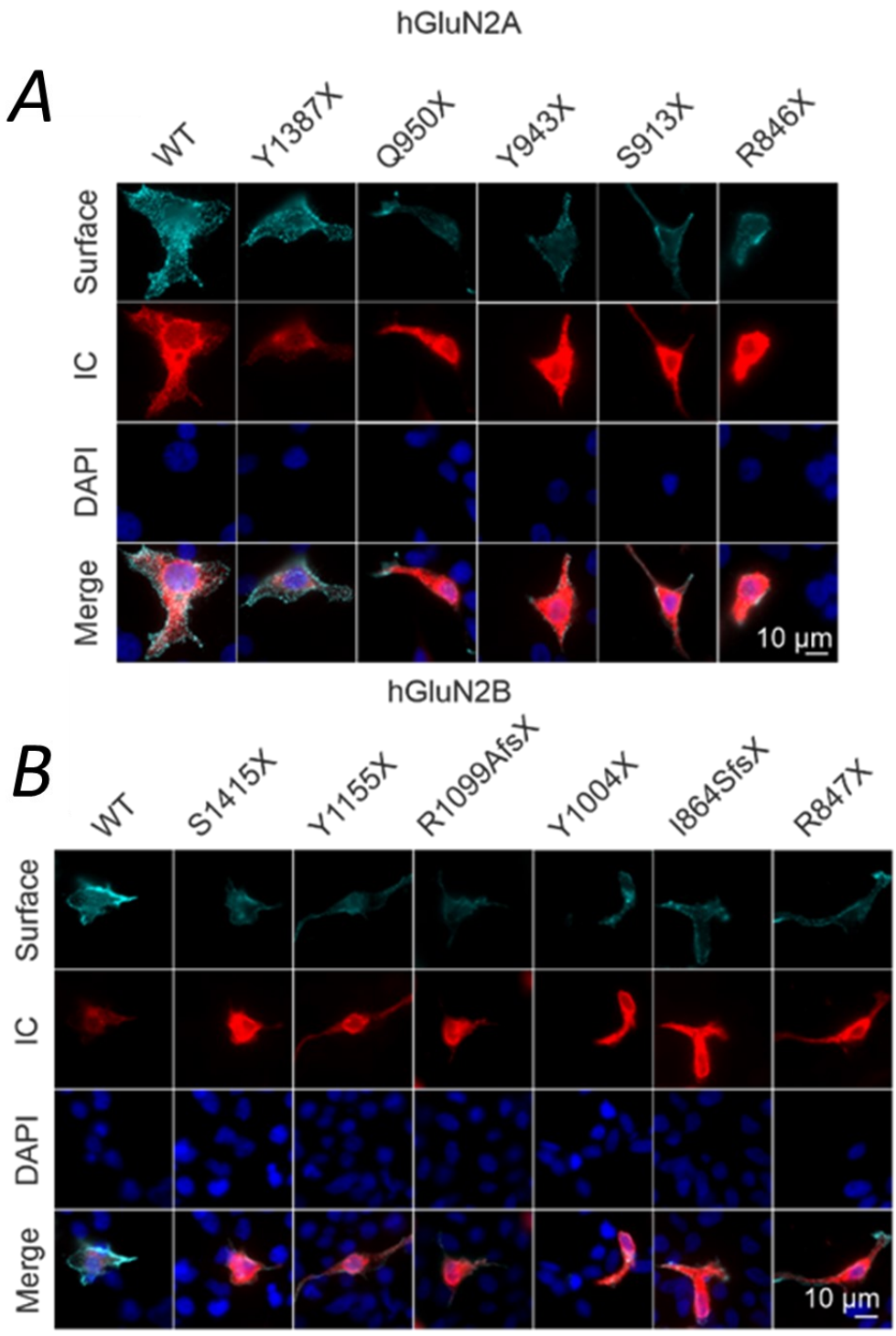
hGluN2A
A
WT
Y1387X
Q950X
Y943X
S913X
R846X
Surface
IC
DAPI
Merge
10 µm
hGluN2B
B
WT
S1415X
Y1155X
R1099AfsX
Y1004X
I864SfsX
R847X
Surface
IC
DAPI
Merge
10 µm

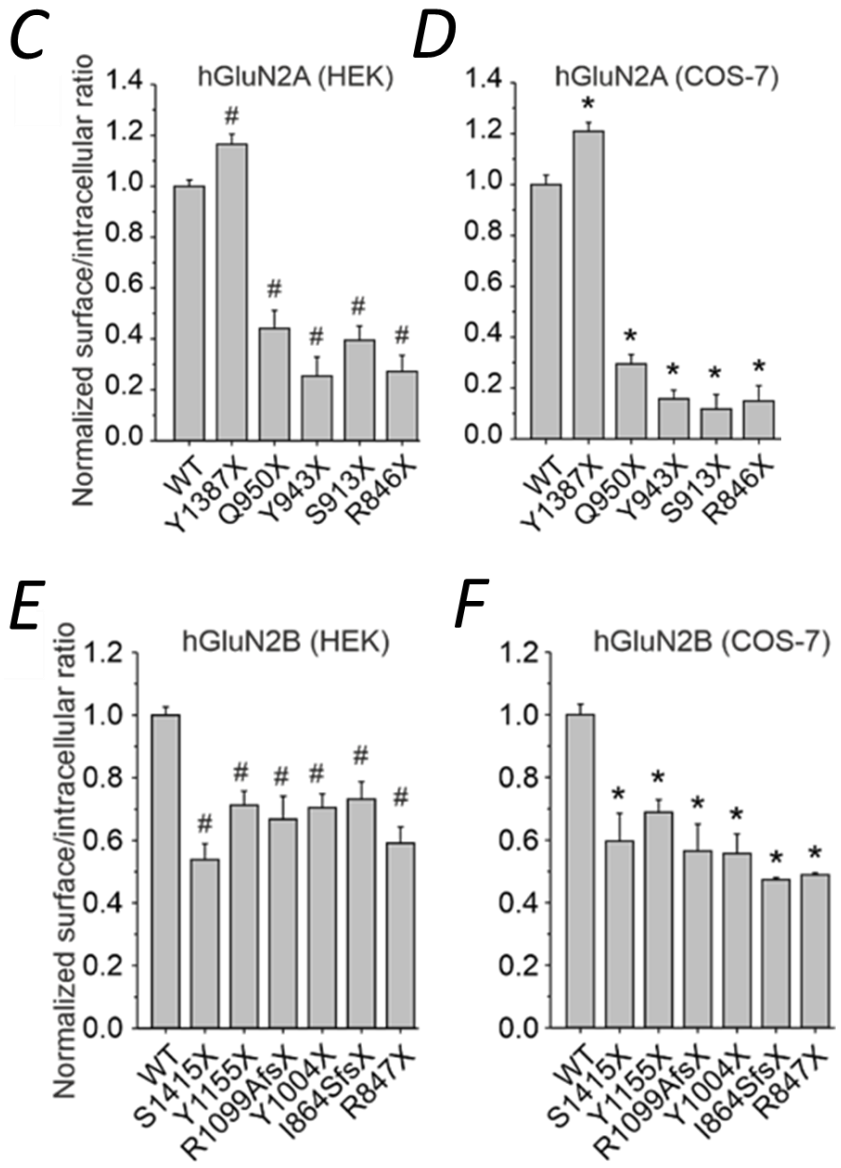

Fig. 26: **Truncations of CTD of hGluN2A and hGluN2B subunits alter surface expression of NMDARs in HEK293 and COS-7 cells.** (***A***,***B***) Representative images of surface and intracellular (IC) eGFP-hGluN2A (***A***) and eGFP-hGluN2B (***B***) subunits measured in HEK293T cells expressing the indicated subunit with WT or truncated CTD. Cells were co-transfected with hGluN1-1a. DAPI was used as an indicator of cell viability. (***C***,***E***) Summary of the mean relative surface expression of eGFP-hGluN2A (***C***) and eGFP-hGluN2B (***E***) subunits measured in HEK293T cells using fluorescence microscopy (n ≥ 100 cells per group from three to four independent experiments). (***D***, ***F***) Summary of the mean relative surface expression of eGFP-hGluN2A (***D***) and eGFP-hGluN2B (***F***) subunits measured in COS-7 cells using a quantitative colorimetric assay. Cells were co-transfected with hGluN1-1a. Relative surface expression was measured in quadruplicate in three to four independent experiments. All summary data are presented as the mean ± SEM. # or *, $p < 0.05$ versus WT, analysed by one-way ANOVA and Tukey's or Dunnett's multiple comparison test.

After that, we used patch-clamp electrophysiology methods to measure the NMDAR current density evoked by glutamate (1 mM) in the presence of 30 μM glycine. The analysis was performed on HEK293T cells co-transfected with both hGluN1-1a and hGluN2A/2B WT or variant subunits. Results indicated a tendency to reduce current density in receptors with truncated CTD compared to WT. Although statistical significance was only confirmed in hGluN1-1a/hGluN2B I864SfsX20 (95% decrease, p = 0.029) and S1415X (89% decrease, p = 0.031) receptors, current densities can vary due to ion channel properties and different transfection efficiencies among cells (Fig. 27).

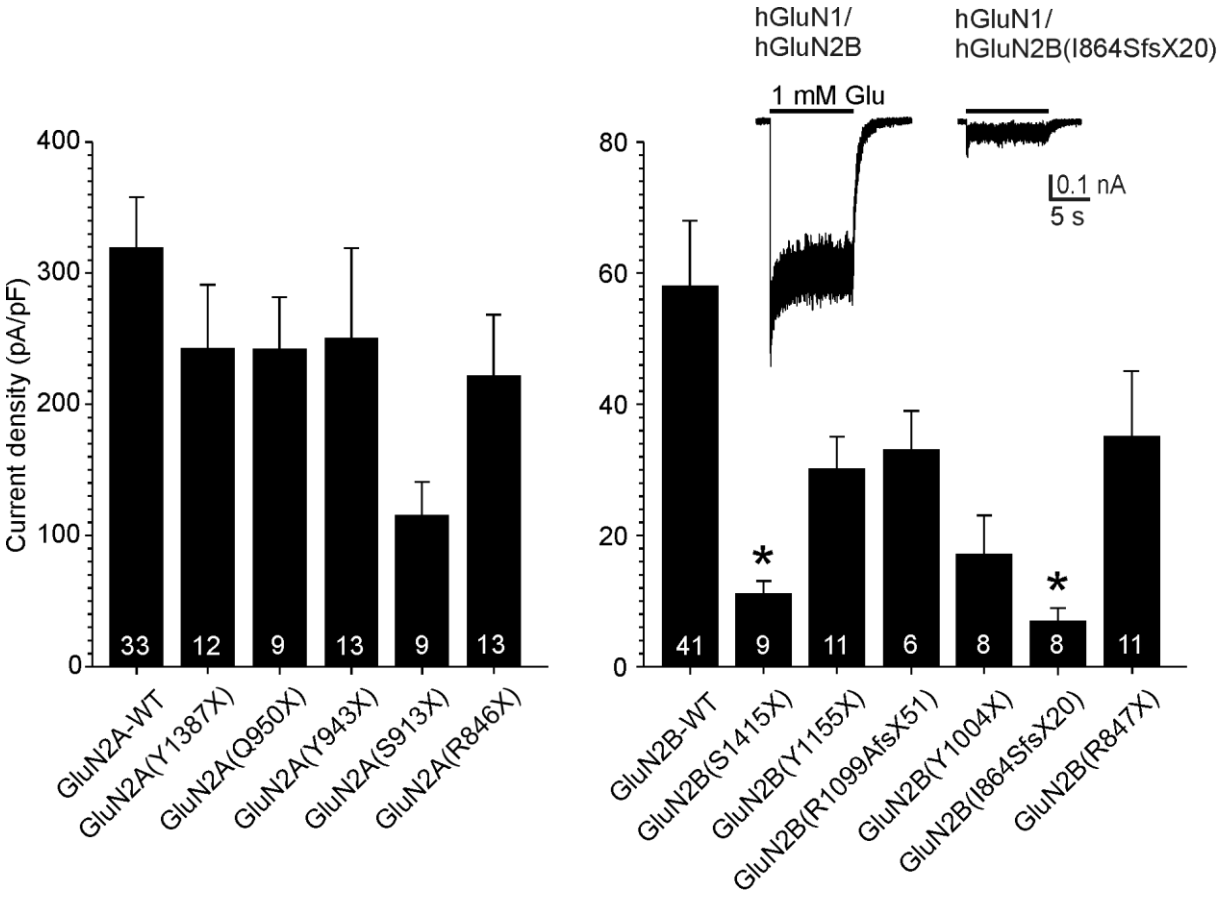

Fig. 27: **Truncations of the CTD of hGluN2A and hGluN2B subunits decrease the current density of NMDARs.** Summary of mean current density of WT or mutated hGluN1-1a/hGluN2A (*left*) or hGluN2B (*right*) NMDAR with the figure illustrating typical whole-cell recordings of currents induced in HEK293T cells that have been transfected with cDNA encoding hGluN1-1a/hGluN2B WT or hGluN1-1a/hGluN2B I864SfsX20 NMDAR. NMDAR's currents were evoked by 1 mM glutamate and normalised with respect to the individual HEK cell capacitance. All summary data are presented as the mean ± SEM. *, $p < 0.05$ versus WT, analysed by one-way ANOVA and Dunnett's multiple comparison test.

5.4.1.2. The effects of the GluN2A CTD nonsense and frameshift variants on receptor ion channel properties

The various functional properties of the disease-associated hGluN2A/2B subunit variants with truncated CTD were further examined using patch-clamp electrophysiology in HEK293T cells co-expressing the hGluN1-1a and hGluN2A/2B variants, or WT subunits.

Analysis of glutamate potency revealed a significant increase in glutamate EC_{50} for hGluN1-1a/hGluN2B R847X receptors (3.9 µM, p = < 0.001); however, glutamate EC_{50} did not significantly differ in any other hGluN2A/2B receptors with truncated CTD compared to WT receptors (1.7 µM) (Fig. 28 A, summarised in Tab. 12).

Analysis of glycine potency revealed a significant reduction in glycine EC_{50} for hGluN1-1a/hGluN2B I864SfsX20 (0.11 µM, p = < 0,001) and R847X (0.12 µM, p = < 0,001) variant receptors. However, glycine potency did not significantly differ in the other truncated hGluN2A and hGluN2B variants, compared to receptors containing hGluN2A/2B WT subunits (0.24 µM) (Fig. 28 B, summarised in Tab. 12).

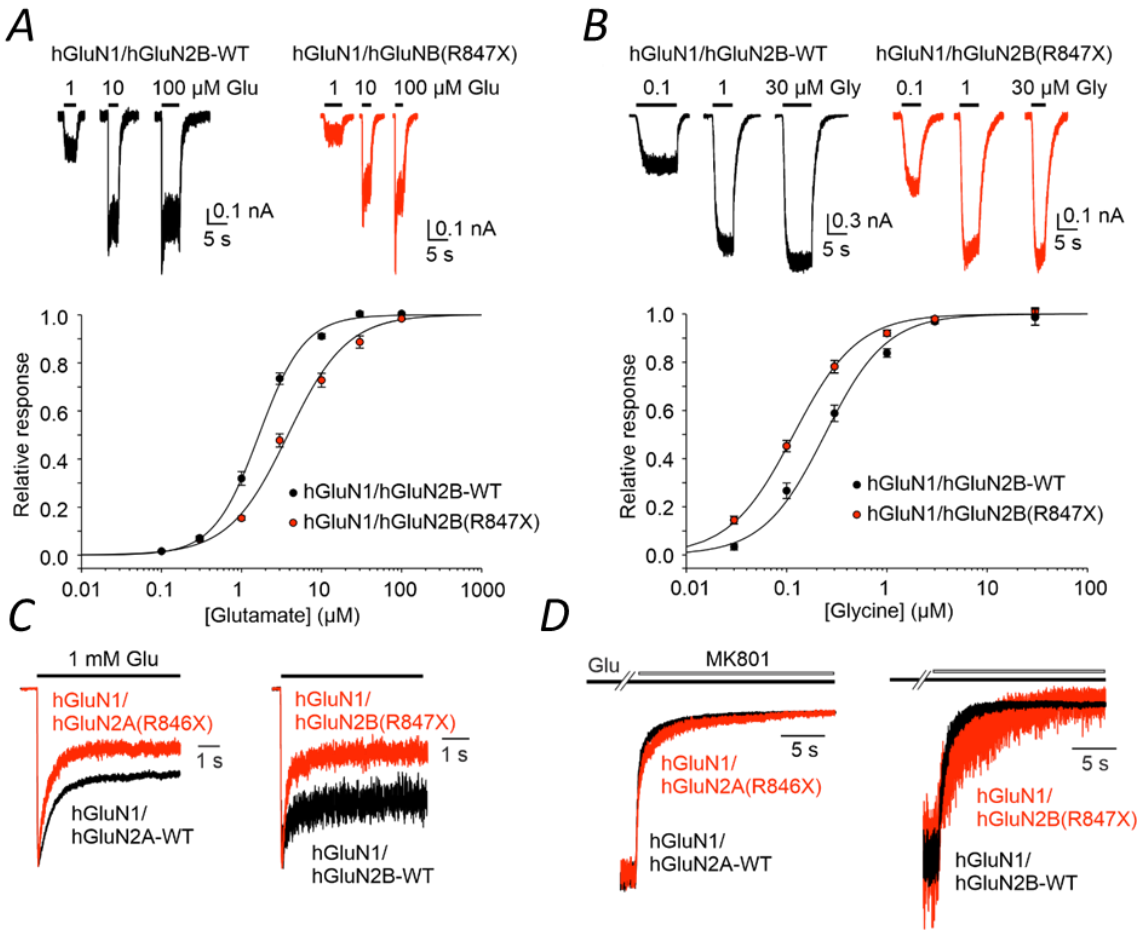

Fig. 28: **Truncations of the CTD of hGluN2A and hGluN2B subunits alter NMDAR functional properties.** (***A***) Representative figures of NMDAR current evoked by 1, 10, and 100 μM glutamate applications in the presence of 30 μM glycine in HEK293T cells expressing hGluN1-1a/hGluN2B WT R847X mutated receptors. The plot shows the relative peak dose-response relationship for glutamate activation of hGluN1-1a/hGluN2B WT (black circles, n = 9) or R847X mutated NMDARs (red circles, n = 5). The data are presented as the mean ± SEM. (***B***) Representative figures of NMDAR current evoked by 0.1, 1, and 30 μM glycine applications in the presence of 1 mM glutamate in HEK293T cells expressing hGluN1-1a/hGluN2B WT or R847X mutated receptors. The plot shows the relative peak dose-response relationship for glycine activation of hGluN1-1a/hGluN2B-WT (black circles, n = 13) and hGluN1-1a/hGluN2B (R847X) receptors (red circles, n = 7). The data are presented as the mean ± SEM. (***C***) Representative recordings of the currents induced in hGluN1-1a/hGluN2A WT or R846X mutated receptors and hGluN1-1a/hGluN2B WT or R847X mutated receptors by fast application of 1 mM glutamate and in the presence of 30 μM glycine. The representative currents are shown normalised with respect to the maximal response. (***D***) Representative recordings of normalised currents induced by application of 1 mM glutamate in the continuous presence of 30 μM glycine hGluN1-1a/hGluN2A WT or R846X mutated receptors and hGluN1-1a/hGluN2B WT or R847X mutated receptors showing the onset of MK-801 (1 μM) inhibition.

Tab. 12: **The impact of hGluN2A and hGluN2B CTD truncations on the potency of NMDAR agonists.** The summary of mean glutamate and glycine EC_{50} for hGluN1-1a/hGluN2A and hGluN2B WT or mutated receptors. Values are the mean ± SEM. Highlighted values indicate significant differences compared to WT, where * is $p < 0.05$ versus WT, analysed by one-way ANOVA and Dunnett's multiple comparison test.

Subunit	Variant	Glutamate			Glycine		
		EC_{50} (μM)	h	*n*	EC_{50} (μM)	h	*n*
hGluN2A	WT	5.0 ± 0.3	1.09 ± 0.02	6	1.50 ± 0.17	1.20 ± 0.07	6
hGluN2A	Y1387X	4.3 ± 0.4	1.24 ± 0.07	5	1.50 ± 0.21	1.29 ± 0.29	5
hGluN2A	Q950X	7.0 ± 0.7	1.29 ± 0.06	7	1.29 ± 0.16	1.30 ± 0.10	5
hGluN2A	Y943X	7.3 ± 0.7	1.27 ± 0.07	11	1.85 ± 0.16	1.43 ± 0.08	5
hGluN2A	S913X	6.0 ± 0.9	1.13 ± 0.08	5	1.85 ± 0.05	1.61 ± 0.07	5
hGluN2A	R846X	5.7 ± 0.5	1.04 ± 0.08	5	0.72 ± 0.05	1.30 ± 0.14	6
hGluN2B	WT	1.7 ± 0.1	1.33 ± 0.03	9	0.24 ± 0.02	1.41 ± 0.08	13
hGluN2B	S1415X	1.9 ± 0.3	1.27 ± 0.08	4	0.26 ± 0.02	1.46 ± 0.06	5
hGluN2B	Y1155X	1.7 ± 0.2	1.32 ± 0.03	7	0.26 ± 0.02	1.29 ± 0.17	5
hGluN2B	R1099AfsX51	1.6 ± 0.1	1.39 ± 0.05	7	0.28 ± 0.01	1.39 ± 0.07	5
hGluN2B	Y1004X	1.5 ± 0.1	1.30 ± 0.05	5	0.19 ± 0.04	1.51 ± 0.19	4
hGluN2B	I864SfsX20	1.5 ± 0.3	1.33 ± 0.04	5	**0.11 ± 0.01***	1.40 ± 0.10	6
hGluN2B	R847X	**3.9 ± 0.3***	1.37 ± 0.05	5	**0.12 ± 0.01***	1.36 ± 0.09	7

We then examined the effects of hGluN2A/2B CTD truncations on NMDAR desensitization, which reflects the time-dependent decline in responses following activation. Using a saturating concentration of glutamate (1 mM) in the presence of glycine (30 μM), we observed that hGluN1-1a/hGluN2A-WT and hGluN1-1a/hGluN2B-WT receptors desensitized by approximately 42% and 19%, respectively. Receptors with the most extensive CTD truncation showed a significantly higher desensitization rate, specifically hGluN1-1a/hGluN2A

R846X (62%, p = < 0.001), hGluN1-1a/hGluN2B I864SfsX20 (48%, p = < 0.001), and hGluN1-1a/hGluN2B R847X (54%, p = < 0.001) receptors when compared to WT receptors (hGluN2A – 42% and hGluN2B – 19%). In contrast, receptors with shorter hGluN2A or hGluN2B CTD truncations displayed relatively the same level of desensitization as WT receptors (Fig. 28 C, summarised in Tab. 13).

The elevated desensitization in receptors with larger CTD truncations was partly due to an increased desensitization rate constant (kd) observed in hGluN1-1a/hGluN2A R846X, hGluN1-1a/hGluN2B I864SfsX20, and R847X receptors, compared to their respective WT receptors. Additionally, the resensitization rate constant (kr) was raised in hGluN1-1a/hGluN2A Q950X, R846X, and hGluN1-1a/hGluN2B I864SfsX20 receptors when compared to the WT receptor values (summarised in Tab. 13).

Tab. 13: The impact of hGluN2A and hGluN2B CTD truncations on NMDAR desensitization and open probability (P_o). The summary of mean desensitization and open probability for hGluN1-1a/hGluN2A and hGluN2B WT or truncated receptors. Values are the mean ± SEM. Highlighted values indicate significant differences compared to WT, where * is p < 0.05 versus WT, analysed by one-way ANOVA and Dunnett's multiple comparison test.

Subunit	Variant	Desensitization				P_o	
		%	k_d	k_r	*n*	%	*n*
hGluN2A	WT	42 ± 4	0.47 ± 0.09	0.59 ± 0.04	7	19.1 ± 1.0	7
hGluN2A	Y1387X	33 ± 3	0.28 ± 0.05	0.54 ± 0.04	5	20.9 ± 1.4	5
hGluN2A	Q950X	46 ± 6	0.67 ± 0.20	**0.66 ± 0.06***	5	23.3 ± 3.8	5
hGluN2A	Y943X	30 ± 3	0.29 ± 0.05	0.65 ± 0.05	7	21.7 ± 2.7	6
hGluN2A	S913X	30 ± 3	0.25 ± 0.06	0.54 ± 0.09	6	17.9 ± 2.3	6
hGluN2A	R846X	**62 ± 5***	**2.50 ± 0.52***	**1.37 ± 0.21***	5	**5.8 ± 1.1***	5
hGluN2B	WT	19 ± 3	0.52 ± 0.19	1.75 ± 0.43	9	9.2 ± 0.8	9
hGluN2B	S1415X	21 ± 3	0.49 ± 0.14	1.84 ± 0.50	5	8.0 ± 1.1	5
hGluN2B	Y1155X	14 ± 2	0.30 ± 0.06	2.40 ± 0.71	6	7.4 ± 1.2	6
hGluN2B	R1099AfsX51	22 ± 2	0.55 ± 0.16	1.86 ± 0.42	5	8.8 ± 0.6	5
hGluN2B	Y1004X	18 ± 3	0.77 ± 0.58	2.36 ± 1.31	5	7.3 ± 0.8	5
hGluN2B	I864SfsX20	**48 ± 5***	**4.23 ± 0.91***	**4.57 ± 0.89***	5	**2.5 ± 0.6***	5
hGluN2B	R847X	**54 ± 3***	**2.32 ± 0.37***	2.32 ± 0.37	6	**3.2 ± 0.4***	6

Finally, we assessed the effects of disease-associated hGluN2A/2B CTD truncations on the channel open probability (Po). We activated the NMDARs with a saturating concentration of glutamate (1 mM) and applied a 1 μM MK-801 channel blocker. From recordings, we used the time course of channel inhibition, fitted it with a kinetic model, and determined Po. The analysis revealed a significant decrease in Po in the shortest GluN2A subunits, dropping from 19.1% in hGluN1-1a/hGluN2A WT receptors to 5.8% in hGluN1-1a/hGluN2A R846X (p = < 0.001) receptors. Likewise, Po decreased from 9.2% in hGluN1-1a/hGluN2B WT receptors to 2.5% in hGluN1-1a/hGluN2B I864SfsX20 (p = < 0.001) and 3.2% in hGluN1-1a/hGluN2B R847X (p = < 0.001) receptors (Fig. 28 D, summarised in Tab. 13).

5.4.1.3. The role of GluN2A CTD nonsense and frame-shift variants in surface expression and synaptic localisation in primary hippocampal neurons

The properties of truncated NMDARs were also tested in a more natural environment of neuronal cells. We used immunofluorescence to analyse the surface expression and synaptic localisation of variant NMDARs in primary hippocampal neurons, where either the WT or variant eGFP-tagged hGluN2A and hGluN2B subunits were introduced into the neurons using lentiviral particles.

Analysis of images of NMDAR-stained cultured hippocampal neurons transduced with WT or variant eGFP-hGluN2A/2B NMDAR subunits confirmed our previous results obtained in surface expression experiments with HEK293T and COS-7 cells. The results revealed a reduction of surface expression in the soma of neurons for all truncated eGFP-hGluN2A/2B subunits, except for the eGFP-hGluN2A Y1387X variant NMDAR, whose surface expression was increased. Except for three eGFP-hGluN2B subunit variants, Y1004X, R1099AfsX51, and Y1155X, all other truncated NMDARs reached statistical significance of altered surface expression (hGluN2A: R846X – 67% decrease, p = < 0,001; S913X – 33% decrease, p = < 0,001, Y943X – 49% decrease, p = < 0,001; Q950X – 52% decrease, p = < 0,001; Y1387X – 35% increase, p = 0.037/ hGluN2B: R847X – 63% decrease, p = < 0,001; I864SfsX20 – 54% decrease, p = < 0,001; Y1004X – 21% decrease; R1099AfsX51 – 20% decrease; Y1155X – 19% decrease; S1415X – 24% decrease, p = 0,016) (Fig. 29 A, B, C , E).

Next, we used immunofluorescence analysis to assess the localisation of NMDARs, which included either the WT or variant hGluN2A and hGluN2B subunits, localised within the synapses of primary hippocampal neurons. The postsynaptic scaffold protein PSD-95 was also stained, and we evaluated the degree of co-localisation between the surface eGFP-hGluN2A/2B and PSD-95 signals within a 20ųm region of secondary dendrites. To analyse synaptic localisation, we wrote our own macro that calculates the percentage of overlapping pixels of surface receptors with PSD-95. The overlapping percentage of surface eGFP-hGluN2A/2B pixels with PSD-95 revealed diminished synaptic localisation across all NMDARs containing truncated eGFP-hGluN2A subunits. Except for the eGFP-hGluN2B R1099AfsX51 and S1415X subunit variants, all other truncated NMDARs reached statistical significance in their reduced synaptic localisations (hGluN2A: R846X – 21% decrease, p = < 0,001; S913X – 15% decrease, p = < 0,005, Y943X – 25% decrease, p = < 0,001; Q950X – 18% decrease, p = < 0,001; Y1387X – 21% increase, p = 0.037/ hGluN2B: R847X – 18% decrease, p = 0,002; I864SfsX20 – 25% decrease, p = < 0,001; Y1004X – 21% decrease, p = < 0,001; R1099AfsX51 – 13% decrease; Y1155X – 14% decrease; p = 0.013; S1415X – 13% decrease). The decrease in synaptic localisation might be related to the absence of the

ESDV PDZ domain-binding motif found at the terminal part of the GluN2A/2B CTDs, which links via PSD-95 interaction the receptor to PSD on the postsynaptic membrane (Fig. 29 A, B, D , F).

Finally, we counted the total number of surface receptor and PSD-95 puncta per 20 µm of secondary dendrites to assess the possible effects of variant subunits on synapse numbers and receptor clusters. The results revealed no significant differences between neurons expressing the WT and variant eGFP-hGluN2 subunits (data not shown).

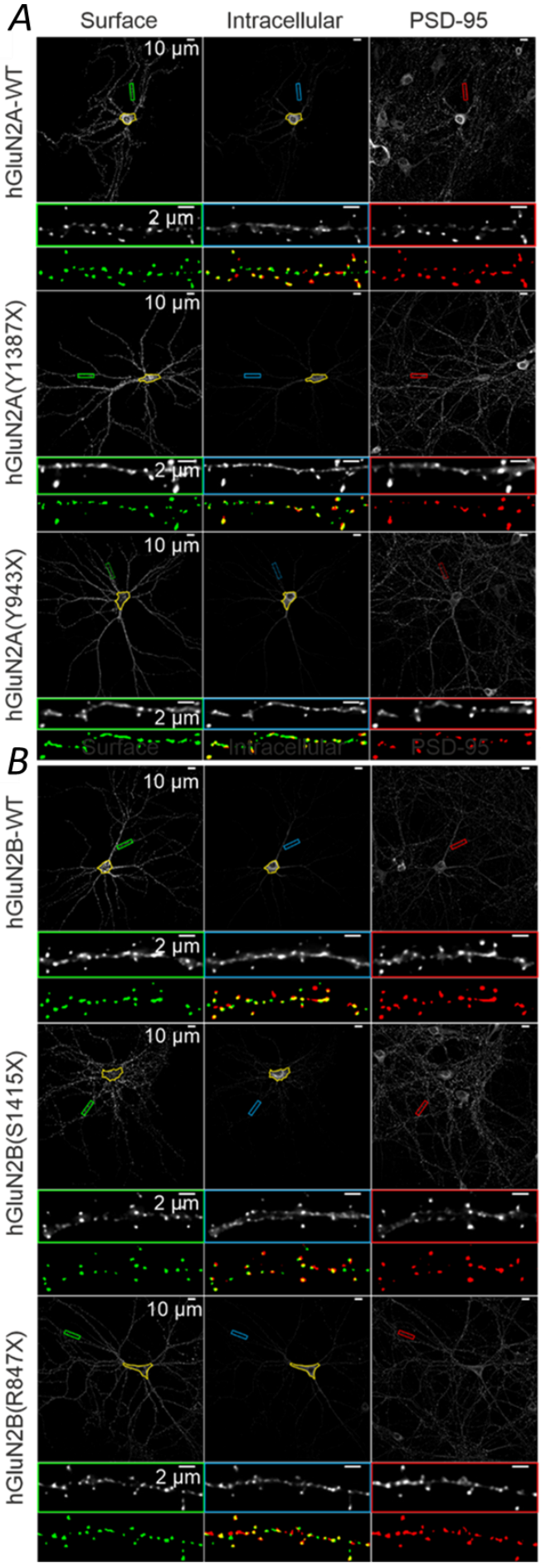
A
Surface
Intracellular
PSD-95
hGluN2A-WT
hGluN2A(Y1387X)
hGluN2A(Y943X)
B
hGluN2B-WT
hGluN2B(S1415X)
hGluN2B(R847X)
10 µm
2 µm

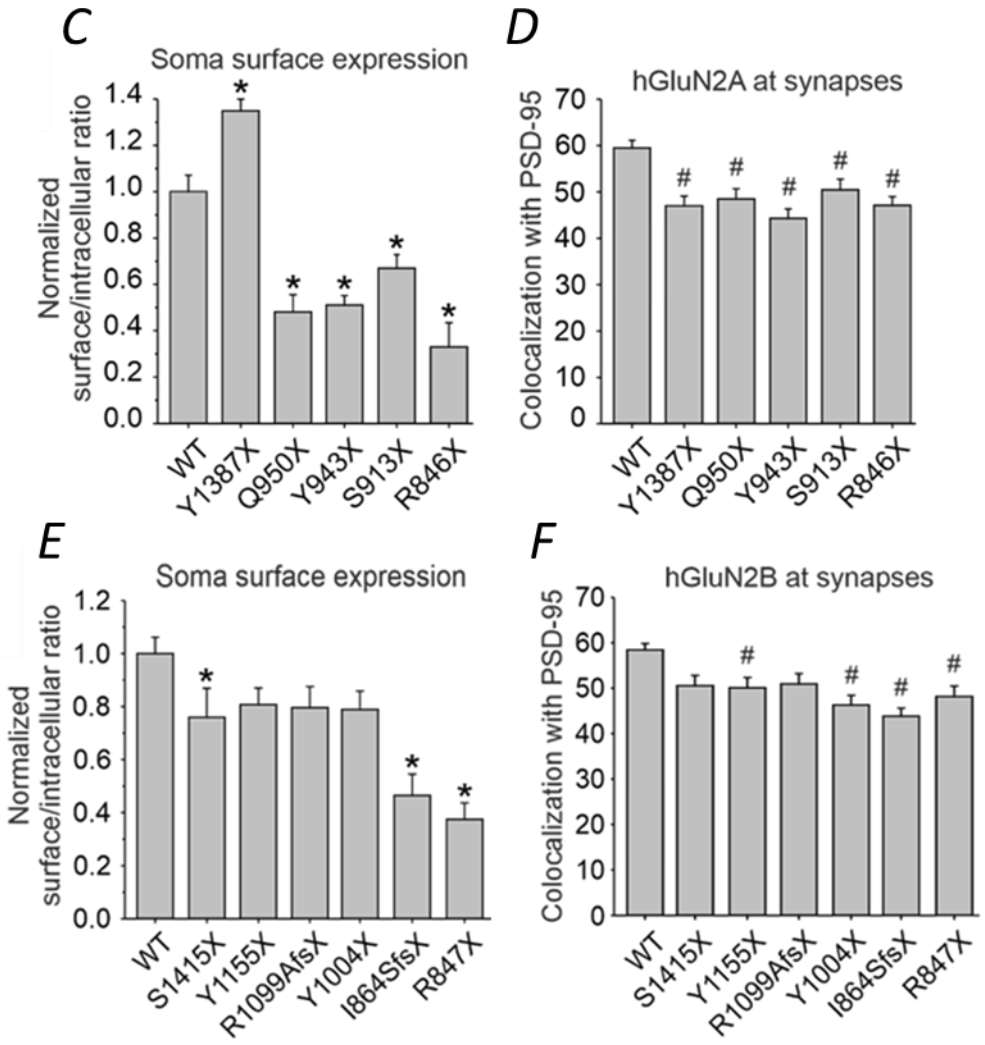

Fig. 29: **Truncations of CTD of hGluN2A and hGluN2B subunits alter surface expression and decrease synaptic localisation of NMDARs in hippocampal neurons.** (***A***,***B***) Representative images show surface and intracellular immunostaining for eGFP-hGluN2A (***A***), eGFP-hGluN2B (***B***) subunits, and immunostaining against the postsynaptic marker PSD-95. The yellow-marked area indicates the soma of neurons, and the green, blue, and red rectangles indicate secondary dendrites, also shown below at a higher magnification. The bottom row shows tresholded surface receptors (green) and PSD-95 (red), with their composite image used to calculate the percentage of receptors at synapses. (***C, E***) Summary of the relative surface expression of eGFP-hGluN2A (***C***) and eGFP-hGluN2B (***E***) subunits measured in somas of hippocampal neurons using fluorescence microscopy. (***D***, ***F***) Summary of the co-localisation analysis determining the percentage of overlapping pixels of the surface eGFP-hGluN2A (***C***) or eGFP-hGluN2B (***F***) with PSD-95. There was no significant difference between the WT and truncated hGluN2 in the total number of puncta of surface receptors and PSD-95 per 20 µm of secondary dendrite (data not shown). n ≥ 24 cells/secondary dendrite per group from three independent experiments. All summary data are presented as the mean ± SEM. # or *, $p < 0.05$ versus WT, analysed by one-way ANOVA and Dunnett's multiple comparison test.

6 Discussion

SCH is a neuropsychiatric disorder with a prevalence reaching almost 1% of the world-wide population. Strong negative health impacts deserving attention, also due to its high socio-economic impact. SCH has a high degree of inheritance, but its genetic background has not been fully understood. However, it is evident that a whole group of genetic changes give rise to the development and emergence of this neuropsychiatric disorder. Molecular pathophysiology mechanisms refer predominantly to impaired synaptic architecture and function. The glutamatergic hypothesis is then the most prominent theory with the capacity to explain a number of pathophysiological mechanisms of SCH (Kahn et al., 2015; Owen et al., 2016; Uno & Coyle, 2019; Kruse & Bustillo, 2022). The largest genetic studies of SCH patients to date pointed to neuronal-specific proteins linked to the function of synapses. Among those, the genes encoding for proteins associated with glutamatergic excitatory synapses were highly represented, which supports the glutamatergic hypothesis of SCH. NMDAR, a crucial protein in glutamatergic synapses, also frequently exhibits genetic variations in SCH patients. All these have led to the theory of NMDAR hypofunction in SCH, which is in line with previous pharmacological and genetic studies linking SCH to dysfunction of NMDARs (Kristiansen et al., 2007; Kirov et al., 2012; Marshall et al., 2017; Singh et al., 2022; Trubetskoy et al., 2022).

6.1. Identifying common and rare variants within NMDAR genes

All seven genes encoding NMDAR subunits were sequenced and analysed in a group of Czech FES patients and matched healthy controls. The study revealed an overall higher genetic variability of *GRIN* genes in the SCH patients compared to the control group. However, the majority of these variations were rare (with a minor allele frequency of ≤ 0.016 in the SCH cases) and appeared to be distributed randomly. Among all NMDAR subunits, *GRIN2A*, *GRIN2B*, GRIN3A, and *GRIN3B* exhibited notably increased genetic variability compared to the *GRIN1*, *GRIN2C*, and *GRIN2D* genes. Since the GRIN1 gene encoding the GluN1 subunit is obligatory in all NMDARs, its dysfunction may lead to more severe neuronal pathophysiology (e.g. early neurodevelopmental disabilities), which is not associated with SCH. GluN2C and GluN2D subunits encoded by the *GRIN2C* and *GRIN2D* genes, on the other hand, are predominantly expressed specifically in the evolutionary older brain structures of the hindbrain and midbrain, potentially having a minor impact on the development of SCH.

The difference in frequency between samples from the SCH subjects and the controls was significant in the case of the variants located in intronic sequences, with a few in 3′ UTRs or promoter regions. The majority of the identified genetic variations within the canonical transcripts were located within introns, likely due to their large sequences' length compared

to coding exons. However, in introns, there are highly conserved nucleotide sequences located in a splicing element, an area forming secondary structures, or an enhancer element that could impact RNA processing and, in turn, protein abundance. Therefore, variants located within the highly conserved intronic sequences may carry potential functional implications (Shaul, 2017).

The increased variability observed in the 3′ UTRs, despite their important role in regulating mRNA stability and localisation, likely results from various sequences subjected to either strong negative selection or milder selective pressures (Hu & Bruno, 2011). In our study, all identified 3′ UTR variants were categorized as potentially non-pathogenic. Previous reports indicated that genetic variations within the 3′ UTRs of NMDAR genes could affect miRNA binding, potentially leading to the suppression of the translation process (H. Shen & Li, 2016; Y. Zhang et al., 2015). However, assessing the functional consequences of 3′ UTR variants remains challenging due to the coordinated binding of multiple proteins to this region, often in a tissue-specific manner.

In addition, we detected numerous synonymous and non-synonymous variations in the coding regions of the *GRIN* genes. However, none of the newly discovered or previously identified variations were significantly associated with SCH, although several *de novo* and rare variants were observed in SCH cases only (García-Recio et al., 2021). The 5′ UTR sequences showed less variability, and the amount of genetic variation was comparable to that found in the exons. This is consistent with the importance of 5′ UTRs for mRNA stability and translation efficiency (Mignone et al., 2002).

6.2. Evaluation of genetic variants within the promoter region of NMDAR genes

We focused on a detailed analysis of the extended promoter region analysed (2000 bp) in five NMDAR genes (*GRIN1, GRIN2A, GRIN2B, GRIN3A*, and *GRIN3B*), where we observed increased genetic variability in SCH. The promoter region of a gene orchestrates the initiation of transcription, thereby exerting direct control over gene expression. The DNA sequence of the promoter regions contains different regulatory elements; thus providing a binding site for RNA polymerase and different transcription factors. The precise length of the individual promoter varies because of the ability of the transcriptional complexes to induce DNA bending, which enables regulatory sequences to be positioned at considerable distances from the TSS. However, since the typical length of the promoter is up to 1000 bp, we believe that our extended promoter regions contain a promoter core with the majority of regulatory elements (Haberle & Stark, 2018; Le et al., 2019).

Genes *GRIN2C* and *GRIN2D* are mostly expressed in the regions with a likely lesser impact on the emergence and development of the SCH; thus, we further did not analyse them. The

other *GRIN* genes and genetic variability within their promoter regions could be more relevant regarding the disorder's pathophysiology. Further, the developmental switch of expression between *GRIN2A* and *GRIN2B* genes, as well as *GRIN3A* and *GRIN3B* genes (decline of the expression of *GRIN2B* and *GRIN3A* and rising of expression of *GRIN2A* and *GRIN3B* until adulthood), in specific brain structures is an interesting phenomenon, with respect to the onset of SCH, that usually starts in early adolescence with no observed symptoms in the earlier developmental stages (Fukaya et al., 2005; Kahn et al., 2015; Monyer et al., 1994; Owen et al., 2016; Wong et al., 2002).

Within the extended promoter regions of the selected genes, we identified a total of sixty-two variants that fulfilled detection quality control criteria. While genes *GRIN1*, *GRIN2A*, *GRIN2B*, and *GRIN3A* exhibited a similar number of genetic variants (7–10), gene *GRIN3B* revealed a considerable number of variants (28). The physiological role of GluN3B subunits encoded by the *GRIN3B* gene is, to date, less understood. The genetic model of GluN3B KO mice revealed, apart from deficits in motor learning, reduced social interaction in a novel environment together with anxiety-like behaviours corresponding to some aspects of SCH (Niemann et al., 2007). Due to the overall lower expression of the subunits and their proposed function as a fine-tuner of neurotransmission, the increased number of genetic variations may reflect less selective pressure on the gene, which could therefore maintain a higher number of variations.

The number of detected variants gave a large number of their theoretical combinations (haplotypes) within specific genes; therefore, we further filtered them according to their predicted pathogenicity and frequency in our samples. Beside the position in a transcriptional regulatory element, other criteria were location within the CpG island (which, when methylated, silences expression of the gene), site of an alternative splicing, position that may alter the effects of chromatin modification, frequency in the population and in our samples, traces in previously published studies, and their CADD and GERP scores (Strahl & Allis, 2000; Cooper et al., 2005; Deaton & Bird, 2011; Rentzsch et al., 2019; Kolathur, 2021).

With the selected promoter variants, we identified several haplotypes for each gene, which were represented at least in one sample. Furthermore, we cloned and functionally analysed only haplotypes whose frequency representation exhibited at least 5% for a group of cases or controls. Among the excluded haplotypes were two within *GRIN2A* and two within *GRIN2B* promoters, which were represented only in a group of patients. These haplotypes could have potentially functional consequences, but they could only describe isolated SCH cases.

Relative promoter activity of selected haplotypes was measured by luciferase assay using reporter plasmids expressed in HEK293T cells. Previous studies of *GRIN* promoters using the

luciferase reporter performed the assay in various types of cell lines, including HEK-293 (A. Liu et al., 2003; Y. Liu et al., 2019, 2022), HeLa (Bai & Kusiak, 1995; Bai et al., 1998; A. Liu et al., 2003), COS-7 (T.-F. Wang et al., 2004), C6 (rat glioma cell line) (Bai & Kusiak, 1995; Bai et al., 1998), U87 (human glioblastoma cell line) (Y. Liu et al., 2022), PC12 (immortalized pheochromocytoma cells from adrenal medulla) (Bai & Kusiak, 1995, 1997; Bai et al., 1998; A. Liu et al., 2001; Miyatake et al., 2002; A. Liu et al., 2003; Tai et al., 2009), N2A (mouse neuroblastoma cell line) (Dhar & Wong-Riley, 2009; Huang & Hsueh, 2009; Priya et al., 2013b), NB1 (human neuroblastoma cell line) (Itokawa, Yamada, Yoshitsugu, et al., 2003), SK-N-SH (human neuroblastoma cell line) (Y. Liu et al., 2019, 2022), P19 (mouse embryonic carcinoma cell line – un/differentiated) (Okamoto et al., 2002; Bai et al., 2003; A. Liu et al., 2003, 2004), primary glia cells (A. Liu et al., 2003), or primary hippocampal (G.-S. Wang et al., 2004; T.-F. Wang et al., 2004) and cortical (A. Liu et al., 2003; Qiang et al., 2005; Qiang & Ticku, 2005; Yeh et al., 2008) neurons.

Although transfected primary neuronal cultures would be the most accurate system regarding the expression of neuronal-specific transcription factors, primary neurons are difficult to transfect to the extent that they give a reasonable luciferase signal, enabling us to compare relatively small changes in promoter activity caused by single nucleotide variants. However, using viral transduction could solve the poor transfection rate and theoretically allow for the use of even more physiologically accurate acute or organotypic brain slices.

To measure the activity of promoters, we did several optimisation steps in the luciferase reporter assay. We initially used the mouse neuroblastoma cell line N2A to express and measure luciferase reporters. Unfortunately, the results produced by the N2A cells showed a very low luciferase signal, with relatively high variability between individual rounds of experiments. Therefore, we decided to use HEK239T cells instead, which resulted in a high level of luciferase signal and reduced variation between experiments. However, the findings from our preliminary data on N2A cells were comparable to those of HEK293T cells, confirming the validity of using the HEK293T cell line. Additionally, previous study reported similar observations when comparing two different promoter haplotypes within the *GRIN1* gene. The study found no differences, neither in assays done on another human neuroblastoma cell line, SK-N-SH, nor in HEK293 cells (Y. Liu et al., 2019). Another study examining twelve different sizes of the *GRIN1* promoter on SK-N-SH and HEK293 cells exhibits similar trends of results, with almost identical results when the promoter size was around 2000 bp, as it was in our experiment (Y. Liu et al., 2022). Last but not least, the *GRIN2A* promoter study comparing differentiated P19 and HEK293 cells also showed identical trends in results. (A. Liu et al., 2003).

Based on our criteria, we selected three potentially deleterious variants within the promoter of the *GRIN1* gene, which were combined into five different haplotypes. Two of the haplotypes did not reach 5% representation; therefore, we did not further test their promoter activity. The haplotype termed GRIN1_1 (CGC) exhibited significantly higher representation within the group of patients. Interestingly, the results from the luciferase assay point to the significantly decreased (several-fold) promoter activity of this haplotype compared to other tested haplotypes. Variant rs11146020 present within the GRIN1_1 haplotype was previously significantly associated with SCH by studies on Italian (Begni et al., 2003), Iranian (Galehdari, 2009), and German (Georgi et al., 2007) populations. However, these three studies associated the C allele with disease, whereas in our study, the haplotype with the rs11146020-G allele was associated with SCH. This is similar to another two studies on the Chinese Han population, which show a comparable significant association of the G allele with SCH (Zhao et al., 2006; Y. Liu et al., 2019). Another two smaller studies on Chinese Han and the Canadian population did not associate the rs11146020 variant with SCH (Hung et al., 2002; Martucci et al., 2003). Nevertheless, the decrease in promoter activity of the GRIN_1 haplotype and its association with SCH were, in our study, probably driven by the combination of two variants, rs7032504-C and rs11146020-G, where the presence of single variants did not exhibit association with SCH. Indeed, similar findings were also discovered in the study of the Chinese Han population, where the haplotype containing variants rs7032504-C and rs11146020-G, combined with four other variants (rs138961287, rs117783907, rs181682830, and rs144123109), was associated with SCH (Y. Liu et al., 2019). We conclude that this particular combination of two rs7032504-C and rs11146020-G variants may significantly contribute to the pathophysiology of SCH.

For the *GRIN2A* promoter, we selected four variants, which give us three haplotypes exceeding 5% representation from all samples. None of the variants or haplotypes exhibited association with SCH. Among the variants present within the haplotypes, only variant rs3785185 was previously described, where the rs3785185-A genotype was revealed as a risk factor for major depressive disorder development (Yin et al., 2016). The haplotype termed GRIN2A_1 (GACC) then showed significantly reduced promoter activity compared to other haplotypes, and the promoter activity of haplotype GRIN2A_3 (GATC) was significantly increased in comparison with haplotype GRIN2A_2 (AACC). However, all haplotypes were equally distributed between SCH patients and controls, and haplotype GRIN2A_1 was the most represented by both, SCH cases and controls. Since all variants in the GRIN2A_1 haplotype were present within two other compared haplotypes, decreased promoter activity might be driven by the combination of variants rs3785185-G and rs117609472-C. Nevertheless, the fact that each haplotype is represented equally in both groups suggests that changes in promoter activity may reflect natural variation in the *GRIN2A* promoter.

In the *GRIN2B* promoter, we selected four different variants, which created five different haplotypes exceeding 5% representation in our sample set. Variant rs3764028-T, represented only by nine patients, exhibited a significant association with SCH. This specific variant was also present in the unique haplotype termed GRIN2B_5 (TTCC), which is also significantly associated with the disorder. Haplotype GRIN2B_3 (AGCC) was then mostly represented by control subjects, which resulted in significance. The other haplotypes were distributed equally among patients and control subjects. The results of the luciferase assay indicate significantly increased promoter activity in haplotype GRIN2B_5 compared to other haplotypes. The result is surprising since the haplotype is represented by only nine SCH cases, and NMDAR hypofunction is hypothesised as a pathophysiological mechanism in SCH. The difference between this haplotype and others is variant rs3764028-T, which may drive the increased promoter activity. Indeed, the finding is also supported by an association study on Alzheimer's disease in the north Han Chinese population, which associated the rs3764028-G variant with the disease and, more importantly, showed by luciferase assay significantly increased promoter activity of the rs3764028-T variant compared to variant rs3764028-G. (H. Jiang & Jia, 2009). A possible explanation for the increased promoter activity of the rs3764028-T variant, apart from alterations in transcription factor binding, can be linked to a change in methylation profile. The rs3764028 variant is located within the CpG island, and substitution of GC bases towards TA bases might disrupt possible methylation within this particular position, which consequently can lead to a reduced methylation profile, which in turn can lead to increased promoter activity (Deaton & Bird, 2011). GluN2B subunits encoded by the *GRIN2B* gene are also often linked to signalling cascades involved in several pathophysiological mechanisms (Lujan et al., 2012), which might provide a possible explanation for the increased *GRIN2B* promoter activity in this specific group of patients.

Additionally, another selected variant, rs3764030-T, was previously associated with an increased *GRIN2B* mRNA level and the maintenance of faster mental processing speed over ageing (Y. Jiang et al., 2017), but also with cognitive impairments (Han et al., 2017). In our analysis of promoter activity, haplotype GRIN2B_1, which contains the rs3764030-T variant, did not exhibit increased activity. Finally, the selected variant rs1019385-A was previously associated with obsessive-compulsive disorder (Kohlrausch et al., 2016); however, in our study, the promoter haplotypes containing this variant showed no difference in activity compared to other haplotypes with variant rs1019385-C. This can be documented in the comparison of promoters GRIN2B_2 and 4, which differ specifically in this particular variant.

In the *GRIN3A* promoter, we selected four variants, which were combined into three haplotypes exceeding 5% representation in our samples. All selected variants and haplotypes exhibited an equal distribution between SCH cases and controls. The results of the luciferase assay

show significantly increased promoter activity of the haplotype termed GRIN3A_3 (GTAT) compared to two other haplotypes. Since haplotypes GRIN3A_3 and GRIN3A_2 differ only in variant rs12338602, it is possible that variant rs12338602-T (GRIN3A_3) may lead to an increase in promoter activity. The strong functional implications of variant rs12338602 were also suggested by its high CADD score (14.46) and its location within the predicted SP1 TF binding site. However, variant rs12338602-T and haplotype GRIN3A_3 exhibit an equal distribution between the SCH cases and control groups, indicating that changes in promoter activity may reflect natural variation within the *GRIN3A* promoter.

Four variants were selected in the *GRIN3B* promoter, resulting in four haplotypes that exceeded 5% representation in our samples. All variants and reconstructed haplotypes exhibited an equal distribution between the SCH patients and control subjects. The results from the luciferase assay revealed reduced promoter activity of the promoter termed GRIN3B_4 (CCAG). The GRIN3B_4 haplotype differs from the haplotype GRIN3B_2 (CTAG) only by variant rs11669927-C, which may, therefore, promote reduced activity of the haplotype GRIN3B_4 in some way. The variant rs11669927-C, characterised as a low-conserved nucleotide with a low CADD score, is positioned within the EGR1 TF binding site and, most importantly, identified as a moderately positive eQTL, supporting its effect on *GRIN3B* promoter activity. Similarly, to promoters *GRIN2A* and *GRIN3A*, changes in promoter activity may reflect natural variation within the *GRIN3A* promoter since all variants and haplotypes are equally distributed.

Additionally, a $(GT)_n$ microsatellite (rs3222791) resides within the *GRIN3B* promoter. Similarly, previous studies located $(GT)_n$ microsatellite (rs3219790) within the promoter of *GRIN2A*, where the longer alleles were significantly associated with SCH (Itokawa, Yamada, Yoshitsugu, et al., 2003; Tang et al., 2006; R. Liu et al., 2015). In addition, a functional *in vitro* assay revealed a length-dependent inhibition of the transcriptional activity of the *GRIN2A* gene by this $(GT)_n$ repeat (Itokawa, Yamada, Yoshitsugu, et al., 2003). According to the published data, in the vast majority (93.34%) of cases, the number of GT repetitions is between 21 and 30, and the difference between these two lengths of $(GT)_n$ repeats should not exceed 16% in their promoter activity (R. Liu et al., 2015). Unfortunately, in our NGS dataset, the quality of reads in the GT repetitive regions within the *GRIN2A* and *GRIN3B* genes was insufficient to reasonably determine the number of GTs in individual samples.

Since the effects of *GRIN2A* $(GT)_n$ microsatellite are fully characterised, we focused on the microsatellite within the *GRIN3B* promoter as an additional risk factor for SCH. We cloned the promoter region containing $(GT)_n$ microsatellite from 23 cases and 22 controls and determined the number of repeats. Although our range of $(GT)_n$ repeats (15–18) was smaller (possibly due

to the low sample size), as in the case of microsatellite within the *GRIN2A* promoter (21–30), the longest allele (18 x GT) was predominantly associated with SCH, while the shortest allele (15 x GT) was only present in control samples.

Additionally, we cloned the full-length *GRIN3B* promoter with varying numbers of $(GT)_n$ repeats (0, 10, 13, 16, 17, and 20). Similarly, to the *GRIN2A* microsatellite, the luciferase assay of the *GRIN3B* promoter with different numbers of $(GT)_n$ repeats revealed a length-dependent inhibition of transcriptional activity. Although potential differences in promoter activity, even between 15xGT and 18xGT repeats, are relatively small, the longer microsatellites within the *GRIN3B* promoter might contribute to the pathophysiology of SCH.

To understand the global *GRIN* genes expression within each case or control subject, we assigned the relative values of the luciferase promoter activity of their two alleles in each sample. Next, we averaged all values within both groups for each gene and normalised the values to the average value of the control group. The results revealed significantly reduced relative promoter activity of the *GRIN3B* and especially *GRIN1* promoters in SCH patients. Considering the obligatory role of GluN1 subunits, which are present in all NMDAR, a 20% decrease in the relative promoter activity of its *GRIN1* promoter may have relatively strong implications for SCH patients. The results of the *GRIN1* and *GRIN3B* gene analysis thus support the hypothesis of NMDAR hypofunction in SCH. Two other genes, *GRIN2A* and *GRIN3A*, did not show any difference in their promoter activity when the two groups were compared. Lastly, promoters of the *GRIN2B* gene exhibited significantly increased relative promoter activity in the group of patients. The increase has its origins in the unique group of SCH patients described above and may reflect another pathophysiological mechanism in which GluN2B subunits play a role.

Next, we combined all normalised data from each gene with a calculated global relative promoter activity for all *GRIN* genes collectively. Despite being aware of the varying expression profiles and physiological roles of the five genes, this comparison could address the question of overall NMDAR hypofunction within our patient group. The results from this comparison then show a reduced relative promoter activity on the edge of significance for the patient group. However, it is important to note that if we exclude the unique nine samples of SCH, which display increases in their promoter activity for the *GRIN2B* gene, the results become significant.

A common characteristic of SCH involves accelerated brain maturation and ageing coupled with an abnormal age-dependent decline in grey matter. BrainAGE, a metric that consolidates the intricate patterns of ageing within the brain or specific brain structure into a single value, quantifies the deviation of brain atrophy from typical brain ageing, expressed in years (Gogtay

& Thompson, 2010). The previous neuroimaging study investigating loss of brain tissue in SCH patients over time revealed BrainAGE 3.36 ± 5.87 years older at their first scan when compared to the expected values of their real age (Schnack et al., 2016). Another study, focusing on individuals in the early stages of SCH as our study, estimated a higher BrainAGE of 2.64 ± 4.15 years compared to their actual chronological age (Hajek et al., 2019). Similarly to these studies, our first-episode SCH patients showed a brain age gap of 2.44 ± 5.54 years relative to the expected values of their actual age. The values of BrainAGE were then also positively correlated with the reduced relative promoter activity of *GRIN* genes.

6.3. Functional characterisation of missense variants identified within the CTD of the GluN2A NMDAR subunit

In our dataset, we identified a total of sixty-two non-synonymous coding variants within all *GRIN* genes. The least affected genes were *GRIN2B*, without any variant assigned, and *GRIN1*, with only one identified variant. The GluN1 subunit encoded by the *GRIN1* gene is an obligatory subunit of NMDAR with crucial functional implications; thus, any non-synonymous variants within the gene may have more severe effects than correspond to SCH symptoms. However, the fact that we did not identify any non-synonymous variants within the *GRIN2B* gene was unexpected, considering many previous reports in which the *GRIN2B* gene shows a similar number of disease-associated variations as the *GRIN2A*, *GRIN2C*, *GRIN2D*, or *GRIN3A* genes (reviewed in Chapter 2.2.3.).

In other *GRIN* genes, we identified five to ten non-synonymous variants, but the gene *GRIN3B* exhibited an increased number of protein-coding variants, thirty-one, which stands for half of all variants we identified. This resembles the results obtained for the promoter region, where the *GRIN3B* gene also exhibited an increased number of variants compared to other genes. The physiological function of GluN3B subunits, encoded by the *GRIN3B* gene, remains relatively uncertain to date. Studies with a genetic model of GluN3B KO mice have demonstrated deficits in motor learning and decreased social interaction in a new environment, accompanied by anxiety-like behaviours that mimic certain symptoms of SCH (Niemann et al., 2007). However, given the overall lower expression of this subunit and its proposed role as a fine-tuner of neurotransmission, the increased presence of genetic variations might just reflect reduced selective pressure on the gene.

Out of all the non-synonymous variants identified, only two exhibited a significant association with SCH. First, the only variant within the *GRIN1* gene, E619del, was found only in nine SCH patients. This variant deletes one full nucleotide triplet, leading to the deletion of one amino acid (glutamate). The deleted amino acid is located within TMD, suggesting a potential

physiological impact on ion channel properties. The E619 is then specifically located in the M1-M2 linker, where we are expecting the compensated effect, although further experiments should validate the functional consequences of the E619del variant. The second significantly SCH-associated variant, P1039R, was identified within the CTD-coding region of the GluN3B subunit, but its potential physiological impact is difficult to estimate. Besides, one variant, R1209S, located within the CTD of the *GRIN2C* gene, exhibited a significant association with the control group. Nevertheless, most of the identified variants were very rare, and specifically, nineteen of them were represented only by SCH patients.

The largest genomic studies on SCH emphasised specifically GluN2A subunits and their genetic variants as potential risk factors for the disorder (Singh et al., 2022; Trubetskoy et al., 2022; Harrison & Bannerman, 2023). Additionally, previously reported variants associated with SCH were located predominantly in the intracellular domains of NMDARs (reviewed in Chapter 2.2.3.). Our NGS data confirmed these observations, revealing that 44% of all variants we found were located within the CTD. Therefore, we further focused on the analysis of the variants located within the intracellular CTD of GluN2A subunits.

Within the CTD of the GluN2A subunit, we identified four variants: P1386L, N1076K, T1064A, and V967L. The variant P1386L (rs1277391984) was unannotated when we performed NGS analysis; thus we classified it as *de novo*. However, in March 2021, the variant was submitted to the ClinVar database (variation ID: 1012393) based on clinical testing. One of the records linked the variant potentially to Landau-Kleffner syndrome (LKS). LKS is characterised by language regression and seizures but is also often associated with social cognitive deficits, which are present in SCH as well (Green et al., 2015). The variant N1076K (rs61758995) was reported by two studies, with a potential link to LKS as well (Endele et al., 2010; Lemke et al., 2013). The variant T1064A (rs138809301) was previously reported by one study, which associated the variant with SCH (Tarabeux et al., 2011). The last variant, V967L (rs61731465), had been reported previously by two studies that linked it to temporal lobe epilepsy, benign epilepsy with centro-temporal spikes, and atypical benign partial epilepsy (Lemke et al., 2013; Lal et al., 2015). Furthermore, the last three variants have, similar to the P1386L variant, multiple entries in the ClinVar database submitted as outcomes of clinical testing.

The CTD of the GluN2A subunit serves as a hub for numerous protein interactions with scaffold, adaptor, cytoskeletal, enzymatic, and other proteins. The GluN2A CTD and its interactions are then crucial for receptor trafficking, surface expression, synaptic localisation, internalisation, degradation, or recycling (Warnet et al., 2021). Since the surface expression may be affected by impaired receptor trafficking, internalisation, recycling, or degradation, we first examined the surface expression of WT or variant heterodimeric

hGluN1-1a/eGFP-hGluN2A-NMDAR using HEK293T (for immunofluorescence microscopy) or COS-7 (for the colorimetric assay) cells. We used the GluN1-1a subunit, which is a highly expressed splice variant, especially in the cortex or hippocampus, and contains the longest CTD among other splice variants, including the C1 cassette with the KKK and RRR signals responsible for ER retention, while it does not contain the C2' cassette, which has an enhancing effect on the trafficking of GluN1 subunits to the cell surface. Surface expression and trafficking of heterodimeric receptors are then preferentially controlled by the GluN2 subunit in the GluN1-1a/GluN2 heterodimer (Laurie & Seeburg, 1994; Standley et al., 2000; Scott et al., 2001; Barria & Malinow, 2002; Horak & Wenthold, 2009).

Our analysis results showed that all four variants have significantly reduced surface expression in both types of analysis, with a decrease between 17% and 31% compared to WT NMDAR, depending on the assay and specific variant. The results were supported by electrophysiological analysis of current densities reflecting a number of receptors on the surface membrane, where all variants showed a reduced mean of current density, although only the P1386L and N1076K variants were statistically significant. However, current densities may be affected by transfection efficiency, which varies widely between cells, and possibly by altered ion channel properties. Similar findings were reported in a functional study of epilepsy-associated missense variants located in the distal CTD of the GluN2A subunit (Mota Vieira et al., 2020). A particular mechanism contributing to the reduction in surface expression is difficult to estimate from these experiments. However, in the immunofluorescence microscopy experiments, there was a noticeable increase in the intracellular localisation of variants in proximity to the nucleus, possibly due to enhanced ER retention. Between the WT and variant receptors, we then did not notice any difference in the total eGFP signal.

A number of studies on the CTD of the GluN2A subunit suggested that the intracellular domain may also influence the ion channel properties of the receptor (Rossi et al., 2002; Krupp et al., 2002; Puddifoot et al., 2009; Maki et al., 2012; Punnakkal et al., 2012; Maki et al., 2013). Therefore, we further performed electrophysiological experiments of the heterodimeric hGluN1-1a/hGlun2A receptor in HEK293T cells to investigate the functional properties of the ion channel in selected variants. The P1386L variant showed significantly reduced receptor desensitisation and, together with the N1076K variant, faster deactivation kinetics (tau weighted). The T1064A variant showed a significantly slower response to the channel blocker MK-801, indicating a lower probability of channel opening. The V967L variant showed significantly increased receptor desensitisation. In addition, variant N1076K exhibited significantly increased glutamate potency, and within variants P1386L and T1064A,

we observed significantly reduced and increased glycine potency, respectively. Although some of the variants significantly altered the channel properties, the changes are relatively small, with a likely minor effect on the general function of NMDAR. The mechanism by which selected variants affect receptor ion channel function in non-neuronal cell lines remains questionable, given the preferential role of the CTD as a hub of protein interaction. However, based on transcriptomic data from HEK293T cells (https://maayanlab.cloud/Harmonizome/; gene set: HEK 293; data set: BioGPS Cell Line Gene Expression Profiles), the cell line expresses several proteins that directly interact with the CTD of GluN2A subunits and could thus affect ion channel properties, including SAP97 (*DLG1*), IQGAP1 (*IQGAP1*) with its interactor ERK1 (*MAPK3*), GIPC1 (*GIPC1*), spectrin (*SPTBN1*), α-actinin (*Actn1*), or PTPN4 (*PTPN4*) (CTD-interacting proteins are discussed in Chapter 2. 1.2.). However, we don't have any data to support the interaction or effects of these CTD-interacting proteins on the activity of the analysed GluN2A variants. Another possibility could be a structural change projected upstream to the TMD.

To refine surface expression analysis, we further employed the more relevant physiological system of primary hippocampal neuronal cultures. Neuronal cells were transduced with WT or variant eGFP-hGluN2A subunits using lentiviral particles. The surface expression of transduced subunits is then absolutely dependent on the endogenous expression of GluN1 subunits. Analysis of surface expression in neuronal somas showed a significant reduction for the T1064A variant and a trend towards a reduction for the P1386L and V967L variants. Differences in the results compared to experiments in HEK293T and COS-7 cells may be due to the expression of neuronal-specific proteins or to the fact that the receptors can either form heterodimeric receptors with different splice variants of GluN1 subunits or heterotrimeric receptors with endogenous WT GluN2A subunits or with one of the GluN2B-D or GluN3A-B subunits, which in turn may affect receptor trafficking. Although the neuronal soma is a morphologically well-defined area, the primary sites of NMDAR activity are synapses. Therefore, we analysed NMDAR surface expression on the dendritic spines, where excitatory synapses are located. The results of the analysis in dendritic spines confirmed all our previous findings, where all four variants showed significantly reduced surface expression between 9% and 36%. Due to the nature of these immunostaining experiments, it is not possible to estimate the specific mechanisms by which variants impair receptor surface expression. However, previous studies of variants within the CTD of GluN2A/2B subunits that altered NMDAR surface expression suggested impaired binding of CTD to other proteins (S. Liu et al., 2017; Mota Vieira et al., 2020; Vieira et al., 2023; X. Wang et al., 2023) or a disrupted functional ER retention motif (Q.-Q. Li et al., 2022a). Thus, the aforementioned or impaired receptor internalisation, recycling, and degradation may potentially play a role in the mechanism.

In previous studies, altered surface expression of CTD variant receptors was associated with impaired synaptic localisation, a critical feature for proper NMDAR function (S. Liu et al., 2017; Mota Vieira et al., 2020). Therefore, we performed similar experiments in which we measured the co-localisation of WT or variant receptors with the postsynaptic scaffold protein PSD-95 to define the localisation of receptors within synapses. Our results showed similarly altered co-localisation with the postsynaptic marker PSD-95, determined as the percentage of overlapping pixels of the surface receptor with PSD-95. Specifically, the eGFP-hGluN2A P1386L (15%) and N1076K (10%) variants exhibited a significantly reduced percentage of co-localisation. While the co-localisation analysis assessed by the determination of Manders' overlap coefficient confirmed a significantly reduced co-localisation of the P1386L variant (11%), the variant N1076K exhibited only a trend towards decrease.

All the variants we tested were found to be heterozygous, which should have a potentially mitigating effect on the observed changes in the function of the variant receptor. Thus, relatively small decreases in the surface expression and alterations in the ion channel properties of the variants might be less severe. In addition, the T1064A, N1076K, and V967L variants were also identified in the control subjects, suggesting that they are not critically deleterious. This is not the case for the P1386L variant, which was only identified in the SCH subject. In addition, apart from reduced surface expression, this variant showed larger alterations of ion channel properties and, most importantly, reduced synaptic localisation, which is critical for NDMAR function.

Previous studies on GluN2 CTD variants have linked altered receptor trafficking and synaptic localisation to impaired CTD protein interaction (S. Liu et al., 2017; Mota Vieira et al., 2020; Vieira et al., 2023; X. Wang et al., 2023). Therefore, we searched for known protein interactions within the position of the P1386L variant, and we found overlaps with binding sites for the proteins CtBP1 (Cousins & Stephenson, 2019), Flot1 (Glebov et al., 2006), and PSD-95 (Cousins et al., 2008, 2009; Cousins & Stephenson, 2012).

PSD-95 is a key postsynaptic scaffolding protein and a member of the MAGUK family of proteins, which are defined by the containment of PDZ, SH3, and guanylate kinase domains. Multiple interaction domains allow PSD-95 to act as a bridge between surface receptors, channels, or adhesion molecules and intracellular signalling proteins, enzymes, or cytoskeletal proteins, which in turn help to hold the synaptic PSD (Kim & Sheng, 2004; Won et al., 2017). PSD-95 contains a total of three PDZ domains, the first two of which bind to the major binding motif ESDV within the GluN2A (and GluN2B) CTD terminal (Kornau et al., 1995; Niethammer et al., 1996; Lim et al., 2002). SH3 domains have an affinity for binding proline-rich sequences, especially those that carry the PxxP motif (Mayer, 2001). Indeed, an additional motif, PSDPYK,

was later described within the CTD of the GluN2A subunit with affinity to bind to the SH3 domain of PSD-95. Although PSD-95 is primarily bound to the ESDV motif, the PSDPYK motif is required for its interaction with the GluN2A subunit in native brain tissue. The proposed mechanism suggests that the first step involves association between the PSDPYK motif and the SH3 domain, followed by docking of GluN2A to PSD-95 via the ESDV motif (Cousins et al., 2008, 2009; Cousins & Stephenson, 2012). In addition, PSD-95 mRNA and protein levels were found to be reduced in the dorsolateral and dorsomedial prefrontal cortex of SCH patients, and genetic variations within the *DLG4* gene encoding PSD-95 were associated with SCH (Coley & Gao, 2018).

Since the P1386L variant is in the fourth position of the PSDPYK binding motif of the synaptic protein PSD-95, we examined the effects of the variant on the interaction of GluN2A-NMDAR with PSD-95. As previously shown, PSD-95 significantly increases surface expression of the NMDAR, but not in the case when receptors contain a deleted ESDV motif. The result also showed that deletion of the ESDV motif did not fully abolish the effect of PSD-95, which could be explained by an additional binding motif within the receptor (Y. Lin et al., 2004). In addition, the impaired interaction also has the capacity to explain deficits in synaptic localisation of the variant receptor, as previous studies show that deletion of the ESDV motif within NMDAR reduced the delivery of receptors to synapses and impaired the anchoring of cell-surface receptors at postsynaptic targets (Barria & Malinow, 2002; Prybylowski et al., 2005; Groc et al., 2006; Standley et al., 2012).

To analyse GluN2A PSD-95 interaction, we performed co-localisation analysis in HEK293T cells co-expressing WT or variant hGlun1-1a/eGFP-hGluN2A-NMDAR and PSD-95. We employed super-resolution microscopy (STED) and analysed the percentage of overlapping pixels between surface eGFP-hGluN2A and PSD-95. The results revealed significantly decreased co-localisation between the variant receptor and PSD-95 (44%), compared to the WT receptor (58%), indicating an impaired protein interaction between the CTD of the GluN2A subunit and PSD-95.

Previous studies also showed direct effects of co-expression of PSD-95 with NMDARs on receptor current density, open probability, and glutamate potency. The effect was diminished when a receptor with a deleted ESDV binding motif was co-expressed with PSD-95 (Rutter & Stephenson, 2000; Y. Lin et al., 2004). Therefore, we carried out a similar test that might indicate an altered interaction of the variant receptor with PSD-95. We performed electrophysiological analysis using HEK293T cells co-expressing WT, P1386L, or ΔESDV hGlun1-1a/eGFP-hGluN2A-NMDAR with or without PSD-95. Similar to the previous study, the results showed that the current density of the WT receptor was significantly increased when

co-expressed with PSD-95. However, this was not the case for the P1386L and ΔESDV receptors, where co-expression with PSD-95 did not result in a significant increase in current density. As in the previous study, we also observed a significant effect of PSD-95 on glutamate potency in WT NMDAR but not in P1386L and ΔESDV receptors. Taken together, all these results suggest an impaired interaction between PSD-95 and the P1386L variant receptors.

Since described co-localisation and electrophysiological analysis do not provide direct evidence for interaction between GluN2A CTD and PSD-95, we performed co-immunoprecipitation and Western blot analysis using HEK293T cells co-expressing WT or P1386L hGlun1-1a/eGFP-hGluN2A-NMDAR together with PSD-95. The results showed a significant decrease of the P1386L receptor (15%) in the IP fraction compared to WT. A similar decrease was then observed in the previous study, where the PSDPYK motif was mutated to ASDAYK (Cousins & Stephenson, 2012). Additionally, we analysed cells co-expressing ΔESDV or P1386L + ΔESDV NMDAR together with PSD-95. We observed a decrease of P1386L + ΔESDV NMDAR (60%) in the IP fraction compared to ΔESDV receptor, but the result did not reach significance likely due to the limited sample size. Our results are intriguing when compared to previously reported, where deletion of the ESDV motif did not result in such a remarkable decrease in the IP fraction as in our study (ΔESDV 3,7% of hGluN2A WT levels) (Cousins et al., 2009; Cousins & Stephenson, 2012). In summary, our results overall confirmed a compromised interaction of the P1386L receptor with PSD-95, and our *in silico* models proposed a possible explanation by predicting that the local structure of CTD with the P1386L variant has much fewer contacts with the SH3 domain of PSD-95 than the CTD of the WT GluN2A subunit.

Our previous results showed that P1386L hGluN2A-NMDAR is less localised within the synapse due to its possibly impaired binding to PSD-95. To further understand the effects of the variant on its distribution within the synapse, we apply transmission electron microscopy together with gold labelling in primary mouse hippocampal neurons transduced with WT or variant 6xHis-eGFP-hGluN2A-NMDAR. We analysed the distribution of the subunits within the synaptic and perisynaptic regions. The perisynaptic region has been loosely defined in previous EM studies as 100–300 nm from the PSD edge (J. Zhang & Diamond, 2006; Pérez-Otaño et al., 2006; J. Zhang & Diamond, 2009; Petralia et al., 2010; Petralia, 2012; Goodman et al., 2017). In our understanding, the difference in PSD size that marks synapses must be projected onto the length of the perisynaptic region. Therefore, in our study, we determined the length of the perisynaptic region as the same length as the PSD (in proximity to the membrane) measured from both edges of the PSD. Next, within these two regions, we measured the distance of GluN2A subunits to the central axis of PSD (in proximity

to the membrane), and the data were normalised within each synapse to the length measured between the central axis and the edge of the PSD. Our results showed striking differences in distribution between WT and P1386L receptors, with the variant receptors having a significantly longer relative distance from the central axis of the PSD and a significantly lower number of receptors per 100 nm of the synapse.

Some previous EM studies suggest that NMDARs are preferentially localised in perisynaptic regions, whereas another member of the iGluR family, AMPARs, are localised predominantly within the synapses (J. Zhang & Diamond, 2006, 2009). However, our results suggest that WT GluN2A-NMDARs are preferentially localised within synaptic rather than perisynaptic regions. Our findings are then supported by recent studies that observed the same localisations with NMDARs at a closer distance to the centre of the synapse and AMPAR located further away from the synaptic centre (S. Li et al., 2021; Hruska et al., 2022). The discrepancy between older (J. Zhang & Diamond, 2006, 2009) and recent studies (S. Li et al., 2021; Hruska et al., 2022) may be explained by different types of samples, brain regions analysed, or staining and sample preparation.

The different number of synaptically available NMDARs will affect synaptic function; therefore, we performed electrophysiology measurements on the primary hippocampal neurons transduced by the WT or P1386L eGFP-hGluN2A subunit. The impaired synaptic distribution of NMDARs with variant hGluN2A subunits may result in a reduction of NMDAR-mediated single-synapse responses. To characterise single-synapse responses, we measured the average charge transfer of NMDAR mEPSCs, which was reduced by 34% in neurons transduced by P1386L compared to the WT eGFP-hGluN2A subunit. This reduction is not significant due to the relatively large variability of the data, which is typical for NMDAR mEPSCs (Korinek et al., 2020; Smejkalova et al., 2021). However, this result is in line with the hypothesis of a reduced synaptic population of hGluN2A P1386L containing NMDARs.

Taken together, our functional analysis suggests that the P1386L variant causes deficits in receptor trafficking and synaptic anchoring, which can contribute to the emergence and development of the SCH on the individual level. Although we cannot exclude the additional impaired receptor interactions with other proteins (CtBP1, Rph3A or Flot1), an impaired interaction between the GluN2A CTD and PSD-95 can explain the observed differences in the P1386L GluN2A-NMDAR function. The disruption of the interaction between the GluN2A subunit and Rph3A then also reduces the amount of synaptic NMDAR, which could thus simultaneously contribute to our findings (Stanic et al., 2015). On the other hand, CtBP1 decreases receptor surface expression (Cousins & Stephenson, 2019) and Flot1 promotes clathrin-independent internalisation of GluN2A (Glebov et al., 2006; Swanwick et al., 2009),

so theoretically, impaired interaction with these proteins should have rather opposite effects than we detected.

Finally, since the PSDPYK motif provides important interaction for receptor subunit and synaptic function, we bioinformatically analysed the sequence of this motif across the vertebrates. Surprisingly, birds and reptiles contained the PSDPYK motif with leucine in the fourth position, the same as analysed human pathogenic variant receptor. Amphibians, fish, and chondrichthyes substituted proline in the fourth position for isoleucine. On the other hand, the larger (71 amino acids) SH3 domain of PSD-95 is highly conserved among vertebrates. This observation thus suggests that P1386L is an evolutionary reversed variant and that possibly evolutionary substitution of the isoleucine and/or leucine for proline has positive functional consequences for the strength of synaptic functions, which is in line with brain complexity and intellectual ability found in mammals.

6.4. Characterisation of the functional determinants of GluN2A and GluN2B subunits' CTD

Given the functional implications of GluN2A CTD missense variants on NMDAR function, we attempted to identify functional determinants of the receptor's intracellular domain. We selected nine GluN2A and GluN2B nonsense and frame-shift variants (and one artificially created variant deleting the whole GluN2A CTD), resulting in the truncation of the CTD, associated with various neurodevelopmental disorders. First, we analysed the surface expression of the WT or variant heterodimeric hGluN1-1a/eGFP-hGluN2A/2B-NMDAR using HEK293T (for immunofluorescence microscopy) or COS-7 (for the colorimetric assay) cells. Our results from both cell lines showed that all variants had significantly reduced surface expression, except for the short truncation hGluN2A Y1387X variant, which had significantly increased surface expression. The results were additionally supported by electrophysiological measurements of receptor current density, where all variants showed a trend towards reduction of overall charge transfer, although only a few variants reached significance. As already mentioned, current density depends not only on the surface expression of the receptor but also on its ion channel properties and the level of transfection, which varies greatly between cells.

Several important functional motifs have been identified within the CTDs of both NMDAR subunits. In the GluN2A subunit, it is the proximal endocytic motif ($YWKL_{842-845}$), the ER retention motif ($KKK_{879-881}$), or the distal endocytic motif ($LL_{1319–1320}$). The CTD of the GluN2B subunit then contains proximal and distal endocytic motifs ($YWQF_{843-846}$, $YEKL_{1474-1477}$). Additionally, endocytosis by the later endocytic motif is disturbed due to the

binding of MAGUKs proteins. We can speculate that the increased surface expression of Y1387X hGluN2A-NMDAR compared to other truncated receptor variants could be explained by the binding of SAP97 (MAGUK family member expressed in HEK293T cells) through its SH3 domain to the PSDPYK motif, whose crucial part, PxxP, is preserved within the variant (Roche et al., 2001; Lavezzari et al., 2003, 2004; Scott et al., 2004; Kim & Sheng, 2004; Cousins et al., 2008; Cousins & Stephenson, 2012; Q.-Q. Li et al., 2022a, 2022a). However, this does not explain the increased surface expression of the Y1387X variant even compared to WT hGluN2A-NMDAR, when the region between 1387 and the CTD terminal may be crucial for the effect. Another explanation can be provided by a recent study of the P1199Rfs*32 GluN2A-NMDAR, which showed increased surface expression similar to our Y1387X receptor. Proposed mechanisms include the loss of all PDZ interactions except for the protein Scribble1, which facilitates NMDAR recycling (Vieira et al., 2023). However, this mechanism requires a neuronal environment, as HEK293T cells do not express Scribble1, or at least not at detectable levels (https://maayanlab.cloud/ Harmonizome/; gene set: HEK 293; data set: BioGPS Cell Line Gene Expression Profiles).

The specific mechanism responsible for reduced surface expression of the rest of the variant receptors is difficult to estimate, but from the microscopy analysis, there was a noticeable increase in the intracellular signal of variants close to the nucleus, suggesting increased ER retention. Within the GluN2B subunits, tested variants covered relatively the whole CTD; therefore, the missing distal part of the domain, downstream of S1415, should be crucial for the observed effect. On the other hand, within GluN2A subunits, the effect should be provided by a part of the domain between Q950X and Y1387 (or P1199). Another possibility could be insufficient masking of retention motifs within the hGluN1-1a subunit or loss of the major binding motif, the PDZ domain, which is important for the stability of the receptor on the surface. A more profound effect on reduced surface expression for the majority of GluN2A variants could then possibly be explained by the preserved proximal endocytic motif within all variants. Although the rate of internalisation is higher for GluN2B than for GluN2A subunits, GluN2A subunits are preferentially sorted from early to late endosomes, whereas GluN2B subunits prefer the recycling pathway (Lavezzari et al., 2004).

Mice expressing truncated CTD of GluN2A and also GluN2B subunits exhibited significantly reduced channel open probability of the NMDAR (Mohrmann et al., 2002; Rossi et al., 2002), and truncation of the CTD in the GluN2A subunit leads to increased glycine potentiation (Puddifoot et al., 2009); therefore, we used electrophysiological measurements to functionally analyse the receptor ion channel properties in HEK293T cells. The analysis of glutamate potency revealed that only the GluN2B variant R847X had significantly changed (increased)

glutamate EC_{50}. In the case of glycine potency, only the GluN2B variants R847X and I864SfsX20 exhibited a significant decrease in glycine EC_{50}. Additionally, the most truncated variants within GluN2A (R846X) and GluN2B (R847X, II864SfsX20) showed significantly increased desensitization and reduced channel open probability. This is in line with previous reports on channel open probability in truncated GluN2 subunits, which were further refined by single channel analysis, where it was shown that the first 100 amino acids of the CTD are critical for the change of properties (Maki et al., 2012; Punnakkal et al., 2012).

Next, we assess the truncated variants in the more physiologically relevant system of primary hippocampal neurons. WT, or variant eGFP-hGluN2A/2B subunits, were introduced into the neurons using lentiviral particles. Surface expression analysis confirmed our previous results in HEK293T and COS-7 cells, where all variants showed reduced surface expression, except for variant Y1387X, which showed the opposite effect. The results are in line with previous experiments in mice expressing CTD-truncated GluN2A or GluN2B subunits, which showed impaired trafficking of receptors to synapses (Mori et al., 1998; Steigerwald et al., 2000). The differences we observed were smaller compared to experiments in the cell lines, which is very likely because the receptors stained in neuronal cells tend to be heterotrimeric, which attenuates the effects of variant subunits assembled as diheteromers. In addition, the difference between HEK293T and COS-7 cell lines and primary neuronal cells is in the expression of a wide range of proteins interacting with the CTD and/or post-translational modifications of the CTD (reviewed in Chapter 2.1.2.), which could all have significant implications. Similar findings were described in the previous study of the GluN2B variant (K1091T), which had reduced interaction with PSD-95 accompanied by reduced surface expression (X. Wang et al., 2023).

In the end, we analysed the synaptic localisations of variants with truncated CTD. We measured the co-localisation of WT or variant receptors with the postsynaptic scaffold protein PSD-95, which was determined as the percentage of overlapping pixels of the surface NMDAR with PSD-95. All selected variants of NMDAR exhibited reduced co-localisation with PSD-95, indicating their reduced synaptic localisation. Our results are consistent with previous reports, when mice expressing GluN2A subunits with truncated CTD showed significantly reduced NMDA synaptic currents and a significantly lower amount of receptors in the synapse, together with an increased density of receptors in perisynaptic regions (Steigerwald et al., 2000; Rossi et al., 2002; Köhr et al., 2003). Similarly, mice expressing GluN2B subunits with truncated CTD showed significantly decreased NMDA synaptic currents and reduced staining of the receptors at synapses (Mori et al., 1998; Mohrmann et al., 2002). Since all tested variants lost their PDZ interactions, we link the reduced anchoring of variant receptors within

the synapses, similar to previous studies of variants that cause loss of interactions with MAGUKs (S. Liu et al., 2017; Mota Vieira et al., 2020; X. Wang et al., 2023).

Taken together, the results demonstrated the important role of the GluN2A and GluN2B subunit CTD for receptor trafficking and synaptic anchoring, together with CTD length-dependent effects on ion channel function. However, further experiments need to be carried out, as so far only a few functional motifs and a limited number of protein interactions have been described within the large CTD of both subunits. From a clinical perspective, our findings concerning variants linked to diverse neuropsychiatric conditions such as epilepsy, intellectual disability, or autism provide the first glimpse at the potential pathophysiological mechanisms that may contribute to the emergence and development of these disorders.

7 Conclusion

NMDAR plays a critical role in excitatory neurotransmission in the CNS, and its dysfunction is associated with several pathophysiological conditions. The present study, unique in its complexity, identified and described common and rare genetic variations across all *GRIN* genes encoding NMDAR subunits in a group of first-episode SCH patients and healthy controls. In particular, the study focuses on the functional analysis of genetic variants located within the promoter and CTD-coding regions of the *GRIN* genes.

Analysis of variants within the promoter regions revealed a SCH-associated promoter haplotype within the critical *GRIN1* gene, whose functional analysis showed reduced promoter activity. In the promoter of the *GRIN3B* gene, we found and analysed a $(GT)_n$ microsatellite whose longer $(GT)_n$ repeats were predominantly associated with SCH and gave rise to reduced promoter activity. Both genes exhibited an overall reduction in promoter activity in SCH patients compared to controls. These results therefore support the general hypothesis of NMDAR hypofunction in SCH.

In addition, we identified a unique variant and haplotype within the *GRIN2B* promoter associated with the disorder. However, functional analysis of this SCH promoter haplotype indicated increased activity, suggesting that GluN2B subunits may contribute to SCH by a distinct mechanism, possibly during the postnatal period.

Functional analysis of missense variants within the CTD of the GluN2A subunits showed reduced surface expression and altered ion channel properties of the variants. The P1386L variant then displayed reduced synaptic localisation due to impaired interaction with the synaptic scaffold protein PSD-95. Interestingly, the P1386L variant alters the PSD-95 binding motif to that found in less complex vertebrates, suggesting that the presence of P1386 has an evolutionary character with positive consequences for synaptic function. Taken together, GluN2A CTD missense variants, especially P1386L, may reduce the number of synaptic NMDARs and thus contribute to the pathogenesis of SCH.

Finally, functional analysis of disease-associated nonsense and frame-shift variants within the GluN2A and GluN2B subunits demonstrates the critical role of the CTD in receptor trafficking and synaptic localisation, as well as the importance of the proximal CTD region for receptor ion channel function. In addition, the results of the analysis provide potential pathophysiological mechanisms that may contribute to the variant phenotype.

8 References

Akazawa, C., Shigemoto, R., Bessho, Y., Nakanishi, S., & Mizuno, N. (1994). Differential expression of five N-methyl-D-aspartate receptor subunit mRNAs in the cerebellum of developing and adult rats. *Journal of Comparative Neurology*, *347*(1), 150–160. https://doi.org/10.1002/cne.903470112

Al-Hallaq, R. A., Conrads, T. P., Veenstra, T. D., & Wenthold, R. J. (2007). NMDA Di-Heteromeric Receptor Populations and Associated Proteins in Rat Hippocampus. *The Journal of Neuroscience*, *27*(31), 8334–8343. https://doi.org/10.1523/JNEUROSCI.2155-07.2007

Alsabban, A. H., Morikawa, M., Tanaka, Y., Takei, Y., & Hirokawa, N. (2020). Kinesin Kif3b mutation reduces NMDAR subunit NR2A trafficking and causes schizophrenia-like phenotypes in mice. *The EMBO Journal*, *39*(1), e101090. https://doi.org/10.15252/embj.2018101090

Aman, T. K., Maki, B. A., Ruffino, T. J., Kasperek, E. M., & Popescu, G. K. (2014). Separate Intramolecular Targets for Protein Kinase A Control N-Methyl-d-aspartate Receptor Gating and Ca2+ Permeability*. *Journal of Biological Chemistry*, *289*(27), 18805–18817. https://doi.org/10.1074/jbc.M113.537282

Amparan, D., Avram, D., Thomas, C. G., Lindahl, M. G., Yang, J., Bajaj, G., & Ishmael, J. E. (2005). Direct interaction of myosin regulatory light chain with the NMDA receptor. *Journal of Neurochemistry*, *92*(2), 349–361. https://doi.org/10.1111/j.1471-4159.2004.02869.x

Andersson, O., Stenqvist, A., Attersand, A., & von Euler, G. (2001). Nucleotide Sequence, Genomic Organization, and Chromosomal Localization of Genes Encoding the Human NMDA Receptor Subunits NR3A and NR3B. *Genomics*, *78*(3), 178–184. https://doi.org/10.1006/geno.2001.6666

Awadalla, P., Gauthier, J., Myers, R. A., Casals, F., Hamdan, F. F., Griffing, A. R., Côté, M., Henrion, E., Spiegelman, D., Tarabeux, J., Piton, A., Yang, Y., Boyko, A., Bustamante, C., Xiong, L., Rapoport, J. L., Addington, A. M., DeLisi, J. L. E., Krebs, M.-O., … Rouleau, G. A. (2010). Direct Measure of the De Novo Mutation Rate in Autism and Schizophrenia Cohorts. *The American Journal of Human Genetics*, *87*(3), 316–324. https://doi.org/10.1016/j.ajhg.2010.07.019

Babault, N., Cordier, F., Lafage, M., Cockburn, J., Haouz, A., Prehaud, C., Rey, F. A., Delepierre, M., Buc, H., Lafon, M., & Wolff, N. (2011). Peptides Targeting the PDZ Domain of PTPN4 Are Efficient Inducers of Glioblastoma Cell Death. *Structure*, *19*(10), 1518–1524. https://doi.org/10.1016/j.str.2011.07.007

Bai, G., & Kusiak, J. W. (1993). Cloning and analysis of the 5′ flanking sequence of the rat N-methyl-d-aspartate receptor 1 (NMDAR1) gene. *Biochimica et Biophysica Acta (BBA) - Biomembranes*, *1152*(1), 197–200. https://doi.org/10.1016/0005-2736(93)90249-Y

Bai, G., & Kusiak, J. W. (1995). Functional Analysis of the Proximal 5′-Flanking Region of the N-Methyl-D-aspartate Receptor Subunit Gene, NMDAR1 (∗). *Journal of Biological Chemistry*, *270*(13), 7737–7744. https://doi.org/10.1074/jbc.270.13.7737

Bai, G., & Kusiak, J. W. (1997). Nerve Growth Factor Up-regulates the N-Methyl-D-aspartate Receptor Subunit 1 Promoter in PC12 Cells*. *Journal of Biological Chemistry*, *272*(9), 5936–5942. https://doi.org/10.1074/jbc.272.9.5936

Bai, G., Norton, D. D., Prenger, M. S., & Kusiak, J. W. (1998). Single-stranded DNA-binding Proteins and Neuron-restrictive Silencer Factor Participate in Cell-specific Transcriptional Control of the NMDAR1 Gene*. *Journal of Biological Chemistry*, *273*(2), 1086–1091. https://doi.org/10.1074/jbc.273.2.1086

Bai, G., Zhuang, Z., Liu, A., Chai, Y., & Hoffman, P. W. (2003). The role of the RE1 element in activation of the NR1 promoter during neuronal differentiation. *Journal of Neurochemistry*, *86*(4), 992–1005. https://doi.org/10.1046/j.1471-4159.2003.01922.x

Bajaj, G., Hau, A. M., Hsu, P., Gafken, P. R., Schimerlik, M. I., & Ishmael, J. E. (2014). Identification of an Atypical Calcium-Dependent Calmodulin Binding Site on the C-terminal domain of GluN2A. *Biochemical and biophysical research communications*, *444*(4), 588–594. https://doi.org/10.1016/j.bbrc.2014.01.111

Bajaj, G., Zhang, Y., Schimerlik, M. I., Hau, A. M., Yang, J., Filtz, T. M., Kioussi, C., & Ishmael, J. E. (2009). N-Methyl-D-aspartate Receptor Subunits Are Non-myosin Targets of Myosin Regulatory Light Chain *. *Journal of Biological Chemistry*, *284*(2), 1252–1266. https://doi.org/10.1074/jbc.M801861200

Balu, D. T., & Coyle, J. T. (2015). The NMDA receptor 'glycine modulatory site' in schizophrenia: D-serine, glycine, and beyond. *Current Opinion in Pharmacology*, *20*, 109–115. https://doi.org/10.1016/j.coph.2014.12.004

Barria, A., & Malinow, R. (2002). Subunit-Specific NMDA Receptor Trafficking to Synapses. *Neuron*, *35*(2), 345–353. https://doi.org/10.1016/S0896-6273(02)00776-6

Barski, A., Cuddapah, S., Cui, K., Roh, T.-Y., Schones, D. E., Wang, Z., Wei, G., Chepelev, I., & Zhao, K. (2007). High-Resolution Profiling of Histone Methylations in the Human Genome. *Cell*, *129*(4), 823–837. https://doi.org/10.1016/j.cell.2007.05.009

Bayer, K.-U., De Koninck, P., Leonard, A. S., Hell, J. W., & Schulman, H. (2001). Interaction with the NMDA receptor locks CaMKII in an active conformation. *Nature*, *411*(6839), Article 6839. https://doi.org/10.1038/35081080

Begni, S., Moraschi, S., Bignotti, S., Fumagalli, F., Rillosi, L., Perez, J., & Gennarelli, M. (2003). Association between the G1001C polymorphism in the GRIN1 gene promoter region and schizophrenia. *Biological Psychiatry*, *53*(7), 617–619. https://doi.org/10.1016/S0006-3223(02)01783-3

Berdenis van Berlekom, A., Muflihah, C. H., Snijders, G. J. L. J., MacGillavry, H. D., Middeldorp, J., Hol, E. M., Kahn, R. S., & de Witte, L. D. (2020). Synapse Pathology in

Schizophrenia: A Meta-analysis of Postsynaptic Elements in Postmortem Brain Studies. *Schizophrenia Bulletin*, *46*(2), 374–386. https://doi.org/10.1093/schbul/sbz060

Birnbaum, R., & Weinberger, D. R. (2017). Genetic insights into the neurodevelopmental origins of schizophrenia. *Nature Reviews Neuroscience*, *18*(12), Article 12. https://doi.org/10.1038/nrn.2017.125

Blanke, M. L., & VanDongen, A. M. J. (2009). Activation Mechanisms of the NMDA Receptor. In A. M. Van Dongen (Ed.), *Biology of the NMDA Receptor*. CRC Press/Taylor & Francis. http://www.ncbi.nlm.nih.gov/books/NBK5274/

Buonarati, O. R., Cook, S. G., Goodell, D. J., Chalmers, N. E., Rumian, N. L., Tullis, J. E., Restrepo, S., Coultrap, S. J., Quillinan, N., Herson, P. S., & Bayer, K. U. (2020). CaMKII versus DAPK1 Binding to GluN2B in Ischemic Neuronal Cell Death after Resuscitation from Cardiac Arrest. *Cell Reports*, *30*(1), 1-8.e4. https://doi.org/10.1016/j.celrep.2019.11.076

Clark, A. G. (1990). Inference of haplotypes from PCR-amplified samples of diploid populations. *Molecular Biology and Evolution*, *7*(2), 111–122. https://doi.org/10.1093/oxfordjournals.molbev.a040591

Coley, A. A., & Gao, W.-J. (2018). PSD95: A synaptic protein implicated in schizophrenia or autism? *Progress in neuro-psychopharmacology & biological psychiatry*, *82*, 187–194. https://doi.org/10.1016/j.pnpbp.2017.11.016

Cooper, G. M., Stone, E. A., Asimenos, G., Green, E. D., Batzoglou, S., & Sidow, A. (2005). Distribution and intensity of constraint in mammalian genomic sequence. *Genome Research*, *15*(7), 901–913. https://doi.org/10.1101/gr.3577405

Cousins, S. L., Kenny, A. V., & Stephenson, F. A. (2009). Delineation of additional PSD-95 binding domains within NMDA receptor NR2 subunits reveals differences between NR2A/PSD-95 and NR2B/PSD-95 association. *Neuroscience*, *158*(1), 89–95. https://doi.org/10.1016/j.neuroscience.2007.12.051

Cousins, S. L., Papadakis, M., Rutter, A. R., & Stephenson, F. A. (2008). Differential interaction of NMDA receptor subtypes with the post-synaptic density-95 family of membrane associated guanylate kinase proteins. *Journal of Neurochemistry*, *104*(4), 903–913. https://doi.org/10.1111/j.1471-4159.2007.05067.x

Cousins, S. L., & Stephenson, F. A. (2012). Identification of N-Methyl-d-aspartic Acid (NMDA) Receptor Subtype-specific Binding Sites That Mediate Direct Interactions with Scaffold Protein PSD-95. *The Journal of Biological Chemistry*, *287*(16), 13465–13476. https://doi.org/10.1074/jbc.M111.292862

Cousins, S. L., & Stephenson, F. A. (2019). Identification of C-Terminal Binding Protein 1 as a Novel NMDA Receptor Interactor. *Neurochemical Research*, *44*(6), 1437–1445. https://doi.org/10.1007/s11064-018-2633-5

Deaton, A. M., & Bird, A. (2011). CpG islands and the regulation of transcription. *Genes & Development*, *25*(10), 1010–1022. https://doi.org/10.1101/gad.2037511

Desai, A., Turetsky, D., Vasudevan, K., & Buonanno, A. (2002). Analysis of Transcriptional Regulatory Sequences of the N-Methyl-d-aspartate Receptor 2A Subunit Gene in Cultured Cortical Neurons and Transgenic Mice*. *Journal of Biological Chemistry*, *277*(48), 46374–46384. https://doi.org/10.1074/jbc.M203032200

Dhar, S. S., & Wong-Riley, M. T. T. (2009). Coupling of Energy Metabolism and Synaptic Transmission at the Transcriptional Level: Role of Nuclear Respiratory Factor 1 in Regulating both Cytochrome c Oxidase and NMDA Glutamate Receptor Subunit Genes. *Journal of Neuroscience*, *29*(2), 483–492. https://doi.org/10.1523/JNEUROSCI.3704-08.2009

Di Maria, E., Gulli, R., Begni, S., De Luca, A., Bignotti, S., Pasini, A., Bellone, E., Pizzuti, A., Dallapiccola, B., Novelli, G., Ajmar, F., Gennarelli, M., & Mandich, P. (2004). Variations in the NMDA receptor subunit 2B gene (GRIN2B) and schizophrenia: A case-control study. *American Journal of Medical Genetics Part B: Neuropsychiatric Genetics*, *128B*(1), 27–29. https://doi.org/10.1002/ajmg.b.30028

Dinamarca, M. C., Guzzetti, F., Karpova, A., Lim, D., Mitro, N., Musardo, S., Mellone, M., Marcello, E., Stanic, J., Samaddar, T., Burguière, A., Caldarelli, A., Genazzani, A. A., Perroy, J., Fagni, L., Canonico, P. L., Kreutz, M. R., Gardoni, F., & Luca, M. D. (2016). Ring finger protein 10 is a novel synaptonuclear messenger encoding activation of NMDA receptors in hippocampus. *eLife*, *5*, e12430. https://doi.org/10.7554/eLife.12430

Dunham, I., Kundaje, A., Aldred, S. F., Collins, P. J., Davis, C. A., Doyle, F., Epstein, C. B., Frietze, S., Harrow, J., Kaul, R., Khatun, J., Lajoie, B. R., Landt, S. G., Lee, B.-K., Pauli, F., Rosenbloom, K. R., Sabo, P., Safi, A., Sanyal, A., … HudsonAlpha Institute, C., UC Irvine, Stanford group (data production and analysis). (2012). An integrated encyclopedia of DNA elements in the human genome. *Nature*, *489*(7414), Article 7414. https://doi.org/10.1038/nature11247

Elagabani, M. N., Briševac, D., Kintscher, M., Pohle, J., Köhr, G., Schmitz, D., & Kornau, H.-C. (2016). Subunit-selective N-Methyl-d-aspartate (NMDA) Receptor Signaling through Brefeldin A-resistant Arf Guanine Nucleotide Exchange Factors BRAG1 and BRAG2 during Synapse Maturation*. *Journal of Biological Chemistry*, *291*(17), 9105–9118. https://doi.org/10.1074/jbc.M115.691717

Endele, S., Rosenberger, G., Geider, K., Popp, B., Tamer, C., Stefanova, I., Milh, M., Kortüm, F., Fritsch, A., Pientka, F. K., Hellenbroich, Y., Kalscheuer, V. M., Kohlhase, J., Moog, U., Rappold, G., Rauch, A., Ropers, H.-H., von Spiczak, S., Tönnies, H., … Kutsche, K. (2010). Mutations in GRIN2A and GRIN2B encoding regulatory subunits of NMDA receptors cause variable neurodevelopmental phenotypes. *Nature Genetics*, *42*(11), 1021–1026. https://doi.org/10.1038/ng.677

Fan, X., Jin, W. Y., & Wang, Y. T. (2014). The NMDA receptor complex: A multifunctional machine at the glutamatergic synapse. *Frontiers in Cellular Neuroscience*, *8*. https://www.frontiersin.org/articles/10.3389/fncel.2014.00160

Firth, H. V., Richards, S. M., Bevan, A. P., Clayton, S., Corpas, M., Rajan, D., Van Vooren, S., Moreau, Y., Pettett, R. M., & Carter, N. P. (2009). DECIPHER: Database of

Chromosomal Imbalance and Phenotype in Humans Using Ensembl Resources. *American Journal of Human Genetics*, *84*(4), 524–533. https://doi.org/10.1016/j.ajhg.2009.03.010

Franke, K., Luders, E., May, A., Wilke, M., & Gaser, C. (2012). Brain maturation: Predicting individual BrainAGE in children and adolescents using structural MRI. *NeuroImage*, *63*(3), 1305–1312. https://doi.org/10.1016/j.neuroimage.2012.08.001

Franke, K., Ziegler, G., Klöppel, S., & Gaser, C. (2010). Estimating the age of healthy subjects from T1-weighted MRI scans using kernel methods: Exploring the influence of various parameters. *NeuroImage*, *50*(3), 883–892. https://doi.org/10.1016/j.neuroimage.2010.01.005

Fromer, M., Pocklington, A. J., Kavanagh, D. H., Williams, H. J., Dwyer, S., Gormley, P., Georgieva, L., Rees, E., Palta, P., Ruderfer, D. M., Carrera, N., Humphreys, I., Johnson, J. S., Roussos, P., Barker, D. D., Banks, E., Milanova, V., Grant, S. G., Hannon, E., … O'Donovan, M. C. (2014). De novo mutations in schizophrenia implicate synaptic networks. *Nature*, *506*(7487), 179–184. https://doi.org/10.1038/nature12929

Fukaya, M., Hayashi, Y., & Watanabe, M. (2005). NR2 to NR3B subunit switchover of NMDA receptors in early postnatal motoneurons. *The European Journal of Neuroscience*, *21*(5), 1432–1436. https://doi.org/10.1111/j.1460-9568.2005.03957.x

Galehdari, H. (2009). Association Between the G1001C Polymorphism in the GRIN1 Gene Promoter and Schizophrenia in the Iranian Population. *Journal of Molecular Neuroscience*, *38*(2), 178–181. https://doi.org/10.1007/s12031-008-9148-5

Gao, C., Frausto, S. F., Guedea, A. L., Tronson, N. C., Jovasevic, V., Leaderbrand, K., Corcoran, K. A., Guzmán, Y. F., Swanson, G. T., & Radulovic, J. (2011). IQGAP1 Regulates NR2A Signaling, Spine Density, and Cognitive Processes. *Journal of Neuroscience*, *31*(23), 8533–8542. https://doi.org/10.1523/JNEUROSCI.1300-11.2011

García-Nafría, J., Watson, J. F., & Greger, I. H. (2016). IVA cloning: A single-tube universal cloning system exploiting bacterial In Vivo Assembly. *Scientific Reports*, *6*(1), Article 1. https://doi.org/10.1038/srep27459

García-Recio, A., Santos-Gómez, A., Soto, D., Julia-Palacios, N., García-Cazorla, À., Altafaj, X., & Olivella, M. (2021). GRIN database: A unified and manually curated repertoire of GRIN variants. *Human Mutation*, *42*(1), 8–18. https://doi.org/10.1002/humu.24141

Gardoni, F., Bellone, C., Cattabeni, F., & Luca, M. D. (2001). Protein Kinase C Activation Modulates α-Calmodulin Kinase II Binding to NR2A Subunit of N-Methyl-D-Aspartate Receptor Complex *. *Journal of Biological Chemistry*, *276*(10), 7609–7613. https://doi.org/10.1074/jbc.M009922200

Gardoni, F., Schrama, L. H., Kamal, A., Gispen, W. H., Cattabeni, F., & Luca, M. D. (2001). Hippocampal Synaptic Plasticity Involves Competition between Ca2+/Calmodulin-Dependent Protein Kinase II and Postsynaptic Density 95 for Binding to the NR2A Subunit of the NMDA Receptor. *Journal of Neuroscience*, *21*(5), 1501–1509. https://doi.org/10.1523/JNEUROSCI.21-05-01501.2001

Garrison, E., & Marth, G. (2012). *Haplotype-based variant detection from short-read sequencing* (arXiv:1207.3907). arXiv. https://doi.org/10.48550/arXiv.1207.3907

Gautam, V., Trinidad, J. C., Rimerman, R. A., Costa, B. M., Burlingame, A. L., & Monaghan, D. T. (2013). Nedd4 is a specific E3 ubiquitin ligase for the NMDA receptor subunit GluN2D. *Neuropharmacology*, *74*, 96–107. https://doi.org/10.1016/j.neuropharm.2013.04.035

Georgi, A., Jamra, R. A., Klein, K., Villela, A. W., Schumacher, J., Becker, T., Paul, T., Schmael, C., Höfels, S., Klopp, N., Illig, T., Propping, P., Cichon, S., Nöthen, M. M., Schulze, T. G., & Rietschel, M. (2007). Possible association between genetic variants at the GRIN1 gene and schizophrenia with lifetime history of depressive symptoms in a German sample. *Psychiatric Genetics*, *17*(5), 308. https://doi.org/10.1097/YPG.0b013e3280c1e5fb

Glebov, O. O., Bright, N. A., & Nichols, B. J. (2006). Flotillin-1 defines a clathrin-independent endocytic pathway in mammalian cells. *Nature Cell Biology*, *8*(1), Article 1. https://doi.org/10.1038/ncb1342

Goebel, D. J., & Poosch, M. S. (1999). NMDA receptor subunit gene expression in the rat brain: A quantitative analysis of endogenous mRNA levels of NR1Com, NR2A, NR2B, NR2C, NR2D and NR3A. *Brain Research. Molecular Brain Research*, *69*(2), 164–170. https://doi.org/10.1016/s0169-328x(99)00100-x

Gogtay, N., & Thompson, P. M. (2010). Mapping gray matter development: Implications for typical development and vulnerability to psychopathology. *Brain and Cognition*, *72*(1), 6–15. https://doi.org/10.1016/j.bandc.2009.08.009

Goodman, L., Baddeley, D., Ambroziak, W., Waites, C. L., Garner, C. C., Soeller, C., & Montgomery, J. M. (2017). N-terminal SAP97 isoforms differentially regulate synaptic structure and postsynaptic surface pools of AMPA receptors. *Hippocampus*, *27*(6), 668–682. https://doi.org/10.1002/hipo.22723

Green, M. F., Horan, W. P., & Lee, J. (2015). Social cognition in schizophrenia. *Nature Reviews Neuroscience*, *16*(10), Article 10. https://doi.org/10.1038/nrn4005

Groc, L., Heine, M., Cousins, S. L., Stephenson, F. A., Lounis, B., Cognet, L., & Choquet, D. (2006). NMDA receptor surface mobility depends on NR2A-2B subunits. *Proceedings of the National Academy of Sciences of the United States of America*, *103*(49), 18769–18774. https://doi.org/10.1073/pnas.0605238103

Grozeva, D., Carss, K., Spasic-Boskovic, O., Tejada, M.-I., Gecz, J., Shaw, M., Corbett, M., Haan, E., Thompson, E., Friend, K., Hussain, Z., Hackett, A., Field, M., Renieri, A., Stevenson, R., Schwartz, C., Floyd, J. A. B., Bentham, J., Cosgrove, C., … Raymond, F. L. (2015). Targeted Next-Generation Sequencing Analysis of 1,000 Individuals with Intellectual Disability. *Human Mutation*, *36*(12), 1197–1204. https://doi.org/10.1002/humu.22901

Guillaud, L., Setou, M., & Hirokawa, N. (2003). KIF17 Dynamics and Regulation of NR2B Trafficking in Hippocampal Neurons. *The Journal of Neuroscience*, *23*(1), 131–140. https://doi.org/10.1523/JNEUROSCI.23-01-00131.2003

Guillaud, L., Wong, R., & Hirokawa, N. (2008). Disruption of KIF17-Mint1 interaction by CaMKII-dependent phosphorylation: A molecular model of kinesin-cargo release. *Nature Cell Biology*, *10*(1), 19–29. https://doi.org/10.1038/ncb1665

Haberle, V., & Stark, A. (2018). Eukaryotic core promoters and the functional basis of transcription initiation. *Nature Reviews Molecular Cell Biology*, *19*(10), Article 10. https://doi.org/10.1038/s41580-018-0028-8

Hajek, T., Franke, K., Kolenic, M., Capkova, J., Matejka, M., Propper, L., Uher, R., Stopkova, P., Novak, T., Paus, T., Kopecek, M., Spaniel, F., & Alda, M. (2019). Brain Age in Early Stages of Bipolar Disorders or Schizophrenia. *Schizophrenia Bulletin*, *45*(1), 190–198. https://doi.org/10.1093/schbul/sbx172

Han, L., Jia, Z., Cao, C., Liu, Z., Liu, F., Wang, L., Ren, W., Sun, M., Wang, B., Li, C., & Chen, L. (2017). Potential contribution of the neurodegenerative disorders risk loci to cognitive performance in an elderly male gout population. *Medicine*, *96*(39), e8195. https://doi.org/10.1097/MD.0000000000008195

Hansen, K. B., Wollmuth, L. P., Bowie, D., Furukawa, H., Menniti, F. S., Sobolevsky, A. I., Swanson, G. T., Swanger, S. A., Greger, I. H., Nakagawa, T., McBain, C. J., Jayaraman, V., Low, C.-M., Dell'Acqua, M. L., Diamond, J. S., Camp, C. R., Perszyk, R. E., Yuan, H., & Traynelis, S. F. (2021). Structure, Function, and Pharmacology of Glutamate Receptor Ion Channels. *Pharmacological Reviews*, *73*(4), 1469–1658. https://doi.org/10.1124/pharmrev.120.000131

Harrison, P. J., & Bannerman, D. M. (2023). GRIN2A (NR2A): A gene contributing to glutamatergic involvement in schizophrenia. *Molecular Psychiatry*, *28*(9), Article 9. https://doi.org/10.1038/s41380-023-02265-y

Hawkins, L. M., Prybylowski, K., Chang, K., Moussan, C., Stephenson, F. A., & Wenthold, R. J. (2004). Export from the Endoplasmic Reticulum of Assembled N-Methyl-D-aspartic Acid Receptors Is Controlled by a Motif in the C Terminus of the NR2 Subunit*. *Journal of Biological Chemistry*, *279*(28), 28903–28910. https://doi.org/10.1074/jbc.M402599200

Hayashi, T., Thomas, G. M., & Huganir, R. L. (2009). Dual Palmitoylation of NR2 Subunits Regulates NMDA Receptor Trafficking. *Neuron*, *64*(2), 213–226. https://doi.org/10.1016/j.neuron.2009.08.017

Hirao, K., Hata, Y., Ide, N., Takeuchi, M., Irie, M., Yao, I., Deguchi, M., Toyoda, A., Sudhof, T. C., & Takai, Y. (1998). A Novel Multiple PDZ Domain-containing Molecule Interacting withN-Methyl-d-aspartateReceptors and Neuronal Cell Adhesion Proteins *. *Journal of Biological Chemistry*, *273*(33), 21105–21110. https://doi.org/10.1074/jbc.273.33.21105

Hirschfeldova, K., Cerny, J., Bozikova, P., Kuchtiak, V., Rausch, T., Benes, V., Spaniel, F., Gregus, D., Horacek, J., Vyklicky, L., & Balik, A. (2021). Evidence for the Association

between the Intronic Haplotypes of Ionotropic Glutamate Receptors and First-Episode Schizophrenia. *Journal of Personalized Medicine*, *11*(12), 1250. https://doi.org/10.3390/jpm11121250

Hisatsune, C., Umemori, H., Mishina, M., & Yamamoto, T. (1999). Phosphorylation-dependent interaction of the N-methyl-D-aspartate receptor epsilon 2 subunit with phosphatidylinositol 3-kinase. *Genes to Cells: Devoted to Molecular & Cellular Mechanisms*, *4*(11), 657–666. https://doi.org/10.1046/j.1365-2443.1999.00287.x

Hollenhorst, P. C., McIntosh, L. P., & Graves, B. J. (2011). Genomic and Biochemical Insights into the Specificity of ETS Transcription Factors. *Annual Review of Biochemistry*, *80*(1), 437–471. https://doi.org/10.1146/annurev.biochem.79.081507.103945

Horak, M., Chang, K., & Wenthold, R. J. (2008). Masking of the Endoplasmic Reticulum Retention Signals during Assembly of the NMDA Receptor. *Journal of Neuroscience*, *28*(13), 3500–3509. https://doi.org/10.1523/JNEUROSCI.5239-07.2008

Horak, M., & Wenthold, R. J. (2009). Different Roles of C-terminal Cassettes in the Trafficking of Full-length NR1 Subunits to the Cell Surface *. *Journal of Biological Chemistry*, *284*(15), 9683–9691. https://doi.org/10.1074/jbc.M807050200

HORNIG, T., GRÜNING, B., KUNDU, K., HOUWAART, T., BACKOFEN, R., BIBER, K., & NORMANN, C. (2017). GRIN3B missense mutation as an inherited risk factor for schizophrenia: Whole-exome sequencing in a family with a familiar history of psychotic disorders. *Genetics Research*, *99*, e1. https://doi.org/10.1017/S0016672316000148

Hruska, M., Cain, R. E., & Dalva, M. B. (2022). Nanoscale rules governing the organization of glutamate receptors in spine synapses are subunit specific. *Nature Communications*, *13*(1), Article 1. https://doi.org/10.1038/s41467-022-28504-4

Hu, Z., & Bruno, A. E. (2011). The Influence of 3′UTRs on MicroRNA Function Inferred from Human SNP Data. *International Journal of Genomics*, *2011*, e910769. https://doi.org/10.1155/2011/910769

Huang, T.-N., & Hsueh, Y.-P. (2009). CASK point mutation regulates protein–protein interactions and NR2b promoter activity. *Biochemical and Biophysical Research Communications*, *382*(1), 219–222. https://doi.org/10.1016/j.bbrc.2009.03.015

Hubalkova, P., Ladislav, M., Vyklicky, V., Smejkalova, T., Hrcka Krausova, B., Kysilov, B., Krusek, J., Naimová, Z., Korinek, M., Chodounska, H., Kudova, E., Cerny, J., & Vyklicky, L. (2021). Palmitoylation Controls NMDA Receptor Function and Steroid Sensitivity. *The Journal of Neuroscience*, *41*(10), 2119–2134. https://doi.org/10.1523/JNEUROSCI.2654-20.2021

Hung, C.-C., Chen, H.-Y., & Chen, C.-H. (2002). Systematic mutation analysis of the human glutamate receptor, ionotropic, N-methyl-D-aspartate 1 gene(GRIN1) in schizophrenic patients. *Psychiatric Genetics*, *12*(4), 225.

Hwang, R., Souza, R. P., Tiwari, A. K., Zai, C. C., Müller, D. J., Potkin, S. G., Lieberman, J. A., Meltze, H. Y., & Kennedy, J. L. (2011). Gene–gene interaction analyses between

NMDA receptor subunit and dopamine receptor gene variants and clozapine response. *Pharmacogenomics*, *12*(2), 277–291. https://doi.org/10.2217/pgs.10.182

Chaudhary, S., Kaushik, M., Kukreti, R., & Kukreti, S. (2017). Structural switch from a multistranded G-quadruplex to single strands as a consequence of point mutation in the promoter of the human GRIN1 gene. *Molecular BioSystems*, *13*(9), 1805–1816. https://doi.org/10.1039/C7MB00360A

Chen, B.-S., Gray, J. A., Sanz-Clemente, A., Wei, Z., Thomas, E. V., Nicoll, R. A., & Roche, K. W. (2012). SAP102 mediates synaptic clearance of NMDA receptors. *Cell reports*, *2*(5), 1120–1128. https://doi.org/10.1016/j.celrep.2012.09.024

Cheung, H. H., & Gurd, J. W. (2001). Tyrosine phosphorylation of the N-methyl-D-aspartate receptor by exogenous and postsynaptic density-associated Src-family kinases. *Journal of Neurochemistry*, *78*(3), 524–534. https://doi.org/10.1046/j.1471-4159.2001.00433.x

Chou, T.-H., Tajima, N., Romero-Hernandez, A., & Furukawa, H. (2020). Structural Basis of Functional Transitions in Mammalian NMDA Receptors. *Cell*, *182*(2), 357-371.e13. https://doi.org/10.1016/j.cell.2020.05.052

Chung, H. J., Huang, Y. H., Lau, L.-F., & Huganir, R. L. (2004). Regulation of the NMDA Receptor Complex and Trafficking by Activity-Dependent Phosphorylation of the NR2B Subunit PDZ Ligand. *The Journal of Neuroscience*, *24*(45), 10248–10259. https://doi.org/10.1523/JNEUROSCI.0546-04.2004

Inoue, H., Yamasue, H., Tochigi, M., Suga, M., Iwayama, Y., Abe, O., Yamada, H., Rogers, M. A., Aoki, S., Kato, T., Sasaki, T., Yoshikawa, T., & Kasai, K. (2010). Functional (GT)n polymorphisms in promoter region of N-methyl-d-aspartate receptor 2A subunit (GRIN2A) gene affect hippocampal and amygdala volumes. *Genes, Brain and Behavior*, *9*(3), 269–275. https://doi.org/10.1111/j.1601-183X.2009.00557.x

Ishchenko, Y., Carrizales, M. G., & Koleske, A. J. (2021). Regulation of the NMDA receptor by its cytoplasmic domains: (How) is the tail wagging the dog? *Neuropharmacology*, *195*, 108634. https://doi.org/10.1016/j.neuropharm.2021.108634

Itokawa, M., Yamada, K., Iwayama-Shigeno, Y., Ishitsuka, Y., Detera-Wadleigh, S., & Yoshikawa, T. (2003). Genetic analysis of a functional GRIN2A promoter (GT)n repeat in bipolar disorder pedigrees in humans. *Neuroscience Letters*, *345*(1), 53–56. https://doi.org/10.1016/S0304-3940(03)00501-9

Itokawa, M., Yamada, K., Yoshitsugu, K., Toyota, T., Suga, T., Ohba, H., Watanabe, A., Hattori, E., Shimizu, H., Kumakura, T., Ebihara, M., Meerabux, J. M. A., Toru, M., & Yoshikawa, T. (2003). A microsatellite repeat in the promoter of the N-methyl-D-aspartate receptor 2A subunit (GRIN2A) gene suppresses transcriptional activity and correlates with chronic outcome in schizophrenia. *Pharmacogenetics and Genomics*, *13*(5), 271. https://doi.org/10.1097/01.fpc.0000054082.64000.63

Iwayama-Shigeno, Y., Yamada, K., Itokawa, M., Toyota, T., Meerabux, J. M. A., Minabe, Y., Mori, N., Inada, T., & Yoshikawa, T. (2005). Extended analyses support the association

of a functional (GT)n polymorphism in the GRIN2A promoter with Japanese schizophrenia. *Neuroscience Letters*, *378*(2), 102–105. https://doi.org/10.1016/j.neulet.2004.12.013

Javierre, B. M., Burren, O. S., Wilder, S. P., Kreuzhuber, R., Hill, S. M., Sewitz, S., Cairns, J., Wingett, S. W., Várnai, C., Thiecke, M. J., Burden, F., Farrow, S., Cutler, A. J., Rehnström, K., Downes, K., Grassi, L., Kostadima, M., Freire-Pritchett, P., Wang, F., … Fraser, P. (2016). Lineage-Specific Genome Architecture Links Enhancers and Non-coding Disease Variants to Target Gene Promoters. *Cell*, *167*(5), 1369-1384.e19. https://doi.org/10.1016/j.cell.2016.09.037

Jeyifous, O., Waites, C. L., Specht, C. G., Fujisawa, S., Schubert, M., Lin, E., Marshall, J., Aoki, C., de Silva, T., Montgomery, J. M., Garner, C. C., & Green, W. N. (2009). SAP97 and CASK mediate sorting of N-Methyl-D-Aspartate Receptors through a novel secretory pathway. *Nature neuroscience*, *12*(8), 1011–1019. https://doi.org/10.1038/nn.2362

Jiang, H., & Jia, J. (2009). Association between NR2B subunit gene (GRIN2B) promoter polymorphisms and sporadic Alzheimer's disease in the North Chinese population. *Neuroscience Letters*, *450*(3), 356–360. https://doi.org/10.1016/j.neulet.2008.10.075

Jiang, Y., Kuan Lin, M., Jicha, G. A., Ding, X., McIlwrath, S. L., Fardo, D. W., Broster, L. S., Schmitt, F. A., Kryscio, R., & Lipsky, R. H. (2017). Functional human GRIN2B promoter polymorphism and variation of mental processing speed in older adults. *Aging (Albany NY)*, *9*(4), 1293–1305. https://doi.org/10.18632/aging.101228

Jones, M. L., & Leonard, J. P. (2005). PKC site mutations reveal differential modulation by insulin of NMDA receptors containing NR2A or NR2B subunits. *Journal of Neurochemistry*, *92*(6), 1431–1438. https://doi.org/10.1111/j.1471-4159.2004.02985.x

Jurd, R., Thornton, C., Wang, J., Luong, K., Phamluong, K., Kharazia, V., Gibb, S. L., & Ron, D. (2008). Mind Bomb-2 Is an E3 Ligase That Ubiquitinates the N-Methyl-d-aspartate Receptor NR2B Subunit in a Phosphorylation-dependent Manner*. *Journal of Biological Chemistry*, *283*(1), 301–310. https://doi.org/10.1074/jbc.M705580200

Kahn, R. S., Sommer, I. E., Murray, R. M., Meyer-Lindenberg, A., Weinberger, D. R., Cannon, T. D., O'Donovan, M., Correll, C. U., Kane, J. M., van Os, J., & Insel, T. R. (2015). Schizophrenia. *Nature Reviews Disease Primers*, *1*(1), Article 1. https://doi.org/10.1038/nrdp.2015.67

Kay, S. R., Fiszbein, A., & Opler, L. A. (1987). The Positive and Negative Syndrome Scale (PANSS) for Schizophrenia. *Schizophrenia Bulletin*, *13*(2), 261–276. https://doi.org/10.1093/schbul/13.2.261

Kim, E., & Sheng, M. (2004). PDZ domain proteins of synapses. *Nature Reviews Neuroscience*, *5*(10), Article 10. https://doi.org/10.1038/nrn1517

Kirov, G., Pocklington, A. J., Holmans, P., Ivanov, D., Ikeda, M., Ruderfer, D., Moran, J., Chambert, K., Toncheva, D., Georgieva, L., Grozeva, D., Fjodorova, M., Wollerton, R., Rees, E., Nikolov, I., van de Lagemaat, L. N., Bayés, À., Fernandez, E., Olason, P. I.,

… Owen, M. J. (2012). De novo CNV analysis implicates specific abnormalities of postsynaptic signalling complexes in the pathogenesis of schizophrenia. *Molecular Psychiatry*, *17*(2), Article 2. https://doi.org/10.1038/mp.2011.154

Klein, M., Pieri, I., Uhlmann, F., Pfizenmaier, K., & Eisel, U. (1998). Cloning and characterisation of promoter and 5′-UTR of the NMDA receptor subunit ϵ2: Evidence for alternative splicing of 5′-non-coding exon. *Gene*, *208*(2), 259–269. https://doi.org/10.1016/S0378-1119(98)00005-5

Kohlrausch, F. B., Giori, I. G., Melo-Felippe, F. B., Vieira-Fonseca, T., Velarde, L. G. C., de Salles Andrade, J. B., & Fontenelle, L. F. (2016). Association of GRIN2B gene polymorphism and Obsessive Compulsive disorder and symptom dimensions: A pilot study. *Psychiatry Research*, *243*, 152–155. https://doi.org/10.1016/j.psychres.2016.06.027

Köhr, G., Jensen, V., Koester, H. J., Mihaljevic, A. L. A., Utvik, J. K., Kvello, A., Ottersen, O. P., Seeburg, P. H., Sprengel, R., & Hvalby, Ø. (2003). Intracellular Domains of NMDA Receptor Subtypes Are Determinants for Long-Term Potentiation Induction. *The Journal of Neuroscience*, *23*(34), 10791–10799. https://doi.org/10.1523/JNEUROSCI.23-34-10791.2003

Kolathur, K. K. (2021). Role of promoters in regulating alternative splicing. *Gene*, *782*, 145523. https://doi.org/10.1016/j.gene.2021.145523

Korinek, M., Gonzalez-Gonzalez, I. M., Smejkalova, T., Hajdukovic, D., Skrenkova, K., Krusek, J., Horak, M., & Vyklicky, L. (2020). Cholesterol modulates presynaptic and postsynaptic properties of excitatory synaptic transmission. *Scientific Reports*, *10*(1), Article 1. https://doi.org/10.1038/s41598-020-69454-5

Kornau, H.-C., Schenker, L. T., Kennedy, M. B., & Seeburg, P. H. (1995). Domain Interaction Between NMDA Receptor Subunits and the Postsynaptic Density Protein PSD-95. *Science*, *269*(5231), 1737–1740. https://doi.org/10.1126/science.7569905

Krainc, D., Bai, G., Okamoto, S., Carles, M., Kusiak, J. W., Brent, R. N., & Lipton, S. A. (1998). Synergistic Activation of theN-Methyl-d-aspartate Receptor Subunit 1 Promoter by Myocyte Enhancer Factor 2C and Sp1*. *Journal of Biological Chemistry*, *273*(40), 26218–26224. https://doi.org/10.1074/jbc.273.40.26218

Krapivinsky, G., Krapivinsky, L., Manasian, Y., Ivanov, A., Tyzio, R., Pellegrino, C., Ben-Ari, Y., Clapham, D. E., & Medina, I. (2003). The NMDA Receptor Is Coupled to the ERK Pathway by a Direct Interaction between NR2B and RasGRF1. *Neuron*, *40*(4), 775–784. https://doi.org/10.1016/S0896-6273(03)00645-7

Kristiansen, L. V., Huerta, I., Beneyto, M., & Meador-Woodruff, J. H. (2007). NMDA receptors and schizophrenia. *Current Opinion in Pharmacology*, *7*(1), 48–55. https://doi.org/10.1016/j.coph.2006.08.013

Krupp, J. J., Vissel, B., Thomas, C. G., Heinemann, S. F., & Westbrook, G. L. (2002). Calcineurin acts via the C-terminus of NR2A to modulate desensitization of NMDA

receptors. *Neuropharmacology*, *42*(5), 593–602. https://doi.org/10.1016/S0028-3908(02)00031-X

Kruse, A. O., & Bustillo, J. R. (2022). Glutamatergic dysfunction in Schizophrenia. *Translational Psychiatry*, *12*(1), Article 1. https://doi.org/10.1038/s41398-022-02253-w

Kurschner, C., Mermelstein, P. G., Holden, W. T., & Surmeier, D. J. (1998). CIPP, a Novel Multivalent PDZ Domain Protein, Selectively Interacts with Kir4.0 Family Members, NMDA Receptor Subunits, Neurexins, and Neuroligins. *Molecular and Cellular Neuroscience*, *11*(3), 161–172. https://doi.org/10.1006/mcne.1998.0679

Lai, T. W., Zhang, S., & Wang, Y. T. (2014). Excitotoxicity and stroke: Identifying novel targets for neuroprotection. *Progress in Neurobiology*, *115*, 157–188. https://doi.org/10.1016/j.pneurobio.2013.11.006

Lal, D., Steinbrücker, S., Schubert, J., Sander, T., Becker, F., Weber, Y., Lerche, H., Thiele, H., Krause, R., Lehesjoki, A.-E., Nürnberg, P., Palotie, A., Neubauer, B. A., Muhle, H., Stephani, U., Helbig, I., Becker, A. J., Schoch, S., Hansen, J., … Lemke, J. R. (2015). Investigation of GRIN2A in common epilepsy phenotypes. *Epilepsy Research*, *115*, 95–99. https://doi.org/10.1016/j.eplepsyres.2015.05.010

Lau, C. G., & Zukin, R. S. (2007). NMDA receptor trafficking in synaptic plasticity and neuropsychiatric disorders. *Nature Reviews Neuroscience*, *8*(6), Article 6. https://doi.org/10.1038/nrn2153

Laurie, D. J., & Seeburg, P. H. (1994). Regional and developmental heterogeneity in splicing of the rat brain NMDAR1 mRNA. *Journal of Neuroscience*, *14*(5), 3180–3194. https://doi.org/10.1523/JNEUROSCI.14-05-03180.1994

Lavezzari, G., McCallum, J., Dewey, C. M., & Roche, K. W. (2004). Subunit-Specific Regulation of NMDA Receptor Endocytosis. *The Journal of Neuroscience*, *24*(28), 6383–6391. https://doi.org/10.1523/JNEUROSCI.1890-04.2004

Lavezzari, G., McCallum, J., Lee, R., & Roche, K. W. (2003). Differential binding of the AP-2 adaptor complex and PSD-95 to the C-terminus of the NMDA receptor subunit NR2B regulates surface expression. *Neuropharmacology*, *45*(6), 729–737. https://doi.org/10.1016/s0028-3908(03)00308-3

Le, N. Q. K., Yapp, E. K. Y., Nagasundaram, N., & Yeh, H.-Y. (2019). Classifying Promoters by Interpreting the Hidden Information of DNA Sequences via Deep Learning and Combination of Continuous FastText N-Grams. *Frontiers in Bioengineering and Biotechnology*, *7*, 305. https://doi.org/10.3389/fbioe.2019.00305

Lee, F. J. S., Xue, S., Pei, L., Vukusic, B., Chéry, N., Wang, Y., Wang, Y. T., Niznik, H. B., Yu, X., & Liu, F. (2002). Dual regulation of NMDA receptor functions by direct protein-protein interactions with the dopamine D1 receptor. *Cell*, *111*(2), 219–230. https://doi.org/10.1016/s0092-8674(02)00962-5

Lee, G. S., Zhang, J., Wu, Y., & Zhou, Y. (2021). 14-3-3 proteins promote synaptic localization of N-methyl d-aspartate receptors (NMDARs) in mouse hippocampal and cortical neurons. *PloS One*, *16*(12), e0261791. https://doi.org/10.1371/journal.pone.0261791

Lemke, J. R., Lal, D., Reinthaler, E. M., Steiner, I., Nothnagel, M., Alber, M., Geider, K., Laube, B., Schwake, M., Finsterwalder, K., Franke, A., Schilhabel, M., Jähn, J. A., Muhle, H., Boor, R., Van Paesschen, W., Caraballo, R., Fejerman, N., Weckhuysen, S., … von Spiczak, S. (2013). Mutations in GRIN2A cause idiopathic focal epilepsy with rolandic spikes. *Nature Genetics*, *45*(9), 1067–1072. https://doi.org/10.1038/ng.2728

Lesca, G., Rudolf, G., Bruneau, N., Lozovaya, N., Labalme, A., Boutry-Kryza, N., Salmi, M., Tsintsadze, T., Addis, L., Motte, J., Wright, S., Tsintsadze, V., Michel, A., Doummar, D., Lascelles, K., Strug, L., Waters, P., de Bellescize, J., Vrielynck, P., … Szepetowski, P. (2013). GRIN2A mutations in acquired epileptic aphasia and related childhood focal epilepsies and encephalopathies with speech and language dysfunction. *Nature Genetics*, *45*(9), 1061–1066. https://doi.org/10.1038/ng.2726

Lesurf, R., Cotto, K. C., Wang, G., Griffith, M., Kasaian, K., Jones, S. J. M., Montgomery, S. B., Griffith, O. L., & The Open Regulatory Annotation Consortium. (2016). ORegAnno 3.0: A community-driven resource for curated regulatory annotation. *Nucleic Acids Research*, *44*(D1), D126–D132. https://doi.org/10.1093/nar/gkv1203

Li, B.-S., Sun, M.-K., Zhang, L., Takahashi, S., Ma, W., Vinade, L., Kulkarni, A. B., Brady, R. O., & Pant, H. C. (2001). Regulation of NMDA receptors by cyclin-dependent kinase-5. *Proceedings of the National Academy of Sciences*, *98*(22), 12742–12747. https://doi.org/10.1073/pnas.211428098

Li, H., & Durbin, R. (2009). Fast and accurate short read alignment with Burrows–Wheeler transform. *Bioinformatics*, *25*(14), 1754–1760. https://doi.org/10.1093/bioinformatics/btp324

Li, Q.-Q., Chen, J., Hu, P., Jia, M., Sun, J.-H., Feng, H.-Y., Qiao, F.-C., Zang, Y.-Y., Shi, Y.-Y., Chen, G., Sheng, N., Xu, Y., Yang, J.-J., Xu, Z., & Shi, Y. S. (2022a). Enhancing GluN2A-type NMDA receptors impairs long-term synaptic plasticity and learning and memory. *Molecular Psychiatry*, *27*(8), Article 8. https://doi.org/10.1038/s41380-022-01579-7

Li, Q.-Q., Chen, J., Hu, P., Jia, M., Sun, J.-H., Feng, H.-Y., Qiao, F.-C., Zang, Y.-Y., Shi, Y.-Y., Chen, G., Sheng, N., Xu, Y., Yang, J.-J., Xu, Z., & Shi, Y. S. (2022b). KKK879-881 motif is an ER-retention signal in GluN2A-NMDA receptor. *Molecular Psychiatry*, *27*(8), Article 8. https://doi.org/10.1038/s41380-022-01868-1

Li, S., Raychaudhuri, S., Lee, S. A., Brockmann, M. M., Wang, J., Kusick, G., Prater, C., Syed, S., Falahati, H., Ramos, R., Bartol, T. M., Hosy, E., & Watanabe, S. (2021). Asynchronous release sites align with NMDA receptors in mouse hippocampal synapses. *Nature Communications*, *12*(1), Article 1. https://doi.org/10.1038/s41467-021-21004-x

Liao, G.-Y., Wagner, D. A., Hsu, M. H., & Leonard, J. P. (2001). Evidence for Direct Protein Kinase-C Mediated Modulation ofN-Methyl-d-aspartate Receptor Current. *Molecular Pharmacology*, *59*(5), 960–964. https://doi.org/10.1124/mol.59.5.960

Lim, I. A., Hall, D. D., & Hell, J. W. (2002). Selectivity and Promiscuity of the First and Second PDZ Domains of PSD-95 and Synapse-associated Protein 102 *. *Journal of Biological Chemistry*, *277*(24), 21697–21711. https://doi.org/10.1074/jbc.M112339200

Lin, R., Duan, Z., Sun, H., Fung, M.-L., Chen, H., Wang, J., Lau, C.-F., Yang, D., Liu, Y., Ni, Y., Wang, Z., Cui, J., Wu, W., Yung, W.-H., Chan, Y.-S., Lo, A. C. Y., Xia, J., Shen, J., & Huang, J.-D. (2019). Kinesin-1 Regulates Extrasynaptic Targeting of NMDARs and Neuronal Vulnerability Toward Excitotoxicity. *iScience*, *13*, 82–97. https://doi.org/10.1016/j.isci.2019.02.009

Lin, Y., Skeberdis, V. A., Francesconi, A., Bennett, M. V. L., & Zukin, R. S. (2004). Postsynaptic Density Protein-95 Regulates NMDA Channel Gating and Surface Expression. *Journal of Neuroscience*, *24*(45), 10138–10148. https://doi.org/10.1523/JNEUROSCI.3159-04.2004

Liu, A., Hoffman, P. W., Lu, W., & Bai, G. (2004). NF-κB Site Interacts with Sp Factors and Up-regulates the NR1 Promoter during Neuronal Differentiation*. *Journal of Biological Chemistry*, *279*(17), 17449–17458. https://doi.org/10.1074/jbc.M311267200

Liu, A., Prenger, M. S., Norton, D. D., Mei, L., Kusiak, J. W., & Bai, G. (2001). Nerve Growth Factor Uses Ras/ERK and Phosphatidylinositol 3-Kinase Cascades to Up-regulate theN-Methyl-d-aspartate Receptor 1 Promoter*. *Journal of Biological Chemistry*, *276*(48), 45372–45379. https://doi.org/10.1074/jbc.M105399200

Liu, A., Zhuang, Z., Hoffman, P. W., & Bai, G. (2003). Functional Analysis of the Rat N-Methyl-D-aspartate Receptor 2A Promoter: MULTIPLE TRANSCRIPTION START POINTS, POSITIVE REGULATION BY Sp FACTORS, AND TRANSLATIONAL REGULATION*. *Journal of Biological Chemistry*, *278*(29), 26423–26434. https://doi.org/10.1074/jbc.M211165200

Liu, R., Dang, W., Du, Y., Zhou, Q., Liu, Z., & Jiao, K. (2015). Correlation of functional GRIN2A gene promoter polymorphisms with schizophrenia and serum d-serine levels. *Gene*, *568*(1), 25–30. https://doi.org/10.1016/j.gene.2015.05.011

Liu, S., Zhou, L., Yuan, H., Vieira, M., Sanz-Clemente, A., Badger, J. D., Lu, W., Traynelis, S. F., & Roche, K. W. (2017). A Rare Variant Identified Within the GluN2B C-Terminus in a Patient with Autism Affects NMDA Receptor Surface Expression and Spine Density. *The Journal of Neuroscience: The Official Journal of the Society for Neuroscience*, *37*(15), 4093–4102. https://doi.org/10.1523/JNEUROSCI.0827-16.2017

Liu, X.-R., Xu, X.-X., Lin, S.-M., Fan, C.-Y., Ye, T.-T., Tang, B., Shi, Y.-W., Su, T., Li, B.-M., Yi, Y.-H., Luo, J.-H., & Liao, W.-P. (2021). GRIN2A Variants Associated With Idiopathic Generalized Epilepsies. *Frontiers in Molecular Neuroscience*, *14*. https://www.frontiersin.org/articles/10.3389/fnmol.2021.720984

Liu, Y., Ding, M., Zhang, X., Liu, Y., Xuan, J., Xing, J., Xia, X., Yao, J., & Wang, B. (2019). Association between polymorphisms in the GRIN1 gene 5′ regulatory region and schizophrenia in a northern Han Chinese population and haplotype effects on protein expression in vitro. *BMC Medical Genetics*, *20*(1), 26. https://doi.org/10.1186/s12881-019-0757-3

Liu, Y., Wu, X., Meng, J., Xing, J., Xuan, J., Xia, X., Yao, J., & Wang, B. (2022). The effect of human GRIN1 gene 5′ functional region on gene expression regulation in vitro. *Gene*, *808*, 145973. https://doi.org/10.1016/j.gene.2021.145973

Lu, W., Fang, W., Li, J., Zhang, B., Yang, Q., Yan, X., Peng, L., Ai, H., Wang, J., Liu, X., Luo, J., & Yang, W. (2015). Phosphorylation of Tyrosine 1070 at the GluN2B Subunit Is Regulated by Synaptic Activity and Critical for Surface Expression of N-Methyl-d-aspartate (NMDA) Receptors. *The Journal of Biological Chemistry*, *290*(38), 22945–22954. https://doi.org/10.1074/jbc.M115.663450

Lu, X., Zhang, H., Li, Y., Zhou, R., He, M., Ma, Y., Tian, X., & Wang, X. (2018). *FRMPD2: A novel GluN2A-interacting scaffold protein in synaptic excitatory transmission* (s. 403360). bioRxiv. https://doi.org/10.1101/403360

Lu, X., Zhang, Q., & Wang, T. (2019). The second PDZ domain of scaffold protein Frmpd2 binds to GluN2A of NMDA receptors. *Biochemical and Biophysical Research Communications*, *516*(1), 63–67. https://doi.org/10.1016/j.bbrc.2019.05.087

Lujan, B., Liu, X., & Wan, Q. (2012). Differential roles of GluN2A- and GluN2B-containing NMDA receptors in neuronal survival and death. *International Journal of Physiology, Pathophysiology and Pharmacology*, *4*(4), 211–218.

Lüscher, C., & Malenka, R. C. (2012). NMDA receptor-dependent long-term potentiation and long-term depression (LTP/LTD). *Cold Spring Harbor Perspectives in Biology*, *4*(6). https://doi.org/10.1101/cshperspect.a005710

Maki, B. A., Aman, T. K., Amico-Ruvio, S. A., Kussius, C. L., & Popescu, G. K. (2012). C-terminal Domains of N-Methyl-d-aspartic Acid Receptor Modulate Unitary Channel Conductance and Gating. *The Journal of Biological Chemistry*, *287*(43), 36071–36080. https://doi.org/10.1074/jbc.M112.390013

Maki, B. A., Cole, R., & Popescu, G. K. (2013). Two serine residues on GluN2A C-terminal tails control NMDA receptor current decay times. *Channels*, *7*(2), 126–132. https://doi.org/10.4161/chan.23968

Makino, C., Shibata, H., Ninomiya, H., Tashiro, N., & Fukumaki, Y. (2005). Identification of single-nucleotide polymorphisms in the human N-methyl-D-aspartate receptor subunit NR2D gene, GRIN2D, and association study with schizophrenia. *Psychiatric Genetics*, *15*(3), 215.

Marshall, C. R., Howrigan, D. P., Merico, D., Thiruvahindrapuram, B., Wu, W., Greer, D. S., Antaki, D., Shetty, A., Holmans, P. A., Pinto, D., Gujral, M., Brandler, W. M., Malhotra, D., Wang, Z., Fajarado, K. V. F., Maile, M. S., Ripke, S., Agartz, I., Albus, M., … Sebat, J. (2017). Contribution of copy number variants to schizophrenia from a genome-wide

study of 41,321 subjects. *Nature Genetics*, *49*(1), Article 1. https://doi.org/10.1038/ng.3725

Martel, M.-A., Ryan, T. J., Bell, K. F. S., Fowler, J. H., McMahon, A., Al-Mubarak, B., Komiyama, N. H., Horsburgh, K., Kind, P. C., Grant, S. G. N., Wyllie, D. J. A., & Hardingham, G. E. (2012). The subtype of GluN2 C-terminal domain determines the response to excitotoxic insults. *Neuron*, *74*(3), 543–556. https://doi.org/10.1016/j.neuron.2012.03.021

Martucci, L., Wong, A. H. C., De Luca, V., Likhodi, O., Wong, G. W. H., King, N., & Kennedy, J. L. (2006). N-methyl-d-aspartate receptor NR2B subunit gene GRIN2B in schizophrenia and bipolar disorder: Polymorphisms and mRNA levels. *Schizophrenia Research*, *84*(2), 214–221. https://doi.org/10.1016/j.schres.2006.02.001

Martucci, L., Wong, A. H. C., Trakalo, J., Cate-Carter, T., Wong, G. W. H., Macciardi, F. M., & Kennedy, J. L. (2003). N-methyl-d-aspartate receptor NR1 subunit gene (GRIN1) in schizophrenia: TDT and case-control analyses. *American Journal of Medical Genetics Part B: Neuropsychiatric Genetics*, *119B*(1), 24–27. https://doi.org/10.1002/ajmg.b.20014

Matsuno, H., Ohi, K., Hashimoto, R., Yamamori, H., Yasuda, Y., Fujimoto, M., Yano-Umeda, S., Saneyoshi, T., Takeda, M., & Hayashi, Y. (2015). A Naturally Occurring Null Variant of the NMDA Type Glutamate Receptor NR3B Subunit Is a Risk Factor of Schizophrenia. *PLOS ONE*, *10*(3), e0116319. https://doi.org/10.1371/journal.pone.0116319

Mattison, H. A., Hayashi, T., & Barria, A. (2012). Palmitoylation at two cysteine clusters on the C-terminus of GluN2A and GluN2B differentially control synaptic targeting of NMDA receptors. *PloS One*, *7*(11), e49089. https://doi.org/10.1371/journal.pone.0049089

Mayer, B. J. (2001). SH3 domains: Complexity in moderation. *Journal of Cell Science*, *114*(7), 1253–1263. https://doi.org/10.1242/jcs.114.7.1253

McCutcheon, R. A., Krystal, J. H., & Howes, O. D. (2020). Dopamine and glutamate in schizophrenia: Biology, symptoms and treatment. *World Psychiatry*, *19*(1), 15–33. https://doi.org/10.1002/wps.20693

McLaren, W., Gil, L., Hunt, S. E., Riat, H. S., Ritchie, G. R. S., Thormann, A., Flicek, P., & Cunningham, F. (2016). The Ensembl Variant Effect Predictor. *Genome Biology*, *17*(1), 122. https://doi.org/10.1186/s13059-016-0974-4

Mignone, F., Gissi, C., Liuni, S., & Pesole, G. (2002). Untranslated regions of mRNAs. *Genome Biology*, *3*(3), reviews0004.1. https://doi.org/10.1186/gb-2002-3-3-reviews0004

Miyatake, R., Furukawa, A., & Suwaki, H. (2002). Identification of a novel variant of the human NR2B gene promoter region and its possible association with schizophrenia. *Molecular Psychiatry*, *7*(10), Article 10. https://doi.org/10.1038/sj.mp.4001152

Mohrmann, R., Köhr, G., Hatt, H., Sprengel, R., & Gottmann, K. (2002). Deletion of the C-terminal domain of the NR2B subunit alters channel properties and synaptic targeting

of N-methyl-D-aspartate receptors in nascent neocortical synapses. *Journal of Neuroscience Research*, *68*(3), 265–275. https://doi.org/10.1002/jnr.10219

Monyer, H., Burnashev, N., Laurie, D. J., Sakmann, B., & Seeburg, P. H. (1994). Developmental and regional expression in the rat brain and functional properties of four NMDA receptors. *Neuron*, *12*(3), 529–540. https://doi.org/10.1016/0896-6273(94)90210-0

Moreno-Cabrera, J. M., del Valle, J., Castellanos, E., Feliubadaló, L., Pineda, M., Brunet, J., Serra, E., Capellà, G., Lázaro, C., & Gel, B. (2020). Evaluation of CNV detection tools for NGS panel data in genetic diagnostics. *European Journal of Human Genetics*, *28*(12), Article 12. https://doi.org/10.1038/s41431-020-0675-z

Mori, H., Manabe, T., Watanabe, M., Satoh, Y., Suzuki, N., Toki, S., Nakamura, K., Yagi, T., Kushiya, E., Takahashi, T., Inoue, Y., Sakimura, K., & Mishina, M. (1998). Role of the Carboxy-Terminal Region of the GluRε2 Subunit in Synaptic Localization of the NMDA Receptor Channel. *Neuron*, *21*(3), 571–580. https://doi.org/10.1016/S0896-6273(00)80567-X

Mota Vieira, M., Nguyen, T. A., Wu, K., Badger, J. D., Collins, B. M., Anggono, V., Lu, W., & Roche, K. W. (2020). An Epilepsy-Associated GRIN2A Rare Variant Disrupts CaMKIIα Phosphorylation of GluN2A and NMDA Receptor Trafficking. *Cell Reports*, *32*(9), 108104. https://doi.org/10.1016/j.celrep.2020.108104

Murphy, J. A., Stein, I. S., Lau, C. G., Peixoto, R. T., Aman, T. K., Kaneko, N., Aromolaran, K., Saulnier, J. L., Popescu, G. K., Sabatini, B. L., Hell, J. W., & Zukin, R. S. (2014). Phosphorylation of Ser1166 on GluN2B by PKA Is Critical to Synaptic NMDA Receptor Function and Ca2+ Signaling in Spines. *The Journal of Neuroscience*, *34*(3), 869–879. https://doi.org/10.1523/JNEUROSCI.4538-13.2014

Nadler, J. V. (2012). Plasticity of Glutamate Synaptic Mechanisms. In J. L. Noebels, M. Avoli, M. A. Rogawski, R. W. Olsen, & A. V. Delgado-Escueta (Ed.), *Jasper's Basic Mechanisms of the Epilepsies* (4th vyd.). National Center for Biotechnology Information (US). http://www.ncbi.nlm.nih.gov/books/NBK98204/

Nagasawa, M., Sakimura, K., Mori, K. J., Bedell, M. A., Copeland, N. G., Jenkins, N. A., & Mishina, M. (1996). Gene structure and chromosomal localization of the mouse NMDA receptor channel subunits. *Molecular Brain Research*, *36*(1), 1–11. https://doi.org/10.1016/0169-328X(95)00225-H

Nakazawa, T., Kuriu, T., Tezuka, T., Umemori, H., Okabe, S., & Yamamoto, T. (2008). Regulation of dendritic spine morphology by an NMDA receptor-associated Rho GTPase-activating protein, p250GAP. *Journal of Neurochemistry*, *105*(4), 1384–1393. https://doi.org/10.1111/j.1471-4159.2008.05335.x

Nakazawa, T., Watabe, A. M., Tezuka, T., Yoshida, Y., Yokoyama, K., Umemori, H., Inoue, A., Okabe, S., Manabe, T., & Yamamoto, T. (2003). p250GAP, a Novel Brain-enriched GTPase-activating Protein for Rho Family GTPases, Is Involved in the N-Methyl-d-

aspartate Receptor Signaling. *Molecular Biology of the Cell*, *14*(7), 2921–2934. https://doi.org/10.1091/mbc.e02-09-0623

Niemann, S., Kanki, H., Fukui, Y., Takao, K., Fukaya, M., Hynynen, M. N., Churchill, M. J., Shefner, J. M., Bronson, R. T., Brown Jr., R. H., Watanabe, M., Miyakawa, T., Itohara, S., & Hayashi, Y. (2007). Genetic ablation of NMDA receptor subunit NR3B in mouse reveals motoneuronal and nonmotoneuronal phenotypes. *European Journal of Neuroscience*, *26*(6), 1407–1420. https://doi.org/10.1111/j.1460-9568.2007.05774.x

Niethammer, M., Kim, E., & Sheng, M. (1996). Interaction between the C terminus of NMDA receptor subunits and multiple members of the PSD-95 family of membrane-associated guanylate kinases. *The Journal of Neuroscience*, *16*(7), 2157–2163. https://doi.org/10.1523/JNEUROSCI.16-07-02157.1996

Nishiguchi, N., Shirakawa, O., Ono, H., Hashimoto, T., & Maeda, K. (2000). Novel polymorphism in the gene region encoding the carboxyl-terminal intracellular domain of the NMDA receptor 2B subunit: Analysis of association with schizophrenia. *The American Journal of Psychiatry*, *157*(8), 1329–1331. https://doi.org/10.1176/appi.ajp.157.8.1329

Okamoto, S., Sherman, K., Bai, G., & Lipton, S. A. (2002). Effect of the ubiquitous transcription factors, SP1 and MAZ, on NMDA receptor subunit type 1 (NR1) expression during neuronal differentiation. *Molecular Brain Research*, *107*(2), 89–96. https://doi.org/10.1016/S0169-328X(02)00440-0

Okamoto, S., Sherman, K., & Lipton, S. A. (1999). Absence of binding activity of neuron-restrictive silencer factor is necessary, but not sufficient for transcription of NMDA receptor subunit type 1 in neuronal cells. *Molecular Brain Research*, *74*(1), 44–54. https://doi.org/10.1016/S0169-328X(99)00250-8

Omkumar, R. V., Kiely, M. J., Rosenstein, A. J., Min, K.-T., & Kennedy, M. B. (1996). Identification of a Phosphorylation Site for Calcium/Calmodulindependent Protein Kinase II in the NR2B Subunit of the N-Methyl-D-aspartate Receptor*. *Journal of Biological Chemistry*, *271*(49), 31670–31678. https://doi.org/10.1074/jbc.271.49.31670

O'Roak, B. J., Stessman, H. A., Boyle, E. A., Witherspoon, K. T., Martin, B., Lee, C., Vives, L., Baker, C., Hiatt, J. B., Nickerson, D. A., Bernier, R., Shendure, J., & Eichler, E. E. (2014). Recurrent de novo mutations implicate novel genes underlying simplex autism risk. *Nature Communications*, *5*, 5595. https://doi.org/10.1038/ncomms6595

Owen, M. J., Sawa, A., & Mortensen, P. B. (2016). Schizophrenia. *Lancet (London, England)*, *388*(10039), 86–97. https://doi.org/10.1016/S0140-6736(15)01121-6

Ozaki, M., Sasner, M., Yano, R., Lu, H. S., & Buonanno, A. (1997). Neuregulin-β induces expression of an NMDA-receptor subunit. *Nature*, *390*(6661), Article 6661. https://doi.org/10.1038/37795

Paoletti, P. (2011). Molecular basis of NMDA receptor functional diversity. *European Journal of Neuroscience*, *33*(8), 1351–1365. https://doi.org/10.1111/j.1460-9568.2011.07628.x

Paus, S., Rietschel, M., Schulze, T. G., Ohlraun, S., Diaconu, C. C., Van Den Bogaert, A., Maier, W., Propping, P., Cichon, S., & Nöthen, M. M. (2004). Systematic screening for mutations in the human N-methyl-D-aspartate receptor 1 gene in schizophrenic patients from the German population. *Psychiatric Genetics*, *14*(4), 233–234. https://doi.org/10.1097/00041444-200412000-00013

Pérez-Otaño, I., Larsen, R. S., & Wesseling, J. F. (2016). Emerging roles of GluN3-containing NMDA receptors in the CNS. *Nature Reviews Neuroscience*, *17*(10), Article 10. https://doi.org/10.1038/nrn.2016.92

Pérez-Otaño, I., Luján, R., Tavalin, S. J., Plomann, M., Modregger, J., Liu, X.-B., Jones, E. G., Heinemann, S. F., Lo, D. C., & Ehlers, M. D. (2006). Endocytosis and synaptic removal of NR3A-containing NMDA receptors by PACSIN1/syndapin1. *Nature neuroscience*, *9*(5), 611–621. https://doi.org/10.1038/nn1680

Petralia, R. S. (2012). Distribution of Extrasynaptic NMDA Receptors on Neurons. *The Scientific World Journal*, *2012*, 267120. https://doi.org/10.1100/2012/267120

Petralia, R. S., Wang, Y.-X., Hua, F., Yi, Z., Zhou, A., Ge, L., Stephenson, F. A., & Wenthold, R. J. (2010). Organization of NMDA receptors at extrasynaptic locations. *Neuroscience*, *167*(1), 68–87. https://doi.org/10.1016/j.neuroscience.2010.01.022

Pieri, I., Klein, M., Bayertz, C., Gerspach, J., van der Ploeg, A., Pfizenmaier, K., & Eisel, U. (1999). Regulation of the murine NMDA-receptor-subunit NR2C promoter by Sp1 and fushi tarazu factor1 (FTZ-F1) homologues. *European Journal of Neuroscience*, *11*(6), 2083–2092. https://doi.org/10.1046/j.1460-9568.1999.00629.x

Piguel, N. H., Fievre, S., Blanc, J.-M., Carta, M., Moreau, M. M., Moutin, E., Pinheiro, V. L., Medina, C., Ezan, J., Lasvaux, L., Loll, F., Durand, C. M., Chang, K., Petralia, R. S., Wenthold, R. J., Stephenson, F. A., Vuillard, L., Darbon, H., Perroy, J., … Sans, N. (2014). Scribble1/AP2 complex coordinates NMDA receptor endocytic recycling. *Cell Reports*, *9*(2), 712–727. https://doi.org/10.1016/j.celrep.2014.09.017

Platzer, K., Yuan, H., Schütz, H., Winschel, A., Chen, W., Hu, C., Kusumoto, H., Heyne, H. O., Helbig, K. L., Tang, S., Willing, M. C., Tinkle, B. T., Adams, D. J., Depienne, C., Keren, B., Mignot, C., Frengen, E., Strømme, P., Biskup, S., … Lemke, J. R. (2017). GRIN2B encephalopathy: Novel findings on phenotype, variant clustering, functional consequences and treatment aspects. *Journal of Medical Genetics*, *54*(7), 460–470. https://doi.org/10.1136/jmedgenet-2016-104509

Poltavskaya, E. G., Fedorenko, O. Y., Kornetova, E. G., Loonen, A. J. M., Kornetov, A. N., Bokhan, N. A., & Ivanova, S. A. (2021). Study of Early Onset Schizophrenia: Associations of GRIN2A and GRIN2B Polymorphisms. *Life*, *11*(10), Article 10. https://doi.org/10.3390/life11100997

Ponjavic, J., Lenhard, B., Kai, C., Kawai, J., Carninci, P., Hayashizaki, Y., & Sandelin, A. (2006). Transcriptional and structural impact of TATA-initiation site spacing in mammalian core promoters. *Genome Biology*, *7*(8), R78. https://doi.org/10.1186/gb-2006-7-8-r78

Portales-Casamar, E., Arenillas, D., Lim, J., Swanson, M. I., Jiang, S., McCallum, A., Kirov, S., & Wasserman, W. W. (2009). The PAZAR database of gene regulatory information coupled to the ORCA toolkit for the study of regulatory sequences. *Nucleic Acids Research*, *37*(suppl_1), D54–D60. https://doi.org/10.1093/nar/gkn783

Priya, A., Johar, K., & Wong-Riley, M. T. T. (2013a). Specificity protein 4 functionally regulates the transcription of NMDA receptor subunits GluN1, GluN2A, and GluN2B. *Biochimica et Biophysica Acta (BBA) - Molecular Cell Research*, *1833*(12), 2745–2756. https://doi.org/10.1016/j.bbamcr.2013.07.002

Priya, A., Johar, K., & Wong-Riley, M. T. T. (2013b). Specificity protein 4 functionally regulates the transcription of NMDA receptor subunits GluN1, GluN2A, and GluN2B. *Biochimica et Biophysica Acta (BBA) - Molecular Cell Research*, *1833*(12), 2745–2756. https://doi.org/10.1016/j.bbamcr.2013.07.002

Prybylowski, K., Chang, K., Kan, L., Vicini, S., & Wenthold, R. J. (2005). The synaptic localization of NR2B-containing NMDA receptors is controlled by interactions with PDZ proteins and AP-2. *Neuron*, *47*(6), 845–857. https://doi.org/10.1016/j.neuron.2005.08.016

Puddifoot, C., Chen, P., Schoepfer, R., & Wyllie, D. (2009). Pharmacological characterization of recombinant NR1/NR2A NMDA receptors with truncated and deleted carboxy termini expressed in Xenopus laevis oocytes. *British Journal of Pharmacology*, *156*(3), 509–518. https://doi.org/10.1111/j.1476-5381.2008.00040.x

Punnakkal, P., Jendritza, P., & Köhr, G. (2012). Influence of the intracellular GluN2 C-terminal domain on NMDA receptor function. *Neuropharmacology*, *62*(5–6), 1985–1992. https://doi.org/10.1016/j.neuropharm.2011.12.018

Purcell, S. M., Moran, J. L., Fromer, M., Ruderfer, D., Solovieff, N., Roussos, P., O'Dushlaine, C., Chambert, K., Bergen, S. E., Kähler, A., Duncan, L., Stahl, E., Genovese, G., Fernández, E., Collins, M. O., Komiyama, N. H., Choudhary, J. S., Magnusson, P. K. E., Banks, E., … Sklar, P. (2014). A polygenic burden of rare disruptive mutations in schizophrenia. *Nature*, *506*(7487), Article 7487. https://doi.org/10.1038/nature12975

Qiang, M., Rani, C. S. S., & Ticku, M. K. (2005). Neuron-Restrictive Silencer Factor Regulates the N-Methyl-d-aspartate Receptor 2B Subunit Gene in Basal and Ethanol-Induced Gene Expression in Fetal Cortical Neurons. *Molecular Pharmacology*, *67*(6), 2115–2125. https://doi.org/10.1124/mol.104.010751

Qiang, M., & Ticku, M. K. (2005). Role of AP-1 in ethanol-induced N-methyl-d-aspartate receptor 2B subunit gene up-regulation in mouse cortical neurons. *Journal of Neurochemistry*, *95*(5), 1332–1341. https://doi.org/10.1111/j.1471-4159.2005.03464.x

Qin, S., Zhao, X., Pan, Y., Liu, J., Feng, G., Fu, J., Bao, J., Zhang, Z., & He, L. (2005). An association study of the N-methyl-D-aspartate receptor NR1 subunit gene (GRIN1) and NR2B subunit gene (GRIN2B) in schizophrenia with universal DNA microarray. *European Journal of Human Genetics*, *13*(7), Article 7. https://doi.org/10.1038/sj.ejhg.5201418

Qiu, Z., & Ghosh, A. (2008). A Calcium-Dependent Switch in a CREST-BRG1 Complex Regulates Activity-Dependent Gene Expression. *Neuron*, *60*(5), 775–787. https://doi.org/10.1016/j.neuron.2008.09.040

Rani, C. S. S., Qiang, M., & Ticku, M. K. (2005). Potential Role of cAMP Response Element-Binding Protein in Ethanol-Induced N-Methyl-d-aspartate Receptor 2B Subunit Gene Transcription in Fetal Mouse Cortical Cells. *Molecular Pharmacology*, *67*(6), 2126–2136. https://doi.org/10.1124/mol.104.007872

Ratnam, J., & Teichberg, V. I. (2005). Neurofilament-light increases the cell surface expression of the N-methyl-d-aspartate receptor and prevents its ubiquitination. *Journal of Neurochemistry*, *92*(4), 878–885. https://doi.org/10.1111/j.1471-4159.2004.02936.x

Rauch, A., Wieczorek, D., Graf, E., Wieland, T., Endele, S., Schwarzmayr, T., Albrecht, B., Bartholdi, D., Beygo, J., Di Donato, N., Dufke, A., Cremer, K., Hempel, M., Horn, D., Hoyer, J., Joset, P., Röpke, A., Moog, U., Riess, A., … Strom, T. M. (2012). Range of genetic mutations associated with severe non-syndromic sporadic intellectual disability: An exome sequencing study. *Lancet (London, England)*, *380*(9854), 1674–1682. https://doi.org/10.1016/S0140-6736(12)61480-9

Rausch, T., Hsi-Yang Fritz, M., Korbel, J. O., & Benes, V. (2019). Alfred: Interactive multi-sample BAM alignment statistics, feature counting and feature annotation for long- and short-read sequencing. *Bioinformatics*, *35*(14), 2489–2491. https://doi.org/10.1093/bioinformatics/bty1007

Rentzsch, P., Witten, D., Cooper, G. M., Shendure, J., & Kircher, M. (2019). CADD: Predicting the deleteriousness of variants throughout the human genome. *Nucleic Acids Research*, *47*(D1), D886–D894. https://doi.org/10.1093/nar/gky1016

Retterer, K., Juusola, J., Cho, M. T., Vitazka, P., Millan, F., Gibellini, F., Vertino-Bell, A., Smaoui, N., Neidich, J., Monaghan, K. G., McKnight, D., Bai, R., Suchy, S., Friedman, B., Tahiliani, J., Pineda-Alvarez, D., Richard, G., Brandt, T., Haverfield, E., … Bale, S. (2016). Clinical application of whole-exome sequencing across clinical indications. *Genetics in Medicine: Official Journal of the American College of Medical Genetics*, *18*(7), 696–704. https://doi.org/10.1038/gim.2015.148

Rice, S. R., Niu, N., Berman, D. B., Heston, L. L., & Sobell, J. L. (2001). Identification of single nucleotide polymorphisms (SNPs) and other sequence changes and estimation of nucleotide diversity in coding and flanking regions of the NMDAR1 receptor gene in schizophrenic patients. *Molecular Psychiatry*, *6*(3), Article 3. https://doi.org/10.1038/sj.mp.4000838

Richter, M., Suau, P., & Ponte, I. (2002). Sequence and analysis of the 5′ flanking and 5′ untranslated regions of the rat N-methyl-d-aspartate receptor 2A gene. *Gene*, *295*(1), 135–142. https://doi.org/10.1016/S0378-1119(02)00833-8

Roche, K. W., Standley, S., McCallum, J., Dune Ly, C., Ehlers, M. D., & Wenthold, R. J. (2001). Molecular determinants of NMDA receptor internalization. *Nature Neuroscience*, *4*(8), 794–802. https://doi.org/10.1038/90498

Rong, Y., Lu, X., Bernard, A., Khrestchatisky, M., & Baudry, M. (2001). Tyrosine phosphorylation of ionotropic glutamate receptors by Fyn or Src differentially modulates their susceptibility to calpain and enhances their binding to spectrin and PSD-95. *Journal of Neurochemistry*, *79*(2), 382–390. https://doi.org/10.1046/j.1471-4159.2001.00565.x

Ross, S., Tienhaara, A., Lee, M.-S., Tsai, L.-H., & Gill, G. (2002). GC Box-binding Transcription Factors Control the Neuronal Specific Transcription of the Cyclin-dependent Kinase 5 Regulator p35*. *Journal of Biological Chemistry*, *277*(6), 4455–4464. https://doi.org/10.1074/jbc.M110771200

Rossi, P., Sola, E., Taglietti, V., Borchardt, T., Steigerwald, F., Utvik, J. K., Ottersen, O. P., Köhr, G., & D'Angelo, E. (2002). NMDA Receptor 2 (NR2) C-Terminal Control of NR Open Probability Regulates Synaptic Transmission and Plasticity at a Cerebellar Synapse. *The Journal of Neuroscience*, *22*(22), 9687–9697. https://doi.org/10.1523/JNEUROSCI.22-22-09687.2002

Roussos, P., Mitchell, A. C., Voloudakis, G., Fullard, J. F., Pothula, V. M., Tsang, J., Stahl, E. A., Georgakopoulos, A., Ruderfer, D. M., Charney, A., Okada, Y., Siminovitch, K. A., Worthington, J., Padyukov, L., Klareskog, L., Gregersen, P. K., Plenge, R. M., Raychaudhuri, S., Fromer, M., … Sklar, P. (2014). A Role for Noncoding Variation in Schizophrenia. *Cell Reports*, *9*(4), 1417–1429. https://doi.org/10.1016/j.celrep.2014.10.015

Rutter, A. R., & Stephenson, F. A. (2000). Coexpression of Postsynaptic Density-95 Protein with NMDA Receptors Results in Enhanced Receptor Expression Together with a Decreased Sensitivity to L-Glutamate. *Journal of Neurochemistry*, *75*(6), 2501–2510. https://doi.org/10.1046/j.1471-4159.2000.0752501.x

Ryan, T. J., Emes, R. D., Grant, S. G., & Komiyama, N. H. (2008). Evolution of NMDA receptor cytoplasmic interaction domains: Implications for organisation of synaptic signalling complexes. *BMC Neuroscience*, *9*, 6. https://doi.org/10.1186/1471-2202-9-6

Ryan, T. J., Kopanitsa, M. V., Indersmitten, T., Nithianantharajah, J., Afinowi, N. O., Pettit, C., Stanford, L. E., Sprengel, R., Saksida, L. M., Bussey, T. J., O'Dell, T. J., Grant, S. G. N., & Komiyama, N. H. (2013). Evolution of GluN2A/B cytoplasmic domains diversified vertebrate synaptic plasticity and behavior. *Nature neuroscience*, *16*(1), 25–32. https://doi.org/10.1038/nn.3277

Sakagami, H., Sanda, M., Fukaya, M., Miyazaki, T., Sukegawa, J., Yanagisawa, T., Suzuki, T., Fukunaga, K., Watanabe, M., & Kondo, H. (2008). IQ-ArfGEF/BRAG1 is a guanine nucleotide exchange factor for Arf6 that interacts with PSD-95 at postsynaptic density of excitatory synapses. *Neuroscience Research*, *60*(2), 199–212. https://doi.org/10.1016/j.neures.2007.10.013

Sakurai, K., Toru, M., Yamakawa-Kobayashi, K., & Arinami, T. (2000). Mutation analysis of the N-methyl-d-aspartate receptor NR1 subunit gene (GRIN1) in schizophrenia. *Neuroscience Letters*, *296*(2), 168–170. https://doi.org/10.1016/S0304-3940(00)01599-8

Salek, A. B., Edler, M. C., McBride, J. P., & Baucum, A. J. (2019). Spinophilin regulates phosphorylation and interactions of the GluN2B subunit of the N-Methyl-D-Aspartate Receptor. *Journal of neurochemistry*, *151*(2), 185–203. https://doi.org/10.1111/jnc.14831

Sans, N., Petralia, R. S., Wang, Y.-X., Blahos, J., Hell, J. W., & Wenthold, R. J. (2000). A Developmental Change in NMDA Receptor-Associated Proteins at Hippocampal Synapses. *The Journal of Neuroscience*, *20*(3), 1260–1271. https://doi.org/10.1523/JNEUROSCI.20-03-01260.2000

Sans, N., Prybylowski, K., Petralia, R. S., Chang, K., Wang, Y.-X., Racca, C., Vicini, S., & Wenthold, R. J. (2003). NMDA receptor trafficking through an interaction between PDZ proteins and the exocyst complex. *Nature Cell Biology*, *5*(6), Article 6. https://doi.org/10.1038/ncb990

Sans, N., Wang, P. Y., Du, Q., Petralia, R. S., Wang, Y.-X., Nakka, S., Blumer, J. B., Macara, I. G., & Wenthold, R. J. (2005). mPins modulates PSD-95 and SAP102 trafficking and influences NMDA receptor surface expression. *Nature Cell Biology*, *7*(12), Article 12. https://doi.org/10.1038/ncb1325

Sanz-Clemente, A., Matta, J. A., Isaac, J. T. R., & Roche, K. W. (2010). Casein Kinase 2 Regulates the NR2 Subunit Composition of Synaptic NMDA Receptors. *Neuron*, *67*(6), 984–996. https://doi.org/10.1016/j.neuron.2010.08.011

Sapkota, K., Dore, K., Tang, K., Irvine, M., Fang, G., Burnell, E. S., Malinow, R., Jane, D. E., & Monaghan, D. T. (2019). The NMDA receptor intracellular C-terminal domains reciprocally interact with allosteric modulators. *Biochemical pharmacology*, *159*, 140–153. https://doi.org/10.1016/j.bcp.2018.11.018

Sasner, M., & Buonanno, A. (1996). Distinct N-Methyl—Aspartate Receptor 2B Subunit Gene Sequences Confer Neural and Developmental Specific Expression *. *Journal of Biological Chemistry*, *271*(35), 21316–21322. https://doi.org/10.1074/jbc.271.35.21316

Scott, D. B., Blanpied, T. A., Swanson, G. T., Zhang, C., & Ehlers, M. D. (2001). An NMDA Receptor ER Retention Signal Regulated by Phosphorylation and Alternative Splicing. *Journal of Neuroscience*, *21*(9), 3063–3072. https://doi.org/10.1523/JNEUROSCI.21-09-03063.2001

Scott, D. B., Michailidis, I., Mu, Y., Logothetis, D., & Ehlers, M. D. (2004). Endocytosis and Degradative Sorting of NMDA Receptors by Conserved Membrane-Proximal Signals. *The Journal of Neuroscience*, *24*(32), 7096–7109. https://doi.org/10.1523/JNEUROSCI.0780-04.2004

Sekar, A., Bialas, A. R., de Rivera, H., Davis, A., Hammond, T. R., Kamitaki, N., Tooley, K., Presumey, J., Baum, M., Van Doren, V., Genovese, G., Rose, S. A., Handsaker, R. E., Daly, M. J., Carroll, M. C., Stevens, B., & McCarroll, S. A. (2016). Schizophrenia risk from complex variation of complement component 4. *Nature*, *530*(7589), Article 7589. https://doi.org/10.1038/nature16549

Sementchenko, V. I., & Watson, D. K. (2000). Ets target genes: Past, present and future. *Oncogene*, *19*(55), Article 55. https://doi.org/10.1038/sj.onc.1204034

Sessoms-Sikes, S., Honse, Y., Lovinger, D. M., & Colbran, R. J. (2005). CaMKIIα enhances the desensitization of NR2B-containing NMDA receptors by an autophosphorylation-dependent mechanism. *Molecular and Cellular Neuroscience*, *29*(1), 139–147. https://doi.org/10.1016/j.mcn.2005.01.006

Setou, M., Nakagawa, T., Seog, D.-H., & Hirokawa, N. (2000). Kinesin Superfamily Motor Protein KIF17 and mLin-10 in NMDA Receptor-Containing Vesicle Transport. *Science*, *288*(5472), 1796–1802. https://doi.org/10.1126/science.288.5472.1796

Shaul, O. (2017). How introns enhance gene expression. *The International Journal of Biochemistry & Cell Biology*, *91*, 145–155. https://doi.org/10.1016/j.biocel.2017.06.016

Sheehan, D. V., Lecrubier, Y., Sheehan, K. H., Amorim, P., Janavs, J., Weiller, E., Hergueta, T., Baker, R., & Dunbar, G. C. (1998a). The Mini-International Neuropsychiatric Interview (M.I.N.I.): The Development and Validation of a Structured Diagnostic Psychiatric Interview for DSM-IV and ICD-10. *The Journal of Clinical Psychiatry*, *59*(suppl 20), 11980.

Sheehan, D. V., Lecrubier, Y., Sheehan, K. H., Amorim, P., Janavs, J., Weiller, E., Hergueta, T., Baker, R., & Dunbar, G. C. (1998b). The Mini-International Neuropsychiatric Interview (M.I.N.I.): The Development and Validation of a Structured Diagnostic Psychiatric Interview for DSM-IV and ICD-10. *The Journal of Clinical Psychiatry*, *59*(suppl 20), 11980.

Shen, H., & Li, Z. (2016). miRNAs in NMDA receptor-dependent synaptic plasticity and psychiatric disorders. *Clinical Science*, *130*(14), 1137–1146. https://doi.org/10.1042/CS20160046

Shen, Y.-C., Liao, D.-L., Chen, J.-Y., Wang, Y.-C., Lai, I.-C., Liou, Y.-J., Chen, Y.-J., Luu, S.-U., & Chen, C.-H. (2009). Exomic sequencing of the glutamate receptor, ionotropic, N-methyl-d-aspartate 3A gene (GRIN3A) reveals no association with schizophrenia. *Schizophrenia Research*, *114*(1), 25–32. https://doi.org/10.1016/j.schres.2009.07.005

Schnack, H. G., van Haren, N. E. M., Nieuwenhuis, M., Hulshoff Pol, H. E., Cahn, W., & Kahn, R. S. (2016). Accelerated Brain Aging in Schizophrenia: A Longitudinal Pattern Recognition Study. *American Journal of Psychiatry*, *173*(6), 607–616. https://doi.org/10.1176/appi.ajp.2015.15070922

Silvennoinen, K., Balestrini, S., Rothwell, J. C., & Sisodiya, S. M. (2020). Transcranial magnetic stimulation as a tool to understand genetic conditions associated with epilepsy. *Epilepsia*, *61*(9), 1818–1839. https://doi.org/10.1111/epi.16634

Singh, T., Poterba, T., Curtis, D., Akil, H., Al Eissa, M., Barchas, J. D., Bass, N., Bigdeli, T. B., Breen, G., Bromet, E. J., Buckley, P. F., Bunney, W. E., Bybjerg-Grauholm, J., Byerley, W. F., Chapman, S. B., Chen, W. J., Churchhouse, C., Craddock, N., Cusick, C. M., … Daly, M. J. (2022). Rare coding variants in ten genes confer substantial risk for

schizophrenia. *Nature*, *604*(7906), Article 7906. https://doi.org/10.1038/s41586-022-04556-w

Smejkalova, T., Korinek, M., Krusek, J., Hrcka Krausova, B., Candelas Serra, M., Hajdukovic, D., Kudova, E., Chodounska, H., & Vyklicky, L. (2021). Endogenous neurosteroids pregnanolone and pregnanolone sulfate potentiate presynaptic glutamate release through distinct mechanisms. *British Journal of Pharmacology*, *178*(19), 3888–3904. https://doi.org/10.1111/bph.15529

Sprengel, R., Suchanek, B., Amico, C., Brusa, R., Burnashev, N., Rozov, A., Hvalby, O., Jensen, V., Paulsen, O., Andersen, P., Kim, J. J., Thompson, R. F., Sun, W., Webster, L. C., Grant, S. G., Eilers, J., Konnerth, A., Li, J., McNamara, J. O., & Seeburg, P. H. (1998a). Importance of the intracellular domain of NR2 subunits for NMDA receptor function in vivo. *Cell*, *92*(2), 279–289. https://doi.org/10.1016/s0092-8674(00)80921-6

Sprengel, R., Suchanek, B., Amico, C., Brusa, R., Burnashev, N., Rozov, A., Hvalby, *Ø*., Jensen, V., Paulsen, O., Andersen, P., Kim, J. J., Thompson, R. F., Sun, W., Webster, L. C., Grant, S. G. N., Eilers, J., Konnerth, A., Li, J., McNamara, J. O., & Seeburg, P. H. (1998b). Importance of the Intracellular Domain of NR2 Subunits for NMDA Receptor Function In Vivo. *Cell*, *92*(2), 279–289. https://doi.org/10.1016/S0092-8674(00)80921-6

Standley, S., Petralia, R. S., Gravell, M., Hamilton, R., Wang, Y.-X., Schubert, M., & Wenthold, R. J. (2012). Trafficking of the NMDAR2B Receptor Subunit Distal Cytoplasmic Tail from Endoplasmic Reticulum to the Synapse. *PLoS ONE*, *7*(6), e39585. https://doi.org/10.1371/journal.pone.0039585

Standley, S., Roche, K. W., McCallum, J., Sans, N., & Wenthold, R. J. (2000). PDZ Domain Suppression of an ER Retention Signal in NMDA Receptor NR1 Splice Variants. *Neuron*, *28*(3), 887–898. https://doi.org/10.1016/S0896-6273(00)00161-6

Stanic, J., Carta, M., Eberini, I., Pelucchi, S., Marcello, E., Genazzani, A. A., Racca, C., Mulle, C., Di Luca, M., & Gardoni, F. (2015). Rabphilin 3A retains NMDA receptors at synaptic sites through interaction with GluN2A/PSD-95 complex. *Nature Communications*, *6*(1), Article 1. https://doi.org/10.1038/ncomms10181

Steigerwald, F., Schulz, T. W., Schenker, L. T., Kennedy, M. B., Seeburg, P. H., & Köhr, G. (2000). C-Terminal Truncation of NR2A Subunits Impairs Synaptic But Not Extrasynaptic Localization of NMDA Receptors. *The Journal of Neuroscience*, *20*(12), 4573–4581. https://doi.org/10.1523/JNEUROSCI.20-12-04573.2000

Stessman, H. A. F., Xiong, B., Coe, B. P., Wang, T., Hoekzema, K., Fenckova, M., Kvarnung, M., Gerdts, J., Trinh, S., Cosemans, N., Vives, L., Lin, J., Turner, T. N., Santen, G., Ruivenkamp, C., Kriek, M., van Haeringen, A., Aten, E., Friend, K., … Eichler, E. E. (2017). Targeted sequencing identifies 91 neurodevelopmental-disorder risk genes with autism and developmental-disability biases. *Nature Genetics*, *49*(4), 515–526. https://doi.org/10.1038/ng.3792

Strack, S., & Colbran, R. J. (1998). Autophosphorylation-dependent Targeting of Calcium/ Calmodulin-dependent Protein Kinase II by the NR2B Subunit of theN-Methyl-d-aspartate Receptor *. *Journal of Biological Chemistry*, *273*(33), 20689–20692. https://doi.org/10.1074/jbc.273.33.20689

Strahl, B. D., & Allis, C. D. (2000). The language of covalent histone modifications. *Nature*, *403*(6765), Article 6765. https://doi.org/10.1038/47412

Suchanek, B., Seeburg, P. H., & Sprengel, R. (1995). Gene Structure of the Murine N-Methyl D-Aspartate Receptor Subunit NR2C (∗). *Journal of Biological Chemistry*, *270*(1), 41–44. https://doi.org/10.1074/jbc.270.1.41

Suzuki, K., Sato, M., Morishima, Y., & Nakanishi, S. (2005). Neuronal Depolarization Controls Brain-Derived Neurotrophic Factor-Induced Upregulation of NR2C NMDA Receptor via Calcineurin Signaling. *Journal of Neuroscience*, *25*(41), 9535–9543. https://doi.org/10.1523/JNEUROSCI.2191-05.2005

Swanwick, C. C., Shapiro, M. E., Yi, Z., Chang, K., & Wenthold, R. J. (2009). NMDA receptors interact with flotillin-1 and -2, lipid raft-associated proteins. *FEBS Letters*, *583*(8), 1226–1230. https://doi.org/10.1016/j.febslet.2009.03.017

Tai, D. J. C., Su, C.-C., Ma, Y.-L., & Lee, E. H. Y. (2009). SGK1 Phosphorylation of IκB Kinase α and p300 Up-regulates NF-κB Activity and Increases N-Methyl-D-aspartate Receptor NR2A and NR2B Expression*. *Journal of Biological Chemistry*, *284*(7), 4073–4089. https://doi.org/10.1074/jbc.M805055200

Takasaki, Y., Koide, T., Wang, C., Kimura, H., Xing, J., Kushima, I., Ishizuka, K., Mori, D., Sekiguchi, M., Ikeda, M., Aizawa, M., Tsurumaru, N., Iwayama, Y., Yoshimi, A., Arioka, Y., Yoshida, M., Noma, H., Oya-Ito, T., Nakamura, Y., … Ozaki, N. (2016). Mutation screening of GRIN2B in schizophrenia and autism spectrum disorder in a Japanese population. *Scientific Reports*, *6*(1), Article 1. https://doi.org/10.1038/srep33311

Takata, A., Iwayama, Y., Fukuo, Y., Ikeda, M., Okochi, T., Maekawa, M., Toyota, T., Yamada, K., Hattori, E., Ohnishi, T., Toyoshima, M., Ujike, H., Inada, T., Kunugi, H., Ozaki, N., Nanko, S., Nakamura, K., Mori, N., Kanba, S., … Yoshikawa, T. (2013). A Population-Specific Uncommon Variant in GRIN3A Associated with Schizophrenia. *Biological Psychiatry*, *73*(6), 532–539. https://doi.org/10.1016/j.biopsych.2012.10.024

Tang, J., Chen, X., Xu, X., Wu, R., Zhao, J., Hu, Z., & Xia, K. (2006). Significant linkage and association between a functional (GT)n polymorphism in promoter of the N-methyl-d-aspartate receptor subunit gene (GRIN2A) and schizophrenia. *Neuroscience Letters*, *409*(1), 80–82. https://doi.org/10.1016/j.neulet.2006.09.022

Tani, A., Kikuta, R., Itoh, K., Joo, A., Shibata, H., Ninomiya, H., Tashiro, N., & Fukumaki, Y. (2002). Polymorphism analysis of the upstream region of the human N-methyl-d-aspartate receptor subunit NR1 gene (GRIN1): Implications for schizophrenia. *Schizophrenia Research*, *58*(1), 83–86. https://doi.org/10.1016/S0920-9964(02)00161-5

Taniguchi, S., Nakazawa, T., Tanimura, A., Kiyama, Y., Tezuka, T., Watabe, A. M., Katayama, N., Yokoyama, K., Inoue, T., Izumi-Nakaseko, H., Kakuta, S., Sudo, K., Iwakura, Y., Umemori, H., Inoue, T., Murphy, N. P., Hashimoto, K., Kano, M., Manabe, T., & Yamamoto, T. (2009). Involvement of NMDAR2A tyrosine phosphorylation in depression-related behaviour. *The EMBO Journal*, *28*(23), 3717–3729. https://doi.org/10.1038/emboj.2009.300

Tarabeux, J., Kebir, O., Gauthier, J., Hamdan, F. F., Xiong, L., Piton, A., Spiegelman, D., Henrion, É., Millet, B., S2D team, Fathalli, F., Joober, R., Rapoport, J. L., DeLisi, L. E., Fombonne, É., Mottron, L., Forget-Dubois, N., Boivin, M., Michaud, J. L., … Krebs, M.-O. (2011). Rare mutations in N-methyl-D-aspartate glutamate receptors in autism spectrum disorders and schizophrenia. *Translational Psychiatry*, *1*, e55. https://doi.org/10.1038/tp.2011.52

Townsend, M., Liu, Y., & Constantine-Paton, M. (2004). Retina-Driven Dephosphorylation of the NR2A Subunit Correlates with Faster NMDA Receptor Kinetics at Developing Retinocollicular Synapses. *The Journal of Neuroscience*, *24*(49), 11098–11107. https://doi.org/10.1523/JNEUROSCI.1207-04.2004

Traynelis, S. F., Wollmuth, L. P., McBain, C. J., Menniti, F. S., Vance, K. M., Ogden, K. K., Hansen, K. B., Yuan, H., Myers, S. J., & Dingledine, R. (2010). Glutamate receptor ion channels: Structure, regulation, and function. *Pharmacological Reviews*, *62*(3), 405–496. https://doi.org/10.1124/pr.109.002451

Trubetskoy, V., Pardiñas, A. F., Qi, T., Panagiotaropoulou, G., Awasthi, S., Bigdeli, T. B., Bryois, J., Chen, C.-Y., Dennison, C. A., Hall, L. S., Lam, M., Watanabe, K., Frei, O., Ge, T., Harwood, J. C., Koopmans, F., Magnusson, S., Richards, A. L., Sidorenko, J., … O'Donovan, M. C. (2022). Mapping genomic loci implicates genes and synaptic biology in schizophrenia. *Nature*, *604*(7906), Article 7906. https://doi.org/10.1038/s41586-022-04434-5

Tu, W., Xu, X., Peng, L., Zhong, X., Zhang, W., Soundarapandian, M. M., Balel, C., Wang, M., Jia, N., Zhang, W., Lew, F., Chan, S. L., Chen, Y., & Lu, Y. (2010). DAPK1 interaction with NMDA receptor NR2B subunits mediates brain damage in stroke. *Cell*, *140*(2), 222–234. https://doi.org/10.1016/j.cell.2009.12.055

Ulfhammer, E., Larsson, P., Magnusson, M., Karlsson, L., Bergh, N., & Jern, S. (2016). Dependence of Proximal GC Boxes and Binding Transcription Factors in the Regulation of Basal and Valproic Acid-Induced Expression of t-PA. *International Journal of Vascular Medicine*, *2016*, e7928681. https://doi.org/10.1155/2016/7928681

Uno, Y., & Coyle, J. T. (2019). Glutamate hypothesis in schizophrenia. *Psychiatry and Clinical Neurosciences*, *73*(5), 204–215. https://doi.org/10.1111/pcn.12823

Varner, M. W., Costantine, M. M., Jablonski, K. A., Rouse, D. J., Mercer, B. M., Leveno, K. J., Reddy, U. M., Buhimschi, C., Wapner, R. J., Sorokin, Y., Thorp, J. M., Ramin, S. M., Malone, F. D., Carpenter, M., O'sullivan, M. J., Peaceman, A. M., Dudley, D. J., Caritis, S. N., & Network, for the E. K. S. N. I. of C. H. and H. D. M.-F. M. U. (2020). Sex-Specific Genetic Susceptibility to Adverse Neurodevelopmental Outcome in Offspring

of Pregnancies at Risk of Early Preterm Delivery. *American Journal of Perinatology*, *37*(3), 281–290. https://doi.org/10.1055/s-0039-1678535

Vieira, M. M., Peng, S., Won, S., Hong, E., Inati, S. K., Thurm, A., Thiam, A. H., Kim, S., Myers, S. J., Badger, J. D., Traynelis, S. F., Lu, W., & Roche, K. W. (2023). A frameshift variant of GluN2A identified in an epilepsy patient results in NMDA receptor mistargeting. *Journal of Neuroscience*. https://doi.org/10.1523/JNEUROSCI.0557-23.2023

Vissel, B., Krupp, J. J., Heinemann, S. F., & Westbrook, G. L. (2001). A use-dependent tyrosine dephosphorylation of NMDA receptors is independent of ion flux. *Nature Neuroscience*, *4*(6), 587–596. https://doi.org/10.1038/88404

von Stülpnagel, C., Ensslen, M., Møller, R. S., Pal, D. K., Masnada, S., Veggiotti, P., Piazza, E., Dreesmann, M., Hartlieb, T., Herberhold, T., Hughes, E., Koch, M., Kutzer, C., Hoertnagel, K., Nitanda, J., Pohl, M., Rostásy, K., Haack, T. B., Stöhr, K., … Borggraefe, I. (2017). Epilepsy in patients with GRIN2A alterations: Genetics, neurodevelopment, epileptic phenotype and response to anticonvulsive drugs. *European Journal of Paediatric Neurology: EJPN: Official Journal of the European Paediatric Neurology Society*, *21*(3), 530–541. https://doi.org/10.1016/j.ejpn.2017.01.001

Vuletić, V., Rački, V., Papić, E., & Peterlin, B. (2021). A Systematic Review of Parkinson's Disease Pharmacogenomics: Is There Time for Translation into the Clinics? *International Journal of Molecular Sciences*, *22*(13), Article 13. https://doi.org/10.3390/ijms22137213

Vyklicky, V., Korinek, M., Smejkalova, T., Balik, A., Krausova, B., Kaniakova, M., Lichnerova, K., Cerny, J., Krusek, J., Dittert, I., Horak, M., & Vyklicky, L. (2014). Structure, function, and pharmacology of NMDA receptor channels. *Physiological Research*, *63*(Suppl 1), S191-203. https://doi.org/10.33549/physiolres.932678

Vyklicky, V., Krausova, B., Cerny, J., Ladislav, M., Smejkalova, T., Kysilov, B., Korinek, M., Danacikova, S., Horak, M., Chodounska, H., Kudova, E., & Vyklicky, L. (2018). Surface Expression, Function, and Pharmacology of Disease-Associated Mutations in the Membrane Domain of the Human GluN2B Subunit. *Frontiers in Molecular Neuroscience*, *11*. https://www.frontiersin.org/articles/10.3389/fnmol.2018.00110

Walsh, T., McClellan, J. M., McCarthy, S. E., Addington, A. M., Pierce, S. B., Cooper, G. M., Nord, A. S., Kusenda, M., Malhotra, D., Bhandari, A., Stray, S. M., Rippey, C. F., Roccanova, P., Makarov, V., Lakshmi, B., Findling, R. L., Sikich, L., Stromberg, T., Merriman, B., … Sebat, J. (2008). Rare Structural Variants Disrupt Multiple Genes in Neurodevelopmental Pathways in Schizophrenia. *Science*, *320*(5875), 539–543. https://doi.org/10.1126/science.1155174

Wang, G.-S., Hong, C.-J., Yen, T.-Y., Huang, H.-Y., Ou, Y., Huang, T.-N., Jung, W.-G., Kuo, T.-Y., Sheng, M., Wang, T.-F., & Hsueh, Y.-P. (2004). Transcriptional Modification by a CASK-Interacting Nucleosome Assembly Protein. *Neuron*, *42*(1), 113–128. https://doi.org/10.1016/S0896-6273(04)00139-4

Wang, J., Liu, S., Fu, Y., Wang, J. H., & Lu, Y. (2003). Cdk5 activation induces hippocampal CA1 cell death by directly phosphorylating NMDA receptors. *Nature Neuroscience*, *6*(10), 1039–1047. https://doi.org/10.1038/nn1119

Wang, T.-F., Ding, C.-N., Wang, G.-S., Luo, S.-C., Lin, Y.-L., Ruan, Y., Hevner, R., Rubenstein, J. L. R., & Hsueh, Y.-P. (2004). Identification of Tbr-1/CASK complex target genes in neurons. *Journal of Neurochemistry*, *91*(6), 1483–1492. https://doi.org/10.1111/j.1471-4159.2004.02845.x

Wang, X., Mei, D., Gou, L., Zhao, S., Gao, C., Guo, J., Luo, S., Guo, B., Yang, Z., Wang, Q., Tan, T., & Zhang, Y. (2023). Functional Evaluation of a Novel GRIN2B Missense Variant Associated with Epilepsy and Intellectual Disability. *Neuroscience*, *526*, 107–120. https://doi.org/10.1016/j.neuroscience.2023.06.018

Warming, H., Pegasiou, C.-M., Pitera, A. P., Kariis, H., Houghton, S. D., Kurbatskaya, K., Ahmed, A., Grundy, P., Vajramani, G., Bulters, D., Altafaj, X., Deinhardt, K., & Vargas-Caballero, M. (2019). A primate-specific short GluN2A-NMDA receptor isoform is expressed in the human brain. *Molecular Brain*, *12*(1), 64. https://doi.org/10.1186/s13041-019-0485-9

Warnet, X. L., Bakke Krog, H., Sevillano-Quispe, O. G., Poulsen, H., & Kjaergaard, M. (2021). The C-terminal domains of the NMDA receptor: How intrinsically disordered tails affect signalling, plasticity and disease. *European Journal of Neuroscience*, *54*(8), 6713–6739. https://doi.org/10.1111/ejn.14842

Wechsler, A., & Teichberg, V. I. (1998). Brain spectrin binding to the NMDA receptor is regulated by phosphorylation, calcium and calmodulin. *The EMBO Journal*, *17*(14), 3931–3939. https://doi.org/10.1093/emboj/17.14.3931

Williams, H. J., Georgieva, L., Dwyer, S., Kirov, G., Owen, M. J., & O'Donovan, M. C. (2012). Absence of de novo point mutations in exons of GRIN2B in a large schizophrenia trio sample. *Schizophrenia Research*, *141*(2), 274–276. https://doi.org/10.1016/j.schres.2012.08.024

Won, S., Levy, J. M., Nicoll, R. A., & Roche, K. W. (2017). MAGUKs: Multifaceted synaptic organizers. *Current opinion in neurobiology*, *43*, 94–101. https://doi.org/10.1016/j.conb.2017.01.006

Wong, H.-K., Liu, X.-B., Matos, M. F., Chan, S. F., Pérez-Otaño, I., Boysen, M., Cui, J., Nakanishi, N., Trimmer, J. S., Jones, E. G., Lipton, S. A., & Sucher, N. J. (2002). Temporal and regional expression of NMDA receptor subunit NR3A in the mammalian brain. *The Journal of Comparative Neurology*, *450*(4), 303–317. https://doi.org/10.1002/cne.10314

Wu, G.-H., Muthaiyan Shanmugam, M., Bhan, P., Huang, Y.-H., & Wagner, O. I. (2016). Identification and Characterization of LIN-2(CASK) as a Regulator of Kinesin-3 UNC-104(KIF1A) Motility and Clustering in Neurons. *Traffic*, *17*(8), 891–907. https://doi.org/10.1111/tra.12413

Wyszynski, M., Lin, J., Rao, A., Nigh, E., Beggs, A. H., Craig, A. M., & Sheng, M. (1997). Competitive binding of α-actinin and calmodulin to the NMDA receptor. *Nature*, *385*(6615), Article 6615. https://doi.org/10.1038/385439a0

XiangWei, W., Jiang, Y., & Yuan, H. (2018). De Novo Mutations and Rare Variants Occurring in NMDA Receptors. *Current Opinion in Physiology*, *2*, 27–35. https://doi.org/10.1016/j.cophys.2017.12.013

Yaka, R., Thornton, C., Vagts, A. J., Phamluong, K., Bonci, A., & Ron, D. (2002). NMDA receptor function is regulated by the inhibitory scaffolding protein, RACK1. *Proceedings of the National Academy of Sciences*, *99*(8), 5710–5715. https://doi.org/10.1073/pnas.062046299

Yang, L., Wei, M., Wang, Y., Zhang, J., Liu, S., Liu, M., Wang, S., Li, K., Dong, Z., & Zhang, C. (2023). Rabphilin-3A undergoes phase separation to regulate GluN2A mobility and surface clustering. *Nature Communications*, *14*(1), Article 1. https://doi.org/10.1038/s41467-023-36046-6

Yang, W., Zheng, C., Song, Q., Yang, X., Qiu, S., Liu, C., Chen, Z., Duan, S., & Luo, J. (2007). A three amino acid tail following the TM4 region of the N-methyl-D-aspartate receptor (NR) 2 subunits is sufficient to overcome endoplasmic reticulum retention of NR1-1a subunit. *The Journal of Biological Chemistry*, *282*(12), 9269–9278. https://doi.org/10.1074/jbc.M700050200

Yang, Y., Li, W., Zhang, H., Yang, G., Wang, X., Ding, M., Jiang, T., & Lv, L. (2015). Association Study of N-Methyl-D-Aspartate Receptor Subunit 2B (GRIN2B) Polymorphisms and Schizophrenia Symptoms in the Han Chinese Population. *PLOS ONE*, *10*(5), e0125925. https://doi.org/10.1371/journal.pone.0125925

Yeh, S.-H., Hung, J.-J., Gean, P.-W., & Chang, W.-C. (2008). Hypoxia-Inducible Factor-1α Protects Cultured Cortical Neurons from Lipopolysaccharide-Induced Cell Death via Regulation of NR1 Expression. *Journal of Neuroscience*, *28*(52), 14259–14270. https://doi.org/10.1523/JNEUROSCI.4258-08.2008

Yi, Z., Petralia, R. S., Fu, Z., Swanwick, C. C., Wang, Y.-X., Prybylowski, K., Sans, N., Vicini, S., & Wenthold, R. J. (2007). The Role of the PDZ Protein GIPC in Regulating NMDA Receptor Trafficking. *The Journal of Neuroscience*, *27*(43), 11663–11675. https://doi.org/10.1523/JNEUROSCI.3252-07.2007

Yin, H., Pantazatos, S. P., Galfalvy, H., Huang, Y., Rosoklija, G. B., Dwork, A. J., Burke, A., Arango, V., Oquendo, M. A., & Mann, J. J. (2016). A pilot integrative genomics study of GABA and glutamate neurotransmitter systems in suicide, suicidal behavior, and major depressive disorder. *American Journal of Medical Genetics Part B: Neuropsychiatric Genetics*, *171*(3), 414–426. https://doi.org/10.1002/ajmg.b.32423

Yu, Y., Lin, Y., Takasaki, Y., Wang, C., Kimura, H., Xing, J., Ishizuka, K., Toyama, M., Kushima, I., Mori, D., Arioka, Y., Uno, Y., Shiino, T., Nakamura, Y., Okada, T., Morikawa, M., Ikeda, M., Iwata, N., Okahisa, Y., … Ozaki, N. (2018). Rare loss of function mutations in N-methyl-D-aspartate glutamate receptors and their contributions

to schizophrenia susceptibility. *Translational Psychiatry*, *8*(1), Article 1. https://doi.org/10.1038/s41398-017-0061-y

Zhang, J., & Diamond, J. S. (2006). Distinct perisynaptic and synaptic localization of NMDA and AMPA receptors on ganglion cells in rat retina. *Journal of Comparative Neurology*, *498*(6), 810–820. https://doi.org/10.1002/cne.21089

Zhang, J., & Diamond, J. S. (2009). Subunit- and Pathway-Specific Localization of NMDA Receptors and Scaffolding Proteins at Ganglion Cell Synapses in Rat Retina. *Journal of Neuroscience*, *29*(13), 4274–4286. https://doi.org/10.1523/JNEUROSCI.5602-08.2009

Zhang, S., Edelmann, L., Liu, J., Crandall, J. E., & Morabito, M. A. (2008). Cdk5 regulates the phosphorylation of tyrosine 1472 NR2B and the surface expression of NMDA receptors. *The Journal of Neuroscience: The Official Journal of the Society for Neuroscience*, *28*(2), 415–424. https://doi.org/10.1523/JNEUROSCI.1900-07.2008

Zhang, Y., Fan, M., Wang, Q., He, G., Fu, Y., Li, H., & Yu, S. (2015). Polymorphisms in MicroRNA Genes And Genes Involving in NMDAR Signaling and Schizophrenia: A Case-Control Study in Chinese Han Population. *Scientific Reports*, *5*(1), Article 1. https://doi.org/10.1038/srep12984

Zhao, X., Li, H., Shi, Y., Tang, R., Chen, W., Liu, J., Feng, G., Shi, J., Yan, L., Liu, H., & He, L. (2006). Significant Association Between the Genetic Variations in the 5′ End of the N-Methyl-D-Aspartate Receptor Subunit Gene GRIN1 and Schizophrenia. *Biological Psychiatry*, *59*(8), 747–753. https://doi.org/10.1016/j.biopsych.2005.10.023

Zheng, F., Gingrich, M. B., Traynelis, S. F., & Conn, P. J. (1998). Tyrosine kinase potentiates NMDA receptor currents by reducing tonic zinc inhibition. *Nature Neuroscience*, *1*(3), Article 3. https://doi.org/10.1038/634

Zhong, Q., Chen, X., Zhao, Y., Liu, R., & Yao, S. (2017). Association of Polymorphisms in Pharmacogenetic Candidate Genes with Propofol Susceptibility. *Scientific Reports*, *7*(1), Article 1. https://doi.org/10.1038/s41598-017-03229-3

Zhou, M.-H., Chen, S.-R., Wang, L., Huang, Y., Deng, M., Zhang, J., Zhang, J., Chen, H., Yan, J., & Pan, H.-L. (2021). Protein Kinase C-Mediated Phosphorylation and α2δ-1 Interdependently Regulate NMDA Receptor Trafficking and Activity. *The Journal of Neuroscience: The Official Journal of the Society for Neuroscience*, *41*(30), 6415–6429. https://doi.org/10.1523/JNEUROSCI.0757-21.2021

Zhou, Q., & Sheng, M. (2013). NMDA receptors in nervous system diseases. *Neuropharmacology*, *74*, 69–75. https://doi.org/10.1016/j.neuropharm.2013.03.030

Zhou, X. (2022). Over-representation of potential SP4 target genes within schizophrenia-risk genes. *Molecular Psychiatry*, *27*(2), Article 2. https://doi.org/10.1038/s41380-021-01376-8

Zimmer, M., Fink, T. M., Franke, Y., Lichter, P., & Spiess, J. (1995). Cloning and structure of the gene encoding the human N-methyl-d-aspartate receptor (NMDAR1). *Gene*, *159*(2), 219–223. https://doi.org/10.1016/0378-1119(95)00044-7

9. List of publications

9.1. Publications *in extenso*, related to this thesis

1. Kysilov, B.*, **Kuchtiak, V.***, Hrcka Krausova, B., Balik, A., Korinek, M., Fili, K., Dobrovolski, M., Abramova, V., Chodounska, H., Kudova, E., Bozikova, P., Cerny, J., Smejkalova, T., & Vyklicky, L. (2024). Disease-associated nonsense and frame-shift variants resulting in the truncation of the GluN2A or GluN2B C-terminal domain decrease NMDAR surface expression and reduce potentiating effects of neurosteroids. *Cellular and Molecular Life Sciences*, *81*(1), 36. IF = 9.23 (2023)

2. Hirschfeldova, K., Cerny, J., Bozikova, P., **Kuchtiak, V.**, Rausch, T., Benes, V., Spaniel, F., Gregus, D., Horacek, J., Vyklicky, L., & Balik, A. (2021). Evidence for the Association between the Intronic Haplotypes of Ionotropic Glutamate Receptors and First-Episode Schizophrenia. *Journal of Personalized Medicine*, *11*(12), 1250. IF = 3.51 (2021)

9.2. Publications *in extenso*, unrelated to this thesis

1. Lebedeva, M., Kubištová, A., Spišská, V., Filipovská, E., Pačesová, D., Svobodová, I., **Kuchtiak, V.**, Balík, A., & Bendová, Z. (2024). The disruption of circadian rhythmicity of gene expression in the hippocampus and associated structures in Gria2R/R mice; a comparison with C57BL/6J and Adar2−/− mice strains. *Brain Research*, *1826*, 148739. IF = 3.61 (2023)

2. Míková, H.*, **Kuchtiak, V.***, Svobodová, I., Spišská, V., Pačesová, D., Balík, A., & Bendová, Z. (2020). Circadian Regulation of GluA2 mRNA Processing in the Rat Suprachiasmatic Nucleus and Other Brain Structures. *Molecular Neurobiology*, *58*(1), 439–449. IF = 5.59 (2020)

* co-first authorship

9.3. Author´s contribution on the publications related to this thesis

1. Kysilov, B.*, **Kuchtiak, V.***, Hrcka Krausova, B., Balik, A., Korinek, M., Fili, K., Dobrovolski, M., Abramova, V., Chodounska, H., Kudova, E., Bozikova, P., Cerny, J., Smejkalova, T., & Vyklicky, L. (2024). Disease-associated nonsense and frame-shift variants resulting in the truncation of the GluN2A or GluN2B C-terminal domain decrease NMDAR surface expression and reduce potentiating effects of neurosteroids. *Cellular and Molecular Life Sciences*, *81*(1), 36. IF = 9.23 (2023)

The author cloned all necessary constructs, produced lentiviruses, prepared primary neuronal cultures, maintained the cell lines, performed all fluorescence microscopy experiments, performed the colorimetric assay, analysed, and graphically processed the data, and participated in the writing of the publication.

2. Hirschfeldova, K., Cerny, J., Bozikova, P., **Kuchtiak, V.**, Rausch, T., Benes, V., Spaniel, F., Gregus, D., Horacek, J., Vyklicky, L., & Balik, A. (2021). Evidence for the Association between the Intronic Haplotypes of Ionotropic Glutamate Receptors and First-Episode Schizophrenia. *Journal of Personalized Medicine*, *11*(12), 1250. IF = 3.51 (2021)

The author participated in the data analysis, processing, and interpretation of the results, as well as in the writing of the publication.

I hereby confirm that the above-stated information about the contribution of Viktor Kuchtiak to all publications is correct.

Prague, 12. 1. 2024 RNDr. Aleš Balík, Ph.D.